Nuclear transport of the nitric oxide synthase interacting protein (NOSIP)

Dissertation

for the award of the degree

“Doctor rerum naturalium”

of the Georg-August-Universität Göttingen

within the doctoral program *Biomolecules: Structure – Function - Dynamics*

of the Georg-August University School of Science (GAUSS)

submitted by

Marius Philip Pörschke

from Datteln

Göttingen 2022

Thesis Committee

Prof. Dr. Ralph H. Kehlenbach

Department of Molecular Biology, University Medical Center Göttingen

Prof. Dr. Michael Meinecke

Department of Cellular Biochemistry, University Medical Center Göttingen

Dr. Achim Dickmanns

Department of Molecular Structural Biology, Georg-August-University Göttingen

Members of the Examination Board

Referee: **Prof. Dr. Ralph H. Kehlenbach**

Department of Molecular Biology, University Medical Center Göttingen

2nd Referee: **Prof. Dr. Hauke Hillen**

Department of Cellular Biochemistry, University Medical Center Göttingen

Further members of the Examination Board

Prof. Dr. Heike Krebber

Institute for Microbiology and Genetics, Georg-August-University Göttingen

Prof. Dr. Michael Meinecke

Department of Cellular Biochemistry, University Medical Center Göttingen

Prof. Dr. Henning Urlaub

Bioanalytical Mass Spectrometry Group, Max Planck Institute for Multidisciplinary Sciences

Dr. Achim Dickmanns

Department of Molecular Structural Biology, Georg-August-University Göttingen

Date of oral examination: 21.10.2022

Declaration

I hereby declare that I have written this PhD thesis independently and with no other aids or sources than quoted.

_____

Marius Philip Pörschke

September 2022, Göttingen

Table of Contents

Abstract

Proteins that need to actively enter the nucleus are thought to be transported by a specific nuclear transport receptor (NTR), depending on the type of the nuclear localization signal (NLS). Some cargoes are reported to be transported by several NTRs, like Histones, HIV-1-Rev or FUS. In a recent proteomic screen for importin 13 cargoes, Lipin 1 and NOSIP were found as potential import cargoes. However, both cargoes had been suggested to be imported by importin α/β. In this study the role of importin 13 and other NTRs in the nuclear import of Lipin 1 and NOSIP was analyzed. Lipin 1 has a dual function as transcriptional coactivator and as phosphatidate phosphatase. For both functions, the subcellular localization is important. Lipin 1 directly interacted with importin 13 and importin α/β. Further, importin α/β was confirmed as the preferred NTR for Lipin 1. However, importin 13 could partially rescue an importin β knockdown, suggesting that importin 13 is involved in the nuclear import of Lipin 1 as well, perhaps under specific conditions or in specific cell types. Moreover, the region comprising amino acids 398-414 was found to contain a CRM1-dependent NES.

The best characterized function of NOSIP is the regulation of eNOS activity by translocating the membrane bound enzyme to the cytoskeleton, specifically in the G2 phase of the cell cycle. For this, NOSIP itself has to translocate from the nucleus to the cytoplasm. The strong nuclear accumulation of NOSIP was shown to depend on active nuclear import, whereas export depends only on passive diffusion. The cytoplasmic enrichment of NOSIP seemed to be regulated through phosphorylation. A phosphomimic mutant of NOSIP was enriched in the cytoplasm, but the nuclear transport was not affected, pointing to a retention of NOSIP through binding to a cytoplasmic binding partner. Moreover, NOSIP specifically interacted with multiple NTRs in a RanGTP-dependent manner. In competition assays, transportin 1 was able to replace all other NTRs from binding to NOSIP. In addition, knockdown experiments showed that transportin 1 is the major NTR for NOSIP. Interestingly, NOISP binds transportin 1 in an unusual binding-mode. The binding-site of NOSIP on transportin 1 was mapped to the N-terminal arch using crosslinking combined with mass spectrometry and interaction studies. This is in contrast to typical PY-NLS or RG/RGG-motif containing transportin 1 cargoes, which bind to the C-terminal arch of transportin 1. This N-terminal binding to NTRs was also observed for importin β and importin 13.

No specific region or NLS like sequence of NOSIP could be identified. Instead, using different NOSIP fragments for binding assay and localization studies in cells, showed that several regions are important for the nuclear localization of NOSIP, suggesting that folded domains of NOSIP function as nuclear localization signals

1 Introduction

1.1 Nuclear Transport

1.1.1 Compartmentalization

In eukaryotic cells, the genetic material in the nucleus is surrounded by a phospholipid-bilayer. Through this compartmentalization, the processes of transcription and translation is locally separated, which leads to a higher organization of eukaryotic cells compared to prokaryotes. Separating both processes is advantageous, since transcribed mRNA is not translated in parallel, as it can be observed in prokaryotes. Based on this separation, proteins with functions in the nucleus, for instance polymerases, transcription factors or histones need to be transported into the nucleus, while at the same time various RNAs or some proteins need to be transported out of the nucleus. The transport of proteins and RNAs between cytoplasm and nucleus occurs through nuclear pores complexes (NPC), which are embedded in the nuclear membrane and are the sole connection between the cytoplasm and the nuclear compartment. NPCs form a barrier for macromolecules, while smaller macromolecules can passively diffuse through these pores, large macromolecules need to be actively transported by specific soluble transport proteins, so-called nuclear transport receptors (NTR). The nuclear transport machinery needs to be tightly regulated to adjust to the cellular environment and this adjustment is mediated through the transport of proteins involved in gene regulatory processes. For instance, under physiological conditions, gene expression differs from that under starvation or oxidative stress requiring a distinct set of transcription factors. Therefore, a subset of transcription factors needs to be transported into the nucleus, whereas another subset needs to be exported. The localization of those proteins is regulated through specific transport signals within the sequence of proteins. Those signals differ depending on the NTR used for nucleocytoplasmic shuttling, which will be explained in detail in the next sections. The transport machinery in cells is precisely orchestrated and a deregulation of this process plays a role in various diseases. Therefore, it is crucial to understand the complex network of nuclear transport under physiological or deregulated conditions.

1.1.2 Nuclear pore complex

The nuclear pore complex was first identified in 1950 (CALLAN and TOMLIN 1950) and further described as a pore embedded in the nuclear membrane, which consists of an inner- and outer-nuclear membrane, connecting the nucleoplasm with the cytoplasm in interphase cells (WATSON 1955). The NPC itself is an enormous multiprotein complex with a mass of ~110 MDa in vertebrates (Ori *et al.* 2013) and ~52 MDa in yeast (Kim *et al.* 2018). Consisting of around 30 different nucleoporins (Nup), each present in multiple copies of eight, the NPC assembles up to ~1000 protein molecules in total (Cronshaw *et al.* 2002). A single NPC mediates up to 10^3 translocation events per second, which corresponds to a mass of ~80-90 MDa. Under physiological conditions, a mass of ~15-40 MDa is transported through a single NPC between the nucleoplasm and cytoplasm (Ribbeck and Görlich 2001). To deal with the huge mass of proteins, which need to be translocated to the different compartments within a short time, the nuclear membrane of human cells is decorated with 2000-4000 NPCs (Maul and Deaven 1977). In *S. cerevisae,* ~120 NPCs can be found per nucleus, while *X. laevis* shows ~3500 NPCs (Maul and Deaven 1977). In the last years, NPC structure and composition have been extensively studied in various organisms, e.g. *S. cerevisae* (Allegretti *et al.* 2020)*, X. laevis* (Huang *et al.* 2020; Fontana *et al.* 2022), *H. sapiens* (Bui *et al.* 2013) or *C. reinhardtii* (Mosalaganti *et al.* 2018). The overall structure (Figure 1, A) shows to be well conserved throughout these species with a certain variability regarding the composition. Those structural studies are conducted using electron microscopy (EM) and X-ray crystallography. Overtime, these techniques have developed to a very powerful tool and have improved the understanding of the atomic structure up to a resolution of ~20 Å (Appen and Beck 2016; Lin and Hoelz 2019). The understanding of the NPC structure further improved by combining crystal structures of Nup-subcomplexes with tomographic maps of cryo-EM structures and in connection with experimental data, for instance mass-spectrometry derived crosslinking data or NMR (nuclear resonance spectroscopy) data (Hoelz *et al.* 2011; Kelley *et al.* 2015; Appen and Beck 2016; Lin *et al.* 2016; Huang *et al.* 2020). Moreover, this NPC structures have improved very recently by using the bioinformatic tool AlphaFold (Fontana *et al.* 2022; Mosalaganti *et al.* 2022). The AlphaFold software is an artificial intelligence system, which predicts protein 3D-structures of the whole human proteome, based on the amino-acid sequences of

proteins (Jumper *et al.* 2021; Tunyasuvunakool *et al.* 2021). It is used to predict high accuracy models of Nups, which are then placed in missing gaps of the tomographic map of *X. laevis* to further complete the picture of the NPC (Fontana *et al.* 2022; Mosalaganti *et al.* 2022).

The dimensions of a human NPC range from ~800 Å in height and a diameter of ~1200 Å with a central opening of about ~425 Å in diameter (Figure 1 B) (Lin and Hoelz 2019). In yeast, the NPC shows smaller dimensions with a diameter of ~950 Å, a height of ~600 Å, but a central channel of about ~450 Å in diameter like human NPCs (Lin and Hoelz 2019). Nevertheless, these dimensions are not rigid. Instead the NPC is dynamic and can dilate or constrict the width of the central channel (Mosalaganti *et al.* 2022). Basically, the NPC shows an 8-fold rotational symmetry and a 2-fold rotational symmetry along the nuclear envelope axis (Gall 1967; Lin and Hoelz 2019). Nucleoporins building up the NPC tend to organize into subcomplexes and are found in different regions of the NPC depending on their structural properties (Hoelz *et al.* 2011). Structurally, Nups are built of β-propellers, α-helical repeats and coiled-coil domains, which are important for their interactions with other Nups (Hoelz *et al.* 2011). A few nucleoporins contain transmembrane domains, namely POM121, gp210 and Ndc1, which anchor the NPC within the nuclear membrane (Onischenko *et al.* 2009; Mitchell *et al.* 2010; Upla *et al.* 2017). Additionally, around one third of the Nups contain long intrinsically disordered regions containing polar residues and several FG (phenylalanine-glycine)-repeats, so called FG-Nups (Rout and Wente 1994). The FG repeats comprise of multiple FG-, GLFG- or FxFG-peptides, which are highly hydrophobic (Patel *et al.* 2007). FG-Nups are mainly present in the inner ring, facing their FG-repeat domains towards the central channel and form the permeability barrier of the NPC (Figure 1, red) (Frey and Görlich 2007; Najbauer *et al.* 2022). Additionally, they are found to be important for nuclear transport regulation through interactions with soluble transport factors in the cytoplasm and nucleoplasm (Radu *et al.* 1995; Bayliss *et al.* 2000; Isgro and Schulten 2005; Hutten *et al.* 2008).

The overall structure of the NPC comprises the inner scaffold, including a permeability barrier in the central channel, and the inner and outer ring structures. Peripheral Nups are attached to the outer and inner structures and build the cytoplasmic filaments and nuclear basket (Schematic structure see Figure 1 A) (Lin and Hoelz 2019). The major

scaffold building block of the NPC is the Y-complex, also called Nup107-Nup160 subcomplex, which is named by its shape (Kelley *et al.* 2015; Stuwe *et al.* 2015; Kosinski *et al.* 2016). This subcomplex contains 10 Nups in humans, namely Nup160, Nup107, Nup133, Nup96, Nup75, Nup37, Nup43, seh1, sec13 and ELYS (Loïodice *et al.* 2004; Kelley *et al.* 2015). It builds the inner ring coat of the scaffold (Figure 1, orange), which is anchored by the transmembrane Nups mentioned above (Onischenko *et al.* 2009; Mitchell *et al.* 2010; Upla *et al.* 2017). A further cylindrical layer around the Y-complex is the adaptor nucleoporin containing Nup93 subcomplex (Figure 1, green and blue) (Amlacher *et al.* 2011; Kosinski *et al.* 2016). Followed by a third cylindrical layer, the Nup62 subcomplex. It is formed by channel Nups, which contain FG-repeats, forming the permeability barrier of the NPC (Figure 1, red) (Finlay *et al.* 1991; Kita *et al.* 1993; Lin *et al.* 2016). The cytoplasmic filaments (CF) nucleoporins are FG-repeat containing Nups and thus more flexible. They are connected to the scaffold ring, protrude towards the cytoplasm (Figure 1, cyan), interact with soluble transport factors and are therefore important for the nuclear transport (Kehlenbach *et al.* 1999; Hutten *et al.* 2008; Hoelz *et al.* 2011; Lin and Hoelz 2019). Nups in the CF include Nup214, Gle1, ALADIN, Nup88, Rae1, Nup98, Nup62 and Nup358 (Lin and Hoelz 2019; Fontana *et al.* 2022), where the latter one is specific for metazoa (Wu *et al.* 1995). Nup98 and Nup62 are found in various subcomplexes as linker molecules (Griffis *et al.* 2003; Lin and Hoelz 2019; Fontana *et al.* 2022). The nuclear basket, named by its basket like structure, comprises Nup153, Nup50 and Tpr, and decorates the nuclear side of the NPC (Figure 1, purple) (Jarnik and Aebi 1991; Panté *et al.* 1994). The nuclear basket is important for anchoring of the NPC and for proper nuclear transport (Walther *et al.* 2001), since blocking of Nup153 using antibodies leads to an abolished nuclear export of some proteins and RNAs (Ullman *et al.* 1999). Most of the mentioned human nucleoporins can be found as homologues in yeast or other species in a high structural and functional similarity, despite a low sequence similarity (Suntharalingam and Wente 2003).

Nucleoporins do not only function in the context of nuclear transport but also play a role in various cellular processes (Fahrenkrog *et al.* 2004). Some Nups directly stimulate the expression of genes. Nup50 and Nup98, for instance, regulate the expression of developmental or cell-cycle genes (Kalverda *et al.* 2010). Further, Nups

are involved in chromatin organization through interaction with histone-modifying proteins (reviewed in (Kuhn and Capelson 2019))

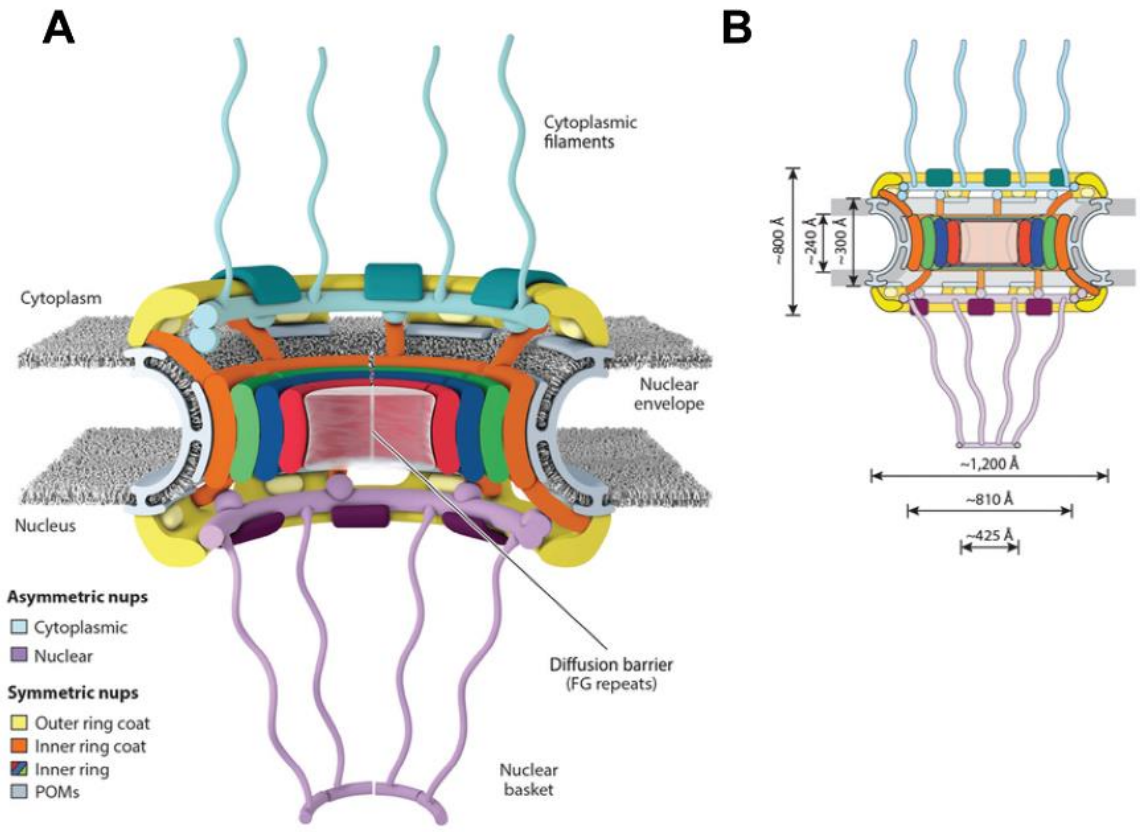

Figure 1: Structure of the nuclear pore complex (NPC). (A) Schematic view of the cross-section of a NPC, structures are colored as indicated. Graphic adapted from (Lin and Hoelz 2019). (B) Schematic view of a cross-section of a human NPC with indicated dimensions. Graphic adapted from (Lin and Hoelz 2019).

1.1.3 Nuclear Transport

Nuclear transport describes the process of proteins crossing the nuclear envelope through the NPC, the direct connection gateway between nucleoplasm and cytoplasm (WATSON 1955). Despite this direct connection, nucleoplasm and cytoplasm are well separated by the permeability barrier built of FG-Nups, which are responsible for controlled nuclear shuttling (Frey and Görlich 2007; Patel *et al.* 2007). The selectivity of the permeability barrier is thought to be dependent on the size or roughly on the mass of the cargo. Cargo molecules smaller than ~30-60 kDa in size or ~5 nm in diameter can enter or exit the nucleus upon passive diffusion (Mohr *et al.* 2009). Macromolecules above this size limit are assumed to need assisted diffusion through the permeability barrier (Wing *et al.* 2022). The detailed composition and regulation of the permeability barrier remains unclear, but several models are proposed to describe

this barrier. The models differ in their description how FG-Nups interact with each other or with transporter molecules. For example, the “selective phase model” describes the diffusion barrier as a meshwork of FG-Nups, that crosslink to each other to form a three-dimensional sieve-like meshwork, which excludes larger molecules from diffusion (Ribbeck and Görlich 2001; Frey *et al.* 2006). In this model, NTRs can penetrate the channel by disrupting FG-Nup crosslinks to pass through this transiently opened meshwork (Ribbeck and Görlich 2001; Frey *et al.* 2006). Another model is the “virtual gate model”, where Rout and Co-workers postulate that FG-Nups protrude into the channel like brushes in a non-interacting way (Rout *et al.* 2003). To facilitate translocation of macromolecules above the size limit, NTRs are assumed to lose entropy when entering the channel and release binding-energy upon interaction with FG-regions, which lowers the activation energy required for the entry in the channel. Inert molecules above the size limit do not interact with FG-regions and are avoided from entering, since entropy costs are too high (Rout *et al.* 2003). In a third model named “forest model”, it is assumed that FG-Nups behave heterogeneously, meaning some FG-regions attract each other forming collapsed coils, whereas others repulse from each other forming more relaxed and extended coils. This heterogeneity is suggested to resemble topological trees and shrubs and forms two zones, called transporter, the central transporter for bigger macromolecules and the lateral transporter for smaller macromolecules (Yamada *et al.* 2010). For several models, indirect experimental evidence is shown, but analysis is mostly performed in *in vitro* systems or in reconstituted FG-Nup gel-like structures, but not *in vivo*.

The transport machinery for assisted active nuclear transport through the NPC requires the RanGTPase system and the soluble nuclear transport receptors. The directionality of nuclear transport is driven by the RanGTP-gradient in the cells, which is maintained by the RanGTPase system (Izaurralde *et al.* 1997). It is composed of Ran (small GTP-binding protein Ran), RanGEF (guanosine nucleotide exchange factor) and RanGAP (RanGTP activating protein) (Bischoff and Ponstingl 1991; Bischoff *et al.* 1994). The high levels of RanGTP within the nucleus are a result of the presence of chromatin bound RCC1 (RanGEF), which loads Ran with GTP (Bischoff and Ponstingl 1991; Renault *et al.* 2001). High RanGTP levels favor the formation of nuclear export complexes and trigger the release of nuclear import complexes (Richards *et al.* 1997). In the cytoplasm, RanGAP bound to the cytoplasmic filament

nucleoporin Nup358 and RanBP1, mediates hydrolysis of RanGTP to RanGDP (Bischoff *et al.* 1994; Bischoff and Görlich 1997; Kehlenbach *et al.* 1999), which leads to a 200-fold lower RanGTP level in the cytoplasm compared to the nucleus (Kalab *et al.* 2002). The hydrolysis of RanGTP to RanGDP leads to the dissociation of nuclear export complexes and the low levels of RanGTP allow the binding of nuclear transport receptors to import-cargoes (Görlich *et al.* 1996; Kehlenbach *et al.* 1999; Koyama and Matsuura 2010). Some nuclear transport receptors are called karyopherins (Kaps) and belong to the importin-β superfamily (Görlich and Kutay 1999; Chook and Süel 2011). Kaps are conserved from yeast to humans (Ström and Weis 2001; O'Reilly *et al.* 2011). In humans, 20 Kaps are known and are originally divided into two groups, classified by the directionality of transport (Wing *et al.* 2022). Importins are named through their ability to import cargoes out of the cytoplasm into the nucleus, while exportins are named by their ability to mediate nuclear export of cargoes to the cytoplasm (GORLICH 1994; Stade *et al.* 1997). Later on, some Kaps have been classified as bi-portins by the capability of mediating both, nuclear import and export (Mingot *et al.* 2001; Gontan *et al.* 2009; Aksu *et al.* 2018). In humans, importins (imp) contain imp β, imp 4, imp 5, imp 7, imp 8, imp 9, imp 11 and TNPO (transportin) 1, TNPO 2 and TNPO 3 (Wing *et al.* 2022). Exportins include exportin 1 (CRM1), exportin 2 (CAS), exportin 3 (exportin t), exportin 5 and exportin 6. Proteins, which function as bidirectional NTRs, are imp 13, exportin 4 and exportin 7 (Mingot *et al.* 2001; Gontan *et al.* 2009; Aksu *et al.* 2018; Wing *et al.* 2022), while the function of RanBP6 and RanBP17 is currently unknown (Wing *et al.* 2022).

Nuclear transport is a well-studied process within cells (Figure 2). For nuclear import, importins bind their cargo depending on a nuclear localization signal (NLS) in a direct manner or with the help of cargo-adaptor proteins, known as importin α proteins (seven isoforms are known for Kap α (karyopherin α) 1-7) (Miyamoto *et al.* 2016). This import complex is transported through the permeability barrier of the NPC, while engaging in multivalent interactions with the FG-nucleoporins and finally dissociates in the nuclear compartment upon RanGTP binding to importin (Görlich *et al.* 1996; Bayliss *et al.* 2000; Allen *et al.* 2001; Lee *et al.* 2005; Hahn and Schlenstedt 2011). Importins bind cargoes or RanGTP in a mutually exclusive manner with a much higher affinity of RanGTP to karyopherins compared to the import-cargo karyopherin binding affinity (Lee *et al.* 2005). The free import cargo is retained in the nucleus, the import

receptor bound to RanGTP is recycled to the cytoplasm. In case of a ternary transport complex out of karyopherin β, karyopherin α and cargo, the cargo-adaptor protein karyopherin α is recycled by exportin 2 (CAS) (Kutay *et al.* 1997; Weis 1998). After hydrolysis of RanGTP to RanGDP, which is mediated by RanGAP, importins are released and ready for another round of import (Bischoff *et al.* 1994). RanBP1, a cofactor of RanGAP, promotes the hydrolysis of RanGTP (Bischoff *et al.* 1995; Kehlenbach *et al.* 1999). Furthermore, the interaction of RanGAP with Nup358, also known as RanBP2, at the cytoplasmic site of the NPC promotes this hydrolysis (Hutten *et al.* 2008; Koyama and Matsuura 2010). RanGDP is then recycled back into the nucleus by a specific transporter protein, named NTF2 (Nuclear transport factor 2), for recharging of RanGDP by chromatin-bound RCC1 to RanGTP (Ribbeck *et al.* 1998; Renault *et al.* 2001). For the process of nuclear export, exportins bind cooperatively to RanGTP and cargoes containing a nuclear export signal (NES) (Monecke *et al.* 2013). This trimeric complex (exportin-RanGTP-export-cargo) shuttles through the NPC and terminates in the cytoplasm upon RanGTP hydrolysis (Koyama and Matsuura 2010). Free RanGDP and free exportin are recycled back to the nuclear compartment and free export cargo is retained in the cytoplasm. RanGDP is then recharged to RanGTP in the nucleus and the free exportin can export another cargo (Bischoff and Ponstingl 1991). The energy used for nuclear translocation against a concentration gradient indirectly results from hydrolysis and recharging of the small GTP-binding protein Ran. Next to this regular nuclear transport via Kaps, some proteins above the size threshold enter the nucleus in a RanGTP- and karyopherin-independent manner (Yokoya *et al.* 1999; Kumeta *et al.* 2012), e.g. β-catenin (Yokoya *et al.* 1999) and actinin-4 (Kumeta *et al.* 2010). The NTR-independent nuclear translocation process depends on the surface hydrophobicity of the respective protein. This was shown for chemical modified BSA, which is able to diffuse into the nucleus after increasing the hydrophobicity of the surface (Naim *et al.* 2009).

The process of nucleocytoplasmic transport (NCT) is tightly orchestrated, and proteins are transported as soon as they are recognized through their signaling sequence. Nonetheless, different proteins need to be re-localized depending on cell-cycle phase or extracellular stimuli, thus, transport needs to be fine-tuned. Regulation of NCT can be achieved by switching on or off respective localization signals or through altering the NTRs. A common feature to pass down signals in cells are posttranslational

modifications (PTM) like phosphorylation, acetylation, ubiquitination or sumolyation (Weinberg 2014). These modifications are known to alter the affinity of cargoes to NTRs when within or near to signaling sequences (reviewed in (Nardozzi *et al.* 2010; Wang *et al.* 2012). Nuclear import of CTP–phosphocholine cytidylyltransferase (CCTα) is blocked by ubiquitination (ub), which disrupts the binding of importin α (Chen and Mallampalli 2009). Contrary to CCTα, ubiquitination of the tumor suppressor PTEN (suppresses phosphatase and tensin homolog on chromosome 10) leads to its nuclear import, whereas a mutation of the ubiquitination-site causes a disposition in the cytoplasm (Trotman *et al.* 2007). Phosphorylation of cargoes also functions as enhancer or inhibitor of nuclear transport, e.g. phosphorylation within or upstream of the NLS of EBNA1 (Kitamura *et al.* 2006) or SV40 large T-antigen (Hübner *et al.* 1997), respectively, increases nuclear import, whereas nuclear import of PTHrP is impaired upon phosphorylation of its NLS (Lam *et al.* 1999). In addition to the direct activation or inactivation of signaling sequences, phosphorylation of STAT leads to its homodimerization and conformational changes, which expose a dimer-specific NLS (Meyer *et al.* 2002). Not only modification of cargoes can regulate transport activities, but also phosphorylation of NTRs, as it is shown for importin 13, which showed resulting in reduced nuclear import activity when modified at Serine 193 (Liu *et al.* 2018).

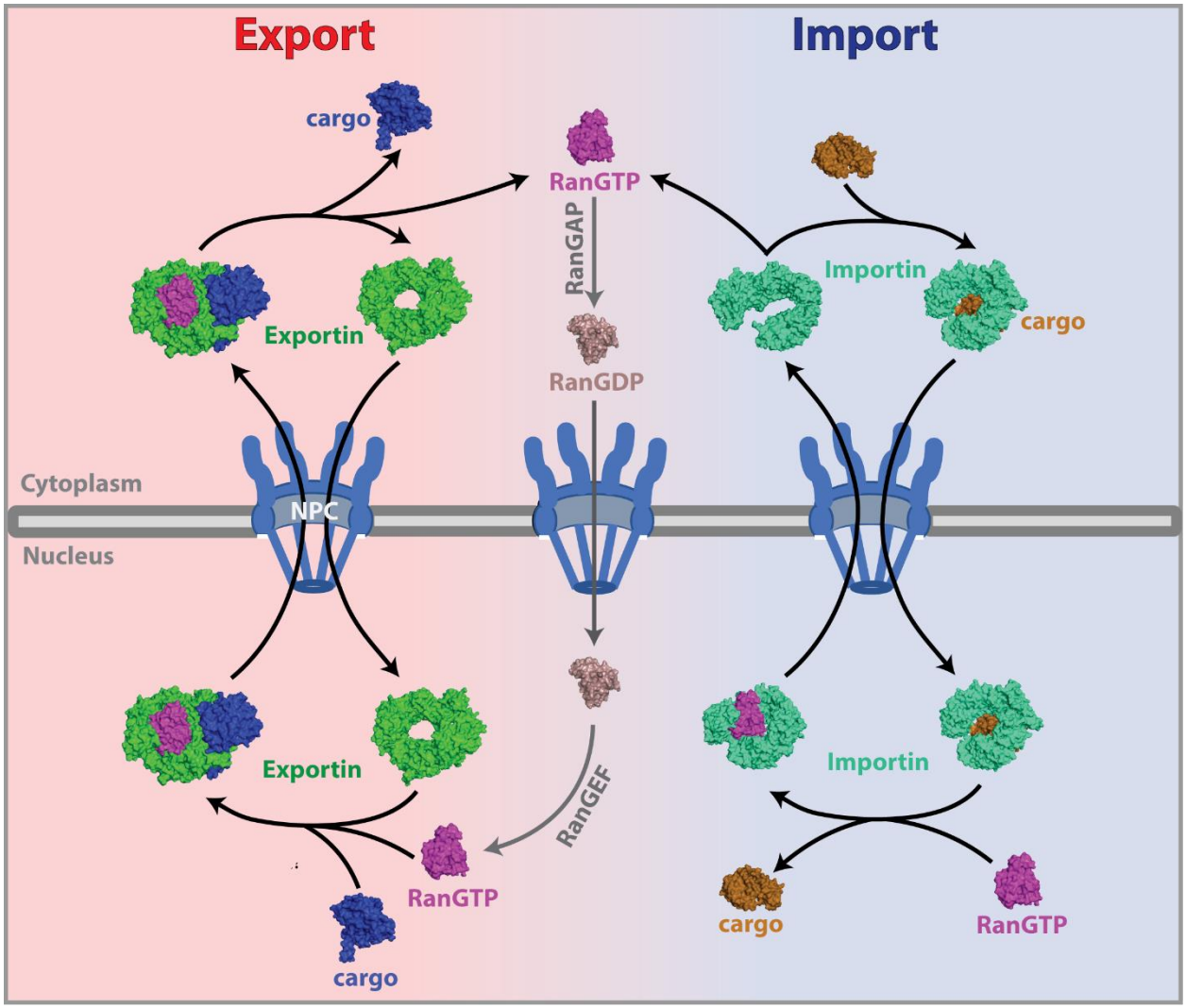

Figure 2: Schematic overview of the nucleocytoplasmic transport pathway. For the process of nuclear import, Importins recognize their cargoes through nuclear localization signals. The Importin-cargo complex passes the nuclear pore complex (NPC) and upon RanGTP-binding to the Importin in the nucleus, the import-cargo is released. The Importin bound to RanGTP shuttles then back to the cytoplasm and is released upon RanGTP hydrolysis to RanGDP. The hydrolysis is mediated by RanGAP. The free Importin mediate another round of import and RanGDP is imported into the nucleus and recharged to RanGTP by RanGEF. For nuclear export, Exportins form a ternary export complex (Exportin-RanGTP-cargo) in the nucleus. This export complex is then transported through the NPC into the cytoplasm, where it dissociates upon hydrolysis of RanGTP. The free Exportin and RanGDP are then recycled back into the nucleus for another round of export and recharging of RanGDP. This figure was created with Adobe Illustrator 6 and is inspired by (Monecke et al. 2014)

1.1.4 Nuclear transport receptors (NTRs)

Nuclear transport receptors enforce nucleocytoplasmic transport by binding to their cargoes via specific localization signals. The dissection of the nuclear transport machinery is challenging since isolation of intact nuclei is difficult. The first functional assay to analyze soluble transport receptors have been established in 1990 by using digitonin to selectively permeabilize the plasma membrane of mammalian cells, whereas the nuclear membrane remains intact (Adam *et al.* 1990). With this simplification, several proteins involved in nuclear transport have been identified, e.g. NTF2 (nuclear transport factor 2), importin β or Ran (Moore and Blobel 1993; Adam and Adam 1994; Paschal and Gerace 1995). Further identification of soluble transport factors and the structural and functional characterization of those lead to their classification into three classes. One class is the NTF2 family named after its most prominent member, since all share striking similarity in their tertiary structure to NTF2, but low sequence homology (Fribourg *et al.* 2001; Eberhardt *et al.* 2013). Another protein of this family that is involved in nuclear transport, precisely in mRNA export, is NXT1 (NTF2-related export protein 1), which shows the same characteristic structure of extensive β-sheets flanked by α-helices (Bullock *et al.* 1996; Katahira *et al.* 1999). NXT1 is an mRNA export receptor, which is only functional as a heterodimer with TAP (tip-associated protein) (Fribourg *et al.* 2001; Fried and Kutay 2003). TAP (Mex67 in yeast) is part of the second class of NTRs, namely NXF family. It contains a NTF2-like domain in its C-terminal half, which is necessary for heterodimerization with NXT1 (Herold *et al.* 2000; Dickmanns *et al.* 2015). The NXF (nuclear export factor) family constitutes of proteins involved in RNA export, comprising in humans NXF 1-6, where NXF1 is also called TAP (Herold *et al.* 2000). All NXF proteins are multidomain proteins consisting an overall structure of a NTF2-like domain, an UBA (Ubiquitin associated)-domain, a RNA-binding domain and 4 leucine-rich repeat (LRR) domains (Herold *et al.* 2000; Liker *et al.* 2000; Fribourg *et al.* 2001).

The third class is the karyopherin (Kap) β superfamily. This class constitutes of 20 members in humans (Wing 2020). The overall structure of karyopherin βs is well conserved, despite a low sequence homology with the highest homology in the N-terminal part (Cook *et al.* 2007; Wing *et al.* 2022). Structurally, karyopherin βs are mainly α-helical proteins consisting of 18-20 so-called HEAT-repeats (Wing *et al.*

2022). HEAT-repeats have first been described in four proteins, from which the motif name originates, namely **H**untingtin, **e**longation factor 3, PR65/**A** subunit of protein phosphatase 2A and the lipid kinase **T**or1 (Andrade *et al.* 2001). A HEAT-repeat consist of 30-50 amino acids (aa), which comprise a secondary structure of two antiparallel oriented α-helices, connected by a short linker (Figure 3 A) (Yoshimura and Hirano 2016). The two α-helices of the HEAT motif interact with further HEAT motifs in a parallel manner, forming a stacked super helical structure (Figure 3 B) (Andrade *et al.* 2001; Yoshimura and Hirano 2016). This stacked super helical structure shows a right-handed twist for karyopherin βs. This twist is based on the tilt between two HEAT motifs (Groves *et al.* 1999; Lee *et al.* 2000; Yoshimura and Hirano 2016). Despite this structural difference, some regions of both, PR65/A and karyopherin β1, show some structural similarity in the arrangement of their HEAT-repeats (Vetter *et al.* 1999).

Overall, this super helical packing results in a two-layered arrangement of the α-helices, which can be more S-shaped or O-shaped (Figure 3 C-D) (Yoshimura and Hirano 2016). The outer convex surface comprises the A-helices of the HEAT motifs and the inner concave surface of the solenoid consist of the B-helices (Figure 3 C) (Cingolani *et al.* 1999; Yoshimura and Hirano 2016). The convex outer side interacts with the intrinsically disordered FG-repeat containing regions of Nups (Yoshimura and Hirano 2016). Crystal-structures of importin β with FxFG or GLFG peptides show that the FG-peptides bind to a hydrophobic grove at the A-helices of HEAT motif 5 and 6 (Bayliss *et al.* 2000; Bayliss *et al.* 2002).

X-ray crystal structures of NTRs with transport-cargoes or Ran show that they bind in the inner concave surface of Kap βs, containing the B-helices (Chook and Blobel 1999; Cingolani *et al.* 1999). More precisely, most transport cargoes bind to the C-terminal arch of Kap β, as it is shown in crystal structures of importin β with SREBP 2 (sterol regulatory element-binding protein 2) (Lee *et al.* 2003) or IBB-domain (Importin β-binding domain of importin α) (Cingolani *et al.* 1999), and of transportin 1 (Kap β2) binding to hnRNP D, JKTBP or hnRNP A (Imasaki *et al.* 2007). The N-terminal half is the conserved binding site for RanGTP among Kap βs (Görlich *et al.* 1997; Chook and Blobel 1999; Lee *et al.* 2005). N-terminal binding of import-cargoes to kap βs is only shown for a few proteins, e.g. for c-Fos and the HIV(human

immunodeficiency virus)-1 Rev protein binding to transportin 1 (Arnold *et al.* 2006a; Arnold *et al.* 2006b), for PTHrP (parathyroid hormone-related protein) binding to importin β (Cingolani *et al.* 2002) and for Ubc9 binding to importin 13 (Grünwald and Bono 2011).

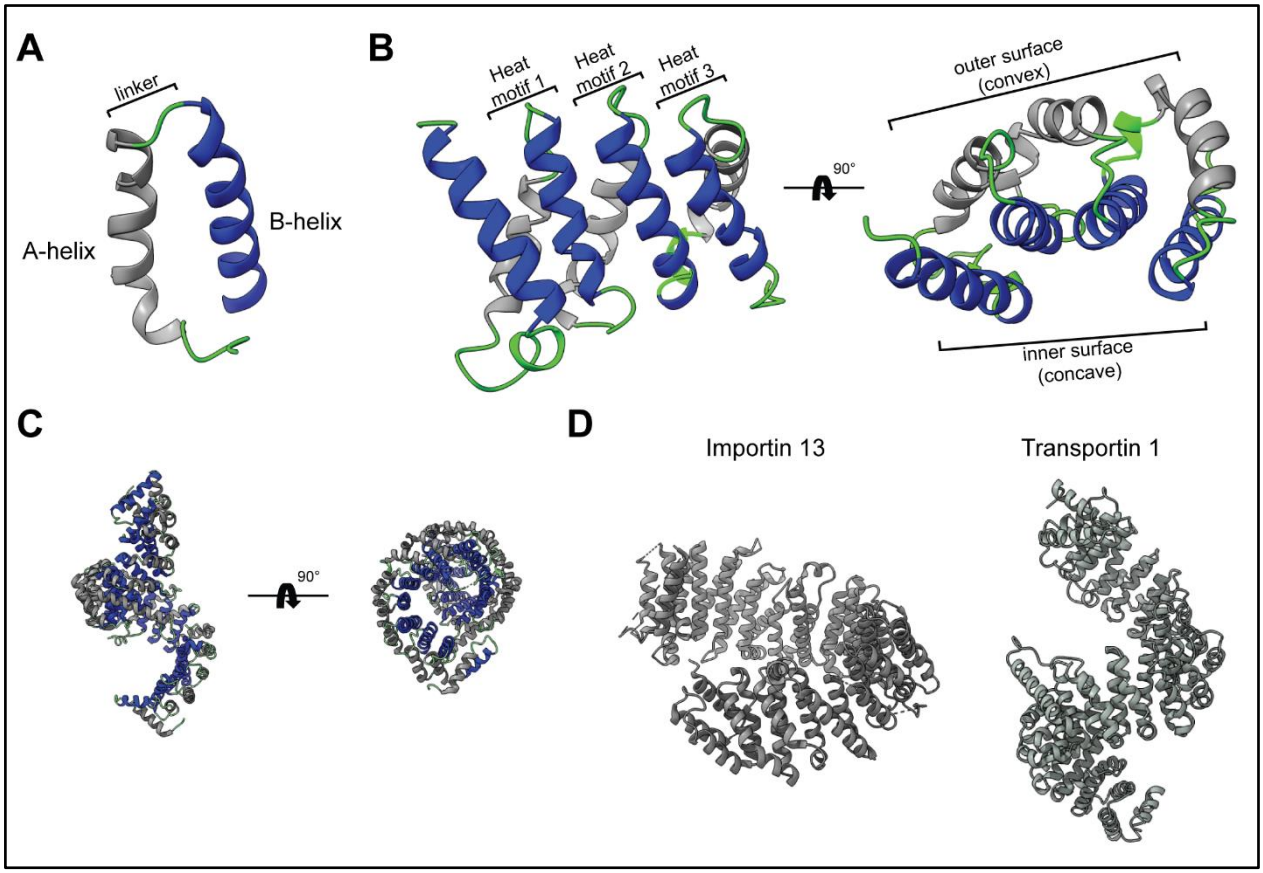

Figure 3: Structure of karyopherin β superfamily members. (A) Single HEAT-repeat consisting of two antiparallel α-helices, helix A (grey) and helix B (blue), which are connected by a linker (green). (B) Several HEAT-repeats stacked, showing a right-handed twist. Both helices and the linker are colored as in A HEAT-motifs taken from transportin 1 crystal structure (PDB:2z5j). (C) Whole crystal structure of transportin 1 (PDB: 2z5j), inner concave surface consisting of B-helices is depicted in blue and outer convex surface formed by A-helices is depicted in grey. (D) Comparison of importin 13 (PDB: 3zkv) and transportin 1 (PDB: 2z5j) crystal structures, tightly packed vs. loosely packed. Graphics were created using Chimera X1-3 software.

The mechanisms of cargo recognition and release from karyopherins is explained in detail in section 1.1.5. Import-cargo release is based on a structural rearrangement of the importin upon RanGTP binding, which replaces cargoes and locks importins in positions, unable to bind import-cargoes ((Lee *et al.* 2005; Grünwald *et al.* 2013; Wing *et al.* 2022), reviewed in (Wing *et al.* 2022)). This mechanism is based on the structural flexibility of NTRs as seen in SAXS (small angle X-ray scattering)-analysis and crystal structures of NTRs in bound and unbound states (Lee *et al.* 2005; Forwood *et al.* 2010; Grünwald *et al.* 2013). The flexibility of NTRs is based on their HEAT-repeats, which are highly flexible structures. Upon different interactions, with Ran or cargoes, HEAT-

repeats can flexible adjust to the size of the bound cargoes (Andrade *et al.* 2001; Tsytlonok *et al.* 2013; Yoshimura and Hirano 2016).

Another karyopherin family is the karyopherin α-family with 7 constituents in humans (Kelley *et al.* 2010; Miyamoto *et al.* 2016). Importin α is an adaptor protein, which binds to classic nuclear localization signals (NLS) of transport-cargoes and to importin β via its IBB-domain (Adam and Gerace 1991; Cingolani *et al.* 1999). Like Karyopherin βs, Karyopherin αs are mainly α-helical proteins, but one major difference is the composition of the α-helices. Importin αs consist of Armadillo (ARM) repeats, which are similar to HEAT-repeats, but consist of three α-helices, referred to as 1-3 (Conti and Kuriyan 2000; Andrade *et al.* 2001). Importin α interacts in a unique way with importin β and mediates translocation of NLS-bearing cargoes (Wing *et al.* 2022).

1.1.5 -Cargo binding modes of karyopherin βs

Assisted transport of macromolecules across the nuclear envelope requires a specific localization sequence, which is bound by specific nuclear NTRs. For import into the nucleus, a NLS (nuclear localization signal) is necessary and for export into the cytosol, a NES (nuclear export signal). The NLS sequence has been described first for the simian virus large T-antigen (SV40) as a linear sequence rich in basic residues, which is required for its nuclear import (Kalderon *et al.* 1984). Importin α is identified to bind these linear NLS and to mediate the import into the nuclei of mammalian cells in concert with Importin β (Adam and Gerace 1991; Adam and Adam 1994). This first import signal is the classical NLS (cNLS) with the consensus sequence K-K/R-X-K/R (where X is every residue), which can be 4-8 basic amino acids long (Kalderon *et al.* 1984). The identification of further cargoes and the characterization of their regions important for nuclear translocation revealed more types of signaling sequences. The classical NLS can be split into two parts, which is defined as bi-partite NLS. This type of NLS has the consensus sequence K/R-K/R-$X_{10–12}$-K/R_{3-5} with a first cluster of basic residues, separated by a linker of 10-12 residues (where X can be any amino acid) from a second basic cluster of 3 to 5 residues (Robbins *et al.* 1991; Lu *et al.* 2021). Classic/bi-partite NLSs are recognized by the adaptor protein importin α, which contains two well conserved binding sites on its concave inner surface (Conti *et al.* 1998), a minor and a major binding site. The latter is mainly bound by cNLSs, whereas

bi-partite NLS bind to both sites on importin α (Conti *et al.* 1998; Fontes *et al.* 2003). Importin α then binds to importin β on the C-terminal site, using its N-terminal IBB-domain (Cingolani *et al.* 1999). This formation of a ternary import-complex is a cooperative interaction, since binding of the IBB-domain to importin β opens the NLS binding sites of importin α (Kobe 1999). The NLS binding sites of importin α are autoinhibited by its NLS bearing IBB-domain (Kobe 1999; Harreman *et al.* 2003). This autoinhibitory function is important for the cargo release of importin α. RanGTP binding to importin β triggers the dissociation of importin α and the freed NLS of the importin α IBB-domain replaces the cargo in the nucleus (Ström and Weis 2001). Additionally, free importin α is recycled by the exportin CAS, which further prevents the rebinding rebinding of import-cargoes in the nucleus (Kutay *et al.* 1997). importin β does not only import cargoes in concert with importin α, but can also bind directly to cargoes or as a heterodimer with importin 7 (Cingolani *et al.* 2002; Ivic *et al.* 2019). The interaction of importin β and cargoes is based on intrinsically disordered regions (IDR), enriched in mainly hydrophobic and basic amino acids (Cingolani *et al.* 1999; Cingolani *et al.* 2002). PTHrP binds directly to importin β through those IDRs (Cingolani *et al.* 1999; Cingolani *et al.* 2002). Localization signals different to those of classic NLSs are categorized as ‘non-classical NLS’.

A second class of linear NLS is the PY-NLS or M9-sequence, first described for hnRNP A1 to be responsible for the binding of transportin 1 (Lee *et al.* 2006). The M9-sequence is also bound by transportin 2 and has the consensus sequence of two regions, an N-terminal hydrophobic or basic cluster, followed by a R/K/H-$X_{2–5}$-P-Y/ϕ motif (where X can be every residue and ϕ=hydrophobic can also be H (histidine), L (leucine) or P (proline)) (Lee *et al.* 2006; Süel *et al.* 2008). Analysis of transportin 1 crystal structures with different PY-NLS-peptides revealed three binding epitopes (referred as epitope 1-3) on transportin 1 (Cansizoglu *et al.* 2007). This three epitopes are defined as binding sites, A and B in the C-terminal arch of transportin 1 (Cansizoglu *et al.* 2007). The first epitope, defined as binding site A, contacts the N-terminal hydrophobic/basic patch. Binding site B contains the second epitope, which binds the ‘R/K/H’-residue in front of the PY-motif and epitope 3, which binds the PY-motif (Cansizoglu *et al.* 2007; Süel *et al.* 2008; Mboukou *et al.* 2021). Studies using untypical PY-NLS revealed that not all 3 epitopes need to be contacted, if the lack of one is compensated by strong interactions to the other epitopes (Soniat and Chook

2016). For instance, TAP (NXF1) binds only to epitope 2 and 3 of transportin 1 or the N-terminal tail of histone H3 resembles a PY-NLS, which lacks the characteristic PY-motif (Imasaki *et al.* 2007; Soniat and Chook 2016). The release of cargoes from transportin 1 in the nucleus is based on conformational changes of transportin 1 upon RanGTP binding. Here, the characteristic H8 loop (present in importin β, transportin 1, transportin 3, CAS and Kap121 (importin 5 yeast homolog) (Wing *et al.* 2022)), which is a long acidic disordered loop, undergoes a conformational change upon RanGTP binding and binds to binding site B (epitope 1) to replace the PY-NLS at this site. An overlap of the H8 loop with binding site A (epitopes 2-3) then leads to the release of the already loosened cargo (Imasaki *et al.* 2007). Moreover, the conformational change prevents reloading of transportin 1 with its import cargo (Chook and Blobel 1999; Imasaki *et al.* 2007). In addition to the well characterized PY-NLS, transportin 1 recognizes another linear NLS, consisting of a RG/RGG (arginine (R)-glycine (G)) rich region (Bourgeois *et al.* 2020). The RG/RGG-NLS binds transportin 1 in regions, which are overlapping with the PY-NLS binding site (Bourgeois *et al.* 2020). These RG/RGG rich motifs are characteristic for RNA-binding proteins, since these regions are additionally involved in RNA binding. This RG/RGG-NLS is observed in FUS (fused in sarcoma) or CIRB (cold-inducible RNA-binding protein) and shown to be important for nuclear import by transportin 1 (Bourgeois *et al.* 2020; Baade *et al.* 2021).

Transportin 3 or transportin-SR import SR (serine-arginine)-rich splicing factors upon recognizing their RS-NLS (Lai *et al.* 2000; Shepard and Hertel 2009). Regions of ~50 residues with >40% RS dipeptides are defined as RS-NLS, usually following a RNA recognition motif (RRM) in these splicing factors (Shepard and Hertel 2009; Wing *et al.* 2022). These RS-NLS often need to be phosphorylated to be recognized and imported by transportin 3 (Lai *et al.* 2000; Jang *et al.* 2019).

In contrast to the above mentioned NLS types, importin 13 binds to folded domains rather than linear motifs of IDRs. Different import-cargoes can bind to different sites on importin 13, which is assumed to be based on the overall substrate structure, because mutants, impaired in the recognition of Ubc9 (import substrate), are still able to import MAGO-Y14 and vice versa (Grünwald and Bono 2011; Grünwald *et al.* 2013). The import-cargo Ubc9 for example binds to the N-terminal arch, as well as RanGTP,

whereas the import-cargoes MAGO-Y14, imported as a heterodimer, binds mainly to the C-terminal portion of importin 13 (Bono *et al.* 2010; Grünwald and Bono 2011). The nuclear release mechanism of cargoes binding to the N-terminal portion of importin 13 is obvious, since they compete with RanGTP for the same binding site, but RanGTP with a much higher affinity (Grünwald *et al.* 2013). The release of cargoes binding like MAGO-Y14 to the C-terminal arch is achieved by conformational changes upon RanGTP binding as seen for other NTRs. Since importin 13 lacks the acidic loop, important for the release of cargoes from transportin 1 and importin β, the mechanism is slightly different (Ström and Weis 2001; Lee *et al.* 2005; Imasaki *et al.* 2007; Grünwald *et al.* 2013). It is shown that RanGTP binding leads to a much tighter packing of importin 13. When bound to RanGTP both ends have a distance of ~1 Å, which prevents rebinding of import substrates, compared to 23.8 Å in unbound cytosolic importin 13 (Grünwald *et al.* 2013). Importin 13 bound to RanGTP then forms a ternary export complex with export-cargoes. Binding of export-cargoes is only weak in the absence of RanGTP (Grünwald *et al.* 2013).

The recognition of cargoes by other import receptors are not fully understood. Some bind not only to linear motifs, but may recognize folded domains, for example importin 4, -5, -7, -8¸ -9 and -11 (reviewed (Wing *et al.* 2022)). The exact rules and mechanisms of binding cargoes are unknown due to a lack of structural studies and a small cargo-spectrum. Only importin 5 is assumed to bind a known type of NLS, the IK (isoleucine (I)-lysine (K))-NLS with a consensus sequence of K-V/I-X-K-$X_{1–2}$-K/H/R (where X is any residue) (Kobayashi and Matsuura 2013). This is based on studies of Kap121, the yeast homolog of importin 5 and the conservation of residues important for the recognition of the IK-NLS (Kobayashi and Matsuura 2013). Importin 7 is known to form either a heterodimer with imp β or to import different, very basic, cargoes like rpL6 and rpL4 (Jäkel *et al.* 2002), the RNA methyltransferase EMG1 (Warda *et al.* 2016) or the histone H1 (Jäkel *et al.* 1999). The formation of the heterodimer is based on the interaction of imp β with the FG-repeat-like regions in the C-terminal tip of imp 7 (Ivic *et al.* 2019). Cargoes of imp β/7 are released upon RanGTP binding and interaction with NPC FG-repeats, which first dissociates imp β, while imp 7 remains bound to the cargo (Jäkel *et al.* 1999; Ivic *et al.* 2019). This is suggested to prevent the protein from aggregation before it reaches its destination (Warda *et al.* 2016; Ivic *et al.* 2019).

All above-mentioned NTRs either bind a linear motif or a folded domain at a time. In contrast to this, the imp β/7 heterodimer bound to histone H1, through a combined motif of the intrinsically disordered histone H1 tail in combination with some parts of its folded globular domain (Ivic *et al.* 2019). Another example for the use of a combined motif is Snurprotein 1 (SPN1) bound to its export receptor CRM1 (chromosome maintenance 1) (Monecke *et al.* 2009). SPN1 functions as an adaptor-protein that binds specifically m_3G-capped spliceosomal snRNPs (small nuclear ribonucleoproteins) in concert with imp β for nuclear import (Huber *et al.* 1998). In the crystal-structure of CRM1 bound to SPN1, SPN1 is recognized through its N-terminal NES and the globular m_3G-cap binding domain, (Monecke *et al.* 2009).

CRM1 binds the only identified NES, consisting of 5 hydrophobic residues within a peptide of up to 15 residues (Fung *et al.* 2017). The sequences of NESs vary strongly in their sequence (Fung *et al.* 2017). The binding of export-cargoes to CRM1 is in stark contrast to the binding of cargoes to other exportins or importins. All NTRs bind their cargoes on the inner concave surface (see above or reviewed in (Wing *et al.* 2022)) but CRM1 binds the NES on its convex, outer surface in a specific groove, but RanGTP at its concave inner surface (Fung *et al.* 2017). Other exportins export either different types of RNA, folded domains in case of exportin 4 and importin 13 or a single cargo like CAS, which exports importin α (Wing *et al.* 2022).

All these linear NLS motifs interact with specific nuclear transport receptors. For the recognition of folded domains, it is not known whether these motifs are more general and bound by several NTRs or if they bind to specific NTRs. Despite some cargoes harbor only one type of NLS, various cargoes interact with multiple NTRs. This redundancy of the transport machinery is reported for histones which bind multiple NTRs. For instance histone H3-H4 binds to importin 4, -5, -7, -9, -β and transportin 1 or histone H2A-H2B interacts with importin α/β, -β, -9 and transportin 1 (reviewed in (Bernardes and Chook 2020)). This is also reported for other cargo-proteins like FUS (fused in sarcoma) (Baade *et al.* 2021), HIV-1 Rev protein (Arnold *et al.* 2006a), c-Fos (Arnold *et al.* 2006b), c-Jun (Waldmann *et al.* 2007) and ribosomal proteins (Jäkel and Görlich 1998). It remains unclear, whether these multiple interactions have any *in vivo* relevance, since most cargoes prefer one NTR, FUS and c-Fos use mainly transportin 1 (Arnold *et al.* 2006b; Baade *et al.* 2021). Binding to multiple NTRs could

serve as a kind of backup system. Alternatively, different NTRs could bind substrates under different cellular conditions to act in a specific cellular context.

1.1.6 Function and cargo specificity of nuclear transport receptors

As already mentioned in section 1.1.1, the hallmark of eukaryotes is the separation of various processes like transcription and translation through compartmentalization. This separation requires a continuous transport of various proteins, depending on cell-cycle stage or as a respond to extracellular stimuli. Therefore, multiple NTRs have evolved in different pathways to regulate a specific cohort of proteins to react to various environmental needs. For some NTRs the specific function is obvious, for example the exportin CAS specifically exports importin α (Kutay *et al.* 1997), NTF2 imports RanGDP (Ribbeck *et al.* 1998), exportin t exports tRNA (Lipowsky *et al.* 1999) and exportin 5 exports miRNA (reviewed in (Wu *et al.* 2018)). In two studies ((Mackmull *et al.* 2017) and (Kimura *et al.* 2017)) a large set of cargoes for several NTRs were identified and the authors tried to define the biological roles of various NTRs based on these sets. Due to the redundancy of NTRs for various cargoes, the allocation of specific biological pathways is not possible. Nevertheless, the authors have been able to link more general roles to specific NTRs, since some specific routes for functionally related proteins are identified (Kimura *et al.* 2017; Mackmull *et al.* 2017).

Recent studies show specific NTRs to be important under certain conditions. A transcriptomic study using mouse embryonic stem cells knocked-out for importin 13 revealed that importin 13 exports the transcription factors SP1 (specificity protein 1) and KLF4 (Krueppel like factor 4), which are important for oxidative stress related genes (Gajewska *et al.* 2021). Another study linked importin 7 to mechano-transduction, showing that the cargo YAP, an important regulator of a mechano-transduction pathway, dominantly binds to importin 7 and outcompetes other cargos under mechanic cues (García-García *et al.* 2022).

1.1.7 Deregulation of nucleocytoplasmic transport is linked to disease

It is not surprising that altering this orchestrated network of reactions and interactions, which is necessary to maintain the cellular homeostasis, is linked to different human

diseases. In general, deregulation of nucleocytoplasmic transport or disruption of NPC structure is linked to neurodegenerative disease, genetic disorders or human malignancies (Kau *et al.* 2004; Dickmanns *et al.* 2015; Ding and Sepehrimanesh 2021). For instance, Nup358 is overexpressed in myeloma and Nup88 in various tumors like endometrial cancer, colorectal and breast cancer (Agudo *et al.* 2004; Felix *et al.* 2009; Schneider *et al.* 2010; Zhao *et al.* 2010; Chow *et al.* 2012). Additionally, Nup98 and Nup214 are associated with leukemia, but the underlining mechanisms remain unclear (Gorello *et al.* 2010; Gough *et al.* 2011). Not only nucleoporins are over-expressed in malignancies, but NTRs as well. The best studied karyopherin's in the context of cancer are CRM1 and importin α and importin β (van der Watt *et al.* 2009; Zheng *et al.* 2010; van der Watt *et al.* 2011). Over-expression leads to mis-localization of many transport cargoes like tumor suppressors, oncogenic proteins or proteins of the DNA damage repair system, which in turn results in abnormal activity of those and in the development of cancer (reviewed in (Teng *et al.* 2006; van der Watt *et al.* 2009; van der Watt *et al.* 2011; Dickmanns *et al.* 2015). In medical research, different drugs have been designed to target NTRs. For instance, LMB (leptomycin B) or SINE (selective inhibitors of nuclear export) specifically inhibit CRM1 mediated nuclear export to prevent the mis-localization of its cargoes (Yashiroda and Yoshida 2003; Zhang *et al.* 2013).

In addition to malignancies, deregulation of nuclear transport is linked to other disorders in humans. Mutations of the NPC proteins ALADIN and Nup358 are found in patients with triple A-syndrome (Allgrove syndrome) and acute necrotizing encephalopathy (ANE), respectively (Huebner *et al.* 2004; Neilson 2010; Sakuma and D'Angelo 2017). Mutations in the NLS binding-site of importin α7 are linked to Lennox-Gastaut syndrome (Paciorkowski *et al.* 2014) and Gle1, a transport factor in mRNA export, is mutated and linked to Lethal congenital contracture syndrome 1 (LCCS1) (Nousiainen *et al.* 2008).

Further, NCT defects are linked to neurotoxicity in neurodegenerative disease like ALS (amyotrophic lateral sclerosis), FTD (frontotemporal dementia), Parkinson or Alzheimer's disease (AD) (reviewed in (Bitetto and Di Fonzo 2020)). Neuronal cells are long-living cells, which do not divide and are therefore more susceptible for defects in NCT. Neurodegenerative diseases are characterized by neuronal protein

aggregates. It is still disputed whether NCT defects cause those neuronal aggregates or if aggregates cause NCT defects, which then promote aggregate formation (Bitetto and Di Fonzo 2020; Hutten and Dormann 2020). For instance, in many cases of FTD, ALS or FTD/ALS, ribonucleoproteins like TDP-43 or FUS are mis-localized and form liquid droplets, which recruit components of the NCT system, resulting in impaired NCT activity (Gopal *et al.* 2017; Chou *et al.* 2018; Ederle *et al.* 2018; Lin *et al.* 2021). Another link between NCT defects and AD is reported for Nup98. A characteristic of AD is the formation of Tau aggregates, which disrupt NPCs. This is triggered by Nup98, which in turn is mis-localized to the cytoplasm (Eftekharzadeh *et al.* 2019). The mis-localization of Nup98 in an AD-mice model can be rescued by dissolving Tau aggregates (Eftekharzadeh *et al.* 2019). As a last example, C9orf72 noncoding hexanucleotide repeats result in toxic dipeptide repeats (DPR), which are linked to the pathology of FTD (DeJesus-Hernandez *et al.* 2011; Jovičić *et al.* 2015). In this context, DPR lead to NCT defects by altering the activity of Nup50, Nup153 and transportins in nuclear import (Freibaum *et al.* 2015) or through binding and mis-localizing RanGAP, an important factor of the RanGTPase system (Zhang *et al.* 2015). In general, the improved understanding of the precisely orchestrated NCT machinery and NPC structure leads to links of NCT deregulation with several human disease. The exact pathology behind NCT defects is an emerging field for researchers and is not fully understood by now.

1.2 Nitric-oxide synthase interacting protein (NOSIP)

Structure and function of NOSIP

The protein nitric oxide synthase interacting protein (NOSIP) a protein of 34 kDa, was originally identified in a yeast-two-hybrid screen as an interaction partner of endothelial nitric oxide synthase (eNOS) (Dedio *et al.* 2001). Furthermore, it interacts with the neuronal nitric oxide synthase (nNOS) (Dreyer *et al.* 2004). Sequence analysis revealed a high similarity to the U-box family of ubiquitin ligases (Friedman *et al.* 2003). The 3D-structure of NOSIP is still unknow but has recently been predicted with high accuracy by the AlphaFold software (Jumper *et al.* 2021; Varadi *et al.* 2022). In the AlphaFold model of NOSIP (from now on referred as NOSIP structure), the predicted secondary structure of the U-box domain is present, except the third beta-sheet

(Figure 4 A). The U-box domain in general is highly similar to the RING-finger domain of many E3-ligases and consists of three β-strands and one α-helix connected by loops, but lacking the characteristic zinc-ion chelating residues, which are replaced by salt bridges and hydrogen bonds to maintain the structure (Aravind and Koonin 2000). As predicted in 2003, the conserved U-box-like domain contains conserved residues important for its function (in NOSIP serin 49 (S49) and proline 186 (P186)) and is atypically split by 104 amino acids behind the Ubox α-helix, which is extended into the linker region (depicted in Figure 4 A, in cyan Ubox-domain, in blue 104 amino acid spacer). Between both halves, the rest of the linker is predicted to be intrinsically disordered (Friedman *et al.* 2003). Despite this atypical structure, the Ubox-domain is functional. NOSIP is an active E3-ubiquitin ligase that mediates the ubiquitination of the erythropoietin receptor (EpoR) or itself (auto-ubiquitination), which is abolished when S49 or P186 are mutated to alanine (Friedman *et al.* 2003). Furthermore, NOSIP is known to monoubiquitinate the catalytic subunit of the protein phosphatase 2A (PP2A) and to interact with the scaffolding- (PR65α) and regulatory-subunit (PR55a) (Hoffmeister *et al.* 2014). The PP2A holoenzyme is a signaling regulator through its phosphatase activity and important during craniofacial development (Latta and Golding 2012). Mono-ubiquitination by NOSIP regulates PP2A activity and a knockout of NOSIP leads to increased PP2A activity, which results in craniofacial malformations and holoprosencephaly (describing the inappropriate separation of the brain-hemispheres) (Hoffmeister *et al.* 2014). Further analysis showed, that NOSIP is involved in early neuronal development. For instance, depletion of NOSIP in *Xenopus* or mice resulted in increased apoptosis and decreased proliferation leading to decreased brain size (Hoffmeister *et al.* 2017). Additionally, it is important in the early development of the eye. The eye-anlagen are formed in the neuronal plate, which is built during early neuronal development (Flach *et al.* 2018). An inhibition of NOSIP causes severe defects of eye formation (Flach *et al.* 2018). Further, a recent study shows that the interaction of NOSIP with nNOS is crucial during neutrophil differentiation (Sadaf *et al.* 2021).

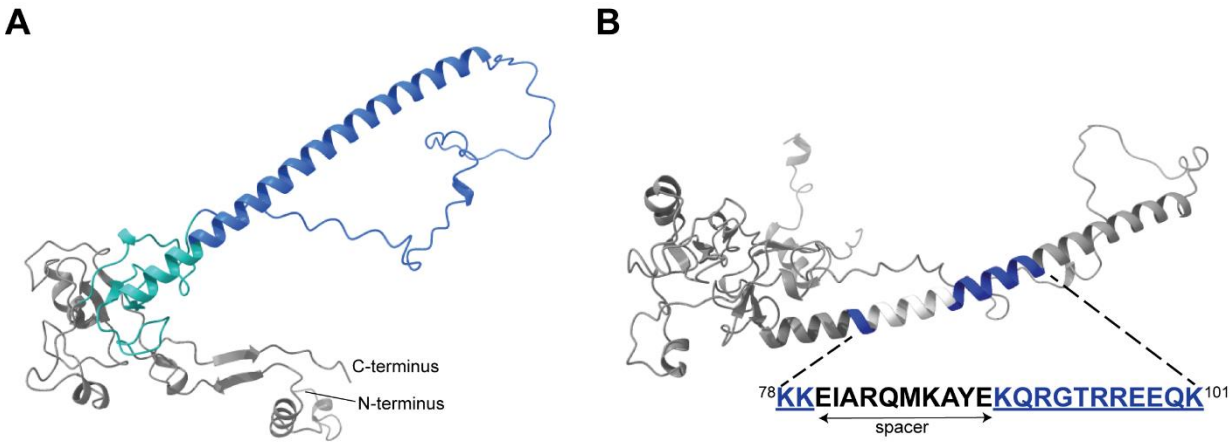

Figure 4: Predicted tertiary structure of NOSIP by the deep learning software AlphaFold. (A) Predicted structure of NOSIP taken from the AlphaFold Databank (Jumper et al. 2021; Varadi et al. 2022). Both halves of the split Ubox-domain are depicted in cyan and the 104 amino acid (aa) long spacer is depicted in blue. (B) The reported bipartite (bp) NLS of NOSIP is marked in blue and white, blue corresponds to the two basic clusters, which are split by a spacer of 10 aa. Depicted below is the sequence of the bp NLS (aa 78-101 defined by (Schleicher et al. 2005)). Images were generated using Chimera X1-3 software.

In view of these crucial roles during neuronal developmental and differentiation, it is not surprising that NOSIP is linked to various human diseases, like mental disorders (Starnawska *et al.* 2017), schizophrenia (Lin *et al.* 2018) or Hirschsprung disease (Tomuschat *et al.* 2017). Further, NOSIP is a significant hit in a genome-wide expression study to identify genes involved in the early traits of osteoporosis and arteriosclerosis (Mishra *et al.* 2021).

Most of these functions or diseases are linked to the association of NOSIP with the nitric oxide pathway (Schleicher *et al.* 2005) and mitogenic signaling (Friedman *et al.* 2003). Nitric oxide (NO) is a very important signal transducer in many cellular processes like neuronal signaling, angiogenesis, vascular tone, platelet aggregation, immune defense and cell proliferation/differentiation (Gow and Ischiropoulos 2001). In the context of cell proliferation, high NO levels block cell-cycle progression at the G1/S transition and G2/M transition or affect mitogenic signaling receptors and their downstream pathway (reviewed in (Villalobo 2006; Napoli *et al.* 2013)).

The best characterized function of NOSIP is the interaction with eNOS and thus its role in the nitric oxide pathway. Nitric oxide synthases are the main source of cellular NO, which need to be tightly regulated. NOSIP is an effector protein and regulates NOS activity (Schleicher *et al.* 2005). The NO production is mediated by NOS catalyzing the reaction of L-arginine, oxygen, and NADPH to the products NO and L-

citruline (Förstermann and Sessa 2012). For sufficient NO production in endothelial cells, eNOS needs to dimerize which is induced upon calmodulin binding, an activator protein of eNOS, under high cellular Ca^{2+}-levels (Fleming and Busse 2003). Under low cellular Ca^{2+}-levels, calmodulin dissociates from eNOS and thus decreases NO production; this is the most rapid mechanism to trigger NO release in cells (Fleming and Busse 2003). Nevertheless, regulation of eNOS activity is controlled through several layers: first, on the transcriptional level, second, through posttranslational modifications and third, by protein-protein interactions. Several effector proteins like caveolin-1, Hsp90, Dynamin-2 , G-protein coupled receptors (GPCR), NOSTRIN and NOSIP regulate eNOS activity (reviewed in (Michel and Vanhoutte 2010; Su 2014)). All these interactions, except with NOSIP, are reported to take place at the plasma membrane (PM) or the Golgi-apparatus, where eNOS is located (Fleming and Busse 2003; Su 2014). The counterpart to calmodulin, the important eNOS activator, is caveolin-1, which suppresses eNOS activity. The binding of calmodulin and caveolin-1 is mutually exclusive, because of overlapping binding-sites and takes place at the PM at high Ca^{2+} levels or at the caveolae (special invaginations of the PM) under low Ca^{2+} levels, respectively (Michel *et al.* 1997b; Michel *et al.* 1997a). Hsp90 (Heat shock protein 90) co-operatively binds with calmodulin to eNOS and additionally exposes phosphorylation sites for the Akt-kinase. Phosphorylation then increases eNOS activity independent of Ca^{2+}-levels (Takahashi and Mendelsohn 2003). Dynamin-2, a Golgi-membrane associated protein, is another activating factor for the eNOS enzyme at the Golgi-apparatus via direct interactions (Su 2014). Next to activating proteins, several inhibitory protein interactions are known. For example, GPCRs like the bradykinin B2 receptor directly bind to eNOS and inhibit its activity (Marrero *et al.* 1999). NOSTRIN, another inhibitory protein, binds co-operatively with caveolin-1 to suppress eNOS activity. Additionally, NOSTRIN is associated with the trafficking of eNOS to intracellular vesicular structures and is suggested to keep eNOS inactive during its transit to other membranous structures (Su 2014). Likewise, NOSIP reduces eNOS activity, but by a different mechanism. The inhibition is not based on directly affecting eNOS activity because in a cell-free system, NOSIP did not alter eNOS activity (Dedio *et al.* 2001). The inhibition of eNOS is based on altering its subcellular localization from the PM to the cytoskeleton (Dedio *et al.* 2001; Dreyer *et al.* 2004; Schleicher *et al.* 2005). As already mentioned, NOSIP interacts also with the neuronal NOS and sequesters away the main NO producer in neurons from its active sites to

attenuate NO production (Dreyer *et al.* 2004). The interaction of NOSIP and eNOS is cell-cycle dependent and involves a re-localization of NOSIP itself (Schleicher *et al.* 2005).

Nuclear transport of NOSIP

The interaction and re-localization of eNOS takes place specifically during the G2-phase of the cell-cycle. Thus it reduces the enzyme activity and basal NO levels in dividing cells (Schleicher *et al.* 2005). This may function as a checkpoint, since higher NO levels are known to inhibit cell-cycle progression (Napoli *et al.* 2013). NOSIP itself is a predominantly nuclear localized protein in cultured cells (König *et al.* 2002; Schleicher *et al.* 2005). During G2-phase of the cell-cycle, when it reduces eNOS activity, NOSIP itself was shown to localize more in the cytoplasm (Schleicher *et al.* 2005). In the same study NOSIP was identified as a nuclear shuttling protein, since the 34 kDa protein NOSIP is below the threshold for passive diffusion through the NPC. Because of the predominant nuclear localization, the nuclear transport of NOSIP has been analyzed. Despite lacking a predictable NLS using the consensus sequences from cNLS or bi-partite NLS (see 1.1.5) with respective software, the authors suggest the region NOSIP$^{78\text{-}101}$ with highly basic character as a non-consensus bi-partite NLS (bpNLS) (Schleicher *et al.* 2005). This bpNLS comprises two basic clusters separated by a 10-residue linker region (Figure 4, white linker and blue basic patches). To validate its functionality, mutational studies have been performed by mutating K (lysine) residues of the first basic cluster to A (alanine) or by deleting either the second basic cluster or the whole NLS. All mutants lead to reduced nuclear accumulation or even exclusion from the nucleus of NOSIP in HeLa cells (Schleicher *et al.* 2005). In line with the identification of this unconventional bpNLS, it was shown that importin α binds to NOSIP in a pulldown assay, using importin α as bait (Schleicher *et al.* 2005). Nuclear export was analyzed using LMB, the potent CRM1 inhibitor, which shows no effect on NOSIP localization (Schleicher *et al.* 2005). Therefore, NOSIP is suggested to be imported through the importin α/β pathway and to be exported in a CRM1 independent manner or only by passive diffusion.

1.3 Lipin 1

Functions of Lipin 1

Lipin 1 (phosphatidate phosphatase LPIN1) is a ~100 kDa protein and belongs to the lipin protein family, consisting of three proteins, Lipin 1, Lipin 2 and Lipin 3 (Péterfy *et al.* 2001). Lipin 1 is expressed in three isoforms α, β and γ (Han and Carman 2010). Lipins are conserved throughout species from yeast, with a single ortholog, to human (Péterfy *et al.* 2001; Han *et al.* 2006) and identified as nuclear proteins being important during lipid metabolism (Péterfy *et al.* 2001). The loss or over-expression of Lipin 1 in a mice model lead to lipodystrophy (loss of body fat) or obesity (excess of body fat) (Péterfy *et al.* 2001; Phan and Reue 2005). These effects of Lipin 1 are based on its function as phosphatidate phosphatase enzyme (Donkor *et al.* 2007). Lipin 1 (as well as Lipin 2 and -3) is the main source of diacylglycerol (DAG) in most cells, since it catalyzes the dephosphorylation of phosphatidic acid (PA) to DAG. DAG is then is further processed to triacylglycerol (TAG), the major energy storage molecule (Ahmadian *et al.* 2007; Donkor *et al.* 2007). Deregulation of TAG storage is linked to human disease like type-2 diabetes, hypertension and arteriosclerosis (Ahmadian *et al.* 2007; Fujiwara *et al.* 2022). Moreover, Lipin 1 is linked to the development of peripheral neuropathy, which is characterized by the demyelination of Schwann cells. The onset of this neuropathy is based on elevated PA levels, which in turn activates the MEK-Erk pathway, leading to the demyelination (Nadra *et al.* 2008). In humans, mutations or deficiency of Lipin 1 cause rhabdomyolysis in early childhood, which is characterized by the fast loss of muscle mass (Michot *et al.* 2010).

In addition to the function as phosphatidate phosphatase, Lipin 1 also functions as a transcriptional co-activator. Lipin 1 activates the fatty acid oxidative metabolism by activation of respective genes through the transcriptional-activation of PPARα (peroxisome proliferator-activated receptor α) (Finck *et al.* 2006). This is regulated through a positive feedback loop. Lipin 1 interacts with its own transcriptional coactivator PGC-1α (PPARγ-coactivator 1α) and PPARα in a co-operative manner to amplify the PGC-1α/PPARα pathway, which regulates fatty acid metabolism (Finck *et al.* 2006). Furthermore, Lipin 1 is a transcriptional coactivator of PPARγ and thereby

amplifies the C/EBPα/PPARγ regulation pathway, which is important during adipogenesis and during adipogenesis maintenance (Koh *et al.* 2008).

Since Lipin 1 acts as a transcriptional coactivator of genes involved in fatty acid oxidation metabolism and is an important enzyme in the lipid synthesis cascade, it is not surprising that Lipin 1 plays a role in cancer (reviewed in (Brohée *et al.* 2021)). In cancer cells, the lipid metabolism is reprogrammed and cells become addicted to fatty acids and cholesterol synthesis or uptake to scope with the lipid amount needed for fastened cell-growth dependent membrane synthesis (Snaebjornsson *et al.* 2020). The product of Lipin 1 is DAG, which is the precursor of several lipid species (Csaki *et al.* 2013). An upregulation of Lipin 1, as seen in various cancer types (reviewed in (Brohée *et al.* 2021)), leads to increased lipid metabolism, which is needed for membrane synthesis (Snaebjornsson *et al.* 2020). This leads to the targeting of Lipin 1 as a potential anti-cancer target (He *et al.* 2017; Fan *et al.* 2018).

Structure and localization of Lipin 1

The different Lipin 1 isoforms, resulting from alternative splicing, are very similar (Han and Carman 2010; Wang *et al.* 2011). It was shown that Lipin 1α and Lipin 1β have different but similar roles, where Lipin 1α functions during the early phase of adipocyte differentiation and Lipin 1β is primarily expressed in mature adipocytes and functions in lipogenesis and lipid storage (Péterfy *et al.* 2005; Chen *et al.* 2015). The third isoform, Lipin 1γ, is mainly expressed in human brains and is assumed to be a specific Lipin 1 form in brain lipid metabolism (Wang *et al.* 2011). Lipin 1β and Lipin 1γ both have an isoform specific insertion compared to Lipin 1α (Péterfy *et al.* 2005; Wang *et al.* 2011). In general, Lipin 1 proteins, as well as the other Lipin-family members, contain two well conserved regions, N-terminal and C-terminal Lipin domains (NLIP, CLIP) (Péterfy *et al.* 2001). The function of the NLIP domain is currently unclear, whereas the CLIP domain contains the two motifs, which are necessary for Lipin's function. The motif 'DXDXT' (haloacid dehalogenase motif) is important for Lipins function as phosphatidate phosphatase (Donkor *et al.* 2009), and the LXXIL motif is important for the function as transcriptional coactivator (Finck *et al.* 2006).

For both functions, as transcriptional coactivator and phosphatidate phosphatase, the subcellular localization is crucial. The role in lipid metabolism is based on its cytoplasmic/ER localization, whereas its activity as transcriptional co-activator requires a nuclear localization of Lipin 1. Originally, Lipin 1 has been described as a nuclear protein (Péterfy *et al.* 2001), but later has been shown to be localized more prominent to the cytoplasm (Péterfy *et al.* 2005; Grimsey *et al.* 2008). As a protein of 100 kDa, Lipin 1 is above the threshold for passive diffusion and therefore needs to be actively imported into the nucleus. Lipins encode a classic NLS (^{153}KKRRKRRRK^{161} in human Lipin 1), which is required for Lipin 1 nuclear localization, since a deletion of the NLS results in a cytoplasmic localization of Lipin 1 (Péterfy *et al.* 2010; Ren *et al.* 2010). Lipin 1 interacts with the 14-3-3 protein via a region (218-260) harboring several 14-3-3 binding motifs (S_pXP). The interaction with 14-3-3 occurs in the cytoplasm upon insulin-induced phosphorylation of Lipin 1, which retains it in the cytoplasm (Péterfy *et al.* 2010). In neuronal cells, the nuclear localization is regulated through its sumoylation status. Sumoylation of Lipin 1 drives its nuclear localization and thereby promotes its transcriptional activity, while a mutation of the sumoylation site leads to cytoplasmic retention of Lipin 1 (Liu and Gerace 2009).

Nuclear export of Lipin 1 seems to be regulated, since it was shown to be LMB sensitive, however no NES is validated (Ren *et al.* 2010). The import could be mediated by importin α/β through the interaction of importin α with the classic NLS, as validated by a GST-pulldown assay using GST-importin α (Ren *et al.* 2010). Recently, a proteomic screen has identified Lipin 1 as a potential importin 13 import-cargo. It was also shown to physically interact with importin 13 *in vitro* (Baade *et al.* 2018). The role of importin 13 in Lipin 1 nuclear transport is currently not known.

1.4 Aim of thesis

Recently, in a proteomic screen for importin 13 import and export cargoes, NOSIP and Lipin 1 were found as potential cargoes of importin 13 (Baade *et al.* 2018). Both cargoes had previously been suggested to be imported by the canonical importin α/β pathway.

The localization of Lipin 1 is important for its dual function as transcriptional coactivator or as phosphatidate phosphatase. The aim of this thesis was to determine the role of importin 13 in the nuclear import of Lipin 1 using different approaches. First, the binding of importin 13 to Lipin 1 was analyzed. Further, inhibitors and interaction studies were used to identify the preferred import pathway, while knock-down experiments were then used to analyze the role of importin 13 in HeLa cells.

NOSIP is a predominantly nuclear protein, but it is known to traffic eNOS to the cytoskeleton, specifically during the G2-phase of the cell-cycle, to inhibit the NO production (Schleicher *et al.* 2005). The import of NOSIP is suggested to be mediated by importin α/β, but the cell-cycle dependent export, which is important for its function in the cytoplasm, remains unknown. The aim of this work was to analyze the nuclear transport of NOSIP in more detail. The interaction of NOSIP with importin 13 and other NTRs was analyzed to understand how NOSIP interacts with different NTRs. The nuclear transport of NOSIP was analyzed in interphase HeLa cells using various transport assays. Additionally, it was examined how the cytoplasmic accumulation of NOSIP, during G2-phase of the cell-cycle, is regulated. Further, the interaction with different NTRs was analyzed and the role of the different NTRs was determined. Moreover, the thesis focused on the identification of regions involved in the interaction with NTRs, since only a bipartite NLS, which binds to importin α, was characterized before (Schleicher *et al.* 2005).

2 Material and Methods

2.1 Material

2.1.1 Technical equipment

Table 1: Technical Equipment

Equipment	Company
Agarose gel running chamber	Home-made, Workshop, UMG
Agarose gel documentation GelSTICK touch	INTAS Science Imaging instruments
Äkta column GSTprep 16/10 FF	GE Healthcare
Äkta column HiLoad 16/60 Superdex 200 pg	GE Healthcare
Äkta column HiLoad 16/60 Superdex 75 pg	GE Healthcare
Äkta column HiLoad 26/60 Superdex 200 pg	GE Healthcare
Äkta column HiLoad 26/60 Superdex 75 pg	GE Healthcare
Äkta column Hisprep 16/10 FF	GE Healthcare
Äkta column HisTrap™HP (5 mL)	GE Healthcare
Äkta column Superdex 200 10/300 GL increase	GE Healthcare
Äkta pure	Amersham Biosciences
Äkta purifier	Amersham Biosciences
Autoclave Sterilizer DX-200	Systec
Biophotometer	Eppendorf
Äkta column Capto HiRes Q 5/50	GE Healthcare
CASY 1, cell counter	Schäfer System
Cell culture hood Herasafe™ KS	Thermo Scientific
Cellculture incubator Herace II™ 150i	Thermo Scientific
Centrifuge 5415R	Eppendorf
Centrifuge 5424	Eppendorf
Allegra X-15R Centrifuge	Beckman Coulter
Confocal microscope LSM 510 meta	Zeiss
Decon FS-100 ultrasonic bath	Decon Laboratories
Documentation system LAS-3000	Fujifilm
Dual Gel Caster for Mini Vertical Units	Hoefer
EmulsiFlex-C3	Avestin
Fluorescence microscope Axioskop 2	Zeiss
FACSCanto II	BD Biosciences
Incubator Heraeus function line	Heraeus
Incubator Shaker INNOVA 4430	New Brunswick Scientific
MBP Trap™ HP (5 mL)	GE Healthcare
Mini Trans-Blot® Cell	Bio-Rad

Table 1 continued

Equipment	Company
Nikon Eclipse Ti2 epifluorescence microscope	Nikon
Odyssey®Sa Infrared Imaging System	LI-COR
SE250 Migthy Small II Mini Vertical Electrophoresis Unit	Hoefer
Spectrophotometer NanoDrop 2000c	ThermoScientific
Thermocycler FlexCycler 2	Analytik Jena AG
Thermomixer comfort	Eppendorf
Thermomixer compact	Eppendorf
Ultracentrifuge Avanti™ J-30I with rotor JA30.50Ti	Backman Coulter
Centrifuge J6-MI with rotor JS4.2	Beckman Coulter
UV sterilizer	Biometra
Mini Trans-Blot® cell	BioRad
Vortexer MS2 Minishaker	IKA
Western blot incubation boxes	LI-COR
Water Bath model 1003	GFL
Olympus CK40 Culture Microscope	Olympus
UV transilluminator	Uvitec

2.1.2 Chemicals, Reagents

Table 2: Table of Chemicals and Reagents

Reagent	Company
2-Propanol (Isopropanol)	AppliChem
Acrylamide 4K Solution (30**%**)	Applichem
Agarose	Fisher Scientific
Adenosine 5’-triphosphate disodium salt hydrate (A3377)	Sigma -Aldrich
Amylose Resin High Flow	New England BioLabs
Bovine Serum Albumin (BSA) (20 mg/mL)	ThermoScientific
BSA, fraction V	AppliChem
Coulter Isoton II diluent	Beckman Coulter
Cyanogen bromide activated Sepharose 4B	Cytiva
Cycloheximide	Sigma-Aldrich
DAPI (D9542)	Sigma-Aldrich
Digitonin	Calbiochem

Table 2 continued

Reagent	Company
Disodium phosphate	Roth
Dimethyl sulfoxide (DMSO)	Roth
dNTP Set, 100 mM Solutions	ThermoScientific
EDTA	Roth
EGTA	Roth
Ethanol 99.9% p.a.	Roth
FBS Superior	Sigma-Aldrich
Formaldehyde solution min. 37%	Millipore
GeneRuler 100bp DNA Ladder	ThermoScientific
GeneRuler 1kb DNA Ladder	ThermoScientific
Gibco® DMEM (1x)	life technologies
Gibco® L-Glutamine	life technologies
Gibco® Opti-MEM® (1x)	life technologies
Gibco® Penicillin Streptomycin (Pen Strep)	life technologies
Glutathione Sepharose 4 Fast Flow	GE Healthcare
Glutathione Sepharose High Performance beads	GE Healthcare
Glycerol	AppliChem
Guanosine 5‘-diphosphate sodium salt (G7127)	Sigma-Aldrich
Guanosine 5‘-triphosphate sodium salt hydrate (51120)	Sigma-Aldrich
Isopropyl β-D-1-thiogalactopyranoside (IPTG)	ThermoScientific
L-Glutathione reduced	AppliChem
Leptomycin B	Enzo life sciences
Lipofectamine 2000®	Life technologies
Magnesium chloride	Roth
Methanol 100**%**	Roth
MOWIOL® 4-88	Calbiochem
Sodium chloride	Roth
Ni-NTA Agarose	Qiagen
NuPAGE® MES SDS Running Buffer (20x)	ThermoScientific
Okadaic acid	Enzo Biolifesciences
Oligonucleotides	Sigma-Aldrich
ortho-Phosphoric acid 85**%** p.A.	AppliChem
PageRuler 1 Kb DNA Ladder	ThermoScientific
PageRuler 100 bp DNA Ladder	ThermoScientific
PageRuler Prestained Protein Ladder	ThermoScientific
PageRuler Unstained Protein Ladder	ThermoScientific

Table 2 continued

Reagent	Company
Poly-L-Lysine Solution 0.1% (w/v)	Sigma-Aldrich
Protein A-Sepharose	Cytiva
S-Protein Agarose	Novagen
SafeView™ Classic (DNA stain)	Applied Biological Materials Inc.
Staurosporine	Sigma Aldrich
TALON® Metal Affinity Resin	Takara Bio Company
Thymidine	Sigma-Aldrich
β-mercaptoethanol	Roth
cOmplete™, Mini, EDTA-free Protease Inhibitor Cocktail	Roche
PhosphoStop Easy pack	Roche
Milk powder	Sigma Aldrich
SDS	Roth
Triton-X-100	Roth

2.1.3 Stock solutions

Table 3: Table of stock solutions

Solution	Composition
1,4-Dithiothreitol (DTT)	1 M in ddH_2O
Ammonium persulfate (APS)	10% APS in H_2O
Ampicillin	100 mg/mL in H_2O
Aprotinin	1 mg/mL in 20 mM HEPES pH 7.4
Adenosine triphosphate (ATP)	100 mM ATP in 100 mM $Mg(OAc)_2$, 20 mM HEPES pH 7.4
Calcium chloride buffer	250 mM $CaCl_2$ in H_2O
Chloramphenicol	34 mg/mL in ethanol
Creatine phosphokinase	2000 U/mL in 50% glycerol, 20 mM HEPES pH7.4
Creatine phosphate	80 mg/mL in H_2O
Guanosine triphosphate (GTP)	100 mM

Table 3 continued

Solution	Composition
Cytosol (ordered from IPRACELL)	14,3 mg/mL; prepared as described in (Kehlenbach *et al.* 1999)
Digitonin	10% (w/v) in DMSO
Isopropyl b-D-1-thiogalactopyranoside (IPTG)	1 M in H_2O
Kanamycin	50 mg/mL in H_2O
Leupeptin/Pepstatin	1 mg/mL each, in DMSO
Phenylmethylsulphonyl fluoride (PMSF)	100 mM in 2-propanol
Wheat germ agglutinin/lectin (WGA)	2 mg/mL in TPB
Okadaic acid	100 mM in DMSO
Staurosporine	100 mM in H_2O
Cycloheximide	25 mg/ml in ethanol
Dexamethasone	100 µM in H_2O
NP-40 Surfact-Amps™ -Detergent	10% (w/v)
Leptomycin B	10 µM in ethanol
2xHBS	50 mM HEPES, 250 mM NaCl, 1.5 mM Na_2HPO_4, pH 6.98

2.1.4 Enzymes

Table 4: Table of used Enzymes

Enzyme	Company
Benzonase	Millipore
Creatine phosphokinase, Rabbit Skeletal Muscle	CALBIOCHEM
DNAseI	AppliChem
Fast alkaline phosphatase (FastAP)	Thermo Scientific
Gibco® Trypsin/EDTA 0.25**%** (1x)	Thermo Scientific
Pfu Ultra II polymerase	Agilent
Phusion High-Fidelity DNA Polymerase	ThermoScientific
PreScision Protease	Self-made
Restriction enzymes	ThermoScientific
T4 DNA ligase	ThermoScientific
TEV Protease	Self-made

2.1.5 Kits

Table 5: Table of used Kits

Kits	Company
Gibson-Assembly master mix	New England biolabs
NucleoBond™ Xtra Midi	Macherey-Nagel
NucleoSpin® Gel and PCR Clean-up	Macherey-Nagel
NucleoSpin® Plasmid	Macherey-Nagel

2.1.6 Consumables

Table 6: Table of used consumables

Consumables	Company
Amersham Protran 0.45 µm NC Nitrocellulose Blotting Membrane	GE Healthcare
Amicon® Ultra Centrifugal Filters, Ultracel®	Milipore
CASY cups with lids	Roche Diagnostics (Fisher Scientific)
Cell culture consumables	Sarstedt
Cell culture plastic ware	Sarstedt, greiner bio-one
Centrifuge Bottle Assembly, Polycarbonate 50 mL	Beckman Coulter
Gravity-flow column	BioRad
Microscope cover slips (12 mm Ø)	Marienfeld
Microscope slides (76x26 mm)	Glaswarenfabrik Karl Hecht GmbH & Co KG
Minisart RC 15, single use syringe filters (0.45 µm, 0.2 µm)	Sartorius Stedim Biotech
Minisart single use filter units (0.45 µm, 0.2 µm)	Sartorius Stedim Biotech
NuPAGE® Novex® 4-12% Bis-Tris Protein Gels (10-, 12-, 15-well)	Thermo fisher scientific
Parafilm “M”	Bemis Company, Inc.
PD-10 columns	GE-Healthcare
pH indicator strips	Machery-Nagel
Reaction tubes (0.5, 1.5, 2, 15, 50 mL)	Sarstedt, greiner bio-one
Spectra/Por® Dialysis Membrane (MWCO 3.5, 6-8 kDa)	Serva serving scientists
Whatman gel blotting paper	GE Healthcare Life Sciences

Table 6 continued

Consumable	Company
Spin-X® UF Concentrator	Corning
Syringes and needles	Braun, servoprax
Whatman Membrane Filters (Mixed cellulose ester) ME25 (0.45 µM)	GE Healthcare Life Sciences
Whatman Membrane Filters (Mixed cellulose ester) NL17 (0.45 µM)	GE Healthcare Life Sciences

2.1.7 Software

Table 7: Table of used Software

Software	Company
Adobe Illustrator CS7	Adobe
Cell Profiler 2.1.1	Broad Institute
Chimera software	https://www.rbvi.ucsf.edu/chimera/
Citavi version 6	Swiss Academic Software
ClusPro webserver	Vajda lab, Boston University
cNLS Mapper webserver	(Kosugi *et al.* 2009)
FACSDiva 6.1.1	BD Biosciences
Fiji (v.2.1.0)	NIH
FlowJo software (v. 10.7.2.)	BD Biosciences
GraphPad Prism 9	GraphPad Software Inc.
Image Reader LAS-3000	Fujifilm
Image Studio, Image Studio Lite 4.0.21	LI-COR
Lasergene 10.1.1 (3)	DNASTAR
LocNES webserver	UT Southwestern Medical Center, Chook Laboratory (Xu *et al.* 2015)
NIS-Elements AR 5.02	Nikon
Rosetta Commons v. 3.4	Rosetta commons
Tm Calculator	Thermo Scientific
Unicorn	GE Healthcare
Xwalk	Dr. A. Kahraman, University Hospital Zurich
Zen System (blue edition)	Carl Zeiss

2.1.8 Buffers, Solutions

Table 8: Table of Buffers and Solutions

Buffer	Composition
2x-YT medium	1.6% (w/v) tryptone, 1% (w/v) yeast extract, 0.5% (w/v) NaCl
2x-YT medium plus	1.6% (w/v) tryptone, 1% (w/v) yeast extract, 0.5% (w/v) NaCl, 30 mM K_2HPO_4, 5% (w/v) glycerol, pH 7.0
Carbonate buffer	0.2 M $NaHCO_3/Na_2CO_3$, pH 8.9
Coomassie destaining solution	10% acetic acid
Coomassie fixation solution	40% ethanol, 10% acetic acid
Coomassie staining solution	10% ethanol, 2% orthophosphoric acid, 5% aluminum sulfate-(14-18)-hydrate, 0.02% CBB-G250
Cross-linking buffer	20 mM Na_2HPO_4/NaH_2PO_4, 150 mM NaCl, 1 mM EDTA and 5% glycerol, pH 8.0
DNA loading buffer (6x)	0.2% bromophenol blue, 0.2% xylene cyanole, 60% glycerol, 60 mM EDTA
GST buffer	50 mM Tris, 300 mM NaCl, 10 mM $Mg(OAc)_2$, 10% (v/v) glycerol, 5 mM β-mercaptoethanol, 1 µg/mL leupeptin pepstatin, 1 µg/mL aprotinin, 0.1 mM PMSF
His-Buffer	50 mM Tris, 300 mM NaCl, 10 mM $Mg(OAc)_2$, 10% (v/v) glycerol, 5 mM β-mercaptoethanol, 1 µg/mL leupeptin pepstatin, 1 µg/mL aprotinin, 0.1 mM PMSF
Laemmli running buffer (10x)	250 mM Tris, 1.92 M glycine, 0.5% SDS
LB medium	1% (w/v) bacto-tryptone, 0.5% (w/v) yeast extract, 1% (w/v) NaCl, pH 7.0
LB-Agar	LB medium with 1.5% (w/v) bacto-agar
Lysis buffer	50 mM Tris, 500 mM NaCl, 10 mM $Mg(OAc)_2$, 5% (v/v) glycerol, 1% (v/v) Triton-X-100, 10 mM β-mercaptoethanol, 1 µg/mL leupeptin, pepstatin, 1 µg/mL aprotinin, 0.1 mM PMSF

Table 8 continued

Buffer	Composition
MBP Buffer	20 mM Tris, 200 mM NaCl, 5% (v/v) glycerol, pH 7.5, 2 mM DTT, 1 µg/mL leupeptin, pepstatin, 1 µg/mL aprotinin, 0.1 mM PMSF
Mowiol mounting medium	13.3% (w/v) Mowiol 4-88, 33.3% (w/v) glycerol, 133 mM Tris-HCl, pH 8.5, optionally: 1 µg/mL DAPI
NaPi buffer	50 mM $NaHPO_4/Na_2PO_4$, pH 8.0, 300 mM NaCl, 5 mM $MgCl_2$, 10% (v/v) glycerol, 10 mM β-mercaptoethanol, 1 µg/mL leupeptin, pepstatin, aprotinin, 0.1 mM PMSF
NOSIP SEC Buffer	20 mM Tris, 150 mM NaCl, 1 mM $MgCl_2$, 1 mM DTT, pH 7.4
PBS (10x)	1.37 M NaCl, 27 mM KCl, 100 mM Na_2HPO_4, 18 mM KH_2PO_4, pH 7.5
PBS-T	1x PBS + 0.1% Tween-20
Resuspension buffer (Res buffer)	50 mM Tris, 500 mM NaCl, 10 mM $Mg(OAc)_2$, 5% (v/v) glycerol, 10 mM β-mercaptoethanol, 1 µg/mL leupeptin, pepstatin, 1 µg/mL aprotinin, 0.1 mM PMSF
SDS-sample buffer (4x)	125 mM Tris pH 6.8, 4% SDS, 0.02% bromophenol blue, 10% glycerol
SEC buffer	50 mM TRIS, 200 mM NaCl, 2 mM DTT, pH 7.4
SOC-medium	10 mM NaCl, 10 mM $MgCl_2$, 10 mM $MgSO_4$, 2.5 mM KCl, 2% (w/v) tryptone, 0.5% (w/v) yeast extract, 0.36% (w/v) glucose, pH 7.0
TAE buffer (50x)	2 M Tris, 0.05 M EDTA, 5.71% acetic acid
TFB-I	100 mM $RbCl_2$, 50 mM $MnCl_2$, 30 mM KAc, 10 mM $CaCl_2$, 15% (v/v) glycerol, 0.5 mM LiCl, pH 5.8
TFB-II	100 mM $RbCl_2$, 50 mM MOPS, 10 mM $CaCl_2$, 15% (v/v) glycerol, pH 7.0
Transport buffer (10x)	200 mM HEPES, 1.1 M KoAc, 20 mM $Mg(OAc)_2$, 10 mM EGTA, pH 7.3

Table 8 continued

Buffer	Composition
Tris buffer	50 mM Tris, 200 mM NaCl, 2 mM β-mercaptoethanol, pH 7.5, 1 µg/mL leupeptin, pepstatin, 1 µg/mL aprotinin, 0.1 mM PMSF
Western blot transfer buffer (10x)	250 mM Tris, 1.93 M glycine, 0.2% SDS
Western blot transfer buffer (1x)	10% 10x Western blot transfer buffer, 20% methanol in ddH_2O

2.1.9 Mammalian Cell lines

Table 9: Table of used Mammalian cell lines

Cell line	Description	Origin
HAP1	human near-haploid cell line derived from the chronic myelogenous leukemia (CML) cell line KBM-7	Horizon Discovery
HeLa P4 (P4 MAGI CCR5+ Cells)	Human adenocarcinoma cell line that expresses CD4; derived from cervix of a 31-year-old woman	NIH AIDS Reagent Program
N2a	Mouse neuroblastoma cell line	D. Doorman (DZNE)
NIH 3T3 cells	Mouse embryonic fibroblasts cell line. Originated from a Swiss NIH embryo.	(Jainchill *et al.* 1969)

2.1.10 Bacterial Strains

Table 10: Table of used Bacterial strains

Bacterial strain	Genotype
BL21(DE3) codon+	F- ompT hsdS(rB- mB-) dcm+ Tetr gal l (DE3) endA Hte [argU proL Camr]
DH5α	F- Φ80lacZΔM15 Δ (lacZYA-argF) U169 recA1 endA1 hsdR17 (rK-,mK+) phoA supE44 λ- thi-1 gyrA96 relA1
JM109	endA1 glnV44 thi-1 relA1 gyrA96 recA1 mcrB+ Δ(lac-proAB) e14- [F' traD36 proAB + lacIq lacZΔM15] hsdR17(rK- mK+)
BL21 DE3	B F^- *ompT gal dcm lon hsdS*$_B$($r_B^-m_B^-$) λ(DE3 [*lacI lacUV5-T7p07 ind1 sam7 nin5*]) [*malB*$^+$]$_{K-12}$(λ^S)
TG1	K-12 *glnV44 thi-1 Δ(lac-proAB) Δ(mcrB-hsdSM)5*($r_K^-m_K^-$) F′ [*traD36 proAB*$^+$ *lacI*^{q} *lacZΔM15*]
SG13009	Nal^s, Str^s, Rif^s, Thi^-, Lac^-, Ara^+, Gal^+, Mtl^-, F^-, $RecA^+$, Uvr^+, Lon^+
BL21(DE3)pLysS	B F^- *ompT gal dcm lon hsdS*$_B$($r_B^-m_B^-$) λ(DE3 [*lacI lacUV5-T7p07 ind1 sam7 nin5*]) [*malB*$^+$]$_{K-12}$(λ^S) pLysS[*T7p20 ori*$_{p15A}$](Cm^R)

2.1.11 Vectors

Table 11: Table of used Vectors

Numb.	Name	Tag	Res.	Application	Origin
52	pcDNA3.1(+)-HA	HA-Tag (C-term.)	Amp	transfection	S.Wälde
87	pQLink-His	His-Tag (C-term.)	Amp	expression	(Scheich *et al.* 2007)
46	pGEX-6P-1	GST-PreSicsion site (C-term.)	Amp	expression	Amersham
82	pGEX-6P-1-MCS2	GST	Amp	expression	I. Baade
#290	pEGFP-C1-GST-MCS	GFP, GST	Kana	transfection	S. Hutten
85	pQLink-GST	GST	Amp	expression	(Scheich *et al.* 2007)
78	pMal-His-MCS-MBP	His (C-term.), MBP (N-term.)	Amp	expression	S. Port

Res: Resistance; Amp: Ampicillin; Kana: Kanamycin

2.1.12 Plasmids

In Table 12, plasmids available in our lab are listed. In Table 13 plasmids that are generated in this work are listed; oligonucleotides used are listed in Table 14.

Table 12: Table of available Plasmids

Number	Name	Origin
23	pRSet-His-Importin α	L. Gerace
26	pET30a-S-His-ImpB	M. Arnold
81	pTYB2-Importinβ (aa1-396)	M. Arnold
82	pTYB2-Importinβ (aa304-876)	M. Arnold
105	pGEX-KG-GST-IBB	M. Arnold
234	pXGmLtn-Rev-GR(aa511-795)-GFP	D. Love
245	pQE32-His-TNPO1	D. Doenecke
246	pGEX-GST-M9	S. Hutten
271	pMal-transportin 1	M. Arnold

Table 12 continued

Number	Name	Origin
275	pMal-transportin (aa 1-517)	M. Arnold
276	pMal-transportin (aa 518-890)	M. Arnold
290	pEGFP-GST-MCS	D. Doenecke
423	pEGFP-Rev$_{47-116}$-GFP$_2$-cNLS	S. Hutten
476	pEF-HA-Importin β	S. Hutten
687	pCS2-FLAG-Imp13	D. Doenecke
687	pCS2plus-FLAG-Imp13	D. Doenecke
813	pCS2plus-FLAG-Imp13 (aa1-410)	D. Doenecke
814	pCS2plus-FLAG-Imp13 (aa1-669)	D. Doenecke
815	pCS2plus-FLAG-Imp13 (aa1-784)	D. Doenecke
816	pCS2plus-FLAG-Imp13 (aa153-963)	D. Doenecke
817	pCS2plus-FLAG-Imp13 (aa153-784)	D. Doenecke
1155	pQE80-His-Importin7	R. Ficner
476	pEF-HA-Importin β	S. Hutten
1511	pQE80-His-Importin 13	D. Doenecke
1513	pCS2plus-FLAG-Importin 13 E436R/D481R	I. Baade
1514	pET23-Ubc9	R. Geiss-Friedländer
1527	pEX-Importin13-GST	I. Baade
1569	pET328-His-zz-tev-Imp13	I. Baade
1684	pEGFP-C1-Bimax2	D. Doorman
1685	Bimax2-RFP	D. Doorman
1686	pEGFP-C1-M9M	D. Doorman
1687	M9M-RFP	D. Doorman
1874	pCS2plus-FLAG-Importin 13 D426R	C. Spillner
1875	pCS2plus-FLAG-Importin 13 K802E/R803E	C. Spillner
1893	pCDNA3-NES-mTag-BFP2-cNLS	M. Blenski
1900	pcDNA3.1(+)-NOSIP-HA	C. Spillner
1910	pEGFP-GST-NOSIP	C. Spillner
1918	pcDNA3.1(+)-Lipin 1-HA	C. Spillner/ I. Baade
1921	pEGFP-GST-Lipin 1	C. Spillner/ I. Baade
1922	pGEX-6P1-GST-Lipin 1	C. Spillner/ I. Baade
1965	pMal-His-NOSIP-MBP	I. Baade
1978	pQE80-His$_{10}$-ZZ-RanQ69L$_{1-180}$	D. Görlich
2013	pQLink-His-NOSIP	C. Spillner
2148	pET21a-CRM1-His-HA	F. Lagadec
2176	pCDNA3-NES-mTag-BFP2-M9	M. Blenski
2219	pQE80-His-Importin7 (aa1-1001)	A. Dickmanns

Table 13: Table of cloned Plasmids

Number	Name	cloning
2162	pEGFP-GST-NOSIP K78A/K79A	Mutagenesis with G2252 and G2253 on plasmid 1910
2185	pQLink-His-NOSIP K78AK79A	Mutagenesis on plasmid 2013 with G2252 & G2253
2213	pGEX-6P-1-GST-PreSc-NOSIP	PCR on plasmid 1900 with G1939 & G2316, digested with EcoRI and XhoI and cloned in vector 46
2233	pEGFP-C1-GR_2-GFP-NOSIP	PCR on plasmid 1900 (G2317 & G2318) digested with BgIII and SalI and cloned in plasmid 649
2238	pcDNA3.1(+)-HA-NOSIP K78AK79A	Mutagenesis with G2252 & G2253 on #1900
2312	pGEX-6P1-GST-Lipin 1_{1-619}	PCR on 1918 with G2456 & G2457 and cloned into vector 82 (generated by G2458 & G2459) by Gibson assembly (cloned by C. Wassong)
2348	pcDNA3.1(+)-HA-NOSIP Y14E S36D	PCR on template with G2550 & G2551 and cloned into vector 52 by Gibson assembly
2349	pcDNA3.1(+)-NOSIP Y14E-HA	PCR on template with G2550 & G2551 and cloned into vector 52 by Gibson assembly
2350	pcDNA3.1(+)-NOSIP S138D-HA	PCR on template with G2550 & G2551 and cloned into vector 52 by Gibson assembly
2351	pcDNA3.1(+)-NOSIP S36D S138D-HA	PCR on template with G2550 & G2551 and cloned into vector 52 by Gibson assembly
2352	pcDNA3.1(+)-NOSIP S36D-HA	PCR on template with G2550 & G2551 and cloned into vector 52 by Gibson assembly
2353	pcDNA3.1(+)-NOSIP Y14E S36D S138D-HA	PCR on template with G2550 & G2551 and cloned into vector 52 by Gibson assembly
2354	pcDNA3.1(+)-NOSIP Y14E S138D-HA	PCR on template with G2550 & G2551 and cloned into vector 52 by Gibson assembly
2357	pQLink-GST-Imp13 (aa1-784)	PCR on plasmid 1511 with G2359 & G2365 and cloned into vector 85 with BamHI and HindIII
2358	pQLink-GST-Imp13 (aa153-784)	PCR on plasmid 1511 with G2366 & G2365 and cloned into vector 85 with BamHI and HindIII

Table 13 continued

Number	Name	cloning
2359	pQLink-GST-Imp13 (aa153-963)	PCR on plasmid 1511 with G2366 & G2360 and cloned into vector 85 with BamHI and HindIII
2386	pEGFP-GST-NOSIP (aa 1-110)	PCR on plasmid 1900 with G2559 & G2560 and cloned into plasmid 290 via HindIII and EcoRI
2387	pEGFP-GST-NOSIP (aa 1-240)	PCR on plasmid 1900 with G2561 & G2562 and cloned into plasmid 290 via HindIII and EcoRI
2388	pEGFP-GST-NOSIP (aa 111-301)	PCR on plasmid 1900 with G2565 & G2566 and cloned into plasmid 290 via HindIII and EcoRI
2389	pEGFP-GST-NOSIP (aa 111-240)	PCR on plasmid 1900 with G2563 & G2564 and cloned into plasmid 290 via HindIII and EcoRI
2391	pEGFP-GST-NOSIP (aa 1-120)	PCR on plasmid 1900 with G2637 & G2642 and cloned into plasmid 290 via XbaI and EcoRI
2392	pEGFP-GST-NOSIP (aa 1-130)	PCR on plasmid 1900 with G2637 & G2641 and cloned into plasmid 290 via XbaI and EcoRI
2393	pEGFP-GST-NOSIP (aa 1-140)	PCR on plasmid 1900 with G2637 & G2640 and cloned into plasmid 290 via XbaI and EcoRI
2394	pEGFP-GST-NOSIP (aa 1-150)	PCR on plasmid 1900 with G2637 & G2639 and cloned into plasmid 290 via XbaI and EcoRI
2395	pEGFP-GST-NOSIP (aa 1-160)	PCR on plasmid 1900 with G2637 & G2638 and cloned into plasmid 290 via XbaI and EcoRI
2396	pEGFP-GST-NOSIP (aa 1-285)	PCR on plasmid 1900 with G2635 & G2636 and cloned into plasmid 290 via HindIII and EcoRI
2397	pMal-His-NOSIP-MBP Y14E	PCR on plasmid 1900 with G2583 & G2584 and cloned with EcoRI & XbaI into vector 78
2398	pMal-His-NOSIP-MBP K78AK79A	PCR on plasmid 1900 with G2583 & G2584 and cloned with EcoRI & XbaI into vector 78

Table 13 continued

Number	Name	cloning
2401	pEGFP-GST-NOSIP (aa 75-102)	PCR on plasmid 1900 with G2609 & G2610 and cloned into plasmid 290 via HindIII and EcoRI
2408	pEGFP-GST-NOSIP Y14E	PCR on plasmid 2349 with G2567 & 2568 and cloned into plasmid 290 using HindIII & EcoRI
2409	pEGFP-GST-NOSIP Y14E S36D S138D	PCR on plasmid 2349 with G2567 & 2568 and cloned into plasmid 290 using HindIII & EcoRI
2410	pEGFP-C1-GR_2-GFP-NOSIP Y14E	PCR on plasmid 2349 with G2317 & G2318 and cloned into plasmid 649 by BgIII and SalI
2411	pEGFP-C1-GR_2-GFP-NOSIP Y14E S36D S138D	PCR on plasmid 2353 with G2317&G2318, digested with BgIII and SalI and cloned in plasmid 649
2445	pEGFP-GST-NOSIP (aa 75-120)	PCR on plasmid 1900 with G2720 & G2721 and cloned into plasmid 290 via HindIII and EcoRI
2446	pEGFP-GST-NOSIP (aa 75-140)	PCR on plasmid 1900 with G2720 & G2722 and cloned into plasmid 290 via HindIII and EcoRI
2447	pEGFP-GST-NOSIP (aa 75-160)	PCR on plasmid 1900 with G2720 & G2723 and cloned into plasmid 290 via HindIII and EcoRI
2448	pEGFP-GST-NOSIP (aa 75-180)	PCR on plasmid 1900 with G2720 & G2724 and cloned into plasmid 290 via HindIII and EcoRI
2449	pEGFP-GST-NOSIP (aa 75-200)	PCR on plasmid 1900 with G2720 & G2725 and cloned into plasmid 290 via HindIII and EcoRI
2464	pEGFP-GST-NOSIP (aa 25-285)	PCR on plasmid 1900 with G2747 & G2636 and cloned into plasmid 290 via HindIII and EcoRI
2465	pEGFP-GST-NOSIP (aa 55-285)	PCR on plasmid 1900 with G2748 & G2636 and cloned into plasmid 290 via HindIII and EcoRI
2466	pEGFP-GST-NOSIP (aa 75-285)	PCR on plasmid 1900 with G2720 & G2636 and cloned into plasmid 290 via HindIII and EcoRI

2.1.13 Oligonucleotides

Table 14: Table of Oligonucleotides used for Cloning

Number	Name	Sequence (5’ to 3’)
G1939	GST-NOSIP_EcoRI_fwd	TTTGAATTCACGCGGCATGGCAAGAAC
G2252	NOSIP_K78A/K79A_fwd	GTACATTCTGCACCAGGCGGCGGAGATTGCCCGGCAG
G2253	NOSIP_K78A/K79A_rev	CTGCCGGGCAATCTCCGCCGCCTGGTGCAGAATGTAC
G2316	GST-NOSIP_XhoI_rev	ACTCGAGTCAGGCCTGCATCACCGC
G2317	GR-GFP-NOSIP_BgIII_fwd	ATAGATCTATGACGCGGCATGGC
G2318	GR-GFP-NOSIP_SaII_rev	TATGTCGACTCAGGCCTGCATCACC
G2359	GST-Imp13_fwd_BamHI	TATAGGATCCATGGAGCGGCGGGAGGA
G2360	GST-Imp13_rev_HindIII	CGCAAGCTTTCAGTAGTCAGCTGTGTAATC
G2365	GST-Imp13 1-784_rev_HindIII	ATAAAGCTTTCAATCCCTGGGCCCTTGCTG
G2366	GST-Imp13 153-963_fwd_BamHI	AGGATCCGAGGACTCACCAGTGGATGGGCA

Table 14 continued

Number	Name	Sequence (5’ to 3’)
G2456	GST-LIPIN1 aa1-619_fwd	CTCCAAAATCGGATTCTCGAATGAATTACGTGGGGCAG
G2457	GST-LIPIN1 aa1-619_rev	GCAGAATTCGAAGCTTGAGCTCAAGGCAGAAGAGGGAG
G2458	V82_GST_LIPIN1-619_fwd	GCTCAAGCTTCGAATTCTG
G2459	V82_GST_LIPIN1-619_rev	TCGAGAATCCGATTTTGG
G2550	NOSIP-HA mutants_fwd_HindIII_GA	CTGGCTAGCGTTTAAACTTAAGCTTATGACGCGGCATGGCAAG
G2551	NOSIP-HA mutants_rev_BamHI_GA	GCTTCGGGCGTCAGCGACGGGATCCAGAAGCTGGGCAGCACTTTG
G2559	GFP-GST-NOSIP 1-110_fwd_HindIII	AAATCGGATTCTCGAGCTCAAGCTTTTACGCGGCATGGCAAGAACTG
G2560	GFP-GST-NOSIP 1-110_rev_EcoRI	CGCGGTACCGTCGACTGCAGAATTCTCAGTCCTGCGAGGCCGC
G2561	GFP-GST-NOSIP 1-240_fwd_HindIII	AAATCGGATTCTCGAGCTCAAGCTTTTATGACGCGGCATGGCAAG
G2562	GFP-GST-NOSIP 1-240_rev_EcoRI	CGCGGTACCGTCGACTGCAGAATTCTCACAGCACAGCGCAGGG
G2563	GFP-GST-NOSIP 111-240_fwd_HindIII	AAATCGGATTCTCGAGCTCAAGCTTTTGTGCGGGGCTTCCTGG
G2564	GFP-GST-NOSIP 111-240_rev_EcoRI	CGCGGTACCGTCGACTGCAGAATTCTCACCGCAGCACAGCGCA
G2565	GFP-GST-NOSIP 111-301_fwd_HindIII	AAATCGGATTCTCGAGCTCAAGCTTTTGTGCGGGGCTTCCTGG
G2566	GFP-GST-NOSIP 111-301_rev_EcoRI	CGCGGTACCGTCGACTGCAGAATTCTCAGGCCTGCATCACCGG
G2567	GFP-GST-NOSIP mutants_fwd	AAATCGGATTCTCGAGCTCAGATGACGCGGCATGGCAAG
G2568	GFP-GST-NOSIP mutants_rev	CGCGGTACCGTCGACTGCAGTCAGGCCTGCATCACCGG
G2583	His-NOSIP -MBP_fwd_EcoRI	GCATCACCATCACCATCACGAATTCATGACGCGGCATGGCAAGAAC
G2584	His-NOSIP -MBP_rev_XbaI	CTTCGATTTTCATGTCGACTCTAGAGGCCTGCATCACCGGCCG
G2609	GFP-GST-NOSIP 75-101_fwd_XhoI	CATCCTCCAAAATCGGATTCTCGAGTTCTGCACCAGAAGAAGG
G2610	GFP-GST-NOSIP 75-101_rev_EcoRI	CGCGGTACCGTCGACTGCAGAATTCTCACTCCTTCTGCTCCTC

Table 14 continued

Number	Name	Sequence (5' to 3')
G2635	GFP-GST-NOSIP 1-285_fwd_HindIII	AAATCGGATTCTCGAGCTCA*AGCTT*TTATGACGCGGCATGGCAAGAACTG
G2636	GFP-GST-NOSIP 1-285_rev_EcoRI	CGCGGTACCGTCGACTGCAG*AATT*CTCAGCCCGCGAAGCCGGT
G2637	GFP-GST-NOSIP 1-X_fwd_EcoRI	ATTCTCGAGCTCAAGCTTCGAATTCTATGACGCGGCATGGCAAG
G2638	GFP-GST-NOSIP 1-160_rev_XbaI	GGCTGATTATGATCAGTTATCTAGACTAGGGCAGCACTTTGTCC
G2639	GFP-GST-NOSIP 1-150_rev XbaI	GGCTGATTATGATCAGTTATCTAGACTAAGGACCCACACTGGG
G2640	GFP-GST-NOSIP 1-140_rev XbaI	GGCTGATTATGATCAGTTAT*CTAGA*CTAATCTGGGCTGGTGCC
G2641	GFP-GST-NOSIP 1-130_rev XbaI	GGCTGATTATGATCAGTTAT*CTAGA*CTATGTGAAAGGGTTGAGGGG
G2642	GFP-GST-NOSIP 1-120_rev_XbaI	GGCTGATTATGATCAGTTATCTAGACTAAGCCGACTCCTTCTCC
G2720	GFP-GST-NOSIP 75-x fwd_HindIII	AAATCGGATTCTCGAGCTCA*AGCTT*TTCTGCACCAGAAGAAGG
G2721	GFP-GST-NOSIP 75-120 rev_EcoRI	CGCGGTACCGTCGACTGCAG*AATT*CCTAAGCCGACTCCTTCTC
G2722	GFP-GST-NOSIP 75-140 rev_ EcoRI	CGCGGTACCGTCGACTGCAG*AATT*CCTAATCTGGGCTGGTGCC
G2723	GFP-GST-NOSIP 75-160 rev_ EcoRI	CGCGGTACCGTCGACTGCAG*AATT*CCTAGGGCAGCACTTTGTC
G2724	GFP-GST-NOSIP 75-180 rev_ EcoRI	CGCGGTACCGTCGACTGCAG*AATT*CCTAGGACGGCTTCTCCAG
G2725	GFP-GST-NOSIP 75-200 rev_ EcoRI	CGCGGTACCGTCGACTGCAG*AATT*CCTACACGGGCGTCAGGTC
G2747	GFP-GST-NOSIP 25-x fwd_HindIII	AAATCGGATTCTCGAGCTCAAGCTTTTGCCTCGGGCTATGGGACC
G2748	GFP-GST-NOSIP 55-x fwd_HindIII	AAATCGGATTCTCGAGCTCAAGCTTTTGATCCTGTTGTCACCCCAGATGGC

2.1.14 siRNAs

Small interfering RNA (siRNAs) were ordered as lyophilized powder, this powder was dissolved in RNAse-free water to a final concentration of 100 µM. Dissolved siRNAs were stored at -80 °C for long-term storage and for short-term at -20 °C as 20 µM working aliquot.

Table 15: Table of used siRNAs

Name	Sequence (5'-3')	Target gene	Company
importin β siRNA 1	ACAGUGCCAAGGAUUGU UA	Importin β	Eurofins genomics
importin β siRNA 2	CUGGAAUCGUCCAGGGA UUAA	Importin β	Sigma-Aldrich
Importin 13 siRNA 1	AACAAUAUCAGGAUGAUCCCT	Importin 13	Ambion
NOSIP siRNA	AAGGAGUCGGCUAUCGUGAG C/ AAGGACUUCGACUGCUGUUG U	NOSIP	Thermo Fisher Scientific
non-targeting siRNA (siNT)	UGGUUUACAUGUCGACU AA	Scrambled sequence	Dharmacon, ON-TARGET plus non-targeting siRNA
Transportin 1 siRNA	siRNA pool	transportin 1	Santa Cruz (sc-35737)

2.1.15 Antibodies

Table 16: Table of primary Antibodies

Number	Name	Species	Origin	IF Dilution	WB Dilution
Ab004	α-CRM1	goat	Self-made	1:1000	1:1000
Ab013	α-FLAG (M2)	mouse	Sigma	1:3000	1:1000
Ab024	α-Imp 9	rabbit	Abcam	-	1:1000
Ab029	α-Imp 13	rabbit	Proteintech	1:200	1:500-1:1000
Ab080	α-GAPDH	rabbit	ProteinTech	-	1:2000
Ab081	α-Tubulin	rabbit	ProteinTech	-	1:2000
Ab140	α-His	mouse	Qiagen	-	1:1000
Ab186	α-HA	mouse	Convance	1:1000	1:1000
Ab197	α-Imp α	mouse	Millipore	-	1:500
Ab198	α-TNPO 1	mouse	Millipore	1:500	1:1000
Ab208b	α-Imp β	rabbit	Self-made	1:600	1:1000
Ab214	α-MBP	Mouse	NEB	1:500	1:1000
Ab228	α-Imp 13	Rabbit	Self-made	1:300	1:1000
Ab246	α-Imp 11	rabbit	Invitrogen	-	1:1000
AB342	α-NOSIP	rabbit	Self-made	Unspecific	1:300
Ab411	α -NOSIP	rabbit	Sigma	1:200	1:500
Ab413	α-GST	rabbit	Sigma	1:500	1:1000
Ab430	α-Imp7	rabbit	Invitrogen	1:300	1:1000
Ab424	α-Lipin1	rabbit	Cell signaling	1:100	-

IF: immunofluorescence; WB: immunoblotting

Table 17:Table of secondary Antibodies

Name	Species	Origin	Application	Dilution
α-mouse 680	donkey	LI-COR	WB	1:10.000
α-mouse 800	donkey	LI-COR	WB	1:10.000
α-rabbit 680	donkey	LI-COR	WB	1:10.000
α-rabbit 800	donkey	LI-COR	WB	1:10.000
α-mouse 680 IgG2a-specific	donkey	LI-COR	WB	1:10.000
α-mouse Alexa Fluor® 488	donkey	Molecular Probes	IF	1:1000
α-mouse Alexa Fluor® 594	donkey	Molecular Probes	IF	1:1000
α-mouse Alexa Fluor® 647	donkey	Molecular Probes	IF	1:1000
α-rabbit Alexa Fluor® 488	donkey	Molecular Probes	IF	1:1000
α-rabbit Alexa Fluor® 594	donkey	Molecular Probes	IF	1:1000
α-rabbit Alexa Fluor® 647	donkey	Molecular Probes	IF	1:1000

2.2 Molecular Biology Methods

2.2.1 Chemical competent cells with rubidium chloride

To prepare chemically competent cells for heat-shock transformation, an aliquot of the respective *Escherichia coli (E. coli)* strains was plated onto a LB-agar plate without antibiotics and grown over-night at 37 °C. The next day, a single colony was picked to inoculate a 5 mL over-night broth-culture. 200 mL of broth-culture were inoculated with 2 mL of over-night culture and grown at 37 °C and 150 rpm until an optical density at 600 nm (OD_{600}) of 0.4 – 0.5 is reached. The culture was then incubated on ice for 10 min before harvesting in a pre-cooled centrifuge at 4000 x g for 10 min and 4 °C. The resulting bacterial cell pellet was resuspended in 200 mL ice-cold TFB-I buffer followed by an incubation for two hours on ice. Afterwards, the cell-suspension was centrifuged at 4000 x g and 4 °C for 10 min. The supernatant was discarded, and the pellet was resuspended in 8 mL ice-cold TFB-II. The resulting cell-suspension was separated into 100 µL aliquots and shock-frozen in liquid-nitrogen. Aliquots were stored at -80 °C for further usage.

2.2.2 Agarose gel electrophoresis

Agarose gel electrophoresis is a method used for separating DNA-fragments according to their size in an agarose gel. Depending on the DNA-fragment size, 0.5 – 2% agarose was dissolved in 1x TAE buffer in a microwave with shaking in between. The dissolved agarose solution was allowed to cool down before adding Safeview™ classic DNA stain (1:15000). After the gel was solidified, DNA samples were mixed with 6x DNA loading dye to a final concentration of 1x and loaded to the agarose gel. Additionally, a DNA molecular weight marker was loaded (GeneRuler 1 kb DNA Ladder, Thermo Fisher Scientific). The gel was run at 120 V for 45 - 60 min to separate DNA-fragments. These separated DNA-fragments were then analyzed in a GelSTICK 'touch' system and bands of interest were cut on an UV transillumination desk and purified as described in 2.2.3.

2.2.3 Purification of DNA fragments from an agarose gel

To extract DNA from an agarose gel, the protocol "DNA extraction from agarose gels" from the NucleoSpin® Gel and PCR Clean-up kit were used according to the manufacturer's instructions. To elute the DNA, 20-30 µL elution buffer was used and the concentration was determined by Nanodrop.

2.2.4 Polymerase Chain Reaction (PCR)

PCR was used to amplify DNA-fragments of interest. For all PCRs Phusion™ High-Fidelity DNA Polymerase (Thermo Scientific) was used according to the manufacturer's protocol. A 50 µL PCR-reaction contained 10 µL 10x HF Phusion Buffer, 20 ng template DNA, 200 µM dNTP's, 5 µM of each primer (Table 14: Table of Oligonucleotides used for Cloning and 0.02 U/µL Phusion™ High-Fidelity DNA Polymerase. PCR reactions were performed with an initial denaturation at 98 °C for 30 seconds, followed by 30-35 amplification cycles. Each cycle started with a denaturation step at 98 °C for 10 seconds, followed by an annealing step with primer dependent temperature (primer melting temperature -2 °C) for 30 seconds and an extension step for 15-30 s/kb at 72 °C. The annealing temperature of all primers were calculated using the 'Tm calculator' from Thermo scientific (Thermo scientific - Tm calculator). The 30-35 amplification cycles were followed by a final extension step for

10 min at 72 °C. Agarose-gel electrophoresis (2.2.2) was used to analyze PCR products and bands of interest were cut and purified as described in 2.2.3.

2.2.5 Site directed mutagenesis

Site directed mutagenesis was used to introduce specific mutations into a DNA-sequence. For mutagenesis, a 50 µL reaction mix was used containing 2.5 U Pfu Ultra HF Polymerase (Agilent Technologies), 200 µM dNTP's, forward and reverse primer each 0.2 µM, 100 ng template DNA and 5 µL 10x Pfu Ultra buffer. The PCR program started with an initial denaturation step at 98 °C for 30 seconds, followed by 18-20 PCR cycles. Each PCR cycle started with a denaturation step for 30 seconds at 98 °C, followed by an annealing step for 1 min/kb with a primer melting temperature minus 5 °C and an extension step for 15 min at 68 °C. The program ends with a final extension step for 15 min at 68 °C. To digest the template DNA, 1 µL DpnI (10 U/µL) was added for one hour at 37 °C. The mutated plasmid was then transformed into chemically competent DH5α cells (2.2.9) and plated onto a LB-agar plate with respective antibiotics and incubated over-night at 37 °C. To check for successful mutagenesis, single colonies were picked and used to inoculate 5 mL LB-cultures and grown over-night at 37 °C. Plasmid DNA of these over-night cultures were purified (2.2.10) and send for sequencing (2.2.11).

For some mutations, gene fragments with respective mutations were ordered by BioCat GmbH. These gene fragments were amplified by PCR (2.2.4) and ligated into pcDNA3.1(+)-HA using the Gibson assembly method. The List of ordered synthetized gene fragments can be found in 0.

2.2.6 Digestion of DNA with restriction enzymes

For the ligation of DNA-fragments of interest into a plasmid both needed to be digested with the same restriction enzymes. In case of the Gibson assembly method, only the vector was digested. The digestion mix contains either 3 µg plasmid DNA or 25 µL PCR-product, 1.5 µL of each restriction enzymes (10 U/µL) and 1x restriction enzyme buffer (10x), resulting in a total volume of 30 to 50 µL. Digestion was performed at 37 °C for 1 h using standard enzymes or 20 min using fast-digest enzymes. Recommended molar ratios between restriction enzymes and buffers were used

according to the DoubleDigest Calculator (Thermo scientific - Double digest calculator).

2.2.7 Test digestion of cloned constructs

A test analysis was performed to analyze cloning success. Therefore, plasmid DNA from small-scale DNA purification was used and digested with restriction enzymes used for cloning. The digestion mixture containing 8.6 µL small-scale purification DNA, 1 µL of respective buffer and 0.2 µL of each restriction enzyme was incubated at 37 °C for 1 hour. Digested DNA was then separated by agarose-gel electrophoresis (2.2.2) and analyzed on an UV transillumination desk. Clones containing the DNA-fragment of interest were send for sequencing (2.2.11).

2.2.8 Ligation of restricted DNA fragments

To ligate restricted DNA-fragments (insert) with restricted vectors, T4 DNA ligase (Thermo Scientific) was used. Therefore, 80 ng of the vector were ligated with the DNA-fragment in a molar ratio of 3:1 (DNA-fragment to vector), the amount of insert was calculated using the formula below. In a total volume of 10 µL ligation mix, the DNA-fragments and the vector were incubated with 1 U of T4 DNA ligase in T4 DNA ligase buffer at room temperature for one hour, followed by transformation in *Escherichia coli* (*E. coli*) strain DH5α (Section 2.2.9).

$$\frac{ng\ of\ vector * kb\ of\ insert}{kb\ of\ vector} * \left(molar\ ratio \frac{insert\ 3}{vector\ 1}\right) = ng\ of\ insert$$

When using the Gibson assembly method, a total of 0.02 – 0.5 pmol of DNA-fragments (insert and vector) were used. To calculate the amount of pmols used for each DNA-fragment, the following formula was used: pmol= (weight in ng) x 1000 / (base pairs x 650 Da). As for conventional cloning, 80 ng of vector was used and a 3-fold molar excess of insert, the amount of insert to use were calculated using the above formula. Respective amounts of DNA-fragments were combined, filled up to 10 µL with ddH_2O and 10 µL of GibsonAssembly master mix (2x) was added. Ligation mix was incubated at 50 °C for 20-60 min, followed by transformation into DH5α (2.2.9)

2.2.9 Transformation of plasmid DNA into bacterial strains

For the transformation of plasmids into *E. coli* strains, chemical competent cells were thawed on ice. The ligation-mix or 1 µg of plasmid DNA was added to 50 µL chemical competent cells and incubated on ice for 20 min. To transform the plasmid DNA into the *E. coli* cells, a heat-shock at 42 °C for 90 seconds was performed, followed by a two min incubation step on ice. After that, 300 µL pre-warmed SOC-medium was added and the cells were incubated for one hour at 37 °C under permanent shaking (800 rpm) in a thermomixer. This transformation mix was then spread on to a LB agar-plate with respective antibiotics, according to the plasmid's resistance, and incubated over-night at 37 °C.

2.2.10 Purification of plasmid DNA

Small-scale plasmid purification

For small-scale purification of plasmid DNA, the kit NucleoSpin® Plasmid was used with the protocol 'Isolation of high-copy plasmid DNA from *E. coli*'. 5 mL LB culture, supplemented with respective antibiotics, was inoculated with a single-colony of a LB-agar plate from freshly transformed *E. coli* and incubated over-night at 37 °C and 150 rpm. The plasmid purification was done according to the manufacturer's instructions and bound plasmid DNA was eluted with 30 µL of 70 °C hot sterile desalted water. This plasmid DNA was sent for sequencing and used for restriction analysis.

Large-scale plasmid purification

For large-scale purification of plasmid DNA, the protocols 'high-copy plasmid DNA' or 'low-copy plasmid DNA' from the kit NucleoBond™ Xtra Midi were used. According to this protocols, 200 mL LB-culture, supplemented with antibiotics, was inoculated with a single-colony of a LB-agar plate from freshly transformed *E. coli*. The culture was grown over-night at 37 °C and 150 rpm. Plasmid purification was done afterwards, according to the manufacturer's instructions until the elution step. Dried plasmid DNA was resuspended in 100 µL sterile desalted water and concentration of DNA was determined by Nanodrop and adjusted to 1 µg/µL.

2.2.11 DNA sequencing

The isolated DNA was sent for sequencing to the company Eurofins Genomics. Sequencing primers were selected from standard primer list.

2.3 Biochemical Methods

2.3.1 SDS-PAGE

SDS-Polyacrylamide gel electrophoresis was used to separate proteins according to their size. Acrylamide percentage (10 – 15%) of the gel was chosen depending on the size of the protein of interest. 4x SDS-sample buffer was added to the protein samples to a final concentration of 2x SDS-sample buffer. Samples were then boiled at 95 °C for 5 – 10 min and loaded on to the SDS-gel. Additionally, a protein ladder (PageRuler Unstained or PageRuler PreStained) was loaded, comprising of proteins of known size. SDS-gels were run in 1x Laemmli running buffer using SE250 Migthy Small II Mini Vertical Electrophoresis Units (Hoefer) with 25 mA per gel for 60 to 70 min. The gel was further used for Western blot analysis (2.3.3) or protein bands were visualized by Coomassie staining (2.3.2).

2.3.2 Coomassie staining of SDS-Gels

To visualize the SDS-gels, they were washed once with water and fixed with Coomassie fixation solution for 15 – 30 min, followed by several washing steps with water to remove residual Coomassie fixation solution. To stain the gel, Coomassie staining solution was used for several h to over-night. Destaining of the gel was done in desalted water or in Coomassie destaining solution until the background was clear. The LAS-3000 documentation System (Fujifilm) was used to digitalize the gels.

2.3.3 Western blot analysis

Western blot analysis was used to detect the protein of interest with specific antibodies. Therefore, the SDS-gel was transferred onto a nitrocellulose blotting membrane (Amersham Protran 0.45 µM NC Nitrocellulose Blotting Membrane, GE Healthcare) in a blotting chamber (Mini Trans Blot® Cell, Bio-Rad) for wet Western blot. For the transfer, Western blot transfer buffer was used, and the transfer was performed at 100 V for 90 min. Optionally, the successful transfer was tested by

Ponceau-S staining, for which the membrane was incubated for 1-2 min in Ponceau-S. Afterwards, the membrane was destained in 0.1% acetic acid and documented by the LAS-3000 documentation system. For further processing, the membrane was completely destained with 1x TBS-T. For the following immuno-detection of proteins, the membrane was blocked in 1x TBS-T with 1% BSA or 4% milk (w/v) for one hour at RT. Blocking of the membrane was followed by an incubation with the primary antibody (Table 16), diluted in blocking solution, over-night at 4 °C. The next day, the membrane was washed three times for 15 min with 1x TBS-T at RT, followed by an incubation with the secondary antibody (diluted 1:10.000 in 1x TBS-T with 4% milk (w/v)) for one hour at RT. Secondary antibodies were coupled to an 800 nm or 680 nm fluorophore. Excess of secondary antibody was removed by washing three times for 15 min with 1x TBS-T. Western blots were visualized by detecting fluorescence signal with the Odyssey®Sa Infrared Imaging System (LI-COR Biosciences).

2.3.4 Protein purification

His-NOSIP

0.5 µg of pQLink-His-NOSIP (or K78AK79A mutant) plasmid was transformed into *E. coli* strain JM109 using the heat shock protocol (2.2.9) and plated on a LB-agar^{ampicillin} plate. The next day, several colonies were picked and a LB medium pre-culture (10 mL/liter of larg-scale culture), supplemented with ampicillin, was incubated over-night at 37 °C and 150 rpm. 10 mL of pre-culture was used to inoculate 1 L LB-medium in a ratio of 1:100 and the cells were grown to an optical density at 600 nm (OD_{600}) of 0.7. Protein expression was then induced with 0.5 mM IPTG for 18 h at 18 °C. Bacterial cells were harvested at 4200 rpm for 20 min at 4 °C, pellets were resuspended in 1x PBS and spun as before to remove medium residuals. Bacterial pellets were resuspended in lysis buffer in the 3-fold volume of the bacterial pellet and disrupted using the EmulsiFlex-C3 system by 4-5 cycles. Lysates were cleared by ultra-centrifugation at 30.000 x g using JLA 30.50 rotor in an Avanti™ J-30I centrifuge, the resulting protein containing supernatant was loaded onto Ni-NTA-Agarose beads and incubated for 1 hour at 4 °C under gentle agitation. Afterwards, unbound protein was removed by centrifugation at 800 x g and 4 °C for 5 min and bound protein was washed with Resuspension buffer (Res buffer) for three times (twice with 10 mM imidazole and

once with 20 mM imidazole). One washing step comprises of a 5 min centrifugation step at 800 x g and 4 °C, followed by a 5 min incubation step at 4 °C under gentle agitation. To elute bound protein, Ni-beads were transferred to a gravity-flow column and eluted using Res buffer, supplemented with 300 mM imidazole. The eluate was concentrated to <5 mL and filtered through a Minisart RC 15 single use syringe filter prior to size exclusion chromatography (SEC) using a Superdex 75 HiLoad 26/60 prep-grade (GE Healthcare) column and NOSIP SEC buffer. SEC fractions were analyzed using SDS-PAGE followed by Coomassie staining (2.3.1;2.3.2). Fractions containing His-NOSIP were pooled and concentrated using Spin-X-UF concentrator (MWCO (molecular weight cut-off) 10 K). Concentration was determined as described in 2.3.5 and His-NOSIP was aliquoted, shock frozen in liquid nitrogen and stored at -80 °C until further usage.

GST-PreSc-NOSIP

For expression and purification of pGEX-6P-1-GST-NOSIP, the respective plasmid was transformed into *E. coli* JM109 and plated on a LB-agar^{ampicillin} plate. Grown colonies were used to inoculate LB-medium starter culture over-night at 37 °C and 150 rpm. LB culture was inoculated 1:100 with starter culture and grown to an OD_{600} of 0.7. Protein expression was induced with 0.5 mM IPTG for 4 h at 30 °C and bacterial cells were collected by spinning at 4200 rpm in an Avanti J6-MI Centrifuge (Rotor: JS 4.2). Bacterial pellets were resuspended in NaPi buffer, supplemented with 1% (v/v) Triton-X-100 and lysed running 5 cycles using an EmulsiFlex-C3 system. Lysed cell suspension was cleared by ultra-centrifugation (Avanti™ J-30I, rotor JA 30.50Ti) for 30 min at 4 °C and 30.000 x g. The cleared lysate was incubated with GST-Sepharose 4 FastFlow for 2 h at 4 °C under gentle agitation, followed by a centrifugation step at 800 x g to collect the beads and remove the unbound proteins in the supernatant. Afterwards, beads with bound GST-NOSIP were washed three times, with NaPi buffer, followed by a high-salt wash with NaPi buffer containing additional 500 mM NaCl and afterwards again NaPi buffer. Each washing step started with a 5 min incubation at 4 °C under gentle agitation, followed by centrifugation for 5 min at 4 °C and 800 x g. Beads were then transferred to gravity-flow columns and eluted using NaPi buffer with 20 mM gluthathione. Eluted GST-protein was either concentrated using Spin-X-UF concentrator and subjected to SEC for further purification or cleaved using GST-

PreScission protease. For SEC, concentrated protein was filtered through Minisart RC 15 single use syringe filter and applied to a Superdex 200 HiLoad 26/600 prep-grade column equilibrated in 20 mM Tris, 100 mM NaCl, 1 mM DTT, pH 7.4. Fractions containing GST-NOSIP were identified by SDS-PAGE (2.3.1) and Coomassie staining (2.3.2) and concentrated using Spin-X UF concentrators (MWCO 30 K). Protein concentration was determined as described in 2.3.5 and the protein was aliquoted for storage at -80 °C. In case of using GST-PreScission protease to remove the GST-tag and obtain untagged NOSIP, eluate from GST-beads was incubated with GST-PreScission protease (1 mg/50 mg GST-protein) for 16 h at 4 °C under gentle agitation. Cleaved NOSIP and free GST have a similar size, to separate both proteins a Superdex 75 HiLoad 16/600 prep-grade column coupled to a GSTprep 16/10 FF column was used. The GSTprep column binds the free GST, whereas the NOSIP protein is in the flow-through. Fractions containing NOSIP were analyzed, concentrated and stored as described for GST-NOSIP.

His-NOSIP-MBP

Plasmids of His-NOSIP-MBP (or respective NOSIP fragments) were transformed into *E. coli* JM109 as described in 2.2.9. The next day, several colonies were picked and used to inoculate a LB starter culture which was incubated over-night at 37 °C and 150 rpm. Starter culture was used in a ratio of 1:100 to inoculate 2xYT expression medium. Cultures were grown to an OD_{600} of 0.7 and induced with 0.5 mM IPTG for 18 h at 16 °C and 90 rpm. Cells were harvested at 4200 rpm for 30 min at 4 °C, pellets were washed once with 1x PBS and afterwards resuspended and lysed in Res buffer, running 4 cycles using an EmulsiFlex-C3 system. Lysates were cleared by ultra-centrifugation at 30.000 x g at 4 °C for 30 min and then incubated with amylose resin for 2 h at 4 °C. Amylose resin was washed three times, as described above, using Res buffer (the 2nd step was a high-salt wash, using Res buffer supplemented with 500 mM NaCl) and eluted with Res buffer containing 20 mM maltose. His-NOSIP-MBP eluate was then incubated with Ni-NTA-Agarose for 1 h at 4 °C under gentle agitation, followed by three washing steps with Res buffer (supplemented with 10-, 10- and 20-mM imidazole). Bound His-NOSIP-MBP was eluted using Res buffer with 300 mM imidazole and was concentrated to <1.5 mL. To remove the eluent and exchange to a new buffer (50 mM Tris, 300 mM NaCl, 10 mM $Mg(OAc)_2$, 5% (v/v) glycerol, 5 mM β-

mercaptoethanol, pH 7.4), protein was concentrated three times to 1 mL and fill up to 15 mL with new buffer using Spin-X-UF concentrator (MWCO 30 K). Concentrated protein was aliquoted, shock frozen in liquid nitrogen and stored at -80 °C until further usage. Purification success was analyzed by SDS-PAGE (2.3.1) and Coomassie staining (2.3.2), while protein concentration was determined as described in 2.3.5.

His-Importin-13

A plasmid coding for His-Importin-13 was transformed into *E. coli* JM109 cells and plated on a LB-agar^{ampicillin} plate. Several colonies were used for inoculation of the LB starter culture which were incubated over-night at 37 °C and 150 rpm. 2xYT plus medium large-scale cultures were inoculated 1:100 with starter culture, grown to an OD_{600} of 1-1.5, diluted 1:1 with ice-cold fresh 2xYT plus medium. Cultures were cooled down to 16 °C, prior to the induction with 0.5 mM IPTG for 18 h at 16 °C and 90 rpm. Cells were harvested and washed once with 1x PBS as described above, followed by resuspension of the pellets in Res buffer and lysing using an EmulsiFlex-C3 system. Lysates were cleared by ultra-centrifugation at 30.000 x g, 30 min and 4 °C and then incubated with Ni-NTA-agarose beads for 1 h at 4 °C. Ni-Beads were washed three times as described above using Res Buffer and eluted using Res buffer with 300 mM imidazole. His-Imp13 eluate was filtered through Minisart RC 15 single use syringe filter and applied in 5 mL batches to SEC using a Superdex 200 HiLoad 26/60 prep-grade column with SEC buffer. Afterwards, fractions containing His-Imp13 were identified as described for His-NOSIP, concentrated in a Spin-X-UF concentrator (MWCO 50 K), aliquoted and stored at -80 °C.

His-Importin 7, His-Importin β and His-transportin 1

His-Importin 7 and His-transportin 1 were transformed into *E. coli* JM109 and His-Importin β into BL21(DE3) codon+ and plated on LB-agar plates with respective antibiotics. Several colonies were used to inoculate a LB starter culture. The next day starter culture was used to inoculate large-scale cultures in a ratio of 1:100. His-Importin β was grown in LB medium to an OD_{600} of 0.8 and protein expression was induced with 1 mM IPTG for 4 h at 26 °C and 90 rpm. His-transportin was cultured in LB medium to an OD_{600} of 0.8 and induced with 0.5 mM IPTG at 25 °C for 16 h and 90 rpm. His-Importin 7 was grown in 2xYT plus medium to an OD_{600} of 0.8 and induced

with 0.5 mM IPTG at 16 °C for 16 h at 90 rpm. Bacterial cells were harvested as described for His-NOSIP, cell pellets were directly used for purification or flash frozen in liquid nitrogen and stored at -80 °C. His buffer was used for His-transportin 1 and His-Importin β and Res buffer for His-Importin-7 unless otherwise indicated. Bacterial pellets were resuspended in respective buffer with the three-fold volume of the pellet and lysed using the EmulsiFlex C3. Cell lysates were cleared by ultra-centrifugation at 30.000 x g and 4 °C for 30 min. Cleared lysates were added to equilibrated Ni-NTA-agarose beads and incubated for 1 h at 4 °C under gentle agitation and unbound proteins were removed by centrifugation at 800 x g at 4 °C for 5 min. Ni-Beads were washed three times using the respective buffer with increasing imidazole concentrations (10-, 10- and 20-mM imidazole). The washing steps were performed as described above. Afterwards, Ni-beads were transferred to a gravity-flow column and bound protein was eluted with elution buffer (respective buffer with 300 mM imidazole). Prior to SEC, the eluate was concentrated to <2.5 mL and filtered through Minisart RC 15 single use syringe filter. SEC was performed using a Superdex 200 HiLoad 16/60 prep-grade column with SEC buffer, supplemented with 5% (v/v) glycerol (for His-Importin-β and His-transportin 1 NaCl concentration was increased to 250 mM). Peaks of interest were identified and analyzed as described for His-NOSIP.

His-Importin-7 ΔC (ΔN= aa 1002-1038)

His-Importin-7 ΔC plasmid was transformed into *E. coli* SG13009 cells and plated on an LB-agar$^{\text{ampicillin, kanamycin}}$ plate. Several colonies were used to inoculate a 2xYT starter culture for 16 h at 37 °C and 150 rpm. Starter culture was used 1:100 to inoculate 2xYT medium, supplemented with 2% (w/v) glucose, and grown to an OD_{600} of 1.6-1.8. Afterwards, 2xYT medium was diluted 1:1 with ice-cold 2xYT medium to reach an OD_{600} of ~0.7-0.9 and 30 mM K_2HPO_4 and 4% (v/v) ethanol was added to buffer the medium and to induce chaperone co-expression. Protein expression was induced by adding 1 mM IPTG at 15 °C for 16 h at 90 rpm. Cells were harvested as described for His-NOSIP. Bacterial cell pellets were resuspended in the three-fold volume of Tris buffer and lysed using the EmulsiFlex-C3 system. Cell lysates were cleared by ultra-centrifugation at 30.000 x g and 4 °C for 30 min. Afterwards, protein containing supernatant was added to Ni-NTA agarose beads and incubated for 3 h at 4 °C under gentle agitation. Unbound protein was removed by centrifugation and

pellets were washed three times using Tris buffer containing 5 mM imidazole, as described for His-NOSIP. Ni-Beads were transferred to a gravity-flow column and bound proteins were eluted using Tris buffer with 300 mM imidazole. The eluate was concentrated using Spin-X-UF concentrator (MWCO 50 K) and filtered through Minisart single use syringe filter (0.45 µM) prior to adding to SEC. For SEC, a Superdex 200 HiLoad 26/60 prep grade column was used with SEC buffer, supplemented with 5% (v/v) glycerol. His-Importin-7 ΔC containing fractions were identified, concentrated, aliquoted and shock frozen as described for His-NOSIP.

GST-Importin-13 constructs

Plasmids coding for GST-Importin-13 constructs were transformed into *E. coli* JM109 and plated on LB-agar^{ampicillin} plates. A LB medium starter culture was inoculated using several colonies and used the next day in a ratio of 1:100 to inoculate large-scale 2xYT plus medium. Cells were grown at 37 °C and 90 rpm to an OD600 of 0.8 and induced with 1 mM IPTG for 16 h at 18 °C. Cultures were harvested and pellets were washed as already described. Pellets resuspended in GST buffer were disrupted using the EmulsiFlex-C3 system and lysates were cleared as described for His-NOSIP. Protein containing cleared lysate was incubated with Glutathione Sepharose 4 FastFlow equilibrated in GST buffer for 2 h at 4 °C under gentle agitation. Unbound proteins were removed by a centrifugation step (800 x g, 4 °C, 5 min) and washed once with GST buffer, once with GST buffer, supplemented with 500 mM NaCl to remove unspecific bound proteins, and again with GST buffer. A washing step was based on a 5 min incubation at 4 °C, followed by 5 min centrifugation at 800 x g at 4 °C. Bound proteins were eluted after transfer to a gravity-flow column with GST buffer containing 20 mM Glutathione. GST-Importin-13 eluate was then dialyzed over-night at 4 °C against GST buffer using Slide-A-Lyzer Dialysis cassettes (MWCO 20 KDa), to remove the eluent. Dialyzed protein was then concentrated using Spin-X-UF concentrator (MWCO 30 K), aliquoted and shock frozen in liquid nitrogen. Purified protein was analyzed by SDS-PAGE (2.3.1), followed by Coomassie staining (2.3.2) and the concentration was determined as described in section 2.3.5.

MBP-transportin 1 constructs

MBP-transportin 1 constructs were transformed into *E. coli* BL21(DE3) cells and plated on LB-agar^{ampicillin} plates. Plates were used to prepare a starter culture, which were used to inoculate the large-scale LB medium cultures (1:100). Cells were cultured to an OD600 of 0.8 and protein expression was induced using 0.5 mM IPTG for 3-4 h at 37 °C. Cultures were harvested, washed and resuspended (in MBP buffer) and lysates were cleared by centrifugation as described for His-NOSIP. Amylose resin was equilibrated in MBP buffer and added to the ultra-centrifugation supernatant for 2 h at 4 °C under gentle agitation, followed by centrifugation to remove unbound proteins. Afterwards, beads were washed three times with MBP buffer, as described above, transferred to a gravity-flow column and MBP-proteins were eluted using MBP buffer containing 20 mM maltose. Eluate was filtered through Minisart RC 15 single use syringe filters and loaded onto a Superdex 200 HiLoad 16/60 prep-grade column using 1x TPB buffer. MBP-transportin containing fractions were identified, concentrated, aliquoted and shock frozen as described for His-NOSIP.

Ran-GTP$_{1-180}$ Q69L

Expression and purification of His$_{10}$-ZZ-[TEV]-Ran$_{1-180}$ Q69L was adapted from the protocol as depicted in (Port *et al.* 2015). Briefly, the plasmid was expressed in BL21(DE3)pLysS in 2xYT medium (supplemented with ampicillin and chloramphenicol and 2% (w/v) glucose) to an OD_{600} of 0.9 while reducing the temperature gradually, and induced with 0.5 mM IPTG for 15 h at 18 °C. Cells were harvested and resuspended in Ran lysis buffer (50 mM HEPES, 500 mM NaCl, 5 mM $MgCl_2$, 10% (v/v) glycerol, 3 mM imidazole, 50 µM GTP, 1 mM DTT, pH 7.0) and incubated for 1 hour at 4 °C with benzonase. Afterwards, cells were lysed using the EmulsiFlex-C3 system and lysates were cleared by ultra-centrifugation. Cleared lysate was loaded on a His-Trap 16/10 FF using an Äkta pure system (GE Healthcare) with Ran lysis buffer. Unbound proteins were washed-out with Ran lysis buffer and eluted in Ran lysis buffer containing 500 mM imidazole. Eluate was then incubated with TEV-protease (1 mg TEV-protease/50 mg protein) over-night at 4 °C to cleave the His$_{10}$-ZZ-tag off. Cleaved Ran$_{1-180}$ Q69L was then loaded again on the His-Trap 16/10 FF column to bind the cleaved His$_{10}$-ZZ-tag and un-cleaved His$_{10}$-ZZ-Ran$_{1-180}$ Q69L. The Ran$_{1-180}$ Q69L containing flow-through was further purified by SEC using a Superdex 75 HiLoad

16/60 prep-grade column and Ran SEC buffer (50 mM HEPES, 500 mM NaCl, 5 mM $MgCl_2$, 10% (v/v) glycerol, 30 µM GTP, 1 mM DTT, pH 7.0). Ran_{1-180} Q69L containing fractions were pooled, concentrated using a Spin-X-UF concentrator (MWCO 5 K), shock frozen in liquid nitrogen and stored at -80 °C.

GST-Lipin 1 constructs

Plasmids coding for GST-Lipin 1 (full length or aa1-619) were transformed into *E. coli* BL21(DE3)codon+ and plated on LB-agar^{Ampicillin} plates. The LB medium starter culture was inoculated using several colonies and to inoculate the large-scale LB medium in a ratio of 1:100 the next day. Cells were grown at 37 °C and 90 rpm to an OD600 of 0.8 and induced with 0.5 mM IPTG for 4 h at 37 °C. Cultures were harvested, pellets were washed with PBS and resuspended in GST buffer (supplemented with 0.1% Triton-X-100. Cells were disrupted using the EmulsiFlex-C3 system and lysates were cleared as described for His-NOSIP. Protein containing cleared lysate was incubated with Glutathione Sepharose 4 FastFlow for 2 h at 4 °C under gentle agitation which was equilibrated in GST buffer. Unbound proteins were removed by a centrifugation step (800 x g, 4 °C, 5 min) and washed once with GST buffer, once with GST buffer, supplemented with 500 mM NaCl to remove unspecific bound proteins, and again with GST buffer. A washing step was based on a 5 min incubation at 4 °C, followed by 5 min centrifugation at 800 x g at 4 °C. Bound proteins were eluted after transference to a gravity-flow column with GST buffer containing 20 mM Glutathione. GST-Lipin 1 was then concentrated using Spin-X-UF concentrator (MWCO 10 K), aliquoted and shock frozen in liquid nitrogen. Purification was analyzed by SDS-PAGE followed by Coomassie staining.

GST-PreScission protease

A plasmid coding for GST-PreScission protease was transformed into *E. coli* BL21(DE3) and plated on LB-agar^{ampicillin} plate. Several colonies were used to inoculate a starter culture which was grown over-night at 37 °C and 150 rpm. Starter culture was used to inoculate large-scale LB medium cultures at a ratio of 1:100 which were grown to an OD_{600} of 0.9 and induced with 0.5 mM IPTG for 16 h at 30 °C. Cells were harvested, washed and lysed in 1x PBS (containing 2 mM DTT, 0.1 µg/mL of each leupeptin, aprotinin, pepstatin and 0.1 mM PMSF). Lysate cleared by ultra-

centrifugation, was loaded onto a GST-prep 16/10 FF column, equilibrated in 1x PBS, using an Äkta pure system. Unbound proteins were removed by washing with two column volumes (CV) of 1x PBS, followed by a high-salt wash with 1x PBS containing 500 mM NaCl to remove unspecific bound proteins. Afterwards, a washing step with two CV of 1x PBS (with 2 mM DTT) was performed before eluting GST-PreScission protease with 1x PBS containing 20 mM glutathione and 2 mM DTT. Fractions containing GST-PreScission protease were dialyzed against 1x PBS with 2 mM DTT over-night at 4 °C, followed by a concentration step, shock freezing and storage at -80 °C.

Other proteins

His-Importin-α was purified as described in (Weis *et al.* 1995) by Dr. Marina Blenski. GST-M9 and GST-IBB (IBB: importin-β-binding domain) were expressed and purified as described in (Arnold *et al.* 2006b) by Dr. M. Arnold. RanWT was expressed and purified as described in (Melchior *et al.* 1995) by U. Moeller. His-Importin-5 protein was kindly provided by Dr. A. Dickmanns.

2.3.5 Protein concentration determination

To determine the concentration of purified proteins, two methods were used, either the determination by Nanodrop or by densitometry. For densitometry, an SDS-gel was loaded with 0.5, 1.0, 1.5 µg of BSA and 1, 2, 3 µL of protein solution and separated. The gel was stained with Coomassie, documented with the LAS-3000 Documentation system and analyzed with Fiji. BSA was used to create a standard curve and to determine the unknown protein concentrations.

2.3.6 Loading Ran with GTP

The RanQ69L$_{1-180}$ was loaded with GTP as described in (Kehlenbach *et al.* 1999). Briefly, RanQ69L$_{1-180}$ was expressed and purified (as described in section 2.3.4) and the recombinant protein was incubated with TPB containing 2.5 mM GTP and 15 mM EDTA for 30 min at RT, followed by the addition of 40 mM $MgCl_2$ for 20 min on ice to stop the reaction. Afterwards, the buffer was exchanged to 1x TPB using PD-10 columns, according to the manufacturer's instructions. Furthermore, the protein was concentrated, aliquoted and shock frozen in liquid nitrogen.

2.3.7 *In vitro* binding assays

Binding assays using recombinant proteins:

The interaction between nuclear transport receptor (NTR) and potential cargoes was studied using recombinant protein. Binding assays were performed with recombinant proteins containing different tags. For GST-tagged proteins, Glutathione Sepharose High Performance beads (GE Healthcare) were used while Amylose Resin High Flow beads (New England BioLabs) were chosen for MBP-tagged proteins and S-protein beads (Novagen) for S-protein-tagged proteins. The beads were washed twice with water and twice with 1x TPB, followed by equilibration with binding buffer (1x TPB with 20 mg/mL BSA or Ovalbumin) for 30 min at 4 °C on a rotation wheel to block the beads. Afterwards, 100 pmol of tagged proteins were immobilized per 10 µL beads for 1-2 h at 4 °C, followed by three washing steps, each with 1 mL binding buffer to remove unbound proteins. Immobilized protein was then incubated with proteins of interest in equimolar amounts or in excess, as indicated for the respective experiments, in a total volume of 0.5 mL for 2-3 h at 4 °C on a rotation wheel. Then,

the beads were washed three times with 1 mL 1x TPB to remove unbound proteins. To elute bound proteins, 50-100 µL 4x SDS sample-buffer were added and samples were boiled at 95 °C and 800 rpm for 10 min, followed by a centrifugation step at 800 x g and 4 °C for 5 min to pellet the beads. The protein containing supernatant was transferred to a fresh reaction tube and analyzed by SDS-PAGE analysis (2.3.1) and Coomassie staining (2.3.2) or Western blot analysis (2.3.3).

Binding assays using cell lysate

For binding assays with cell lysate, 600 pmol His-NOSIP-MBP (wildtype and mutants) or MBP were immobilized to 62.5 µL equilibrated MBP-selector Beads (Nanotag Biotechnologies) for 1 h at 4 °C using 1x TPB containing 10 mg/mL BSA, 1 µg/mL each of leupeptin, pepstatin and aprotinin and 2 mM DTT. Immobilized His-NOSIP-MBP was incubated with 200 µL HeLa cytosol (Ipracell, 14.3 mg/mL) in the presence or absence of 2000 pmol RanQ69L$_{1-180}$-GTP in a final volume of 1 mL for 6 h at 4 °C under continuous gentle rotation. Unbound proteins were removed by 4 washing steps, each with 1 mL 1x TPB for 2 min at 800 x g and 4 °C. Bound proteins were eluted using 150 µL of 4x SDS sample buffer at 95 °C for 10 min shaking at 800 rpm in a Thermomixer comfort (Eppendorf). Afterwards, a centrifugation step at 16,100 x g was used to pellet the beads and the protein containing supernatant was transferred to a fresh tube. Samples were analyzed by SDS-PAGE (2.3.1) followed by Western blotting (2.3.3).

2.3.8 Complex formation

To analyze if a potential cargo is forming a protein-complex with a nuclear transport receptor, analytical size exclusion chromatography (SEC) was performed. Therefore, 20 µM of each nuclear transport receptor was mixed with equimolar (or excess amount in case of ternary complexes) of His-NOSIP or optionally 60 µM of RanQ69L$_{1-180}$-GTP in a total volume of 250 µL and incubated for one hour on ice. Before applying this complex to a Superdex 200 (or 75) 10/300 GL (increase) column on an Äkta pure/Äkta purifier system, it was centrifuged at 16,000 x g and 4 °C for 15 min. The run was performed with a flowrate of 0.5 mL/min and 0.5-1.0 mL fractions were collected and analyzed by SDS-PAGE (2.3.1), followed by Coomassie staining (2.3.2).

2.3.9 Antibody purification

The polyclonal anti-NOSIP antibody (Table 16) was purified from serum of two rabbits which were immunized against recombinant full-length His-NOSIP by Davids Biotechnology GmbH company. For purification of anti-NOSIP antibody, 1.2 mg of His-NOSIP-MBP were dialyzed against carbonate buffer (0.2 M Na_2CO_3/$NaHCO_3$ pH 8.9) at 4 °C over-night. Dialyzed His-NOSIP-MBP was immobilized to 1.4 g cyanogen bromide-activated Sepharose 4B (Sigma Aldrich) for one hour at RT, followed by an incubation over-night at 4 °C. Cyanogen bromide-activated Sepharose was prepared by swelling in 1 mM ice-cold HCl for 1 hour, washing two times with water and brief washing in carbonate buffer. The next day, beads were washed twice with carbonate buffer and remaining free reactive amide groups were blocked using 100 mM ethanolamine in carbonate buffer for one hour at RT while rotating. Afterwards, three washing steps with carbonate buffer and one with 0.5 M NaCl in 1x PBS were performed. Prior to adding the serum to the immobilized His-NOSIP-MBP for an over-night incubation at 4 °C, the immune serum was diluted 1:1 with 1x PBS and filtered through a 0.2 µm sterile filter. Beads were transferred to a gravity-flow column (BioRad) and washed with 1x PBS containing 0.5 M NaCl until no more protein was present in the flow-through fraction. The antibody was eluted with 0.2 M acetic acid and 0.5 M NaCl in 1x PBS at pH 2.5 in fractions of 0.5 mL, these fractions were immediately neutralized with 100 µL of 100 µM Tris base (pH 8). Ponceau S staining was used to identify antibody containing fractions. First elution step was followed by a second elution step with 100 µM Triethylamine pH 11.5 in 500 µL fractions after neutralization of the beads by 1x PBS containing 0.5 M NaCl. Again, fractions were checked for antibodies by Ponceau S staining, all antibody containing fractions were combined and concentrated in a 30 K MWCO Spin-X UF concentrator to a volume of 0.5 mL. Antibodies were supplemented with 500 µL 87% glycerol and stored at -20 °C until further use. Self-made antibodies were tested in Western blotting (2.3.3) and indirect immunofluorescence (2.4.8).

2.4 Cell Biology Methods

2.4.1 Cultivation of mammalian cells

Mammalian cells were cultivated in Dulbecco's Modified Eagle Medium (DMEM), supplemented with Fetal Bovine Serum (10%), L-glutamine (2 mM) and penicillin/streptomycin (each 100 µg/mL). The cells were grown in a humidified cell incubator at 37 °C and 5% CO_2. To keep cells growing, they were sub-cultured twice a week in fresh medium when they reached a confluency of ~80%. For cell passaging, old medium was aspirated and the cells were washed once with 1x PBS. To detach cells, 1 mL of pre-heated trypsin was added and incubated at 37 °C. For inactivating trypsin, 9 mL of DMEM was added and the cell suspension was pipetted up and down to separate cells and dissolve cell clumps. A certain amount of this cell suspension was transferred to a new sterile 10 cm dish and supplemented with fresh DMEM to a total volume of 10 mL. Cells were distributed equally in the dish and incubated in a humidified cell incubator at 37 °C and 5% CO_2. HeLa P4 cells and NIH 3T3 cells were passaged twice a week with a dilution of 1:10 up to 1:20.

2.4.2 Determination of Cell concentration

The number of cells per milliliter were determined using the CASY 1 system (Schäfer System). Therefore, 100 µL of the detached and separated cell suspension were added to 10 mL of Coulter ISOTON II Diluent and measured according to the manufacture's protocol.

2.4.3 Transfection of Plasmids

Calcium phosphate

To transfect mammalian cells with plasmid DNA, the calcium phosphate method was used. 50.000 cells were seeded per well in a 24-well plate and cultivated in 0.5 mL DMEM in a humidified cell incubator at 37 °C and 5% CO_2. For transfection, the cells need to be at a confluency of ~50%. 0.5-1 µg of plasmid DNA were added to 20 µL 250 mM calcium chloride and vortexed for 10 seconds. Then, 20 µL of 2x HBS buffer was added and vortexed for 10 seconds. This transfection solution was incubated at RT for 20 min to form phosphate-DNA complexes before adding dropwise to the cells.

Transfected cells were grown in a humidified cell incubator at 37 °C and 5% CO_2 until the next morning.

Lipofectamine® 2000

For transfection of plasmid DNA with the lipofectamine method, 80.000 cells were seeded per well in a 24-well plate in 0.5 mL DMEM. The confluency at the day of transfection needed to be around ~70%. Prior to the transfection with lipofectamine, DMEM medium was changed to DMEM without penicillin and streptomycin. 0.5-1 µg of plasmid DNA was added to 25 µL OptiMEM and 1.5 µL of Lipofectamine® 2000 were added to 23.5 µL OptiMEM, both solutions were mixed and incubated for 5 min at RT. Then, both solutions were combined and incubated for 20 min at room temperature to form DNA containing lipid-droplets. Afterwards, the solution was added dropwise to the cells and cells were incubated at 37 °C and 5% CO_2, followed by a medium exchange to DMEM, supplemented with penicillin and streptomycin, after 4-5 h because of the toxicity of lipofectamine. The cells were then incubated in a humidified cell incubator at 37 °C and 5% CO_2.

Lipofectamine™ RNAiMAX

Lipofectamine™ RNAiMax was used to transfect siRNA to knockdown specific proteins. Here, 30.000 cells were seeded onto cover-slips in a 24-well plate. The next day 50-100 nM siRNA were mixed with OptiMEM in a total volume of 25 µL, while 1.5 µL Lipofectamine™ RNAiMax were incubated with 23.5 µL OptiMEM for 5 min at RT. Afterwards, both solutions were combined, incubated for 20 min at RT and then added dropwise to the cells and incubated at 37 °C and 5% CO_2, followed by a medium exchange after 6 h. Optionally the next day cells were re-transfected with 50 nM of siRNA as described above. At the third day after seeding, 0.5-1 µg of plasmids of interest were transfected using the calcium-phosphate method and incubated at 37 °C and 5% CO_2.

2.4.4 Treatment of HeLa P4 cells

Cells were treated with Leptomycin B (LMB) to block CRM1 dependent nuclear export. To analyze the effect of okadaic acid (OA), a general phosphatase inhibitor or of

staurosporine (ST), a protein kinase inhibitor or of both on NOSIP, cells were treated with these reagents. Therefore, cells were grown as described for the respective application. For immunofluorescence, cells were seeded and transfection was performed the next day, as described in 2.4.3. For cell treatment, transfected cells were washed once with 1x PBS to replace the medium with fresh DMEM containing the reagent. For LMB treatment, cells were incubated with 10 nM LMB (dissolved in ethanol) for 1-4 h. In case of the Heterokaryon assay (2.4.11), cells were incubated 3 h while co-cultivation with NIH 3T3 cells and throughout the whole experiment. For treatment with 0.1, 0.25, 0.5 µM OA or 0.5, 1 µM ST or both together, the cells were incubated for 1-2 h at 37 °C and 5% CO_2 in DMEM. After the treatment, cells were washed twice with 1x PBS and subjected to indirect immunofluorescence (2.4.8). For Western blot analysis, 70.000 cells were seeded in 24-well plates and the next day cells were treated with respective amounts of OA, ST or OA/ST for 2 h at 37 °C and 5% CO_2. Afterwards, cells were washed with 1x PBS and collected using 100 µL trypsin and cells were pellet by centrifugation at 800 x g for 5 min. Cells were resuspended and lysed in 50 µL 4xSDS-sample buffer and boiled for 10 min at 95 °C prior to Western blot analysis.

2.4.5 Synchronization of HeLa cells by a double-thymidine block

40.000 HeLa P4 cells per well in 24 well-plates (for indirect immunofluorescence on cover slips) were seeded and cultivated at 37 °C and 5% CO_2. The next day, cells were incubated for 18 h with DMEM containing 2 mM thymidine, followed by a release for 8 h in DMEM lacking thymidine. For a second block, cells were again incubated with DMEM containing 2 mM thymidine for 16 h at 37 °C and 5% CO_2. Afterwards, cells were released by washing twice with pre-warmed PBS and the addition of fresh DMEM for another 8-9 h. Cells collected immediately after the release represent cells in G1-phase of the cell-cycle and cells harvested after 8-9 h represent cells in G2-phase of the cell-cycle. When harvesting cells for indirect immunofluorescence, cells were washed twice with PBS and fixed with 3.7% formaldehyde for 10 min at RT. Flow cytometry analysis was used to determine the stage of the cell-cycle. For this, the DNA content was stained and analyzed, since the amount of DNA is doubled in the G2-phase compared to the G1-phase of the cell-cycle. For flow cytometry, cells were washed with twice with PBS, fixed in 70% ethanol overnight at 4 °C, followed by a

treatment with 50 µg/µl RNAse for 4 h on ice. DNA was then stained with 50 µg/ml propidium iodide for 30 min at RT. Fluorescence was measured using a FACSCanto II (BD Biosciences) with FACS Diva 6.1.1 software and data were analyzed using Flowjo software (Version 10.7.2).

2.4.6 Coating of coverslips with Poly-L-Lysine

For transport assays (described in 2.4.7), cells were grown in 24-well plates on poly-L-Lysine coated coverslips to obtain a better attachment of the cells. Therefore, coverslips were washed with isopropanol and were air-dried separately on filter paper. Poly-L-Lysine was diluted to 0.01% (v/v) with sterile H_2O and spread on to the coverslips for a 30 min incubation at room temperature. Afterwards, poly-L-Lysine solution was aspirated carefully and coverslips were washed once with sterile H_2O. The air-dried cover slips were then sterilized in a UV oven with 0.12J/cm^2 for 3 min.

2.4.7 *In vitro* transport assays

To analyze the nuclear transport of specific proteins, an *in vitro* transport assay was performed. The assay is based on the protocol from (Adam *et al.* 1990). For the transport assay, 60.000 mammalian cells were seeded in 0.5 mL DMEM on poly-L-Lysine coated cover slips in a 24-well plate. The cells needed to exhibit a confluency of ~50-70% and were first washed twice with ice-cold 1x TPB. Afterwards, the plasma membrane was permeabilized for 5 min on ice with 0.005-0.006% digitonin in 1x TPB while the nuclear membrane remained intact (Adam *et al.* 1990). The efficiency of permeabilization was checked by trypan blue staining. The permeabilized cells were then washed 3 times with 1x TPB, each for 3 min at room temperature or 4°C, to remove the cytosol. Afterwards, 40 µL of the transport reaction mixture were added on top of the cover slips and the transport reaction was performed either at 4 °C on ice or at 30 °C in a dark humidity chamber for 30 min. The transport reaction mixture consisted of 1 µL ATP regenerating system (1 mM ATP, 5 mM creatine phosphate, 20 U/mL creatine-phosphokinase), 500 µM protein of interest, 1 mM Nuclear Transport Receptor, 2 mg/mL BSA in 1x TPB, 4 µM RanWT and optionally instead of NTR 4 µL cytosol (14.3 mg/mL) or 100 µg/mL WGA (wheat germ agglutinin). To stop the transport reaction, the cells were washed three times for 5 min with ice-cold 1x TPB, followed by a fixation step with 3.7% formaldehyde in 1x PBS for 20 min at room

temperature. Afterwards, indirect immunofluorescence (2.4.8) was used to visualize the proteins.

2.4.8 Indirect immunofluorescence

Indirect Immunofluorescence was used to detect transfected or endogenous proteins in mammalian cells. Therefore, mammalian cells grown on cover slips were washed twice with 1x PBS the day after transfection. Afterwards, cells were fixed with 3.7% formaldehyde for 15 min, followed by washing twice with 1x PBS, each for 5 min to remove residual fixing solution. Then, cells were incubated with 0.5% Triton-X100 in 1x PBS for 5 min on ice to permeabilize the cells. To avoid unspecific binding of the antibodies, cells were blocked with 1% BSA or 10% FCS in 1x PBS for 10-20 min. For the detection of the proteins, the cover slips were placed in a dark humidity chamber and incubated with the primary antibody (Table 16) diluted in blocking solution for one hour at RT. To remove the excess of primary antibody, cells were washed three times with 1x PBS for 5 min each step. Afterwards, the cells were incubated with the secondary antibody (Table 17) diluted in blocking solution for one hour at RT. The excess of antibody was removed by three washing steps, each with 1x PBS for 5 min. The cover slips were air-dried in the dark after an additional washing step with sterile water. The cover slips were then mounted in Mowiol mounting medium containing 1 µg/mL DAPI to stain the nuclei (except for constructs containing mTagBFP (blue fluorescence protein)).

2.4.9 Microscopy

Cells transfected with fluorescently labeled proteins or stained by indirect immunofluorescence were analyzed using either a confocal microscope (LSM 510 META system) or an epifluorescence microscope (Nikon Eclipse Ti2). When using confocal microscopy, an Axiovert 200 M inverted microscope (Zeiss) was used, and images were acquired using the LSM 510 META confocal imaging system. The following objectives were used: 63x Plan-Neofluar 1.3 NA water-corrected objective or 100x Plan-Neofluar 1.3 NA water-corrected objective. For the excitation of DAPI and mTag-BFP2, the diode laser 405 nm was used, for AlexaFluor488 and GFP the 458/477/488/514 nm argon laser and for RFP or AlexFluor594 the 594nm HeNe laser. For acquisition of confocal images, the Zeiss Zen System (blue edition) software was

used. As a standard the pinhole was set to 1 airy unit. Laser intensity was set to a level to obtain a good signal intensity and prevent bleaching effects. For image acquisition, 4 images were averaged at a data depth of 8 bit, the scan speed was adjusted between speed 5 and speed 7. Intensity and background signal was adjusted using the Detector Gain and the Amplifier Offset. Images were analyzed using Fiji (version 2.1.0) software or Cell Profiler software (2.4.12). If needed for printing, brightness and contrast were linearly enhanced.

2.4.10 Glucocorticoid receptor assay (GR assay)

To analyze nuclear import and export, glucocorticoid-receptor assays (GR Assay) was used, adapted from (Love *et al.* 1998). For this assay, 50.000 HeLa P4 cells were grown on coverslips in 24-well plates and transfected with GR2-GFP-NOSIP (or mutant) or Rev-GR-GFP. Upon addition of 10 µM dexamethasone in DMEM (containing 100 µg/µL cycloheximide (CHX)) for up to 2 h at 37 °C, import of GFP-reporter proteins was induced. To fix cells at indicated timepoints, they were washed three times with 1x PBS, followed by a 10 min fixation step at RT in 3.7% formaldehyde in 1x PBS. After fixation, cells were washed three times with 1x PBS and once with sterile water prior to drying and mounting in Mowiol containing DAPI. For analysis of nuclear export, import was induced as described above and dexamethasone was removed. After washing three times with 1x PBS, cells were incubated in DMEM containing 100 µg/µL CHX for up to 2 h at 37 °C. Cells were fixed and mounted at different time-points as described above. Mounted cells were analyzed by fluorescence microscopy using a Nikon Ti-2 eclipse with a 60x Plan Apo 1.4 NA oil objective.

2.4.11 Heterokaryon assay

Shuttling of NOSIP was analyzed using a heterokaryon assay (HKA). 50.000 HeLa cells were seeded on poly-L lysine coated-coverslips in 24-well plates and incubated for 24 h at 37 °C and 5% CO2. The next day, cells were transfected with respective plasmids coding for NOSIP-HA (wildtype and mutants), GFP-GST-NOSIP (wildtype and mutants) or $Rev_{47\text{-}116}$-GFP2-cNLS, using the calcium-phosphate method (2.4.3). After 24 h, cells were co-cultured with NIH 3T3 mouse fibroblasts in DMEM, supplemented with 100 µg/µL CHX to stop protein translation for 3 h at 37 °C and 5%

CO2. Afterwards, heterokaryons were formed by fusing settled NIH 3T3 cells and HeLa P4 cells, therefore coverslips were placed on 40 µL 50% (w/v) PEG200 or on sterile PBS as control for 3 min at RT. To remove residual PEG2000, coverslips were washed four times extensively with 1x PBS. Fused cells were then incubated in DMEM containing 100 µg/µL CHX for 3 h at 37 °C and 5% CO_2. Afterwards, cells were washed three times with 1x PBS, fixed in 3.7% formaldehyde in 1x PBS for 10 min at RT and washed again three times with 1x PBS. Fluorescently labeled proteins were directly mounted in Mowiol containing DAPI while other proteins were visualized and analyzed by indirect immunofluorescence (2.4.8) followed by microscopy (2.4.9).

2.4.12 Image analysis using Cell profiler

Microscopy images were acquired as described in 2.4.9 and analyzed using Cell profiler software (Carpenter *et al.* 2006). For analysis of the nucleocytoplasmic ratio (N/C ratio), cell nuclei were identified by DAPI staining using the 'Otsu thresholding' method. The identified nuclear region was then expanded depending on the intensity using the 'Minimum Cross Entropy' method and a minimal intensity of 0.01 to obtain the whole cell region. The cytoplasmic region was then defined by subtracting the nuclear region from the whole cell region. After the definition of the whole cell, cytoplasmic and nuclear region, images were filtered for transfected cells in the 488 nm channel or, in the case of co-transfected cells, for 488 nm and 594 nm channel. Therefore, cells were filtered depending on the intensity in one or both channels with a cutoff intensity of 0.01. In filtered cells, the cytoplasmic and nuclear fluorescence intensity were measured in the channel of interest, followed by the division of the nuclear intensity by the cytoplasmic intensity to obtain the N/C ratio. For each condition, 500-1000 cells were analyzed and the results were visualized in Graph Pad Prism 9. Statistical analysis was performed using OneWay ANOVA, followed by Bonferroni post-test. P-values <0.05 were considered as significant (*: ≤0.05, **: ≤ 0.01, ***: ≤0.001).

For the analysis of *in-vitro* transport assays (2.4.7), the nuclear intensities of 50 – 100 cells per condition were measured using the Cell profiler software. Cell nuclei were identified by their DAPI staining using the 'Otsu thresholding' method. The identified nuclear region was then expanded depending on the intensity using the 'Minimum Cross Entropy' method and a minimal intensity of 0.01 to obtain the whole cell region.

Afterwards, cells were filtered for a minimum intensity of 0.01 in 488 nm (optionally 594 nm, depending on the staining) channel. The identified nuclei were shrunken by 10 pixels to measure only the fluorescence within the nucleus. The mean fluorescence intensity was measured in the shrunken nuclear region of filtered cells. In these transport assays, all conditions were performed at 37 °C and as control at 4 °C. To overcome the problem of varying background intensities which depended on the nuclear transport receptor used, the mean fluorescence of the 4 °C controls (condition without active transport) were subtracted from respective 37 °C samples. The corrected mean fluorescence intensity was normalized to a positive control (condition with whole transport mix containing cytosol instead of recombinant NTR) which was set to 1 as 100% transport. Data were plotted in Graph Pad Prism 9.

2.5 Structural Methods

2.5.1 Circular dichroism spectroscopy

CD-spectroscopy was performed to analyze whether recombinantly expressed and purified NOSIP was folded. For this, untagged NOSIP was purified as described in 2.3.4 and the buffer was exchanged by 100 mM Na_2HPO_4/$NaHPO_4$ (pH 8.0) using SlideALyzer dialysis cassettes (10K MWCO) over-night at 4 °C. Dialyzed protein was then centrifuged at 16,100 x g for 10 min and 4 °C to remove aggregates and was adjusted to a concentration of 0.1 mg/mL in a total volume of 370 µL. Samples were measured using a Chirascan™ CD spectrometer with respective cuvettes. Measurements were acquired with the following settings: with 1 nm steps from 180-260 nm, 0.5 s per time-point in millidegrees (mdg), at a temperature pf 20 °C and with 20 spectra repeats. Data were acquired and analyzed using Chirascan Software v.4.2.27, a sample of buffer was used as blank. For analysis, all 20 spectra were averaged, and the blank average was subtracted to obtain the CD-spectrum. This resulting CD-spectrum was compared to a data bank of proteins with known structure and CD-spectrum to calculate the amounts of secondary structure elements. Data were plotted using GraphPad Prism 9.

2.5.2 Cross-linking of NTR-NOSIP complexes

To form NOSIP-NTR complexes, 100 µM His-NOSIP were incubated with 100 µM His-transportin 1 or His-importin 13 for 2 h on ice in a final volume of 300 µL in Cross-

linking Buffer (20 mM Na2HPO4/NaH2PO4 pH 8.0, 150 mM NaCl, 1 mM EDTA and 5% glycerol). Preformed complexes were purified using a Superdex 200 analytical 10/300 GL increase column (GE Healthcare) equilibrated in cross-linking buffer. Purified complexes were used for cross-linking with bis(Sulfosuccinimidyl)Suberate (BS3). BS3 is an amine-to-amine cross-linker, both reactive groups are separated by a spacer-arm of 11.4 Å, which crosslinks primarily lysine sidechains. Cross-linking was performed at RT, BS3 was added in 50, 100, 200, 300, 400 and 800 -fold molar excess and reactions were stopped by adding TRIS-buffer (pH 8.8) to a final concentration of 50 mM. Afterwards, 4x SDS-sample buffer was added and samples were analyzed by SDS-PAGE and Coomassie staining (2.3.1, 2.3.2). Shifted bands corresponding to the size of cross-linked proteins were subjected to LC-MS analysis.

Additionally, purified NOSIP-Importin-13 complex was crosslinked using formaldehyde. His-NOSIP/His-Importin-13 complex was purified as described above and incubated with 0.4, 0.8, 1 or 1.3% of formaldehyde in buffer (20 mM HEPES, 100 mM NaCl, 15% glycerol, 4 mM $MgCl_2$, 10 mM ß-mercaptoethanol; pH 7.5) for 30 min at RT. Formaldehyde crosslinks everything in close proximity and cannot be mapped to a single residue while BS3 can. To stop the crosslinking reaction, 2-fold molar excess of TRIS compared to formaldehyde was added. Afterwards, 4x SDS sample buffer was added to the crosslinked complex and was heated no more than 37 °C, since higher temperature break the crosslinks. After heating the samples at 37 °C for 10 min, they were separated via SDS-PAGE, followed by Coomassie staining. Bands corresponding to the size of the complex were excised and subjected to LC-MS-analysis. LC-MS analysis was performed by Iwan Parfentev (MPI, Bioanalytical Mass Spectrometry, Göttingen, Prof. Dr. Hennig Urlaub group).

2.5.3 Molecular Docking

The AlphaFold structure of NOSIP (AlphaFold database: AF-Q9Y314-F1-model_v2) was docked to the crystal structure of transportin 1 using mass spectrometry derived crosslinking data as restrains. For transportin 1 the crystal structure of RanGppNHp-transportin 1 (PDB: 1QBK) was used. Therefore, the RanGppNHp structure was removed and transportin 1 was used as input for the initial docking. The structures of NOSIP and transportin 1 were initially docked using the protein-protein docking ClusPro webserver (https://cluspro.bu.edu/). The transportin 1 structure was used as

receptor and the NOSIP structure as ligand. The identified crosslinked residues were given as attraction sites for transportin 1 (K66, K81, K85, K128, K197, K385, K502, K889) and for NOSIP (K21, K90, K100, K117, K132, K153, K155, K157, K172, K175, K178, K289). For further analysis the model saturating the most crosslinks, the highest ClusPro score and NOSIP positioned in the inner-concave surface of transportin 1 was chosen. This initial model was further refined using the local docking protocol of the Rosetta software. Prior to the local docking by Rosetta, the input complex was energy minimized using the relax protocol generating 500 constructs. The complex with the lowest total energy was chosen as input structure for the local docking protocol. The docking protocol was performed using the options listed in Table 18 and the constrains listed in Table S 1 and Table S 2. The model with the lowest energy and highest interface score and additionally saturating the most crosslinks with a maximum distance of 30 Å was used for visualization. The complex structure was visualized using Chimera software (Pettersen *et al.* 2004).

Table 18: Options used for local docking of NOSIP and transportin 1

Options
-partners B_A
-docking local refine
-dock_pert 3 8
-sc_min
-ex1
-ex2aro
-use_input_sc
-construct 10000
-constraints:cst_file
-score:docking_interface_score 1

3 Results

In a recent proteomic screen to identify importin 13 cargoes, several new import and export-cargoes were identified (Baade *et al.* 2018). Two of these cargoes are NOSIP and Lipin 1, which were defined as potential importin 13 import-cargoes. Here, the role of importin 13 in the nuclear transport of NOSIP and Lipin 1 was analyzed in detail.

Lipin 1 was shown to harbor a classic NLS (^{153}KKRRKR^{158}) and to be imported by importin α/β (Ren *et al.* 2010). The LMB sensitivity of Lipin 1 points to CRM1 mediated nuclear export (Ren *et al.* 2010). To determine the role of importin 13 in Lipin 1 nuclear transport, the interaction of Lipin 1 with importin 13 was analyzed. Further, the role of importin 13 in Lipin 1 nuclear transport in HeLa cells was determined by performing knock-down experiments.

Like Lipin 1, NOSIP was suggested to be imported through the canonical NTRs importin α/β. However, it was found to be a potential import substrate of importin 13 with a rather high score. Therefore, the nuclear transport of NOSIP was analyzed in more detail in this work using various assays, followed by the analysis of its interaction with NTRs in a systematic way and a structural analysis of these interactions using cross-linking combined with mass-spectrometry. Moreover, regulation of nuclear transport, especially during the cell-cycle, was analyzed since NOSIP was observed to be relocated to the cytosol in a cell-cycle dependent manner.

3.1 Characterization of Lipin-1 interaction with importin 13

Lipin 1 is an important protein in fatty acid metabolism through its action as a transcriptional coactivator of lipid metabolic gene expression (Finck *et al.* 2006). Its transport was shown to depend on importin α/β and probably CRM1 (Ren *et al.* 2010). Additionally, its identification as an importin 13 cargo led to the question if importin 13 may play a role in its nuclear import. To analyze the nuclear import of Lipin 1, the localization of endogenous Lipin 1 was compared to the localization of over-expressed Lipin 1-HA protein in HeLa cells.

3.1.1 Lipin 1 localization in cultured cells

First, the localization of endogenous and HA-tagged Lipin 1 in HeLa and HAP1 cells was analyzed. Endogenous Lipin 1 was detected all over the cell with an equal distribution between nucleus and cytoplasm. Over-expressed Lipin 1-HA was localized in a similar way, however, with a more pronounced cytoplasmic staining (Figure S 2). GFP-GST-Lipin 1 instead was mainly localized in the cytoplasm and only barely detected in the nucleus. For further experiments Lipin 1-HA, which localizes similar to the endogenous Lipin 1, was used.

To confirm the previous reports that Lipin 1 may be exported through the major export receptor CRM1 (Ren *et al.* 2010), HeLa cells, transfected with Lipin 1-HA, were treated with 10 nM LMB. As observed before, in the absence of LMB most cells showed an equal distribution between nucleus and cytoplasm and in some cells slightly enriched in the cytosol. When treated with 10 nM LMB for 45 min, a more pronounced nuclear localization was observed. After 90 min of treatment, the nuclear signal increased, indicating a CRM1 dependent nuclear export of Lipin 1 (Figure 5).

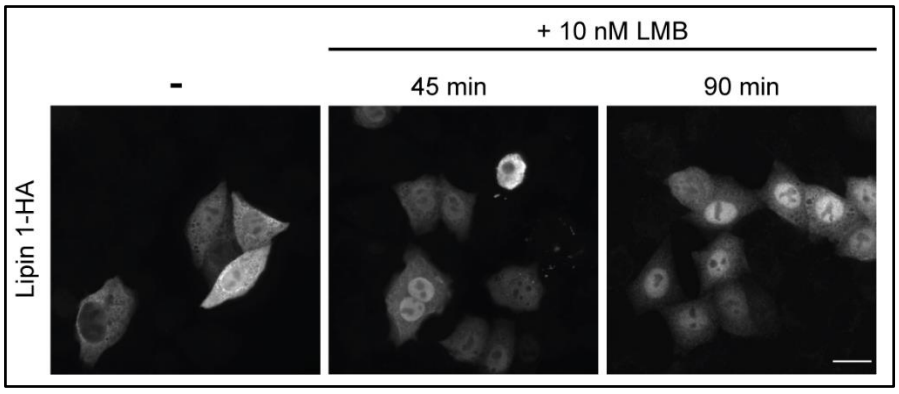

Figure 5: Lipin 1-HA accumulates in the nucleus after LMB treatment. HeLa P4 cells were transfected with a plasmid coding for Lipin 1-HA using the calcium phosphate method. Cells were treated with 10 nM Leptomycin B (LMB) for up to 90 mins. Lipin 1-HA was visualized by indirect immunofluorescence using an antibody against the HA-tag. Samples were analyzed by epifluorescence microscopy, scale bar 20 µm.

To validate the role of importin α/β in the nuclear import of Lipin 1, established peptide inhibitors of this pathway were used, as well as transportin 1 inhibitors as a control for the import pathway. Bimax2 is an optimized cNLS sequence, which was shown to bind with picomolar affinity to importin α and thereby prevents dissociation by RanGTP (Kosugi *et al.* 2008). Transportin 1 is inhibited by a peptide comprising an optimized M9 sequence, named M9M, which binds 200-fold stronger than typical M9-cargoes

(Cansizoglu *et al.* 2007). For importin 13 no such inhibitors are available. In order to analyze if the peptide inhibitors are selective for the respective pathways, shuttling reporter proteins were used. These shuttling proteins contain an NES fused to an mTagBFP2 (blue fluorescent protein) and either an cNLS or an M9-sequence.

The M9-shuttling construct (NES-mTagBFP2-M9, or in short BFP-M9) shows mainly a nuclear localization under steady state conditions. Control constructs were transfected with GFP-tagged inhibitors. The co-transfection with GFP-M9M abolished the nuclear accumulation of BFP-M9, whereas the co-transfection with GFP-bimax2 did not alter its localization. The cNLS-shuttling construct (NES-mTagBFP2-cNLS, or in short BFP-cNLS) showed a shift to the cytoplasm when co-transfected with GFP-bimax2 but was not affected by GFP-M9M (Figure 6 A). This indicates the specificity of the respective inhibitory peptides. Endogenous Lipin 1 is localized in the nucleus and the cytoplasm but when co-transfected with GFP-bimax2 it was excluded from the nucleus (Figure 6 B). Co-transfection of GFP-M9M lead to a weak shift to the cytoplasm in single cells, but not as pronounced as for GFP-Bimax2. When transfecting these peptide inhibitors in HeLa cells together with Lipin 1-HA, GFP-M9M did not show any effect. GFP-Bimax2 led to a strong accumulation of Lipin 1-HA in the cytoplasm, similar as for endogenous Lipin 1 (Figure 6 B). This indicates that importin α/β plays a major role in the nuclear import of Lipin 1 in HeLa cells.

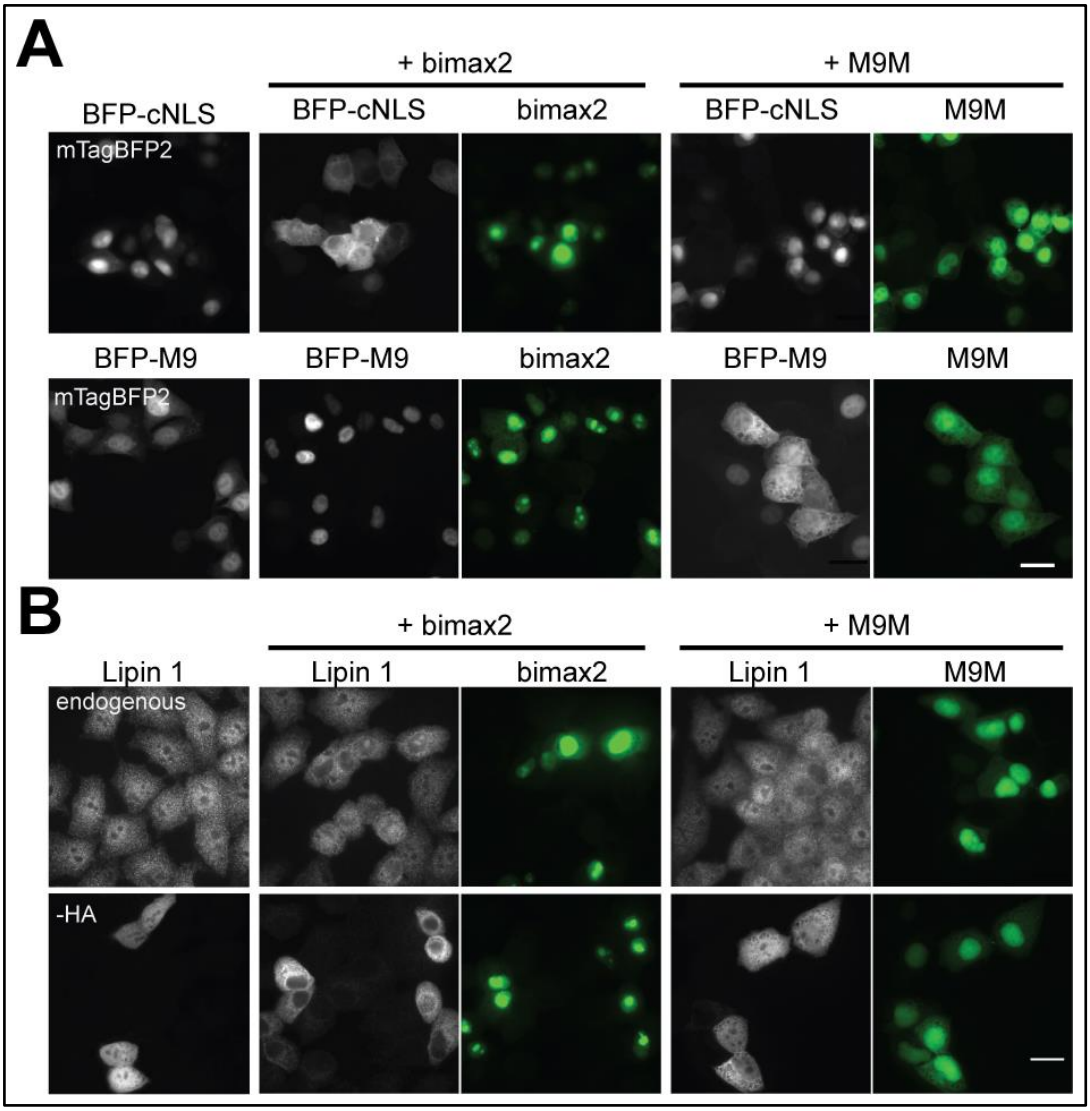

Figure 6: Effect of the inhibitors bimax2 and M9M on Lipin 1. A) HeLa P4 cells were transfected with shuttling constructs containing an NES, a fluorescence tag (mTagBFP2) and a cNLS or M9-signal (NES-mTagBFP2-cNLS/M9, in short BFP-cNLS/M9) to validate the specificity of the inhibitors. M9M is an optimized M9 sequence and established as a transportin 1 inhibitor, bimax2 is an optimized cNLS sequence, which binds and inhibits importin α. M9M or bimax2 were transfected as GFP-tagged fusion proteins, together with the shuttling constructs. (B) Transfection of GFP-M9M or bimax2 as GFP- or RFP-tagged variants respectively. Cells were transfected either with GFP-M9M or GFP-bimax2 alone or in combination with Lipin 1-HA. Lipin 1 was visualized by indirect immunofluorescence using antibodies against the HA-tag or Lipin 1. Scale bar 20 µm.

3.1.2 Interaction of Lipin 1 with importin 13

Lipin 1 is known to be imported by importin α/β (Ren *et al.* 2010), which was confirmed in this work. However, in a proteomic screen Lipin 1 was identified as a potential import substrate of importin 13. To compare the binding of importin 13 and importin α/β to Lipin 1, all proteins were purified and used in a binding assay. Full-length GST-Lipin 1 (aa 1-890) was barely soluble. To improve the solubility, a C-terminal truncated Lipin 1 fragments were tested (data not shown). GST-Lipin $1^{1\text{-}619}$ showed the highest solubility and bound comparable to the full-length Lipin 1 (Figure S 3). GST-Lipin $1^{1\text{-}619}$ was

immobilized on glutathione sepharose beads and incubated with His-importin 13 and His-importin α/β or both. To test whether importin α/β can replace importin 13 from binding to GST-Lipin 1^{1-619}, the concentration of His-importin 13 was kept constant and increasing amounts of His-importin α/β were added. Additionally, the assay was performed in the reverse way, keeping His-importin α/β concentration constant and increasing His-importin 13. Bound proteins were analyzed by Western blotting, since His-importin β (103 kDa) and His-importin 13 (108 kDa) have a similar size and could not be analyzed by Coomassie staining.

When GST-Lipin 1^{1-619} was incubated with an equimolar amount of His-importin 13, binding of importin 13 was observed (Figure 7, first lane). The addition of 2-fold or 4-fold molar excess of His-importin α/β reduced the bound fraction of His-importin 13. A 10-fold molar excess abolished binding of His-importin 13 almost completely. The band intensities of His-Importin α and His-importin β were increasing. In the reverse reaction, where importin α/β were kept constant, neither a 2-fold nor a 4-fold molar excess of importin 13 could compete with importin α/β for binding to Lipin 1. Only the presence of importin 13 in 10-fold molar excess decreased the binding of importin α/β slightly (Figure 7). As a control, the GST-tag alone was immobilized and incubated with the His-tagged NTRs. No binding of importin 13 or importin α/β to GST-alone was observed, indicating the specificity of this reaction. This assay demonstrates that importin 13 binds to Lipin 1 in an *in vitro* binding assay. However, importin 13 could not compete with importin α/β for Lipin 1 binding. Instead, importin α/β could prevent binding of importin 13 to Lipin 1 when present in molecular excess, indicating a higher affinity of importin α/β under these experimental conditions.

The specificity of the binding of importin 13 or importin α/β to GST-Lipin 1^{1-619} was tested using Ran_{1-180} Q69L-GTP, which is a Ran mutant deficient for GTP hydrolysis. In the nucleus, RanGTP is present in a high concentration and leads to the dissociation of import complexes. Therefore, using Ran_{1-180} Q69L-GTP in high molecular excess in a binding reaction should prevent or reduce the binding of importins and mediate the binding of exportins to immobilized Lipin 1. In a binding assay, GST-Lipin 1^{1-619} was incubated with 100 pmol of His-importin 13, CRM1-His-HA or His-importin α/β in the presence or absence of 3-fold molar excess of Ran_{1-180} Q69L-GTP. Both,

importin 13 and importin α/β, bound only to immobilized Lipin 1 in the absence of Ran but not in its presence, demonstrating the specificity of this interaction (Figure S 3 B). CRM1-His-HA bound to GST-Lipin 1^{1-619} and to GTS-Lipin 1 full-length only in the presence of Ran_{1-180} Q69L-GTP (Figure S 3 C).

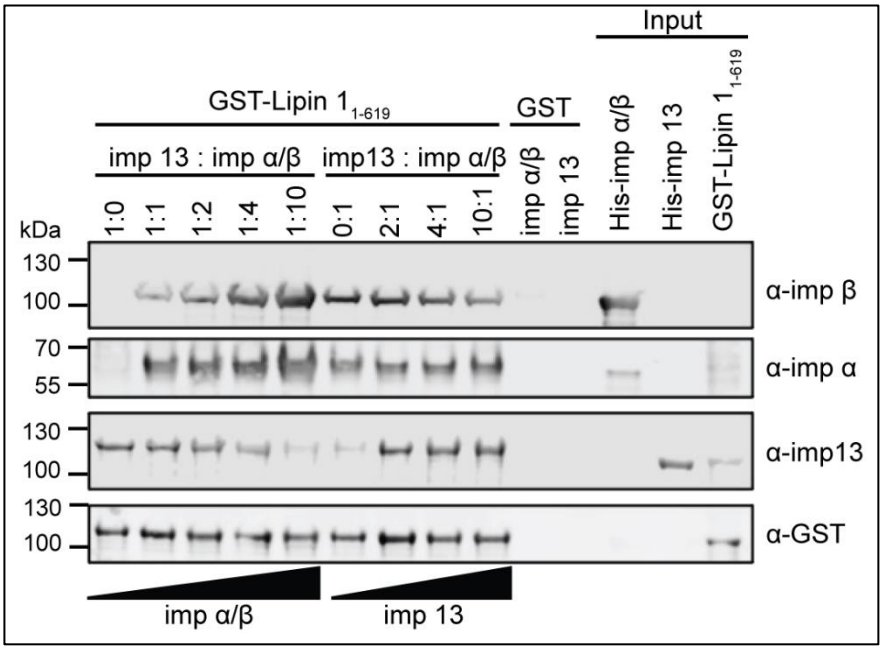

Figure 7: Competition of importin α/β and importin 13 for Lipin 1. For the competition binding assay, 100 pmol GST-Lipin 1^{1-619} was immobilized to glutathione sepharose beads and incubated with 100 pmol of His-importin 13 and increasing amounts of His-importin α/β (0, 100, 200, 400, 1000 pmol) or vice versa. Unbound proteins were washed out and bound proteins were eluted using 4xSDS-sample buffer. Eluted proteins were analyzed by SDS-PAGE, followed by Western blotting. Importin β, importin α and importin 13 were detected using respective antibodies, GST-Lipin 1^{1-619} was detected using an antibody directed against GST.

To analyze if importin 13 interacts with Lipin 1 in HeLa cells, transfection experiments were performed. Cells were transfected with constructs coding for different FLAG-tagged importin 13 mutants and Lipin 1-HA. The mutants are deficient in binding to single cargoes, whereas other cargoes can still bind to importin 13 (Grünwald and Bono 2011; Grünwald *et al.* 2013). For instance, K802E/R803E is deficient in binding and importing MAGO-Y14 but still can bind and import Ubc9. D426R, a mutant unable to import and bind Ubc9, is still able to bind MAGO-Y14 and export eIF1a. The last mutant is E436R/D481R, which is deficient in exporting eIF1a but is able to import Ubc9 and MAGO-Y14 (Grünwald and Bono 2011; Grünwald *et al.* 2013).

Lipin 1-HA transfected in HeLa cells localized equally between nucleus and cytoplasm, whereas co-transfecting FLAG-imp 13 showed a nuclear enrichment of Lipin 1-HA. The same was observed when co-transfecting FLAG-Imp13

K802E/R803E. Co-transfection of D426R or E436R/D481R had no effect on Lipin 1-HA (Figure 8), indicating that the N-terminal arch of importin 13 is involved in binding to Lipin 1. Importin 13 induced the translocation of over-expressed Lipin 1-HA to the nucleus, showing that a NTR was rate-limiting for its localization.

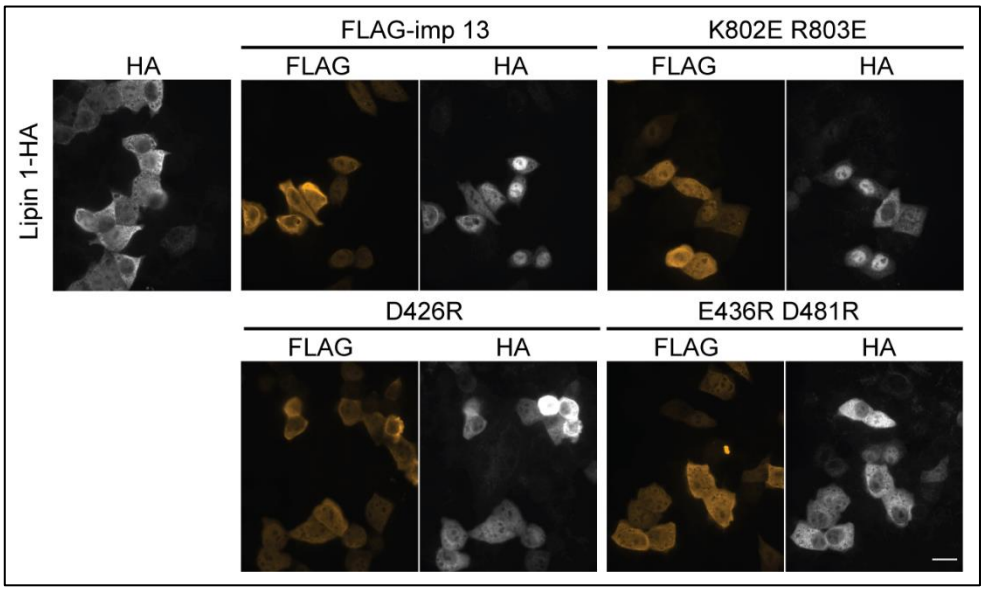

Figure 8: FLAG-Importin 13 is able to import Lipin 1-HA in HeLa P4 cells. HeLa P4 cells were transfected with Lipin 1-HA or together with FLAG-tagged importin 13 constructs using the calcium phosphate method. Different mutants of importin 13 were used, which are deficient in binding a specific cargo, K802E/R803E (deficient in MAGO-Y14 import), D426R (unable to import Ubc9) and E436R/D481R (unable to export eIF1a). Proteins were visualized by indirect immunofluorescence using anti-FLAG and anti-HA antibodies. Images were acquired by epifluorescence microscopy. Scale bar 20 µm.

3.1.3 The role of importin 13 in Lipin 1 nuclear import in HeLa cells

To examine the role of importin 13 in living cells, a knock-down was performed and analyzed for the effect on endogenous Lipin 1, as well as Lipin 1-HA. For the knock-down, 50 nM of siRNA or non-targeting control siRNA were transfected. The efficiency of knock-down was validated by Western blotting (Figure 9). In parallel to importin 13, an importin β knock-down was performed to abolish the known transport pathway of Lipin 1. The effect on endogenous or over-expressed Lipin 1-HA was assessed using indirect immunofluorescence. Endogenous Lipin 1 localized equally to the cytoplasm and nucleus, the same was observed for over-expressed Lipin 1-HA (Figure 9 B). Knock-down of importin 13 led to a shift of endogenous Lipin 1 to the cytoplasm, whereas Lipin 1-HA was only slightly shifted to the cytosol. Knocking down importin β led to an exclusion of endogenous Lipin 1 from the nucleus (Figure 9 B). Lipin 1-HA showed a similar exclusion from the nucleus.

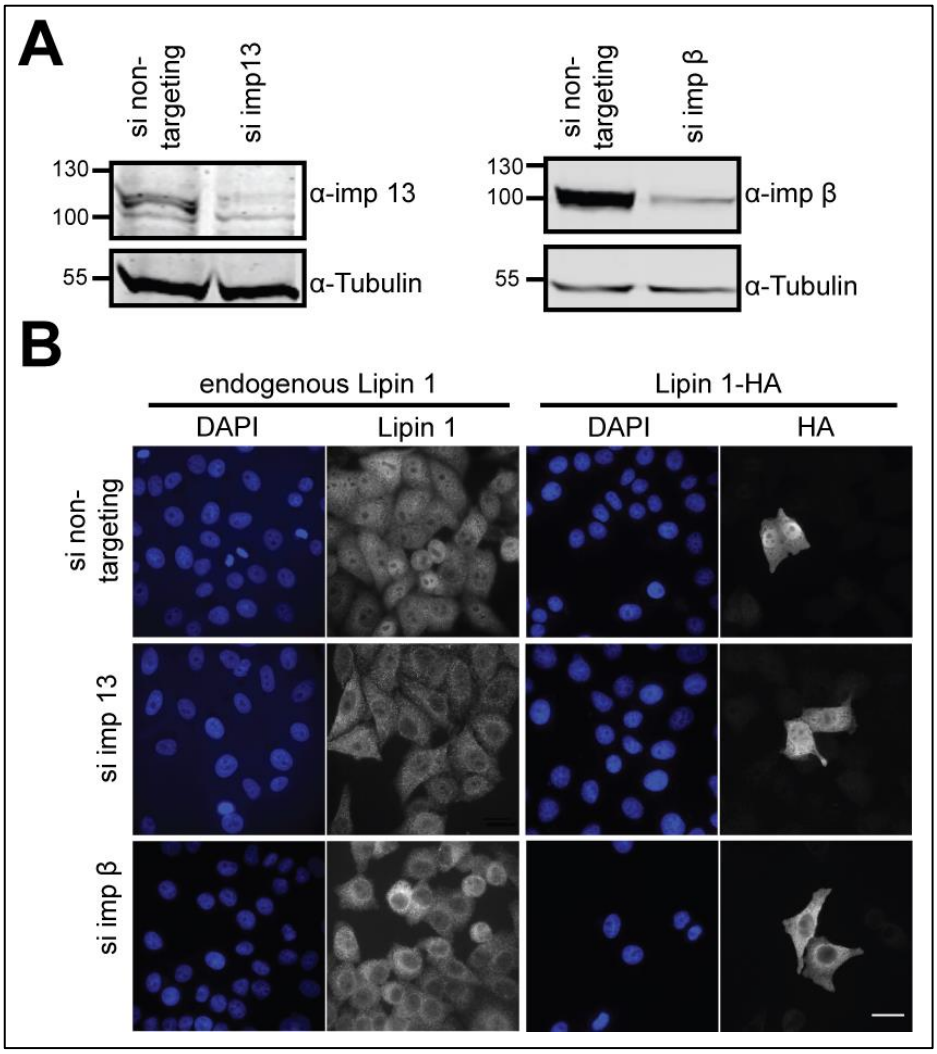

Figure 9: A knock-down of importin 13 or importin β alters the localization of Lipin 1 in HeLa cells. HeLa P4 cells were transfected with 50 nM of siRNA directed against importin 13 (si imp 13) or importin β (si imp β) or else a non-targeting control siRNA (si non-targeting). After 48 h, cells were harvested and knock-down efficiency was analyzed by Western blotting (A) or cells were transfected with Lipin 1-HA and the next day subjected to indirect immunofluorescence (B). Endogenous Lipin 1 was visualized using an anti-Lipin 1 antibody and Lipin 1-HA was detected using an anti-HA antibody. Images were acquired on an epifluorescence microscope. Scale bar 20 µm.

Further, it was analyzed whether importin 13 can rescue the knock-down of importin β, since the availability of the NTR is a limiting factor for the localization of Lipin 1-HA (Figure 8). Therefore, FLAG-importin 13 was co-transfected with Lipin 1 (endogenous and Ha-tagged) in importin β knock-down cells. As shown in Figure 10 (A), co-transfection could partially reverse the importin β knock-down and led to a re-localization of endogenous and HA-tagged Lipin 1 to the nucleus. The reverse experiment, in which importin 13 was knocked-down and HA-importin β was co-transfected, showed a similar rescue effect on endogenous Lipin 1, but the re-localization of Lipin 1-HA seemed to be more pronounced (Figure 10 B).

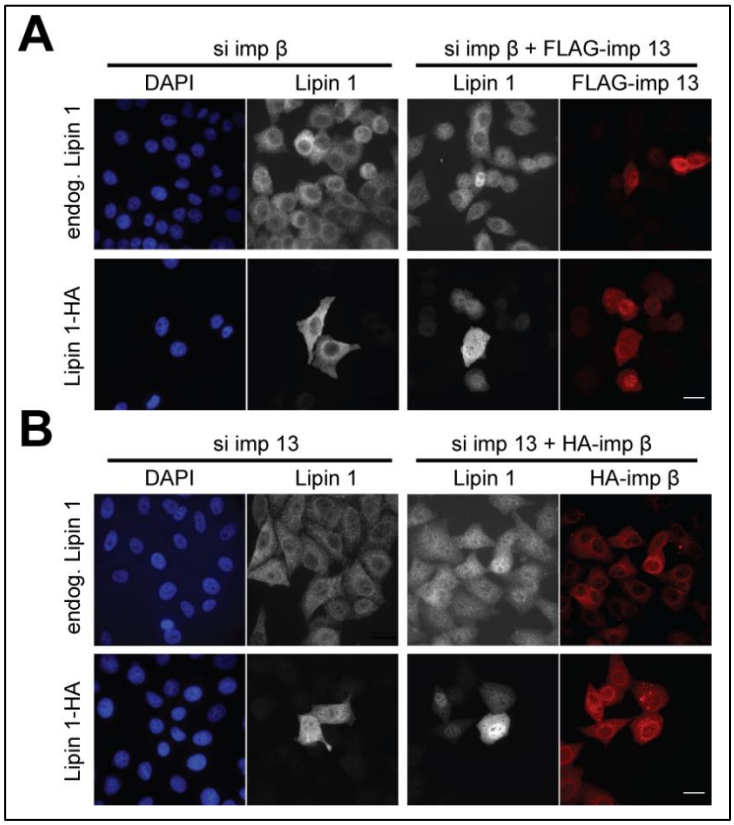

Figure 10: Importin 13 can rescue the importin β knock-down effect on Lipin 1-HA. A knock-down of Importin β (A) or importin 13 (B) was performed in HeLa P4 cells. After 48 h, cells were transfected with Lipin 1-HA and with or without FLAG-importin 13 (A) or HA-importin β (B). Indirect immunofluorescence was used to visualize respective proteins using an anti-Lipin 1 antibody and anti-HA or anti-FLAG antibody. Images were acquired on an epifluorescence microscope and analyzed using Fiji software. Scale bar 20 µm.

Taken together, the knock-down of importin β had a stronger effect on Lipin 1 than the importin 13 knock-down. Both knock-downs could be, at least partially, rescued when co-transfected with the other NTR, but the rescue of the importin 13 knock-down was more efficient. These results point to a more important role of importin α/β compared to importin 13, which was shown to play a minor role in Lipin 1 nuclear localization under these experimental conditions.

3.2 Characterization of NOSIP nuclear transport

3.2.1 Localization of NOSIP in cultured cells

The localization of NOSIP differs depending on cell types and tissues, but in cultured cells it is reported to be mainly nuclear (König *et al.* 2002; Schleicher *et al.* 2005). To test whether this holds true for the cell-lines used in this thesis and if the protein-tag influences NOSIP localization, cells were transfected with different NOSIP fusion proteins. Additionally, the localization of endogenous NOSIP was examined. Hela cells were transfected with plasmids coding for NOSIP-HA, GFP-GST-NOSIP or GFP-GST. The specificity of anti-NOSIP antibody was validated by knockdown of endogenous NOSIP using siRNA directed against NOSIP (see Figure S 1). Endogenous NOSIP as well as NOSIP tagged with HA showed mainly a nuclear localization (Figure 11 A). This is in line with the observation for myc-tagged NOSIP transfected in normal HeLa cells (Schleicher *et al.* 2005). Endogenous or HA-tagged NOSIP with 33 and 34 kDa, respectively, is small enough to passively diffuse through the NPC. To increase the size above the limit for passive diffusion, a GFP-GST-NOSIP (87 kDa) fusion protein was used. This fusion protein showed a mostly nuclear localization (Figure 11 A), but in some cells an equal distribution between nucleus and cytoplasm or even more cytoplasmic localization could be seen. To exclude that the added GFP-GST-tag drives the nuclear accumulation of the fusion protein, cells were transfected with GFP-GST-tag alone. GFP-GST alone was excluded from the nucleus, showing that the nuclear accumulation of GFP-GST-NOSIP is based on NOSIP (Figure 11 B). This shows, at least for HeLa cells, that NOSIP localizes mainly nuclear.

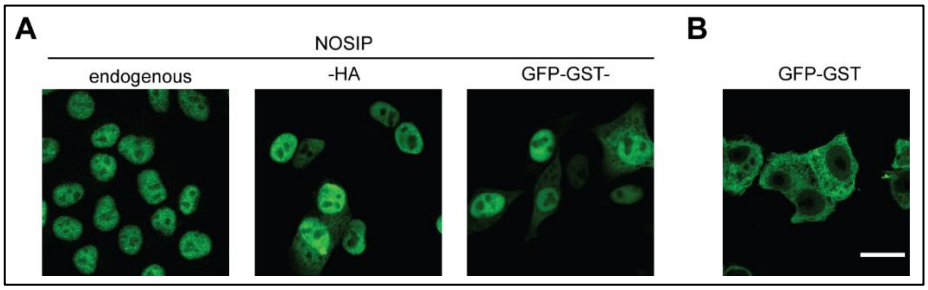

***Figure 11: NOSIP localization in HeLa P4 cells**. HeLa P4 cells were transfected using the calcium phosphate method (2.4.3) with NOSIP-HA, GFP-GST-NOSIP or GFP-GST-tag alone and analyzed for their localization in cultured cells. NOSIP was visualized using the GFP-tag or by indirect immunofluorescence using antibodies directed against the HA-tag or against endogenous NOSIP. Scale bar 20 µM.*

3.2.2 NOSIP is a nuclear shuttling protein

Based on the size of NOSIP, the protein can passively diffuse through the NPC and one would expect NOSIP to be equally distributed. The nuclear localization of NOSIP under steady state conditions results either from retention of NOSIP in the nucleus upon binding to a nuclear binding partner or through continuous nuclear shuttling, where import outbalances nuclear export. The latter was suggested by (Schleicher *et al.* 2005) and co-workers using a heterokaryon assay (HKA), where NOSIP was fused to a myc-tag, resulting in a fusion protein of 34.5 kDa, in size similar to NOSIP-HA. To confirm this observation, the shuttling of NOSIP-HA and additionally of GFP-GST-NOSIP was analyzed in an HKA. In this assay HeLa cells and NIH 3T3 were used, because these can be distinguished based on their DNA staining. The localization of NOSIP proteins or the control protein Rev (Rev^{47-111}-GFP_2-cNLS) was analyzed. A nuclear signal of NOSIP or Rev within the nuclei of NIH 3T3 cells would indicate shuttling out of HeLa nuclei into NIH 3T3 nuclei. As expected, the control protein Rev, which contains a cNLS and an NES, was observed to shuttle between HeLa- and NIH 3T3-nuclei when cells were fused, but not in control cells (see Figure 12 upper lane). This confirms the functionality of the HKA.

For NOSIP tagged with an HA-tag, small enough for passive diffusion through the NPC, nuclear shuttling could be observed (see Figure 12 second lane). This is in line with the observation of Schleicher and co-workers (Schleicher *et al.* 2005). In contrast to NOSIP-HA, GFP-GST-NOSIP, with 87 kDa clearly above the size for passive diffusion, did not show nuclear shuttling between HeLa and NIH 3T3 cells (Figure 12 third lane). The accumulation of GFP-GST-NOSIP within HeLa nuclei indicates that there is no active export, at least under these experimental conditions. To further analyze nuclear export and to exclude the possibility that the GFP-GST-tag shapes a usually functional NES, the same assay was performed in the presence of LMB, a potent inhibitor of the main exportin, CRM1. In the presence of LMB, nuclear shuttling of the control protein Rev, whose nuclear export depends on CRM1, was abolished (Figure 12 fourth lane). NOSIP-HA, on the other hand, was still able to shuttle between nuclei and GFP-GST-NOSIP did not shuttle (Figure 12 last two lanes), indicating that NOSIP is a nuclear shuttling protein. This showed that NOSIP is actively imported into the nucleus, whereas nuclear export depends more likely on passive diffusion.

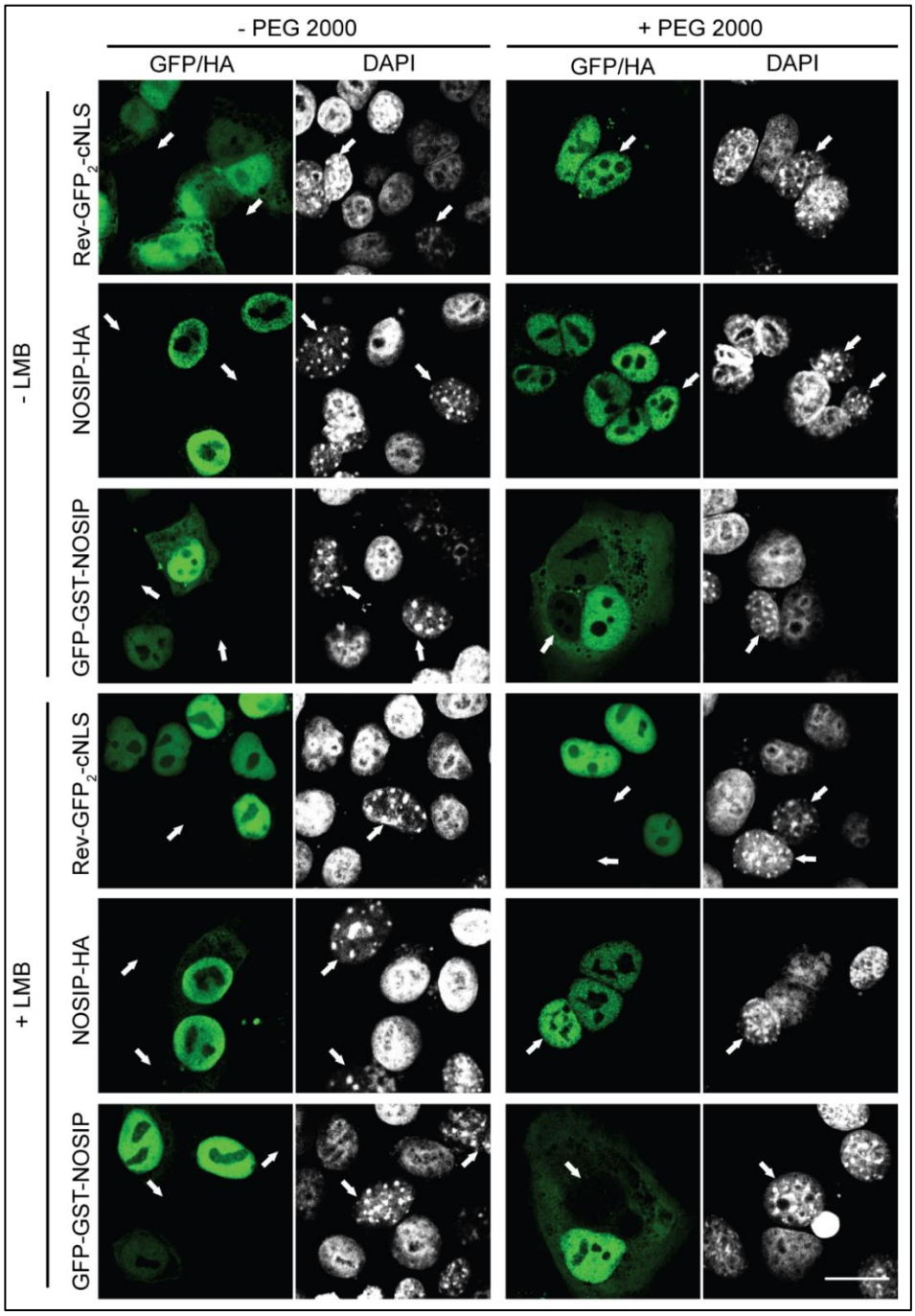

Figure 12: NOSIP is a nuclear shuttling protein. Heterokaryon assays were performed by fusing (+ PEG 2000 or as control – PEG 2000) HeLa P4 cells, transfected with Rev^{47-116}-GFP_2-cNLS, NOSIP-HA or GFP-GST-NOSIP, and NIH 3T3 cells in the presence (+LMB) or absence (-LMB) of leptomycin B. Cell nuclei were distinguished by their DAPI staining, NIH 3T3 nuclei show several bright dots and are indicated by arrows. Proteins of interest were detected by their fluorescence tag or in case of NOSIP-HA by indirect immunofluorescence using an anti-HA antibody. Nuclear shuttling of fluorescently labeled proteins was analyzed by confocal microscopy. Scale bar 20 µm.

3.2.3 Analysis of NOSIP nuclear export using the glucocorticoid receptor assay

For further analysis of NOSIP nuclear export, a nuclear transport assay was used, where nuclear import and nuclear export can be controlled. This assay uses the hormone responsive domain of the glucocorticoid receptor (GR, aa 511-795) (Love *et al.* 1998). The glucocorticoid receptor is in absence of steroid localized in the cytoplasm and imported into the nucleus in the presence of steroid (Picard and Yamamoto 1987). The GR-responsive domain is fused to the protein of interest and to GFP and the resulting chimeric protein is above the size limit for passive diffusion (control plasmid Rev-GR-GFP, ~67 kDa and GR_2-GFP-NOSIP, ~127 kDa). Upon addition of hormone, in this assay dexamethasone, the nuclear translocation of the fusion protein is induced (Import).

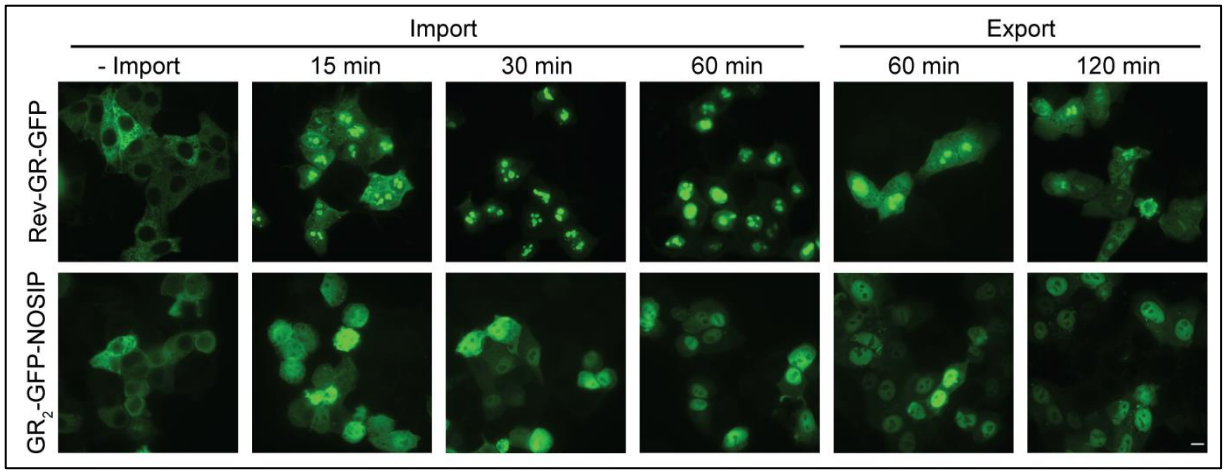

Figure 13: NOSIP is not actively exported in HeLa cells. In this in vivo transport assay nuclear import and nuclear export can be controlled by treatment with dexamethasone or removal of steroid, respectively. Rev protein fused to the hormone responsive domain of the glucocorticoid receptor (GR, aa 511-795) and GFP serves as a control. The GR fragment is bound to cytoplasmic structures in the absence of steroid and is imported upon steroid treatment. Import was induced with 5 µM dexamethasone and cells were fixed at indicated time-points. After removal of steroid proteins, will be exported and retained in the cytoplasm if an NES is present. Localization of proteins was analyzed by fluorescence microscopy. Scale bar 10 µM.

To analyze nuclear export, dexamethasone was washed out by replacing the old medium with fresh medium lacking dexamethasone to induce export. In these controlled transport assay (or GR (Glucocorticoid-receptor) assay) the control protein, Rev-GR-GFP, was imported within 30 min after dexamethasone addition and showed a typical nucleoli localization. After 1 or 2 h of export, Rev was enriched in the cytoplasm (Figure 13). The GR_2-GFP-NOSIP protein was imported in the same manner and showed a predominantly nuclear accumulation after 60 min. In contrast to Rev, the nuclear accumulation of GR_2-GFP-NOSIP could not be reversed upon

dexamethasone wash out (Figure 13). Rev, containing an NES, showed nuclear export, but NOSIP was not actively exported. This is in line with the observations of the HKA above.

3.3 NOSIP interaction with nuclear transport receptors (NTR)

3.3.1 NOSIP binds to several NTRs *in vitro*

Recently, NOSIP was identified in a proteomic screen for importin 13 cargoes (Baade *et al.* 2018), in contradiction to the report that NOSIP is transported by the canonical NTRs importin α/β (Schleicher *et al.* 2005). Therefore, the interaction of NOSIP with different NTRs was analyzed in detail. NOSIP fused to His (6x Histidine (H)) and MBP (Maltose binding protein) was immobilized using the MBP-tag and incubated with HeLa lysate to identify binding NTRs by immuno-blotting (Western blot). To verify that detected NTRs bind specifically, binding reactions were performed in the presence or absence of RanGTP$_{1-180}$ Q69L, a Ran mutant insensitive to GTP-hydrolysis (Klebe *et al.* 1995). To exclude that NTRs interact with the His- and MBP-tag, His-MBP (referred from here on as MBP) was immobilized as a control. As seen in Figure 14 B either His-NOSIP-MBP or MBP were specifically immobilized to MBP-Trap, detected by Western blotting using anti-MBP and anti-NOSIP antibodies. In the eluate of the pulldown reactions with His-NOSIP-MBP, several NTRs were detected, namely importin β, importin α, importin 7, importin 13 and transportin 1 (Figure 14 A). The binding of all NTRs was reduced in the presence of RanGTP$_{1-180}$ Q69L demonstrating the specificity of their binding. The import-receptors importin 11 and importin 9 were only detected in the input and thus not binding to immobilized NOSIP. For the nuclear export receptor, CRM1, a strong binding was observed in the presence of RanGTP$_{1-180}$ Q69L (Figure 14 A). No NTRs were bound when MBP was immobilized instead of His-NOSIP-MBP, further demonstrating the specificity of the interaction with NOSIP (Figure 14 A).

Clearly, NOSIP interacted with multiple NTRs. To further analyze the binding of NTRs to NOSIP, recombinant proteins, expressed in *E. coli*, were used. Again, His-NOSIP-MBP was immobilized and incubated with purified His-tagged NTRs in the presence or absence of RanGTP. Binding of importin 7, importin 13, transportin 1, importin β and importin 5 (which could not be tested in the pulldown assay, due to a lack of a

specific antibody) could be detected and was specifically reduced in the presence of RanGTP$_{1-180}$ Q69L (Figure 14 C). Interestingly, importin β alone bound independently of importin α to NOSIP. In a reaction with importin α, neither a binding of importin α nor a further increase in binding of importin β could be observed (Figure 14 C). This is contradictory to the current literature, which suggested importin α to be essential for NOSIP nuclear import. Since the NTRs importin 7 and importin β are known to form heterodimers and facilitate nuclear import (Jäkel *et al.* 1999) and both were shown to bind NOSIP individually, it was tested if they bind simultaneously. As seen in Figure 14 C, when incubating His-NOSIP-MBP with importin β and importin 7 both were detected in the eluate, suggesting that they may form a ternary import complex. As in the pulldown experiments, specific binding of CRM1 in the presence of RanGTP could be observed (Figure 14 C). A control reaction, where MBP was immobilized instead of NOSIP showed no significant binding of NTRs (Figure 14 D). Of all NTRs tested, transportin 1 showed the strongest binding to His-NOSIP-MBP.

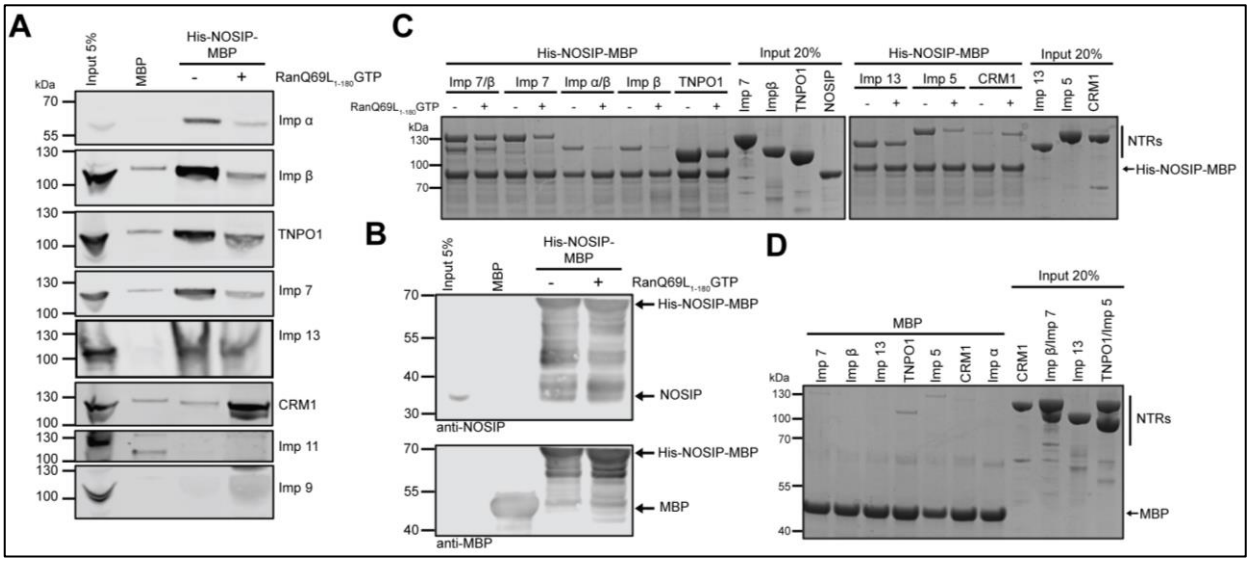

Figure 14: NOSIP binds to several nuclear transport receptors. (A) Pulldown of NTRs from HeLa cytosol using His-NOSIP-MBP. His-NOSIP-MBP or His-MBP protein (600 pmol) was immobilized on MBP-Trap and incubated with HeLa cytosol in the presence or absence of RanGTP$_{1-180}$ Q69L (2000 pmol). Unbound proteins were washed out and bound proteins were eluted using 4xSDS-sample buffer. Eluted proteins were separated by SDS-PAGE and analyzed using Western blotting with respective antibodies as indicated. (B) To control the immobilization of MBP or His-NOSIP-MBP, the eluate was analyzed by Western blot using anti-MBP or anti-NOSIP antibodies. (C) The binding of purified NTRs to immobilized His-NOSIP-MBP was analyzed. His-NOSIP-MBP (100 pmol) was immobilized on amylose resin and incubated with 100 pmol of purified His-tagged NTR in the presence or absence of 300 pmol RanGTP$_{1-180}$ Q69L. Bound proteins were eluted using 4xSDS-sample buffer and analyzed by SDS-PAGE followed by Coomassie staining. (D) As a control, MBP-protein was immobilized instead of His-NOSIP-MBP and incubated with His-tagged NTRs.

3.3.2 Competition of NTRs for His-NOSIP-MBP

His-transportin 1 showed the strongest binding to immobilized His-NOSIP-MBP, suggesting that this NTR has the highest affinity to NOSIP. This was analyzed by performing competition binding assays, where transportin 1 competes with other NTRs for NOSIP binding. Basically, the binding assays were performed as above: His-NOSIP-MBP was immobilized and incubated either with 100 pmol of His-importin 13, His-importin 7 or His-S-importin β and His-transportin 1 was added with increasing molar ratios (0.5, 1, 2, 4, 10-fold molar excess). A nuclear transport receptor with a higher affinity to His-NOSIP-MBP should replace or prevent binding of other NTRs. All tested NTRs were shown to bind to His-NOSIP-MBP in the absence of transportin 1. His-S-Importin β was already strongly reduced at a ratio of 1:0.5 (imp β:TNPO 1) and its binding to His-NOSIP-MBP was abolished when His-transportin 1 was added in 2-fold molar excess (Figure 15 C), indicating a lower affinity of importin β compared to transportin 1. His-importin 13 showed a prominent reduction at a 1:1 ratio and His-transportin 1 in a 2-fold molar excess replaced His-importin 13 (Figure 15 A), demonstrating a weaker affinity than transportin 1. Performing the assay using His-importin 13 at a constant concentration and increasing His-S-importin β concentration up to 10-fold molar excess, showed that importin β reduced the binding of importin 13 partially (Figure S 4 A). His-importin 7 and His-importin 5, in contrast, were still detectable when His-transportin 1 was in a 4-fold molar excess and even very weak at a 10-fold molar excess (Figure 15 B, D). This competition assays were also performed in a reversed way, where the His-transportin 1 concentration was kept constant and increasing amounts of the other NTRs were added. In the reverse experiment, importin 7, importin 13 and importin β could not compete with transportin 1 (Figure S 4). His-importin 5, in contrast, could compete with transportin 1 and was able to replace transportin 1 at a 4-fold molar excess. When MBP protein was immobilized instead of His-NOSIP-MBP, no binding was observed showing the specificity of the binding to NOSIP (Figure S 4 B). His-transportin 1 was able to replace all NTRs from NOSIP binding. Only His-importin 5 showed a similar strong binding to NOSIP.

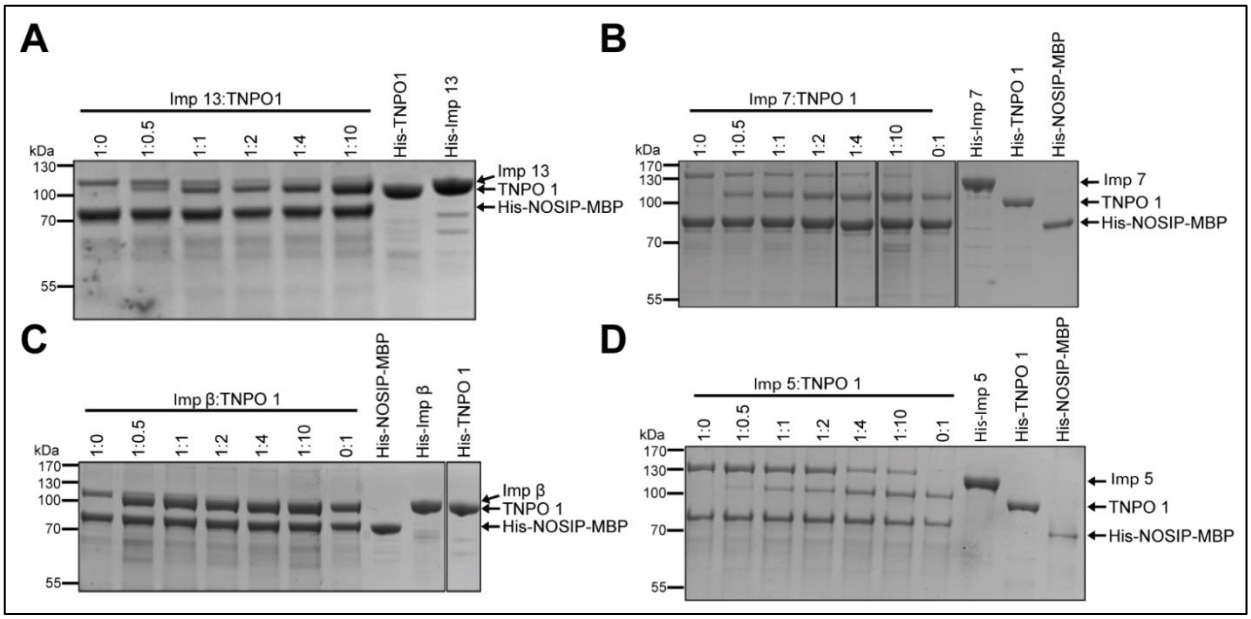

Figure 15: Transportin 1 and importin 5 bind with a higher affinity to NOSIP than importin 13, importin 7 or importin β. For competition binding assays 100 pmol His-NOSIP-MBP was immobilized to amylose resin and incubated with 100 pmol of His-tagged importin 13 (A), importin 7 (B) importin β (C) or importin 5 (D) and increasing amounts of His-transportin 1 (as indicated). Unbound proteins were washed out and bound proteins were eluted using 4xSDS-sample buffer. Eluted proteins were analyzed by SDS-PAGE followed by Coomassie staining. Lines in B and C indicate cropping-sites of the SDS-Gel, all slices belong to the same SDS-Gel and were arranged in the appropriate order.

3.3.3 Importin β and importin 7 are binding to NOSIP in a cooperative manner

In the previous section, His-NOSIP-MBP was shown to interact with importin β and importin 7 when both are present in the reaction. To further analyze if they bind simultaneously to different binding sites on NOSIP or if they bind cooperatively forming a ternary import complex, another binding assay was performed. Again His-NOSIP-MBP was immobilized and incubated with only one NTR or in excess of importin β while importin 7 remains constant or vice versa (Figure 16 A). Both importins were observed to bind to NOSIP independently. Increasing the concentration of importin β to 3- or 5-fold molar excess compared to importin 7 did not affect binding of importin 7, but more importin β bound to NOSIP. In the reverse way, increasing the concentration of importin 7 led to an increased binding of both NTRs to NOSIP (Figure 16 A). This could indicate a cooperative binding of both NTRs, which is limited through the amount of importin 7.

In the previous competition assays, transportin 1 was one of the strongest binding NTRs and was therefore used in the next assay. To test whether the heterodimer of importin β/7 binds stronger than the individual NTRs, a competition assay was

performed. Importin β/7 in the absence of transportin 1 showed binding to NOSIP, whereas in presence of transportin 1 in a molar ratio of 1:1 (heterodimer: TNPO 1) the binding was strongly reduced. Increasing the molar ratio up to 5:1 (importin β/7: TNPO1), increased the amount of bound importin β/7, but it was still less than in the absence of transportin 1 (Figure 16 B). A 3-fold molar excess of His-transportin 1 compared to His-importin β/7 abolished the binding of importin β/7.

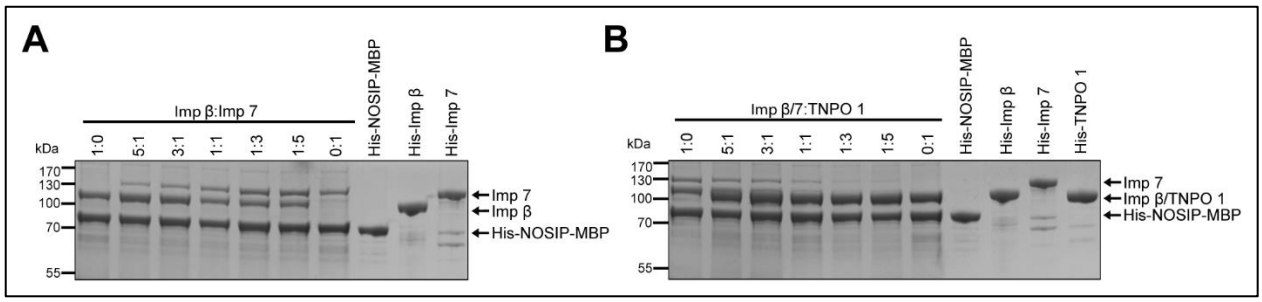

Figure 16: Importin β/7 shows a cooperative binding to NOSIP, but with a lesser affinity than transportin 1. (A) To analyze cooperative binding of importin β/7 to NOSIP, His-NOSIP-MBP was immobilized to amylose resin and incubated with His-imp 7 and His-S-imp β at indicated molar ratios. Unbound proteins were washed out and bound proteins were eluted using 4xSDS-sample buffer. Eluted proteins were analyzed by SDS-PAGE, followed by Coomassie staining. (B) Competition binding assay of importin β/7 and transportin 1 for His-NOSIP-MBP binding. The assay was performed as described in A.

3.3.4 Imp 7, imp β, imp β/7, imp 13 and transportin 1 form stable transport complexes with NOSIP

Various NTRs could be identified to interact with His-NOSIP-MBP in 3.3.1. These interactions were shown to be RanGTP-dependent (Figure 14). To analyze if purified NTRs can form a stable import-complex with NOSIP, size-exclusion chromatography (SEC) was used. SEC is a method to separate proteins or protein-complexes according to their size. Larger proteins or protein complexes elute earlier, and small proteins elute later from the column. To increase the difference in size of His-NOSIP-MBP (~ 77 kDa) to nuclear transport receptors, typically 90-120 kDa, His-tagged NOSIP (~37 kDa), lacking the MBP-tag, was used. A complex of His-NOSIP and His-NTR would have ~130-150 kDa in size, a complex of this size would elute earlier than the unbound NTR.

Transport complexes were formed by incubating His-tagged NTRs with His-NOSIP on ice, prior to injection to the analytical SEC columns. First the formation of an import complex of NOSIP with one NTR was tested. The peaks corresponding to Importin 13 or transportin 1 in complex with NOSIP (brown curves), were shown to elute earlier

than peaks corresponding to importin alone (blue curves) (Figure 17 A-B, graph). Analyzing respective fractions form the SEC runs by SDS-PAGE followed by Coomassie staining, showed that NOSIP, which eluted usually in fractions 5-6, was detected in fractions 3-4 together with importin 13 or transportin 1 (Figure 17 A-B, SDS-gels). To examine whether the formed complex is stable, fractions comprising importin 13-NOSIP complex were pooled, concentrated, and reapplied to SEC. The complex was stable, since only one peak comprising importin 13-NOSIP was observed and addition of $RanGTP_{1-180}$ Q69L resulted in disassembly of the complex. The disassembled SEC curve comprises 3 peaks, corresponding to importin 13, NOSIP and $RanGTP_{1-180}$ Q69L (Figure S 5). Further, the specificity of the formed NOSIP-NTR complex was tested by the addition of a three-fold molar excess of $RanGTP_{1-180}$ Q69L, similar to the conditions in binding- and pull-down assays. Addition of Ran resulted in a dissociated NTR-NOSIP complex (green curves). The reaction importin 13-NOSIP-$RanGTP_{1-180}$ Q69L resulted in a peak comprising free NOSIP and a peak for importin 13 bound to $RanGTP_{1-180}$ Q69L. The size of the importin 13-$RanGTP_{1-180}$ Q69L complex (127 kDa) is similar to importin 13-NOSIP (145 kDa), but eluted later from the SEC column. The later elution can be explained by the flexibility of NTRs and the different packing according to their bound state. Importin 13 was reported to be tighter packed when bound to Ran and more loose when unbound in the so-called cytosolic state or even more extended when bound to its import cargoes MAGO-Y14 (Grünwald *et al.* 2013).

His-NOSIP-MBP bound to importin 7 and importin β individually as well as simultaneously in binding assays (Figure 14). Both NTRs were used to form complexes with His-NOSIP individually and analyzed by SEC. For both NTRs, His-NOSIP co-eluted in the same fractions as the NTR, showing the formation of an import complex (Figure 17 C-D). Peaks of importin 7 or importin β in complex with NOSIP (brown curves) showed a smaller shift than imp 13 or transportin 1 bound to NOSIP and a small shoulder eluting earlier. Further, both chromatograms showed still free NOSIP, indicating an incomplete binding of NOSIP. Another NTR used for complex formation with His-NOSIP was importin 5. When testing importin 5, His-NOSIP was used in a 2-fold molar excess, since a 1:1 ratio did not result in an interaction. Importin 5, in 2-fold molar excess, was observed to bind to NOSIP and form a complex, as seen in the additionally appearing peak (Figure 17 E, brown curve).

Nevertheless, still free importin 5 and NOSIP were detectable indicating that the interaction is weak and possibly requires additional factors.

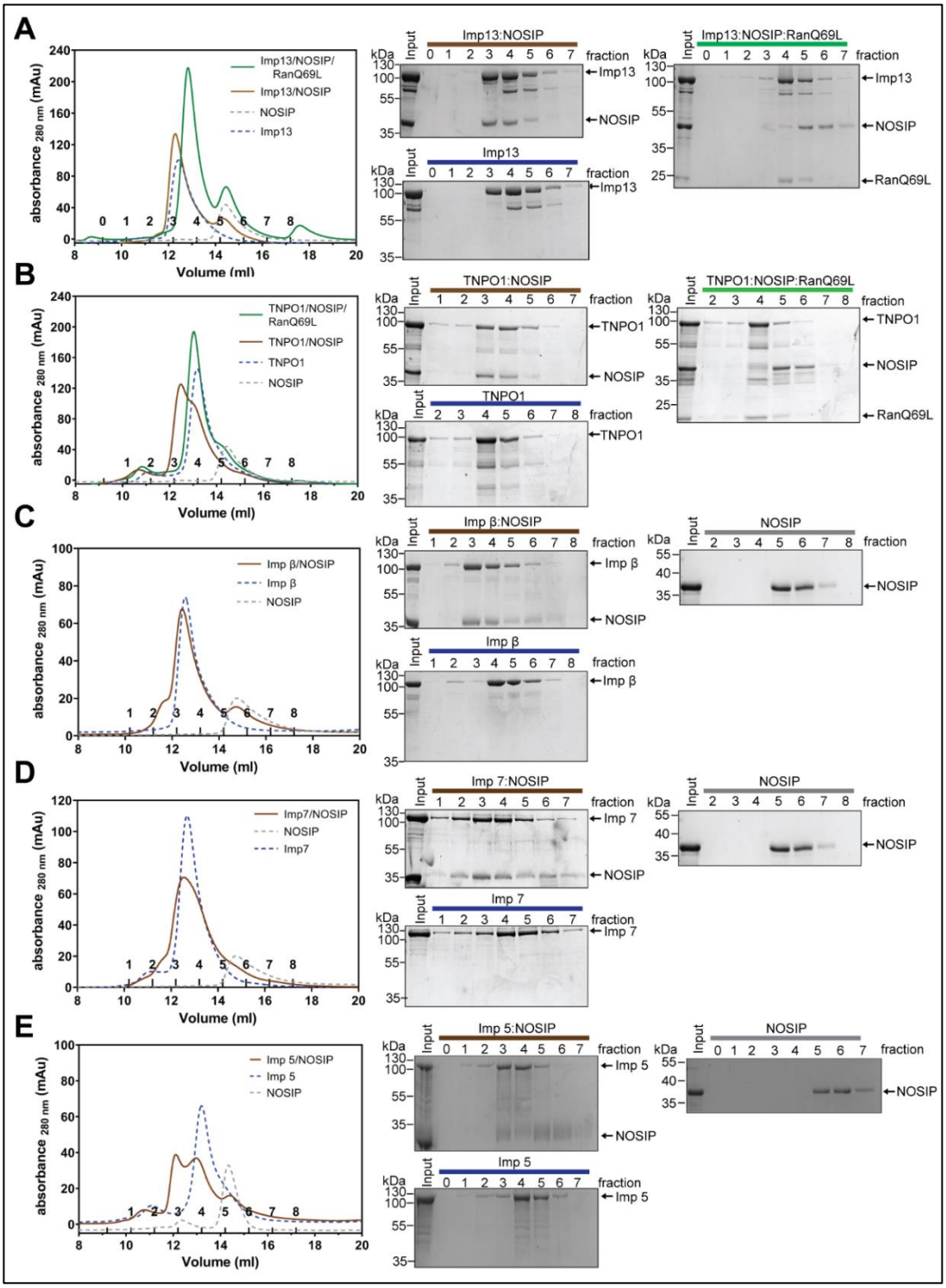

Figure 17: NOSIP forms stable complexes with imp 7, imp 13, imp β and transportin. The transport complexes were formed by incubating His-NOSIP with His-NTR (in a ratio of 1:1, except for importin 5, which was used in a 1:2) for one hour on ice prior to analyses by size exclusion chromatography (SEC). Complex formation was performed using a physiological buffer (TPB), and protein elution was followed by measuring the absorbance at 280 nm. Fractions of eluted peaks were analyzed using SDS-PAGE, followed by Coomassie staining. Transport complexes of His-NOSIP were formed with His-importin 13 (A), His-transportin 1 (B), His-importin β (C), His-importin 7 (D) and His-importin 5 (E). Data were plotted using GraphPad prism 9.

As seen in the binding assays (Figure 14), binding of importin β to NOSIP was independent of importin α. In a previous work NOSIP was suggested to be imported by importin α/β (Schleicher *et al.* 2005), therefore the possible formation of a ternary complex of NOSIP with importin α/β was examined. Formation of a heterodimer of importin α/β (green curve) could be observed, nevertheless the heterodimer formation was incomplete, since there were still peaks for unbound importin α and importin β. The curve of importin α/β with His-NOSIP were the same as for importin α/β alone, except an additional peak of free His-NOSIP (brown curve) (Figure 18). This indicates that no ternary complex of importin α/β and NOSIP was formed. Additionally, the SDS-Gel showed no co-elution of importin α/β and NOSIP under these experimental conditions (Figure 18 A, SDS-gels).

The observations that importin 7 and importin β bind simultaneously or partially cooperatively (Figure 16) and that both formed import complexes individually, suggests the formation of a ternary import complex with NOSIP. This hypothesis was tested by incubating NOSIP together with both NTRs. First, the formation of an importin β/7 heterodimer was tested. As seen in Figure 18 B (cyan curve), the peak of importin β bound to importin 7 eluted ~1 mL earlier and contained both NTRs. This heterodimer formed a ternary complex with His-NOSIP, as seen in the brown curve (Figure 18 B). The addition of a 3-fold molar excess of $RanGTP_{1\text{-}180}$ Q69L led to the dissociation of His-NOSIP from the heterodimer and a partial dissociation of the heterodimer (Figure 18 B, green curve). Furthermore, a shortened importin 7 construct (importin 7ΔC) comprising importin 7 aa 1-1001 was used. This construct lacks the last 37 residues, which were shown to be necessary for the heterodimer formation with importin β (Ivic *et al.* 2019). Importin 7ΔC did not form a heterodimer with importin β (Figure 18 D). Further, no ternary import complex with importin β and NOSIP (Figure 18 C) was formed. The eluted peak corresponds to the retention volume of the individual NTRs bound to NOSIP (Figure 18 C), indicating the formation of a ternary complex. All together NOSIP formed transport complexes with all tested NTRs or with combinations of them, except a ternary complex with importin α/β.

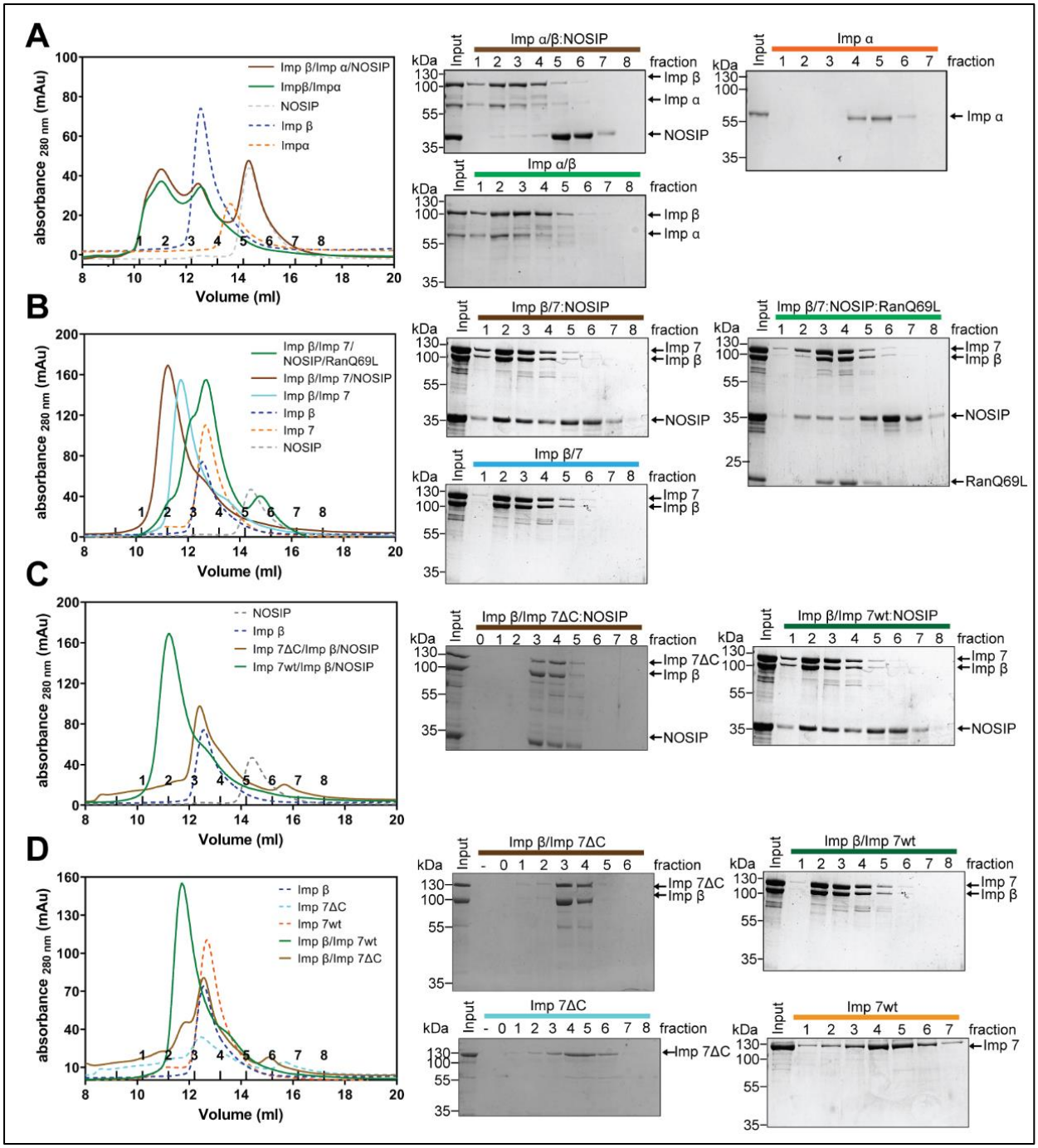

Figure 18: NOSIP forms a stable complex with imp β/7 but not with importin α/β. (A-D) The transport complexes were formed by incubating His-NOSIP with His-NTR1/His-NTR2 (in a ratio of 3:1:1) for one hour on ice prior to analyses by size exclusion chromatography (SEC). Complex formation was performed using physiological buffer (TPB) and protein elution was followed by measuring the absorbance at 280 nm. Fractions of eluted peaks were analyzed using SDS-PAGE followed by Coomassie staining. Transport complexes of His-NOSIP were formed with importin α/β (A) and imp β/7 (B). As specificity control of imp β/7 ternary complex formation an importin 7 deletion construct, lacking the last 37 residues (importin 7ΔC), important for heterodimer formation with importin β, was used. (C) Complex formation of imp β/7 or imp β/7ΔC with His-NOSIP. (D) Formation of importin β/7 heterodimer, using either full-length importin 7 (Imp 7wt) or importin 7ΔC. Data were plotted using GraphPad prism 9. wt - wildtype

3.3.5 Binding of NOSIP or Importin α to importin β is mutually exclusive

Importin α was suggested to bind NOSIP by a non-conventional bpNLS and to import NOSIP in concert with importin β (Schleicher *et al.* 2005).This was determined by a pull-down assay using immobilized GST-importin α. In this work a similar experiment was performed, where His-NOSIP-MBP was immobilized and incubated with HeLa lysate. Binding of importin α to NOSIP was detected. Nevertheless, using purified proteins to perform binding assays, no binding of His-importin α in combination with His-S-importin β was observed. Rather a binding of His-S-importin β, independent of His-importin α was detected (Figure 14). Additionally, no stable import complex of His-importin α/β with NOSIP could be formed, but a complex of His-S-importin β with NOSIP could be formed (Figure 17 C, Figure 18 A). In view of these results NOSIP probably interacts with importin β directly, like PTHrP (Cingolani *et al.* 2002), Rev (Truant and Cullen 1999) or SREBP (Lee *et al.* 2003) and therefore would compete for binding of importin β with importin α. The competition of importin α and NOSIP for importin β was analyzed in a binding assay. His-S-importin β was immobilized using the S-protein tag and incubated with both or each binding partner individually in different molar ratios. His-Importin α as well as His-NOSIP bound to importin β individually. When His-importin α and His-NOSIP were used in a 1:1 ratio, both proteins were binding, but His-NOSIP bound less compared to the reaction lacking His-importin α. Increasing the amount of His-importin α to a 3- or 10-fold molar excess prevented binding of His-NOSIP (Figure 19 A). In the reverse reaction, where His-NOSIP was increased, binding of His-importin α was only partially decreased and His-NOSIP, when in 10-fold molar excess, bound in a similar amount as in the absence of His-importin α (Figure 19 A).

Since both compete for importin β binding, it was tested if they compete for the same binding-site. Importin α binds to importin β via the IBB domain of importin α (Cingolani *et al.* 1999). Therefore, the binding of His-S-importin β full-length (FL) or N-terminal and C-terminal His-S-importin β fragments to GST-NOSIP or GST-IBB was analyzed. The N-terminal fragment, His-S-importin βΔC (aa 1-396), is deficient in binding the GST-IBB-domain and the C-terminal fragment, His-S-importin βΔN (aa 304-876), is deficient in binding RanGTP. The GST-IBB domain bound to His-S-importin βΔN

(comprising all residues shown to be important for IBB binding (Cingolani *et al.* 1999)) and His-S-importin β FL, but not to His-S-importin βΔC, as expected. In contrast to this, GST-NOSIP bound strongly to His-S-importin βΔC or His-S-importin β FL and additionally weaker to His-S-importin βΔN (Figure 19 B).

In conclusion, NOSIP was shown to compete with importin α for importin β binding. In contrast to importin α, NOSIP bound to the N-terminal arch of importin β, whereas the IBB domain of importin α bound to the C-terminal arch of importin β. The binding of NOSIP or importin α seems to be mutually exclusive, despite binding to different sites on importin β. This can be explained through partially overlapping binding-sites, as seen for NOSIP which interacts in addition to the N-terminal also weakly with the C-terminal arch.

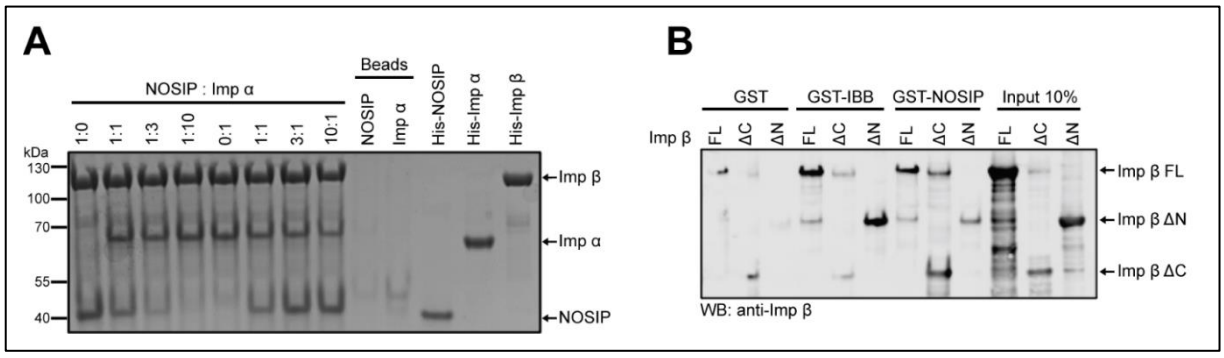

Figure 19: Binding of NOSIP or importin α to importin β is mutually exclusive. (A) For a competition binding assay of importin α and NOSIP for importin β, 100 pmol His-S- importin β was immobilized on S-protein beads and incubated with different ratios of His-NOSIP to His-importin α, as indicated (a ratio of 1:1 corresponds to 100 pmol:100 pmol). As control only S-Protein Beads (Beads) were incubated with His-NOSIP or His-importin α. Unbound proteins were washed out and bound proteins were eluted using 4xSDS-sample buffer, analyzed by SDS-PAGE followed, by Coomassie staining. (B) To analyze if NOSIP and importin α bind to the same binding-site on importin β, GST-tagged IBB (importin β-binding domain of importin α)-domain, NOSIP or GST alone were immobilized to glutathione-sepharose beads and incubated with importin βΔC (aa 1-396), importin βΔN (aa 304-876) or importin β FL (full-length). Unbound proteins were washed out and bound proteins were eluted using 4xSDS-sample buffer. Eluted proteins were separated by SDS-PAGE and analyzed by Western blotting using an anti-importin β antibody.

3.3.6 Imp 13, -7, -7/β, -β and TNPO1 can mediate nuclear import of His-NOSIP-MBP in digitonin permeabilized HeLa cells

In the previous section it was shown that NOSIP interacts with various NTRs and forms stable import complexes with them. To test if these import complexes can mediate nuclear import of NOSIP, the established import-assay in digitonin-permeabilized cells was used (Adam *et al.* 1990). In this assay, the plasma membrane of HeLa cells was selectively permeabilized with digitonin, while the nuclear membrane remained intact.

This allows for the replacement of the cytosol with a transport reaction mix, to analyze the import of a specific protein by a specific NTR (Figure 20 A). The transport reactions were performed at 30 °C or at 4 °C, where no or very little transport occurs. In this assay His-NOSIP-MBP was used. In a control reaction lacking any NTRs or cytosol, and only containing His-NOSIP-MBP and buffer, no nuclear signal was observed, indicating that NOSIP, which is too big for passive diffusion, is not able to enter the nucleus on its own (Figure 20 C). A transport reaction containing all components and cytosol (cytosol) could import His-NOSIP-MBP specifically into the nucleus. Additionally, the same reaction was performed in the presence of WGA (wheat germ agglutinin), which binds to the N-acetylglucosamine of some Nups, and thereby inhibits active nuclear import. The reaction with WGA led to the cytoplasmic retention of His-NOSIP-MBP (Figure 20 C), indicating the specificity of this assay.

To analyze the import of His-NOSIP-MBP by a single NTR, the purified His-tagged NTRs were added to the transport reaction instead of cytosol. Transportin 1 and importin 13 were observed to import NOSIP and most cells showed a clear nuclear signal for His-NOSIP-MBP (Figure 20 B). Importin β, importin 7 and importin β/7 were shown to import His-NOSIP-MBP in some cells, the heterodimer more efficiently than the monomers. Under these conditions some cells showed a nuclear signal, whereas almost all cells showed a cytoplasmic signal for NOSIP. For importin α/β, import was less efficient than for importin β alone, which is in line with the observation of previous experiments that importin α/β, at least *in vitro,* does not play a significant role. Importin 5 did not show any import activity, since all cells showed only a strong cytoplasmic signal for His-NOSIP-MBP (Figure 20 B). In summary, His-NOSIP-MBP was shown to be imported by transportin 1, importin 13, importin β, importin 7 and importin β/7, where transportin 1 and importin 13 showed the highest efficiency compared to the other NTRs.

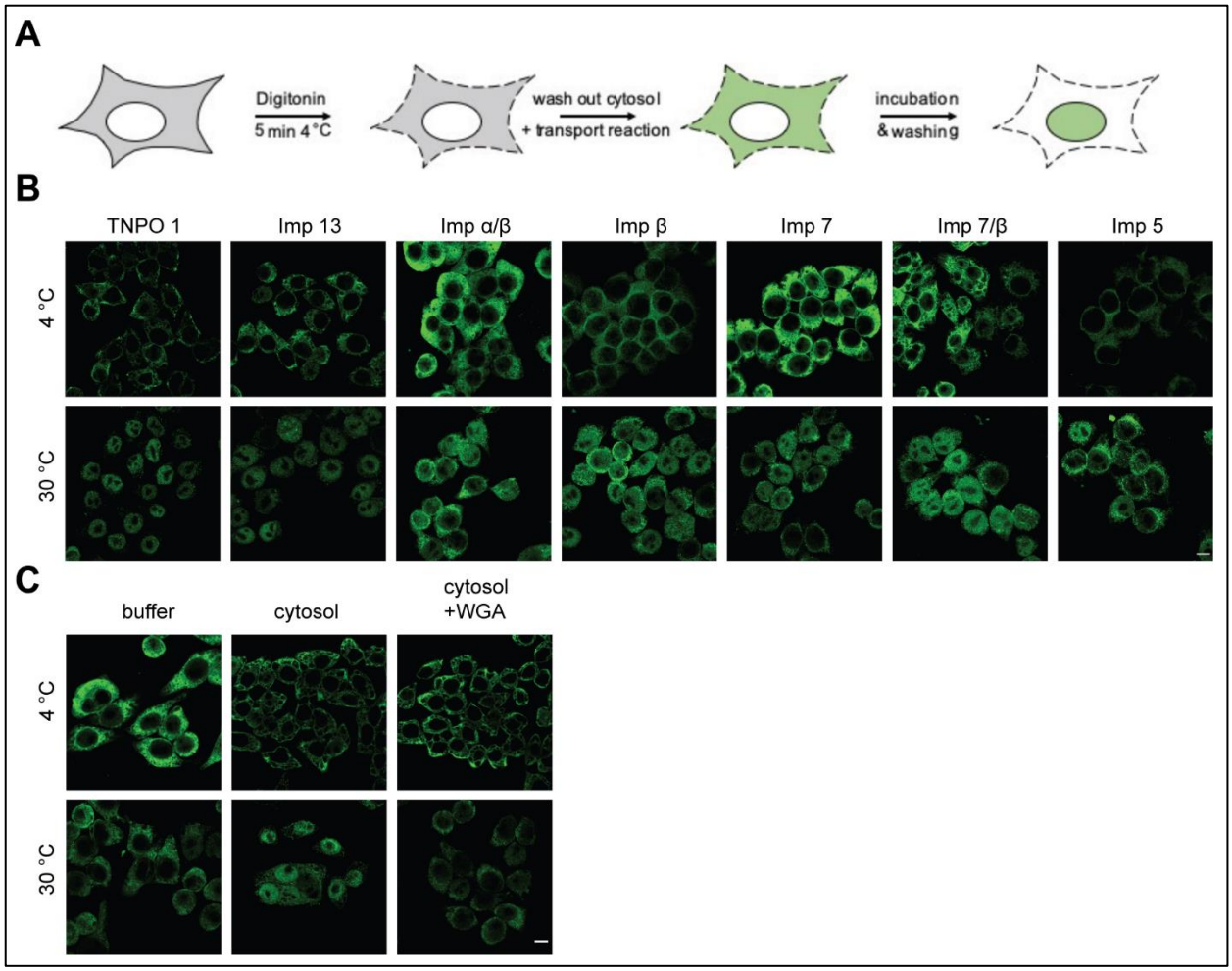

Figure 20: His-NOSIP-MBP can be imported by Imp 13, -7, -7/β, -β and TNPO 1 in digitonin-permeabilized HeLa P4 cells. (A) Schematic overview of the import assay in digitonin permeabilized HeLa P4 cells. The plasma membrane was permeabilized, while the nuclear membrane remained intact, using 0.004% Digitonin for 5 min at 4 °C. Cytosol was washed out by 1x TPB and replaced by a transport reaction mix, containing an energy-regeneration system, Ran, BSA, 500 nM His-NOSIP-MBP and 1 µM NTR or cytosol (optionally WGA (wheat-germ agglutinin) was added to cytosol to block active nuclear import). Cells were incubated for 30 min at 30°C or at 4 °C, after the incubation, cells were washed three times to wash out cytosolic proteins and fixed. (B-C) Nuclear import assay was performed as described in A and the used NTRs are indicated. His-NOSIP-MBP was visualized by indirect immunofluorescence using an anti-MBP antibody. Scale bar 10 µM.

3.4 Characterization of the previously defined nuclear localization signal

3.4.1 Mutation of NOSIP bpNLS impairs the interaction with NTRs

A common technique to analyze nuclear transport are mutational studies, where the residues of the NLS are mutated, mostly the basic residues lysine (K) or arginine (R) to Alanine (A). For NOSIP a non-conventional bpNLS was suggested and shown to be important for the localization of transiently transfected myc-NOSIP. It was shown that mutating the bpNLS or deleting parts of it led to a cytoplasmic accumulation of NOSIP, whereas the wildtype variant of NOSIP was localized to the nucleus (Schleicher *et al.* 2005). To study the relevance of the identified bpNLS for the binding

of NOSIP to all NTRs, a mutant, where the first basic patch was mutated was chosen for analysis in this work. In this mutant, named NOSIP^{K78AK79A}, two lysine residues were mutated to alanine residues (Figure 21 A). The double mutation was inserted into NOSIP-HA and GFP-GST-NOSIP and was shown to prevent NOSIPs nuclear accumulation in HeLa cells (Figure 21 B). NOSIP^{K78AK79A}-HA showed an equal distribution between nucleus and cytoplasm, whereas the wildtype showed mainly a nuclear localization. GFP-GST-NOSIP^{K78AK79A} was excluded from the nucleus and was localized exclusively to the cytoplasm in contrast to the wildtype which is mainly nuclear and, in some cells, equally distributed. This demonstrates that the earlier identified bpNLS is needed for the localization of NOSIP.

To analyze whether the altered localization of NOSIP is based on a loss of interaction with NTRs binding assays were performed (Figure 14). Either His-NOSIP-MBP or His-NOSIP^{K78AK79A}-MBP was immobilized and incubated with respective purified NTRs. Imp β, Imp 7, Imp 7/β and Imp 13 showed a strongly reduced binding to His-NOSIP^{K78AK79A}-MBP compared to His-NOSIP-MBP. In contrast, the binding of transportin 1 to His-NOSIP^{K78AK79A}-MBP was still partially detectable (Figure 22 A). Importin 5, which was shown to bind in a RanGTP-dependent manner to His-NOSIP-MBP, but unable to form a stable complex or to be imported in digitonin-permeabilized HeLa cells (Figure 17, Figure 20), bound His-NOSIP^{K78AK79A}-MBP surprisingly in the same manner as the wildtype (Figure 22 A). The main nuclear exportin, CRM1, did not bind to His-NOSIP^{K78AK79A}-MBP or the wildtype, as expected, since binding to the wildtype can only be observed in the presence of RanGTP (compare Figure 14).

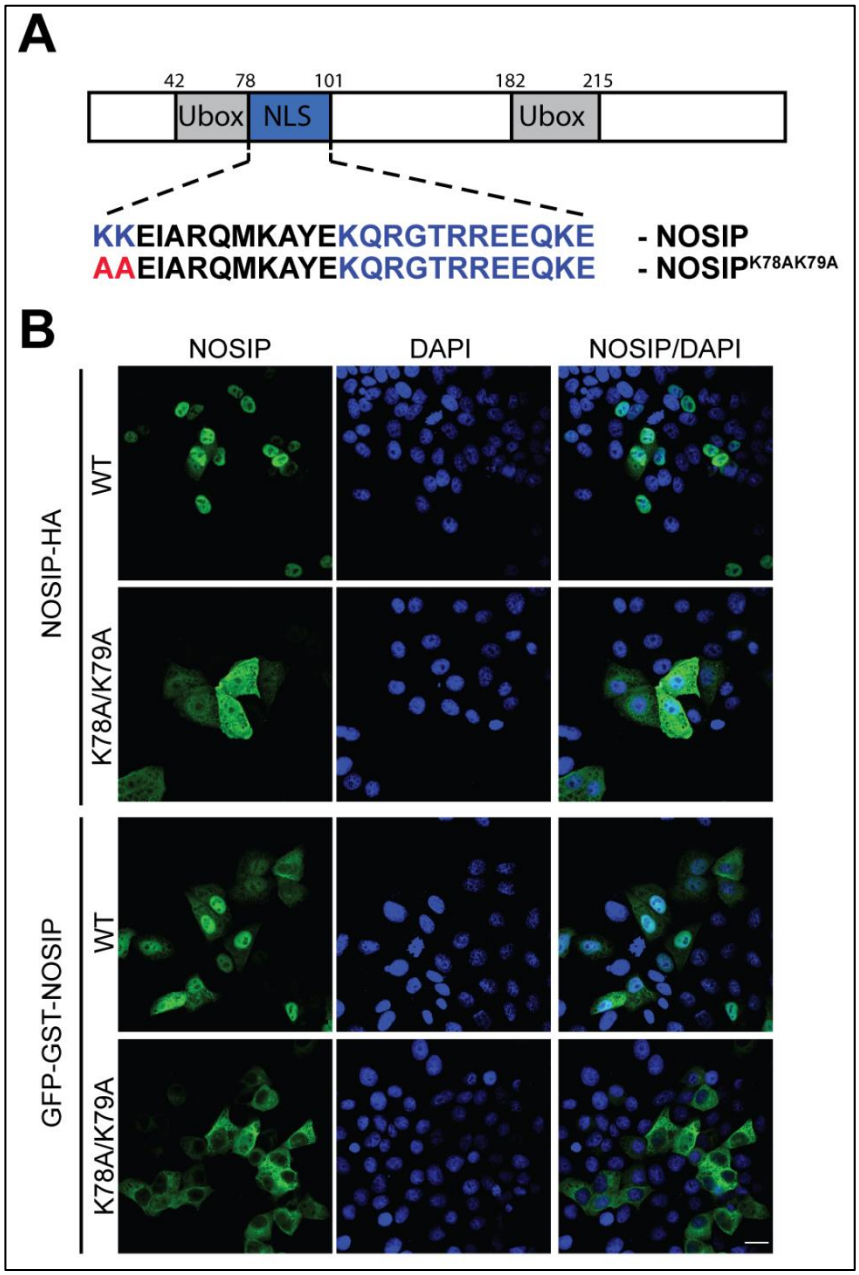

Figure 21: Localization of the NOSIP^{K78AK79A} mutant in HeLa cells. (A) Schematic overview of NOSIP. Depicted in gray is NOSIPs conserved Ubox-like domain, which is split into two halves by 104 amino acids. The bi-partite nuclear localization signal (NLS) comprising amino acids 78 to 101 is depicted in blue. The bi-partite NLS consist of two basic clusters (marked in blue in the sequence), which are separated by a 10 amino acid linker (maker in black in the sequence). In the mutant NOSIP^{K78AK79A} the first basic cluster, consisting of two lysine residues, is mutated to alanine residues. (B) The mutation K78AK79A was introduced in NOSIP-HA and GFP-GST-NOSIP and was used for transfection into HeLa cells to analyze the localization of NOSIP NLS mutant. GFP-GST-NOSIP was visualized using the GFP-tag. NOSIP-HA was visualized by indirect immunofluorescence using an antibody against the HA-tag. Scale bar 20 µM.

To further characterize the bpNLS, the mutation was inserted in the His-NOSIP construct. His-NOSIP^{K78AK79A} was used to form a stable complex with NTRs. His-transportin 1 showed a strong binding and the most efficient import in the import assay and was therefore assumed to be representative for the other NTRs that NOSIP interacts with. For complex formation, His-NOSIP^{K78AK79A} was used in 2-fold molar

excess and incubated with His-transportin for 1 h on ice and then subjected to SEC. As seen in Figure 22 (B), two peaks were eluted, one contained free His-NOSIP^{K78AK79A} and one His-transportin- His-NOSIP^{K78AK79A}. The analysis of the fractions by SDS-PAGE showed that only a minor fraction of His-NOSIP^{K78AK79A} co-eluted with His-transportin 1, whereas the majority of His-NOSIP^{K78AK79A} eluted without His-transportin 1.

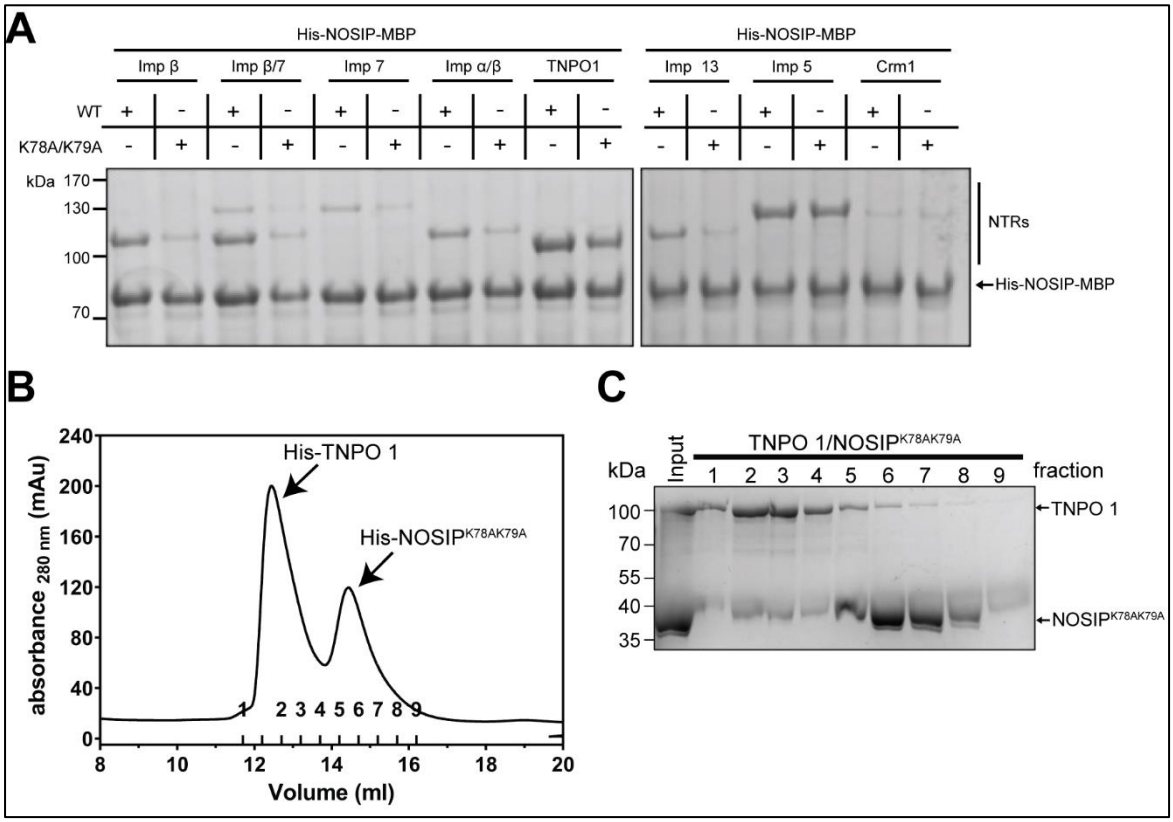

Figure 22: Mutation of NOSIPs NLS impairs its interaction with nuclear transport receptors. (A) The binding of purified NTRs to immobilized His-NOSIP-MBP wildtype or K78AK79A mutant was analyzed in a binding assay. Therefore 100 pmol of His-NOSIP-MBP was immobilized on 10 µL amylose resin and incubated with 100 pmol purified NTR as indicated. Unbound proteins were washed out and bound proteins were eluted using 4x SDS-sample buffer and analyzed by SDS-PAGE followed by Coomassie staining. (B) 40 µM His-NOSIP^{K78AK79A} were incubated with 20 µM His-transportin 1 and subjected to size exclusion chromatography. The absorbance at 280 nm was monitored and (C) fractions corresponding to peaks were analyzed by SDS-PAGE followed by Coomassie staining.

Taken together, these results indicate that the identified bpNLS is crucial for the interaction with nuclear transport receptors. The mutation of the first basic cluster lead to reduced interaction with NTRs and prevents the formation of stable transport complexes.

3.4.2 Nuclear import of NOSIP^{K78AK79A} is impaired *in vitro*

As shown above, the bpNLS of NOSIP is crucial for the binding to importins and the formation of transport complexes. Next, it was analyzed if the mutation had an effect on nuclear import in digitonin-permeabilized HeLa cells. The assay was performed as before using His-NOSIP-MBP or His-NOSIP^{K78AK79A}-MBP as import cargo. Overall, the import efficiency was reduced compared to the wildtype. The controls using only buffer or cytosol with WGA demonstrate the functionality of the assay. The positive control with cytosol showed nuclear import of His-NOSIP^{K78AK79A}-MBP, but less efficient than the wildtype. Transportin 1 showed still some import activity and importin 13, -β, -7/β, -7 and -α/β showed import activity only in single cells, albeit with diminished efficiency (Figure 23 A). Since the import efficiency varied from cell to cell, 300-1000 cells were analyzed for their nuclear fluorescence to quantify the transport efficiency. This quantification was done for wildtype and mutant NOSIP. The import efficiency of His-NOSIP^{K78AK79A}-MBP was strongly reduced when compared to wildtype His-NOSIP-MBP (Figure 23 B).

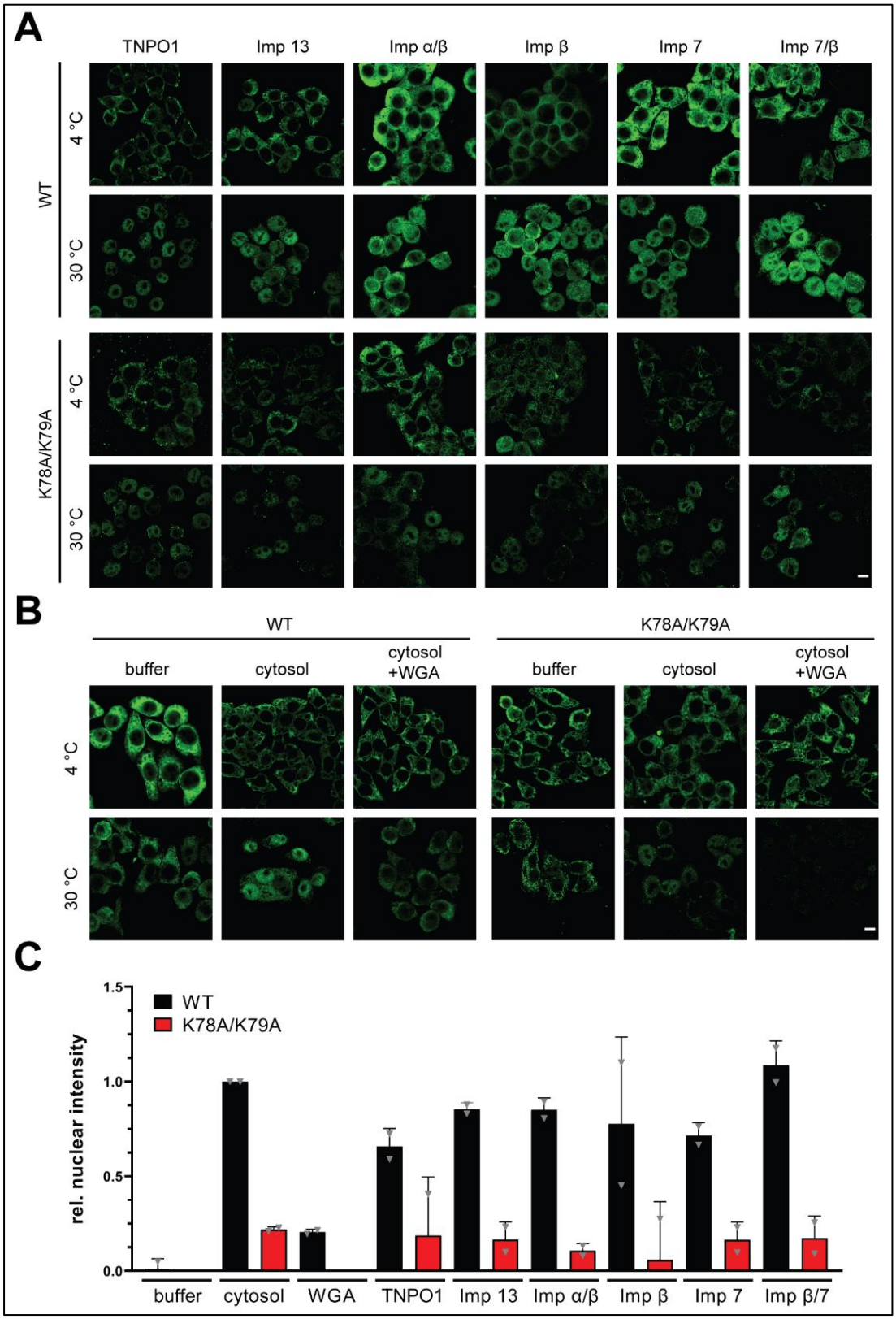

Figure 23: Mutation of the NOSIP bpNLS lead to diminished nuclear import of NOSIP in digitonin-permeabilized HeLa cells. (A) Nuclear import assay was performed using purified Imp 13, -7, -α, -β and TNPO 1. As a cargo either His-NOSIP-MBP wildtype (WT) or His-NOSIP^{K78AK79A}-MBP (K78A/K79A) was used and visualized by indirect immunofluorescence using an anti-MBP antibody. Scale bar 10 µM. (B) Quantification of the results presented in A. The mean nuclear fluorescence intensities of 4 °C reactions were subtracted from the respective 37 °C values and normalized to the value obtained for the reaction containing cytosol of wildtype His-NOSIP-MBP, which was arbitrarily set to 1.

3.4.3 The non-consensus bi-partite NLS alone is not sufficient for the localization of NOSIP

As shown previously, the bpNLS of NOSIP is important for the interaction with NTRs. Classic NLS or bi-partite NLS are usually known to bind to importin α/β. For other NTRs, like transportin 1 or importin 13 these are PY-NLSs and RG/RGG motifs or folded domains, respectively. NOSIPs bpNLS was shown to be important for the interaction with various NTRs (Figure 14-Figure 20), except for importin 5, which still bound to His-NOSIP-MBP when the bpNLS was mutated, but was not able to import NOSIP. To further analyze the interaction of NOSIP with its NTRs and if different NTRs bind different regions, NOSIP fragments were used.

The following His-NOSIP-MBP fragments of NOSIP were cloned and used for binding assays: NOSIP$^{1-110}$, NOSIP $^{111-240}$, NOSIP$^{1-240}$ and NOSIP$^{111-301}$. These fragments were immobilized and incubated with His-tagged NTRs as indicated. As a specificity control, MBP was immobilized. When immobilizing His-NOSIP-MBP FL (full-length), all tested NTRs (imp 7, imp β, TNPO 1 and imp13) bound, as seen before, and none bound to immobilized MBP (Figure 24 E-F). Using the bpNLS-containing fragment, His-NOSIP$^{1-110}$-MBP, binding of all NTRs was observed but to a lesser extent than to His-NOSIP-MBP full-length (Figure 24 A). Surprisingly, the extended fragment His-NOSIP$^{1-240}$-MBP bound as strongly as His-NOSIP-MBP FL to the NTRs (Figure 24 B). For His-NOSIP$^{111-240}$-MBP or His-NOSIP$^{111-301}$-MBP, which lack the bpNLS (aa 78-101), no binding was observed (Figure 24 C-D).

Assuming that the identified bpNLS is crucial for the interaction with NTRs and for the localization of NOSIP in cells, it would be expected that the fragment His-NOSIP$^{1-110}$-MBP, which contains the bpNLS, would bind to the NTRs as the FL protein. But surprisingly it did not, instead the fragment extended to the C-terminal end His-NOSIP$^{1-240}$-MBP, bound to NTRs like the full-length protein.

This led to the question if the bpNLS alone, fused to a bigger protein above the size-limit for passive diffusion, would locate in the nucleus in cells. Therefore, NOSIP$^{75-102}$ containing the bpNLS, was fused to GFP and GST to increase the size to ~60 kDa. GFP-GST-NOSIP$^{75-102}$ showed an equal distribution between nucleus and cytoplasm (Figure 25 A). The fused GFP-GST tag alone did not enter the nucleus, but the GFP-

GST tag fused to full-length NOSIP localized predominantly to the nucleus (Figure 25 A). This showed that the bpNLS fused to GFP-GST was not sufficient to localize mainly to the nucleus as GFP-GST-NOSIP FL did.

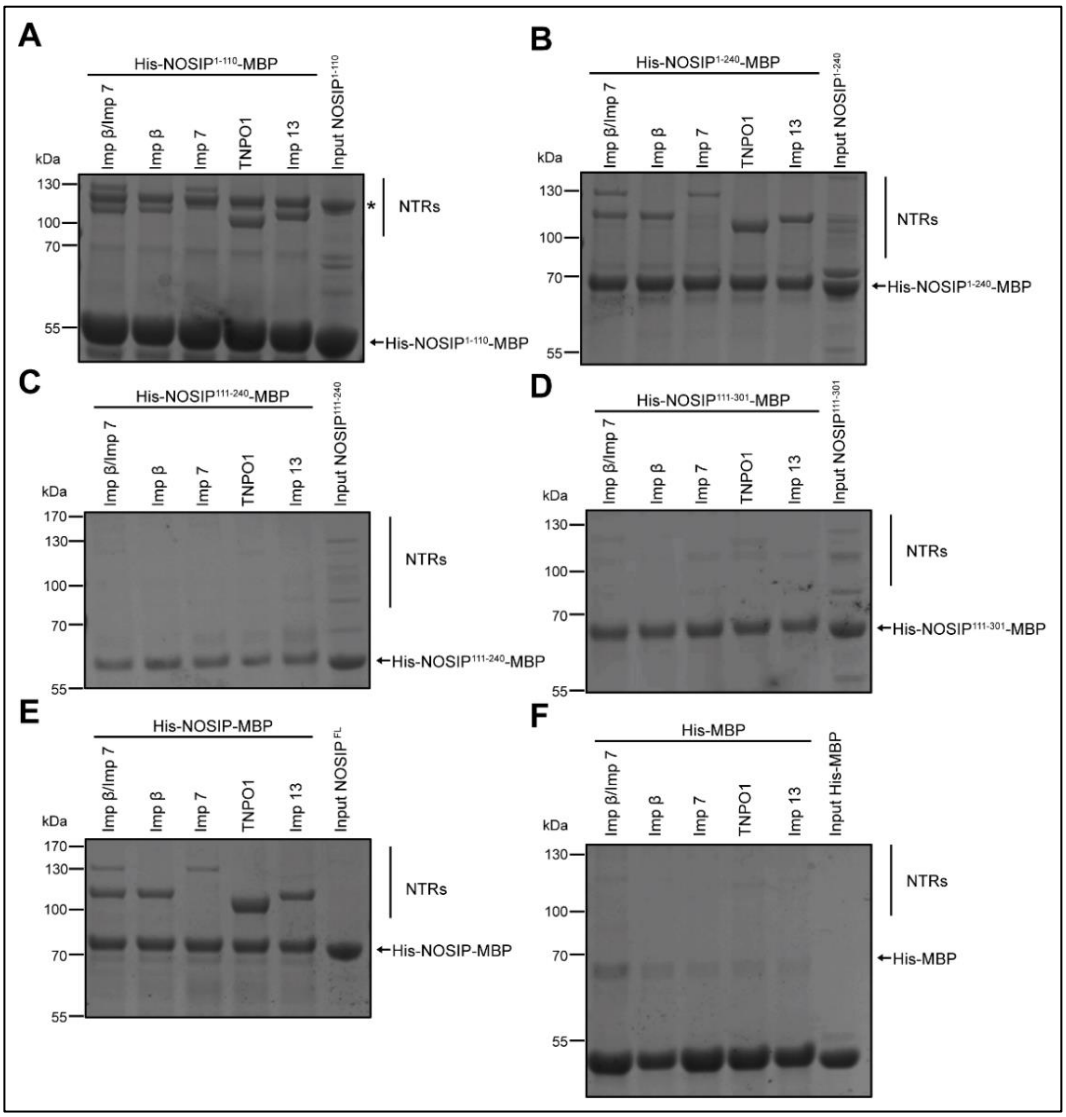

Figure 24: The bpNLS is not sufficient enough for the interaction with NTRs. The binding of NTRs to different His-NOSIP-MBP fragments was analyzed using binding assays. His-NOSIP-MBP fragments aa 1-110 (A), aa 1-240 (B), aa 111-240 (C), aa 111-301 (D), full-length (E) or His-MBP alone (F) were immobilized to amylose resin beads and incubated with purified NTRs as indicated. Unbound proteins were washed out and bound proteins were eluted using 4xSDS-sample buffer. Eluates were analyzed by SDS-PAGE followed by Coomassie staining. Asterisks (*) indicate impurities resulting from the immobilized protein. Note the strength that the band intensity of immobilized His-NOSIP- His-NOSIP$^{1-110}$-MBP is stronger, which resulted from different loading of the SDS-Gels

To further analyze, which regions of NOSIP are important for the nuclear localization of NOSIP, several fragments of NOSIP were used. The fragments 1-110, 1-240, 111-240 and 111-301, were fused to GFP-GST and analyzed for their localization. Surprisingly, the construct GFP-GST-NOSIP$^{1-110}$ only localized to the cytoplasm and not as expected like the bpNLS fragment (Figure 25 A-B). The fragment GFP-GST-NOSIP$^{1-240}$ aggregated within the cytoplasm. GFP-GST-NOSIP$^{111-240}$ partially localized to the nucleus, in a similar way as the bpNLS fragment (Figure 25 B). The extended fragment GFP-GST-NOSIP$^{111-301}$ localized similar as GFP-GST-NOSIP$^{111-240}$ (Figure 25 B). These results were in parts contrary to the binding assay, where NOSIP$^{1-240}$ bound to NTRs like the FL protein, but here it aggregated in the cytoplasm of HeLa cells. Since the construct His-NOSIP$^{1-240}$-MBP bound to NTRs and the construct GFP-GST-NOSIP$^{111-240}$ localized partially to the nucleus, as the bpNLS, the GFP-GST-NOSIP$^{1-110}$ fragment was extended C-terminally. The fragment was extended in steps of 10 amino acids up to residue 160. None of these fragments localized to the nucleus, instead they were mainly cytoplasmic (Figure 25 C). To exclude that N-terminal residues in front of the NLS inhibit the nuclear localization, the bpNLS fragment starting at residue 75 was extended to residue 120, 140, 160, 180 and 200. When extended up to residues 120 or 140, the nuclear accumulation was slightly increased, but showed still a clear signal in the cytoplasm (Figure 25 D). Further extension resulted in a more pronounced cytoplasmic localization. In a next step, the construct GFP-GST-NOSIP$^{1-240}$, which was seen to bind as His-MBP-tagged protein similar to the NTRs as the wildtype, was extended to the C-terminal end to prevent aggregation. GFP-GST-NOSIP$^{1-285}$ did not aggregate anymore and localized, like the full-length protein, mainly nuclear in HeLa cells (Figure 25 E). Shortening the N-terminal end of this construct by 25 residues (GFP-GST-NOSIP$^{25-285}$) did not affect the localization, but shortening it to GFP-GST-NOSIP$^{55-285}$ or GFP-GST-NOSIP$^{75-285}$ led to a loss of nuclear NOSIP (Figure 25 E).

Overall, these constructs demonstrate that the nuclear import of NOSIP is more complex than expected. The bpNLS of NOSIP is not sufficient for its strong nuclear accumulation. Predicting potential cNLSs using the cNLS-Mapper (Kosugi *et al.* 2009) resulted in several predictions with a very low score, only NOSIP$^{150-180}$ resulted in a higher score of 6.7 for a bpNLS (Table S 8). A score of 6.7 corresponds to a partially nuclear localization. However, the construct NOSIP$^{75-180}$, which includes the bpNLS

and the potential predicted second bpNLS did not localize to the nucleus as the FL protein. In general, some residues between the bpNLS up to residue 285, as well as residues between 25 and 55 of NOSIP, are important for a strong nuclear accumulation (Figure 25 F). This points to a more complex recognition by NTRs through several interaction sites, instead of a linear sequence.

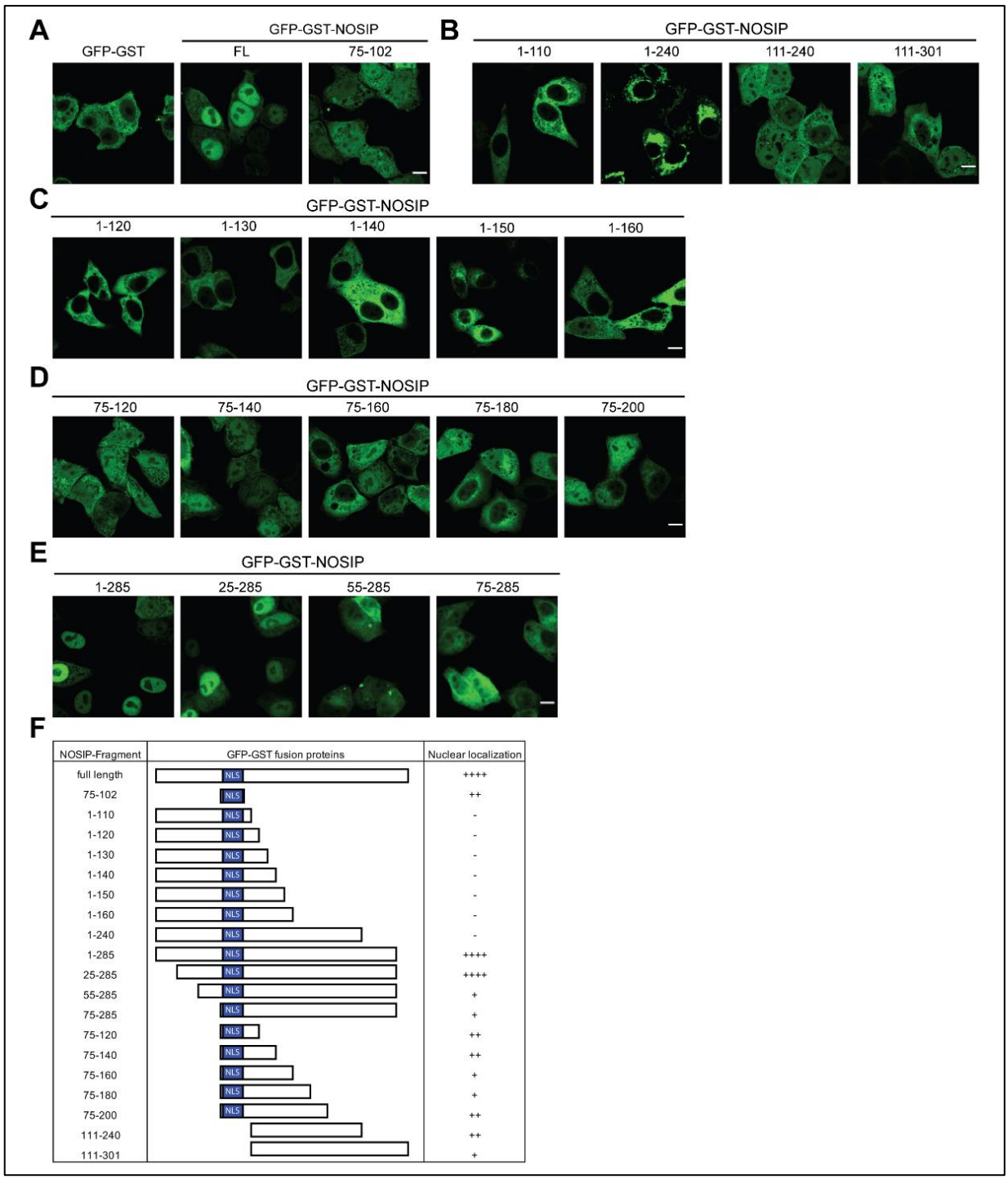

Figure 25: Transfection of GFP-GST-NOSIP fragments in HeLa P4 cells. Plasmids coding for respective GFP-GST-NOSIP fragments were transfected using the calcium phosphate method. (A) Transfection of GFP-GST vector, full-length GFP-GST-NOSIP or the bpNLS fragment fused to GFP-GST. (B) Transfection of C-terminal

deletion fragments of GFP-GST-NOSIP (1-120, -130, -140, -150, -160). (C) Transfection of extended bpNLS GFP-GST-NOSIP fragments (75-120, -140, -160, -180, -200). (E) Transfection of different GFP-GST-NOSIP fragments deleted for the last 16 residues or deleted for those in combination with N-terminal deletions (first 24, 54 or 74 residues). Scale bar 10 µm. (F) Schematic overview of the used fragments in combination with localization to the nucleus. Strong nuclear accumulation (++++), slightly enriched in the nucleus (++), more cytoplasmic localization with a minor nuclear signal (+), exclusively cytoplasmic signal (-)

3.5 Transportin 1 is the major nuclear transport receptor for NOSIP

As shown before, NOSIP binds to various NTRs in HeLa cell lysate or to recombinantly expressed and purified NTRs (Figure 14). Among all the NTRs tested, the interaction with transportin 1 was observed to be the strongest, since His-transportin 1 could outcompete all other tested NTRs except importin 5 which was shown to bind similar (Figure 15). Despite the similar binding of importin 5, no proper import complex could be formed and no active import of NOSIP by importin 5 could be observed. However, His-transportin 1, as well as His-Importin 13, were observed to import His-NOSIP-MBP with the highest efficiency in digitonin-permeabilized HeLa cells (Figure 20 and Figure 23).

These experiments suggest that transportin 1 is the preferred NTR for NOSIP. This is in contrast to the literature, where importin α/β was shown to import NOSIP (Schleicher *et al.* 2005). To further analyze nuclear transport of NOSIP in living cells, HeLa cells were transfected with the established peptide inhibitors of the importin α/β or transportin 1 import pathway, Bimax2 or M9M, respectively.

3.5.1 Inhibition of transportin 1 or importin α leads to a mis-localization of NOSIP

To analyze the effect of the peptide inhibitors M9M or bimax2, the peptide fragments were fused to RFP (red fluorescence protein) or to GFP and transfected in HeLa cells. Inhibitors were either transfected alone to analyze the effect on endogenous NOSIP or together with NOSIP-HA or GFP-GST-NOSIP to analyze the effect on over-expressed NOSIP. As specificity control for the peptide inhibitors shuttling constructs, containing an NES fused to an mTagBFP2 (blue fluorescent protein) and either a cNLS or an M9-sequence, were used as before (see section 3.1.1).

The nuclear accumulation of BFP-M9 was abolished by GFP-M9M, but not by GFP-Bimax2 (Figure 26 A). The BFP-cNLS was affected by GFP-Bimax2, but not by GFP-M9M, demonstrating the specificity of the inhibitors. Control constructs were

transfected with GFP-tagged inhibitors, and nuclei were detected by a far-red DNA staining using DRAQ5.

Co-transfection of NOSIP-HA with GFP-bimax2 or GFP-M9M showed an effect of both inhibitors. In general, both inhibitors shift the mainly nuclear NOSIP-HA to an equal distribution between nucleus and cytoplasm (Figure 26 B). For quantification, 300-1000 cells per condition were analyzed with respect to their nucleocytoplasmic ratio (N/C ratio). A value around 1 corresponds to an equal distribution between nucleus and cytoplasm, above 1 to a more pronounced nuclear accumulation and below 1 to an enrichment in the cytoplasm. For NOSIP-HA both inhibitors showed a significant shift to an almost equal distribution between nucleus and cytoplasm. RFP-M9M co-transfection with GFP-GST-NOSIP resulted in a pronounced shift towards the cytoplasm, whereas RFP-bimax2 co-transfection resulted in a more equal distribution of NOSIP between nucleus and cytoplasm. In contrast to the overexpressed NOSIP proteins, no effect of GFP-bimax2 on endogenous NOSIP was observed. Endogenous NOSIP showed an exclusive nuclear localization and transfection of GFP-M9M led to a slight cytoplasmic enrichment of NOSIP. The controls were co-transfected with GFP-tagged inhibitors, whereas GFP-GST-NOSIP with RFP-tagged inhibitors instead of GFP-tagged inhibitors. To exclude that the tag, GFP or RFP, had an influence, NOSIP-HA and endogenous NOSIP were additionally co-transfected with RFP-tagged inhibitors. It was observed that there is no difference between either RFP- or GFP-tagged inhibitors (Figure S 6).

Over-expressed NOSIP was affected by both inhibitors, whereas M9M showed the stronger effect for GFP-GST-NOSIP. Further, only M9M altered the distribution of endogenous NOSIP within HeLa cells, where bimax2 had no effect. This points towards a preference of transportin 1 for nuclear import of NOSIP in living cells.

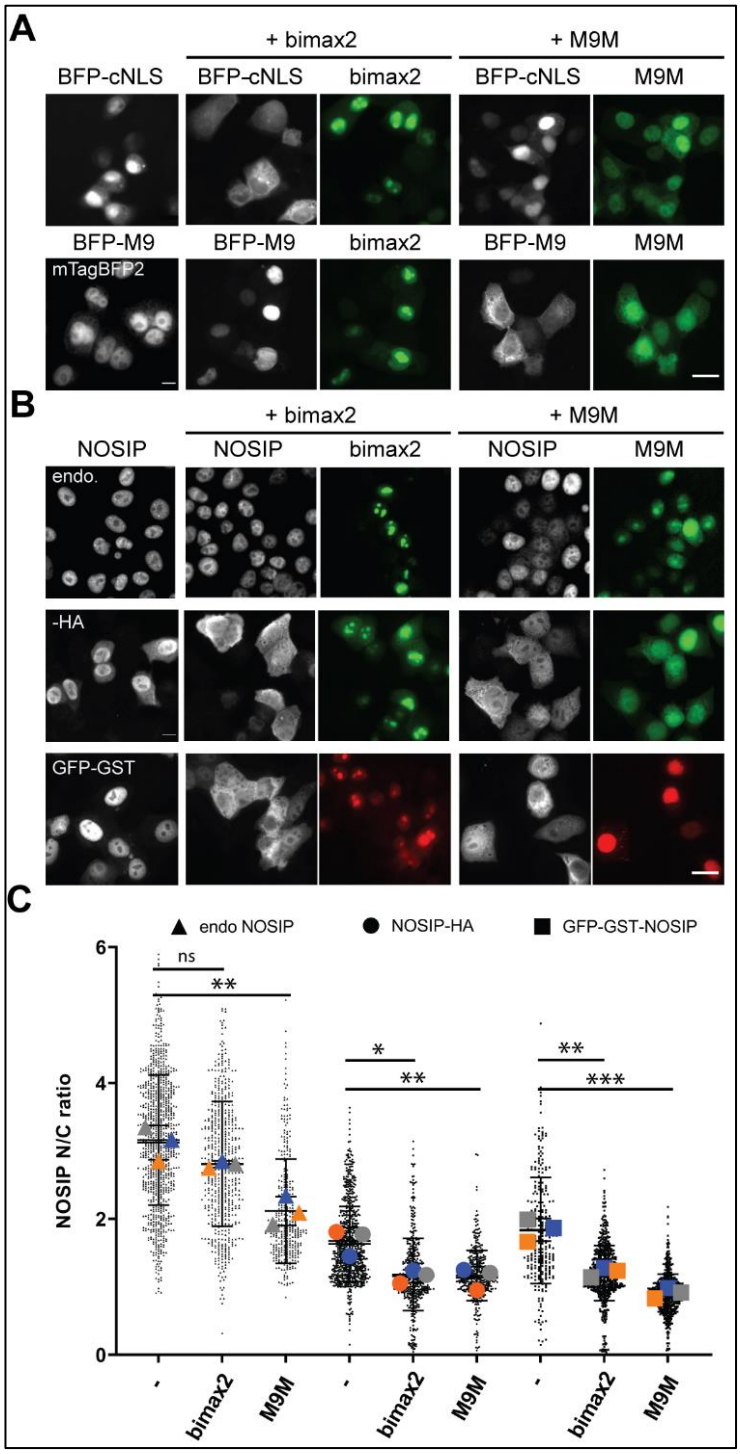

Figure 26: The peptide inhibitors M9M and bimax2 inhibit nuclear import of NOSIP. (A) HeLa P4 cells were transfected with shuttling constructs containing an NES, a fluorescence tag (mTagBFP2) and a cNLS or an M9-signal to validate the specificity of the used inhibitors. M9M is an optimized M9 sequence and established as transportin 1 inhibitor and bimax2 is an optimized cNLS sequence which binds and inhibits importin α. M9M or bimax2 were transfected as GFP-tagged fusion proteins, together with the shuttling constructs. (B) Transfection of NOSIP-HA or GFP-GST-NOSIP with M9M or bimax2 as GFP- or RFP-tagged variant respectively. To analyze the effect on endogenous NOSIP, only GFP-M9M or GFP-bimax2 were transfected. NOSIP was visualized by its GFP-tag or by indirect immunofluorescence using antibodies directed against the HA-tag or NOSIP. Scale bar 20 µm. (C) Quantification of B using Cell Profiler software. 300-1000 cells were analyzed, the nuclear and cytoplasmic fluorescence intensity was determined and divided to obtain the nucleocytoplasmic ratio (N/C ratio). Values of all measured cells are depicted as black dots, the mean value of each of the three independent experiments are depicted as bigger symbols (orange, blue, grey). For statistical analysis one-way ANOVA test with Bonferroni post-test was used. p-values <0.05 were defined as significant (= <0.05, ** = <0.01, *** = <0.001).*

3.5.2 Transportin 1 is important for the localization of NOSIP *in vivo*

The co-transfection with the inhibitory peptides, M9M and bimax2, showed that transportin 1 seems to be the preferred NTR of NOSIP. This is in line with the observations that His-transportin 1 bound the strongest to His-NOSIP-MBP. In order to further analyze the role of transportin 1 and importin β in the nuclear import of NOSIP, knock-down experiments were performed. In parallel to importin β and transportin 1, an importin 13 knock-down was performed, because importin 13 and transportin 1 showed the most efficient import in digitonin-permeabilized cells.

For knock-down experiments, cells were either transfected with siRNA (small interfering RNA) against the respective NTR or with non-targeting siRNA (siNT) as a control. Knock-down efficiency was confirmed by Western blot analysis, as shown in Figure 27 (A). The effect of knocked-down of these NTRs on endogenous NOSIP and for over-expressed NOSIP-HA and GFP-GST-NOSIP was analyzed. Knock-down cells were subsequently transfected with respective NOSIP constructs. The control transfection with siNT did not alter the localization of NOSIP, all three constructs were mainly nuclear localized as seen before (Figure 27 B). Knock-down of transportin 1 caused a shift of NOSIP-HA and GFP-GST-NOSIP to the cytoplasm. For endogenous NOSIP, a slight shift to the cytoplasm could be observed (Figure 27 B), comparable to endogenous NOSIP co-transfected with M9M inhibitor. Neither knock-down of importin 13, nor of importin β altered the localization of endogenous NOSIP. For knock-down of importin 13, a slight shift of NOSIP-HA or GFP-GST-NOSIP in some cells was observed. The knock-down of Importin β had no effect on over-expressed NOSIP-HA or GFP-GST-NOSIP (Figure 27 B).

The specific transportin 1 inhibitor, M9M, altered the localization of over-expressed NOSIP and of endogenous NOSIP. Further, a knock-down of transportin 1 prevents the nuclear accumulation of over-expressed NOSIP constructs and affected also endogenous NOSIP slightly to the cytoplasm. Altogether, this points to transportin 1 as the preferred NTR for NOSIP nuclear import, at least in HeLa cells

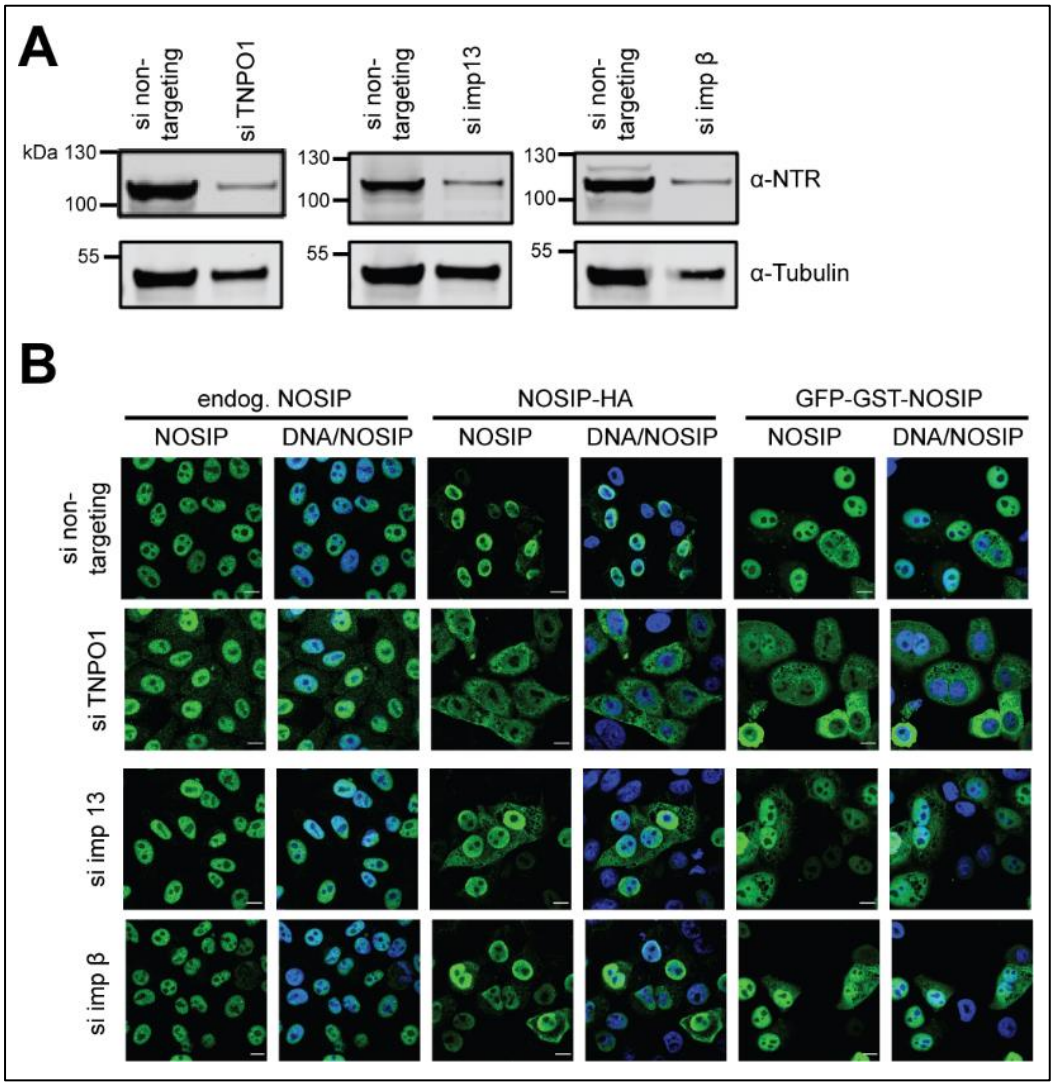

Figure 27: Knock-down of transportin 1 alters NOSIP localization in HeLa cells. Cells were transfected with 50 nM siRNA (non-targeting, TNPO 1, importin 13 or importin β) using Lipofectamine RNAiMAX, after 24 h a second transfection of siRNA was performed. After 24 h, plasmids for NOSIP-HA or GFP-GST-NOSIP were transfected using the calcium phosphate method. (A) Cells were lysed in 4xSDS-sample buffer and knock-down efficiency was analyzed by SDS-PAGE followed by Western blotting with respective antibodies. An antibody directed against Tubulin was used as loading control. (B) Cells were fixed in 3.7% formaldehyde and subjected to indirect immunofluorescence for visualization of proteins. NOSIP was either detected by the GFP-tag or by antibodies directed against the HA-tag or NOSIP. Cell nuclei were stained using DAPI. Scale bar 10 µm.

3.6 Characterization of NOSIP – NTR interactions

In this work, it was shown that the nuclear import of NOSIP is more complex than expected and that the identified bpNLS is not sufficient to mediate nuclear import when fused to a GFP-GST fusion protein (Figure 25 A). Further, it was shown that the His-NOSIP$^{1-110}$-MBP fragment, containing the bpNLS (aa 78-101), was only weakly binding to NTRs in a binding assay, but an extended fragment to residue 240 did bind to NTRs as the FL protein (Figure 24). To further analyze regions involved in the interaction with NTRs, beside the bpNLS, cross-linking combined with mass

spectrometry (MS) was used. This is a powerful approach, where two or more interacting proteins are linked using a chemical crosslinker and linked regions are identified by MS analysis. A BS3 crosslinker was used, which has two amine-reactive N-Hydroxysulfosuccinimid (NHS)-Esters separated by a spacer-arm of 11.4 Å. This crosslinker links primary amines of lysine sidechains which are in close proximity. Crosslinked lysine sidechains of the same protein are intra-protein crosslinks and crosslinked lysine sidechains of different proteins, here NOSIP and NTR (imp 13 or TNPO1) are inter-protein crosslinks. These identified interacting regions were then further analyzed using biochemical assays.

3.6.1 Crosslinking of NOSIP with transportin 1 or importin 13

Transportin 1, which was shown to be the preferred NTR for NOSIP, and importin 13, which was originally identified to bind to NOSIP, were used for cross-linking experiments. For cross-linking with BS3, complexes of His-NOSIP with His-transportin 1 or His-importin 13 were purified by gel filtration. Purified complexes were titrated against BS3 cross-linker (Figure 28). For the transportin 1-NOSIP complex, a band above transportin 1, corresponding to the size of complex (~140 kDa) appeared in the presence of BS3, while the band intensities of NOSIP and transportin 1 were decreased gradually. In contrast to this, cross-linking of importin 13-NOSIP resulted in a weak band around 140 kDa, comprising the complex. A second more prominent band appeared above the marker, corresponding to a much higher molecular weight (marked with an asterisk), probably comprising multiple copies of both proteins (Figure 28 B). In case of importin 13-NOSIP, the higher and lower bands were analyzed by MS. For further experiments, transportin 1-NOSIP complex was crosslinked with 300-fold molar excess of BS3 and importin 13-NOSIP was crosslinked in 200-fold molar excess.

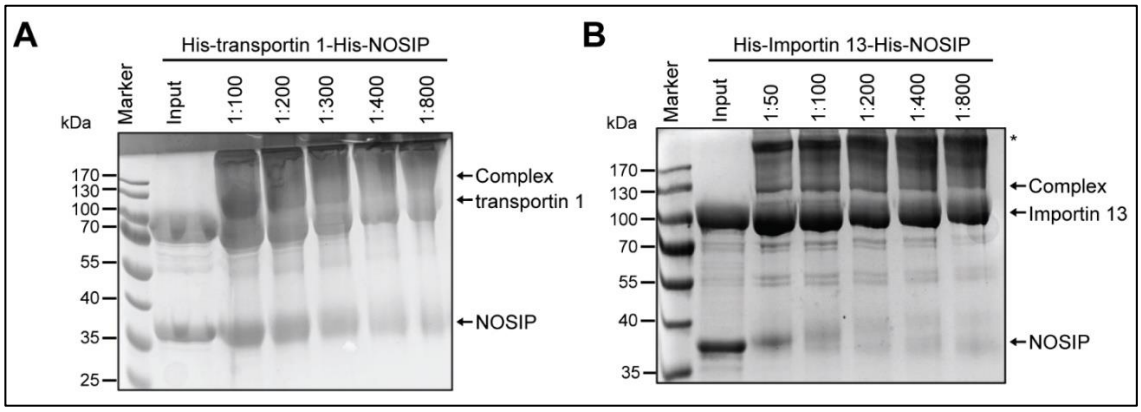

Figure 28: Crosslinking of transportin 1-NOSIP and importin 13-NOSIP using BS3. Mixtures of 100 µM His-NOSIP with 100 µM His-NTR were incubated for 1 h on ice and purified by SEC. Fractions containing complex were pooled and concentrated. Purified complexes were crosslinked with BS3 in molar excess as indicated for 30 min at RT and reaction was stopped with 50 nM TRIS. 4xSDS-sample buffer was added to separate bands according to their size by SDS-PAGE followed by Coomassie staining. Bands corresponding to complex, for importin 13 additionally the higher band (marked with an asteriks, were cut out and subjected to LC-MS analysis.

Crosslinking of importin 13 and NOSIP using BS3 and formaldehyde

For importin 13, bands corresponding to the size of importin 13/NOSIP complex and the band running much higher were cut out and subjected LC-MS analysis. For the band corresponding to the complex, 5 inter-protein crosslinks could be identified of the very N- or C-terminal parts of NOSIP to the C-terminal $K941^{imp13}$ (Figure 29, all filtered crosslinks are listed in Table S 3). As seen in the AlphaFold structure of NOSIP, these residues ($K6^{NOSIP}$, $K19^{NOSIP}$, $K21^{NOSIP}$, $K289^{NOSIP}$, $K294^{NOSIP}$) are near to each other and are therefore defined as region-I (Figure 29 B). However, no cross-links to the bpNLS of NOSIP were identified (marked in blue).

When analyzing the high molecular weight band, the region-I was observed to be crosslinked, as before. In total, four lysins (K) of importin 13 were found to be crosslinked, $K117^{imp\ 13}$, $K835^{imp\ 13}$, $K941^{imp\ 13}$, $K945^{imp\ 13}$ (Figure 29 C-D, all filtered crosslinks are listed in Table S 4). The C-terminal residues ($K835^{imp\ 13}$, $K941^{imp\ 13}$, $K945^{imp\ 13}$) of importin 13 were crosslinked to region-I of NOSIP. The N-terminal $K117^{imp13}$ crosslinked to several lysins in the middle part of NOSIP ($86\text{-}178^{NOSIP}$) including $K86^{NOSIP}$, $K90^{NOSIP}$ and $K100^{NOSIP}$ of the bpNLS. The middle part of NOSIP consist of the long α-helix and the IDR (intrinsically disordered region) was defined as region-II (Figure 29 D). However, for importin 13 only a few interacting regions could be mapped to its very N- and C-terminal ends. Crystal structures of importin 13 with its cargoes or RanGTP showed that the cargoes usually interact with the inner concave surface of either the N- or C-terminal arch of importin 13 (Grünwald and Bono

2011; Grünwald *et al.* 2013). Since the BS3 crosslinker is limited to the presence of lysine sidechains in near proximity to each other, regions lacking those could not be identified. Additionally, the BS3 crosslinker with a spacer-arm of 11.4 Å would be excluded from very tightly packed regions. To identify more interacting regions, formaldehyde was used as crosslinker. Formaldehyde crosslinks all residues in very close proximity, since it is a small molecule (Tayri-Wilk *et al.* 2020).

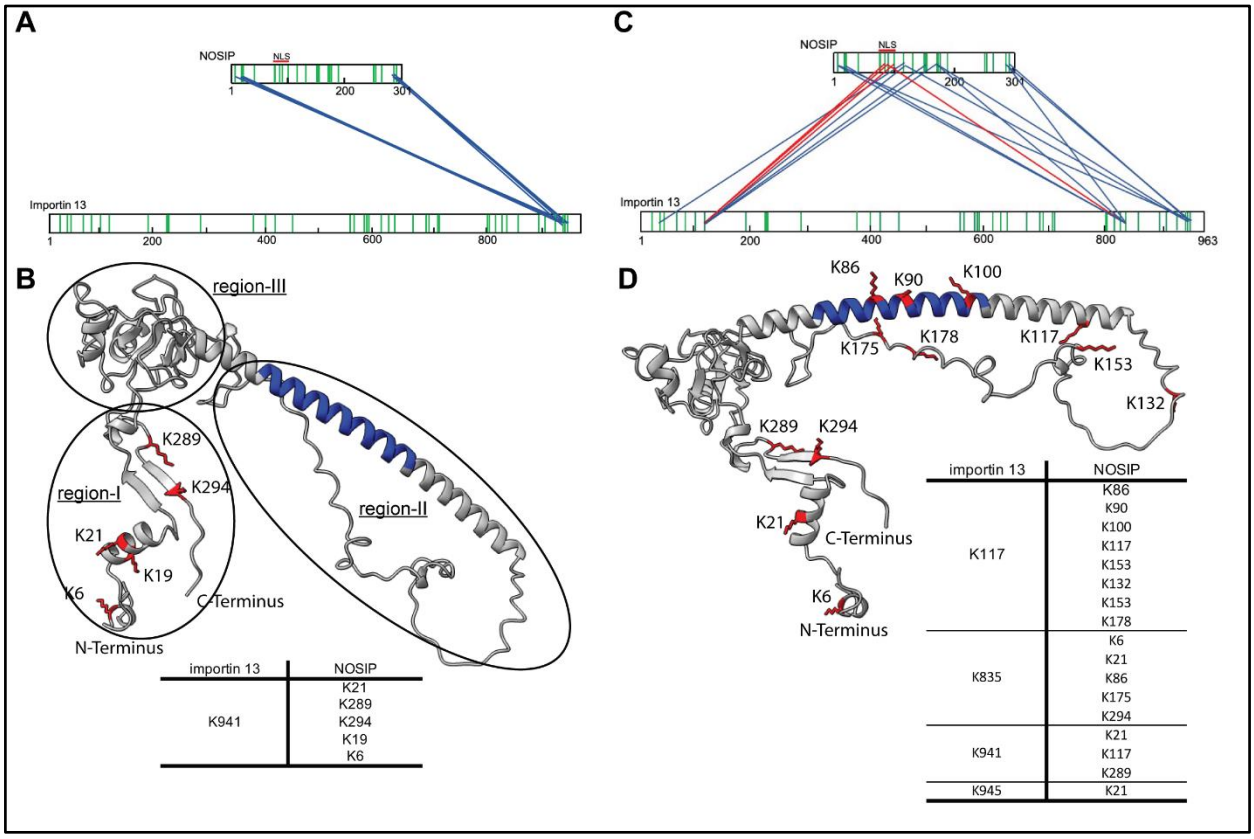

Figure 29: Crosslinking of importin 13/NOSIP using BS3. His-NOSIP/His-importin 13 complex was formed as described before, purified by gel filtration and concentrated. Purified complex was then crosslinked using 200-fold molar excess of BS3 for 30 min at RT, the reaction was stopped by adding TRIS pH 8 to a final concentration of 50 mM. Crosslinked proteins were seperated by SDS-PAGE and bands corresponding to the size of importin 13/NOSIP complex (~140 kDa, lower band) (A) and a band with higher molecular weight (upper band) (C) were analyzed by mass-spectrometry. Crosslinks were depicted in a schematic of importin 13 to NOSIP, green lines indicate lysins of the proteins. Identified and filtered crosslinks are depicted in blue or in case of crosslinks to NOSIP bpNLS in red. Crosslinks were filtered for a minimum score of 5 and at least two spectrum identifications. (B, D) Lysines of NOSIP, which were crosslinked to importin 13, are depicted in red on the AlphaFold model of NOSIP. The bpNLS of NOSIP is marked in blue and crosslinks are listed in a table (B, D).

Purified importin 13-NOSIP complex was crosslinked using 0.8% (v/v) formaldehyde, the crosslinked complex was analyzed by SDS-PAGE followed by Coomassie staining (Figure 30 A) and bands corresponding to complex were subjected to MS analysis. In the SDS-Gel it could be seen that NOSIP and importin 13 bands are decreasing, while a band above the 130 kDa marker band appeared, comprising NOSIP crosslinked to importin 13. In contrast to BS3, the band corresponding to the expected weight of the

complex was stronger than the heigh molecular weight band, which was here only faint. With formaldehyde as a crosslinker, interacting peptides could be identified, and the crosslink could not be mapped to a specific residue, as in case of BS3. In general, formaldehyde resulted in more cross-links of NOSIP to importin 13. All filtered crosslinked regions are listed in Table S 5 and the crosslinked residues indicated are in the middle of the crosslinked peptides. Like BS3 crosslinking, regions around $116^{imp\ 13}$, $867^{imp\ 13}$ and $924^{imp\ 13}$ were crosslinked. In addition to this, regions at the very C-terminal part $37^{imp\ 13}$ and two additional areas in the middle of importin 13 $410^{imp\ 13}$ and 650^{imp13} were crosslinked to NOSIP. Region-I (27^{NOSIP}, $261\text{-}286^{NOSIP}$) and region-II ($82\text{-}163^{NOSIP}$) of NOSIP were crosslinked to importin 13, as seen before for BS3. Furthermore, an additional region was mapped to $200\text{-}215^{NOSIP}$. Like for BS3 crosslinking, the N-terminal site of importin 13 was mainly crosslinked to region-II of NOSIP. The C-terminus observed to bind mainly to region-I of NOSIP and additionally to some parts of region-II.

To conclude, NOSIP binds with mainly two regions to importin 13. Region-I, comprising of the very N- and C-terminal tips of NOSIP, was shown to interact mainly with the C-terminal site of importin 13. The region-II, which comprises the long α-helix and the IDR from residues $86\text{-}178^{NOSIP}$, was observed to interact with the N-terminal tip of importin 13. This is in line with the binding assay using NOSIP fragments, where the fragment $1\text{-}110^{NOSIP}$ was only weakly binding to NTRs, whereas the extended fragment $1\text{-}240^{NOSIP}$bind comparable to the full-length protein.

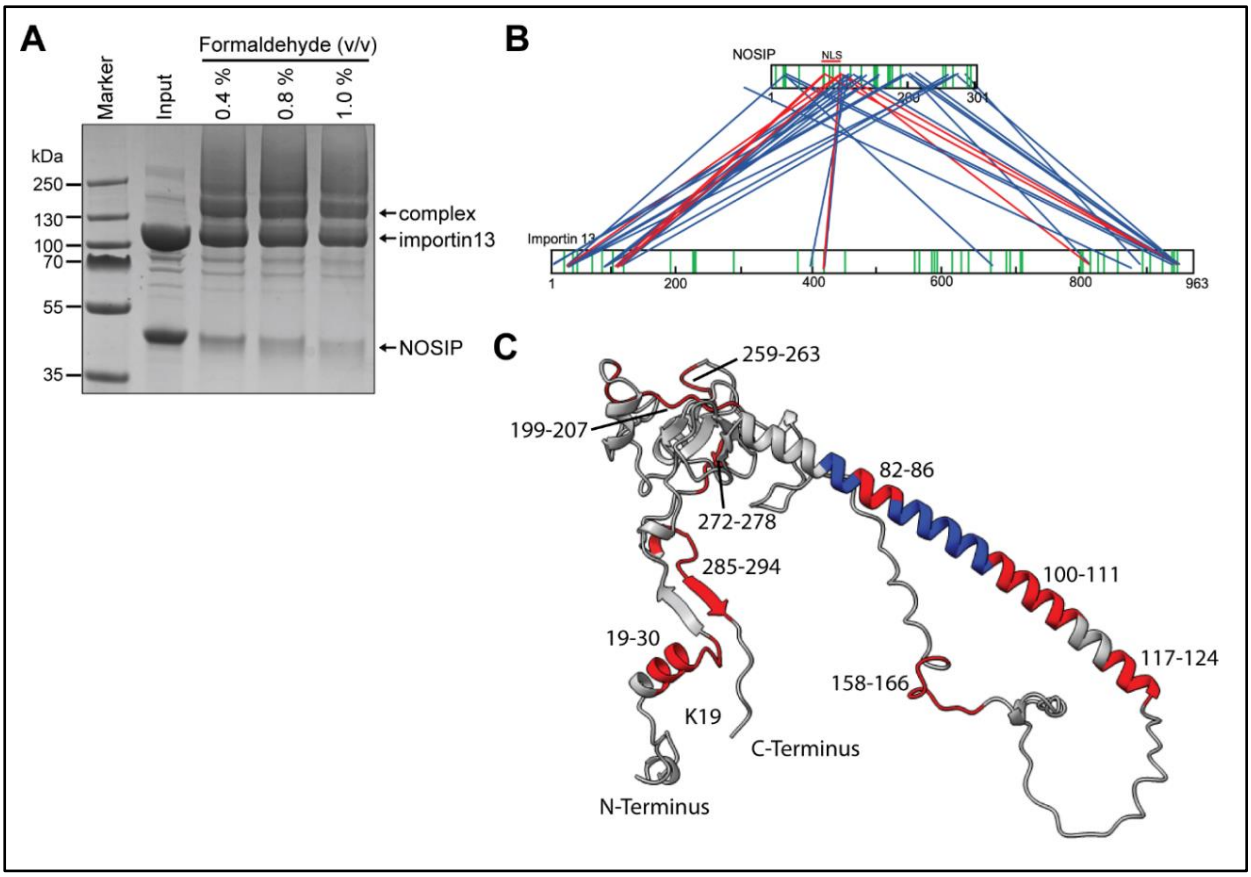

Figure 30: Crosslinking of importin 13-NOSIP using Formaldehyde. To identify more interacting regions of NOSIP and importin 13, the purified complex was crosslinked using 0.4, 0.8 or 1% (v/v) of formaldehyde. (A) The crosslinked complex was separated by SDS-PAGE and visualized using Coomassie staining. Bands corresponding to complex were cut-out and subjected to MS analysis. (B) Identified crosslinks were mapped on the schematic representation of importin 13 and NOSIP (lysins are marked in green), crosslinks are depicted as blue lines and crosslinks involving the bpNLS of NOSIP are depicted in red. Note that here no specific positions could be mapped, since with formaldehyde crosslinking only interacting peptides were identified. The crosslinks were mapped to the middle of identified peptides. (C) Crosslinked regions of NOSIP were marked in red on the AlphaFold structure of NOSIP and the bpNLS of NOSIP is marked in blue.

Crosslinking of transportin 1 and NOSIP using BS3

Crosslinking of His-transportin 1 with His-NOSIP using BS3 resulted in a prominent band around 130 kDa, which was analyzed by MS. The analysis revealed that similar regions of NOSIP were crosslinked, like for importin 13 (all filtered inter- and intra-protein crosslinks are listed in Table S 6). Noticeable, only a few crosslinks were observed to region-I of NOSIP, whereas more crosslinks were identified to region-II. As seen for importin 13, residues of NOSIPs bpNLS, $K90^{NOSIP}$ and $K100^{NOSIP}$ were crosslinked to transportin 1 (Figure 31 B, C). Of transportin 1, eight lysins were crosslinked to NOSIPs region-I and -II. Mainly the N-terminal arch of transportin 1 was crosslinked to NOSIP (Figure 31 A). This was surprising, since the conserved N-terminal arch of NTRs is the binding-site for RanGTP (Görlich *et al.* 1997; Chook and

Blobel 1999). Cargoes usually bind to the C-terminal arch of transportin 1, as well as for other NTRs (Lee *et al.* 2005; Mboukou *et al.* 2021). The N-terminal lysins K66^{TNPO1}, K81^{TNPO1}, K85^{TNPO1} and K128^{TNPO1} were crosslinked to NOSIP. In addition, crosslinks of NOSIPs region-I to K385^{TNPO1} and K502^{TNPO1} were identified. Moreover, K889^{TNPO1} was crosslinked to region-I of NOSIP.

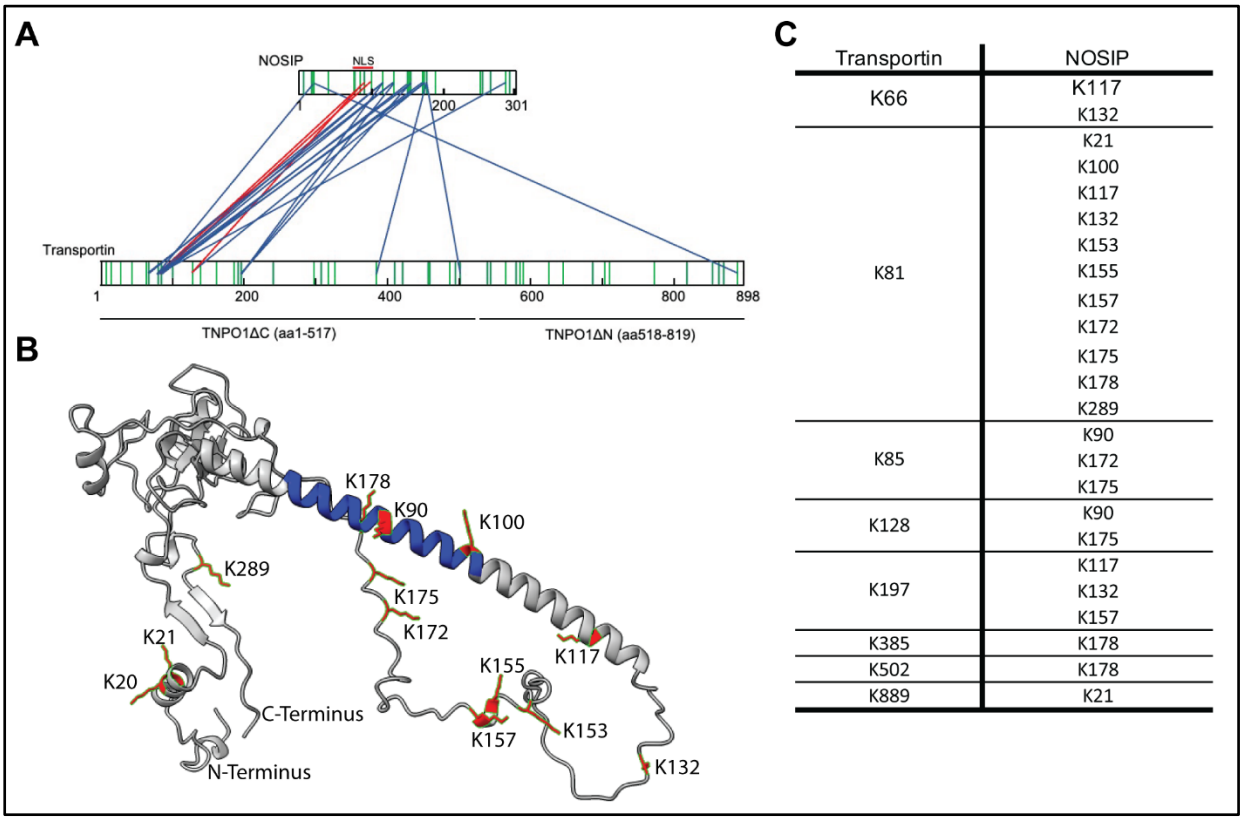

C

Transportin	NOSIP
K66	K117
	K132
K81	K21
	K100
	K117
	K132
	K153
	K155
	K157
	K172
	K175
	K178
	K289
K85	K90
	K172
	K175
K128	K90
	K175
K197	K117
	K132
	K157
K385	K178
K502	K178
K889	K21

Figure 31: Crosslinking of transportin 1/NOSIP using BS3. His-NOSIP/His-transportin 1 complex was formed as before, purified by gel filtration and concentrated. Purified complex was then crosslinked using 300-fold molar excess of BS3 for 30 min at RT, the reaction was stopped by adding TRIS pH 8 to a final concentration of 50 mM. Crosslinked proteins were seperated by SDS-PAGE and bands corresponding to the size of transportin 1/NOSIP complex (~140 kDa) were analyzed by mass-spectrometry. Crosslinks are filtered for a minimum score of 5 and at least 2 spectrum identifications. (A) Filtered crosslinks are depicted as blue lines, or when the bpNLS of NOSIP is involved, as red lines. Transportin 1 and NOSIP proteins are depicted as bars with lysin-residues depicted in green. (B) Lysins of NOSIP which were crosslinked are colored in red and mapped on the AlphFold structure of NOSIP. The bpNLS, including the spacer-arm, of NOSIP is colored in blue. (C) Table of filtered crosslinks. K is the one letter code for lysine.

Taken together, NTRs were observed to interact mainly with region-II of NOSIP containing the bpNLS within the long α-helix and the IDR. For transportin 1, the interacting region could be clearly mapped to the N-terminal arch, which contrasts with the C-terminal binding of typical transportin 1 cargoes. Like for transportin 1, the N-terminal RanGTP-binding site of importin 13 was observed to bind mainly to region-II. The C-terminal tip bound mainly to region-I and additionally to region-II, pointing to an

unusual binding of NOSIP to NTRs, which usually bind with the C-terminal arch to their cargoes.

3.6.2 NOSIP binds to the N-terminal arch of transportin 1

Crosslinking of transportin 1 and NOSIP showed that NOSIP binding is clearly different from most other transportin 1 cargoes. To validate the MS result, transportin 1 deletion constructs were analyzed for their binding to M9 or NOSIP. Either full-length transportin 1, an N-terminal deletion (ΔN) or a C-terminal deletion (ΔC) fragments of transportin 1 were incubated with immobilized GST-M9 or GST-NOSIP in the presence or absence of Ran_{1-180} Q69L-GTP.

In this binding assay, GST-M9 bound to transportin 1 FL in the absence of Ran and to the C-terminal arch of transportin 1 (MBP-TNPO1 ΔN) in both, presence and absence of Ran. This is explained by the lack of the N-terminal RanGTP binding-site in the MBP-TNPO1 ΔN construct (Figure 32 A). MBP-TNPO1 ΔC did not bind to GST-M9, as expected. In contrast to GST-M9, GST-NOSIP bound to MBP-TNPO1 ΔC, comprising the N-terminal arch, to the same extent as to the MBP-TNPO1 FL. Additionally, GST-NOSIP bound to the C-terminal arch of transportin 1 (MBP-TNPO1 ΔN), however to a lesser extent (Figure 32 B).

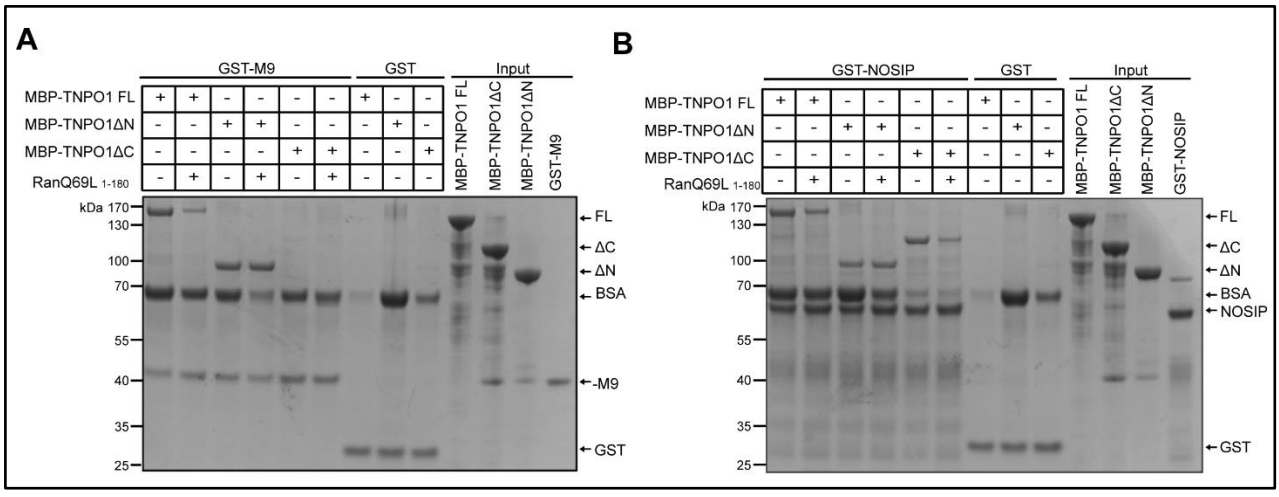

Figure 32: NOSIP binds differently than M9 to transportin 1. Either 100 pmol GST-M9 (A) or GST-NOSIP (B) were immobilized on glutathione sepahrose beads and incubated with 100 pmol of MBP-TNPO1 fulllength (FL, aa 1-890), N-terminal arch (ΔC, aa 1-517) or C-terminal arch (ΔN, aa 518-890). Unbound proteins were washed out and bound proteins were eluted and analyzed by SDS-PAGE followed by Coomassie staining.

3.6.3 Molecular docking of NOSIP and transportin 1 using MS-derived crosslinks as distance restrains

NOSIP was assumed to bind to NTRs via its identified bpNLS, but here it was shown that the bpNLS alone is not sufficient to mediate NOSIP's nuclear import. Crosslinking combined with mass spectrometry analysis revealed, that NOSIP bound to importin 13 and transportin 1 via region-II (residues around 86-178^{NOSIP}), which contains the bpNLS and the IDR of NOSIP. In addition, NOSIP was observed to bind to the very N-terminal arch of transportin 1, like RanGTP does. NOSIP also bound to the N-terminal tip of importin 13, but N-terminal binding to importin 13 is reported for other cargoes (Grünwald and Bono 2011). The binding to transportin 1 was unusual. To gain more information about the interaction, NOSIP was docked to transportin 1 using Rosetta software. Unfortunately, no experimental structure of NOSIP was available, but in 2021 AlphaFold, an AI (artificial intelligence) system, predicted the 3D-structures of the whole human proteome, including NOSIP. The structure of human NOSIP was predicted with an overall high accuracy according to the confidence score AlphaFold provided (Figure 33 A). For transportin 1, several crystal structures in complex with various cargoes are available.

Comparing the AlphaFold model of NOSIP to experimental data

The predicted AlphaFold model of NOSIP was analyzed for its reliability using experimental data. First, the AlphaFold model was compared to the secondary structure distribution of NOSIP, which was generated using CD (circular dichroism)-spectroscopy (Figure S 7). The secondary structure distribution of untagged NOSIP was nearly similar to the distribution in the AlphaFold model (Figure 33 B). Additionally, the intra-protein crosslinks of NOSIP lysin-residues to each other were mapped on the NOSIP model using the Xwalk webserver (https://www.xwalk.org/, (Kahraman *et al.* 2011)). This webtool analyses the solvent accessible surface distances (SASD), which is the shortest way between crosslinked residues, using a surface accessible way. The Euclidean distance, which is usually used when measuring distances, was additionally calculated and represents the shortest way in the three-dimensional room.

41 intra-protein crosslinks were identified (using the data of the transportin 1-NOSIP complex, Table S 6) and analyzed using Xwalk. 21 of these crosslinks had a reasonable distance <34 Å SASD (the upper limit for DSS crosslinked lysin residues) between the Cβ-atoms (Figure 33 C, all measured distances are listed in Table S 7) using the AlphaFold model. The remaining crosslinks were above the threshold of 34 Å SASD. Most crosslinks above this cutoff were lysins, which are located in the IDR region of NOSIP. The IDR region has a higher flexibility, and it can be assumed that this region can be oriented in various positions.

In general, the CD data and the crosslinking data fit to the predicted AlphaFold model of NOSIP, except some crosslinks of the IDR. Obviously, the IDR was only predicted with a low accuracy in the AlphaFold model (Figure 33 A).

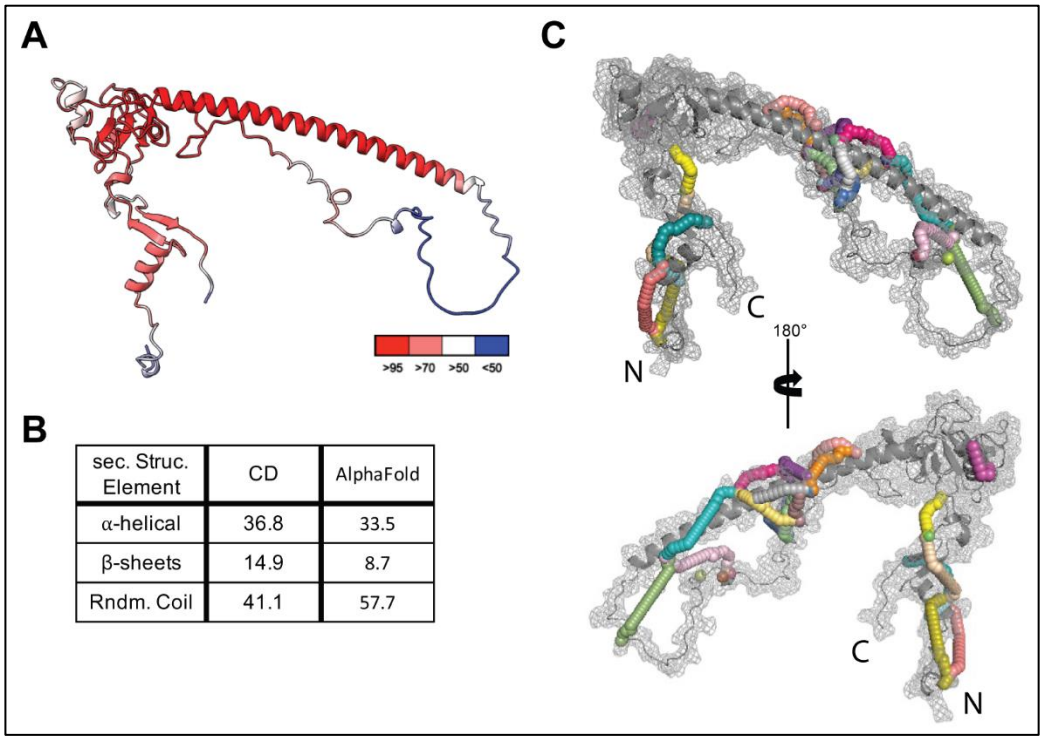

sec. Struc. Element	CD	AlphaFold
α-helical	36.8	33.5
β-sheets	14.9	8.7
Rndm. Coil	41.1	57.7

Figure 33: The AlphaFold model of NOSIP. (A) The 3D-protein structure was predicted by AlphaFold using the amino acid sequence of human NOSIP. The confidence of the model is given as a per-residue confidence score, red residues have a confidence of >95, pale red of <90 to >70, white <70 to >50 and blue <50. (B) Comparing the relative distribution of secondary structure elements (α-Helices, β-sheets, random (Rndm) coil) from the AlphaFold model of NOSIP to the distribution obtained from CD (circular dichroism)-spectroscopy measurements. For CD-spectroscopy, untagged NOSIP, present in 100 mM Na_2HPO_4/NaH_2PO_4 pH 8, was measured and secondary structure distribution was calculated. (C) Identified intra-protein crosslinks of NOSIP are depicted on the AlphaFold model of NOSIP. The Xwalk webserver was used to measure the solvent accessible surface distance (SASD) of intra-protein crosslinks. Here, crosslinks with a SASD distance < 34 Å are depicted as colored spheres. The structure of NOSIP is displayed in gray with a mesh around the cartoon-structure to indicate the surface.

Docking of NOSIP to transportin 1

For docking of NOSIP to transportin 1, the AlphaFold model was used for NOSIP, while a crystal-structure of transportin 1 was used. The structure of transportin 1 bound to Ran·GppNHp (PDB: 1QBK, GppNHp is a non-hydrolysable form of GTP) was used, because NOSIP bound N-terminally to transportin 1, similar to Ran (Chook and Blobel 1999). For docking, Ran·GppNHp of the crystal-structure was removed to obtain transportin 1.

The initial docking was performed using the ClusPro webserver (https://cluspro.org) with the option “protein-protein docking”. As input, the prepared PDB structure of transportin 1 and the AlphaFold model of NOSIP were used. Additionally, crosslinked residues of both, NOSIP and transportin 1, were set as attraction sites in the advanced options (Table 19). Attraction sites are defined as regions in proximity to the binding partner and involved in the interaction. As output, the ClusPro webserver provides

models with the lowest energy and the most clusters. A cluster is defined as a region with neighbors in a 9 Å radius around the Cα-atoms, which bind to the binding partner. The models are ranked according to the cluster-size and best energy score.

Table 19: Residues given as interaction-sites for ClusPro docking of NOSIP and transportin 1

Attraction sites of transportin 1	Attraction sites of NOSIP
K66	K21
K81	K90
K85	K100
K128	K117
K197	K132
K385	K153
K502	K155
K889	K157
	K172
	K175
	K178
	K289

Further, the ClusPro output was filtered for structures, where NOSIP was docked to the inner concave surface of transportin 1, since cargoes were shown to bind to the inner concave surface of NTRs (Cingolani *et al.* 1999). Additionally, the crosslinks identified by MS analysis were used to filter for models saturating the most crosslinks. A saturated crosslink was defined as maximum distance of 30 Å between the lysin Cα-Cα atoms. According to the literature, the maximum distance of the Cα-Cα atoms is 24 Å when crosslinked by DSS (Gong *et al.* 2020). As the structure of NTRs is flexible and some crosslinks involved the flexible IDR of NOSIP, an additional flexibility of 6 Å was allowed. The best model was used as initial starting model for a further refinement using the Rosetta software (for the docking protocol see section 2.5.3.). The local refinement protocol of the Rosetta docking protocol was used to optimize the initially docked transportin 1-NOSIP complex.

In the final model, NOSIP was positioned within the inner-surface near to the N-terminal end of transportin 1 with a cluster around $K81^{TNPO\ 1}$, $K85^{TNPO\ 1}$ and $K128^{TNPO\ 1}$ (Figure 34 B-C). NOSIP mainly bound with its region-II, containing the long α-helix and the IDR, to transportin 1, involving $K90^{NOSIP}$, $K100^{NOSIP}$, $K117^{NOSIP}$, $K132^{NOSIP}$, $K155^{NOSIP}$, $K172^{NOSIP}$ and $K175^{NOSIP}$ (Figure 34 B-C). However, the long α-helix was oriented at the very end in the cleft between the C- and N-terminal arch. The IDR, instead, was oriented within the lumen of transportin 1 and possibly interacted with the

acidic H8-loop of transportin 1. In this model, region-I of NOSIP was not involved in the interaction. For instance, K21^{NOSIP} and K889$^{TNPO\ 1}$, which were crosslinked by BS3, were not near each other (Figure 34 A). Region-I could not be docked closer to K889$^{TNPO\ 1}$, because the IDR sterically hindered the respective orientation. Region-III of NOSIP was not involved in the interaction with transportin 1 and some crosslinks exceeded the cutoff of 30 Å (Figure S 8).

IDRs are flexible structures without secondary structure elements. The IDR of NOSIP was only predicted with a low accuracy in the AlphaFold model. In order to improve the positioning of the accurately predicted NOSIP structure, the IDR (126-188^{NOSIP}) was deleted. This shortened NOSIP structure (NOSIP∆IDR) was then used for docking to transportin 1, as described before. In comparison to NOSIP, NOSIP∆IDR was oriented more luminally within the N-terminal arch of transportin 1 (Figure 35). Additionally, region-I of NOSIP could be oriented more closely to the C-terminal arch of transportin 1 (Figure 35 B). Region-II was docked, as before, to the cluster around K81$^{TNPO\ 1}$, K85$^{TNPO\ 1}$ and K128$^{TNPO\ 1}$. The IDR of NOSIP is probably oriented more luminal, as it was crosslinked to K385$^{TNPO\ 1}$ and K502$^{TNPO\ 1}$. However, remodeling of the IDR failed, because only smaller loops up to 12 residues can be modeled by the Rosetta software. Besides, two crosslinks contrasted with this model. These crosslinks indicate that NOSIP may be bound in different orientations. For instance, region-I of NOSIP (K21^{NOSIP} and K289^{NOSIP}) was docked to the C-terminal end (K889$^{TNPO\ 1}$) and the N-terminal end (K81$^{TNPO\ 1}$) of transportin 1 (Figure S 8 and Figure S 9). Alternatively, NOSIP could be bound as an antiparallel oriented dimer. This would explain the docking of NOSIP's region-I to both ends of transportin 1.

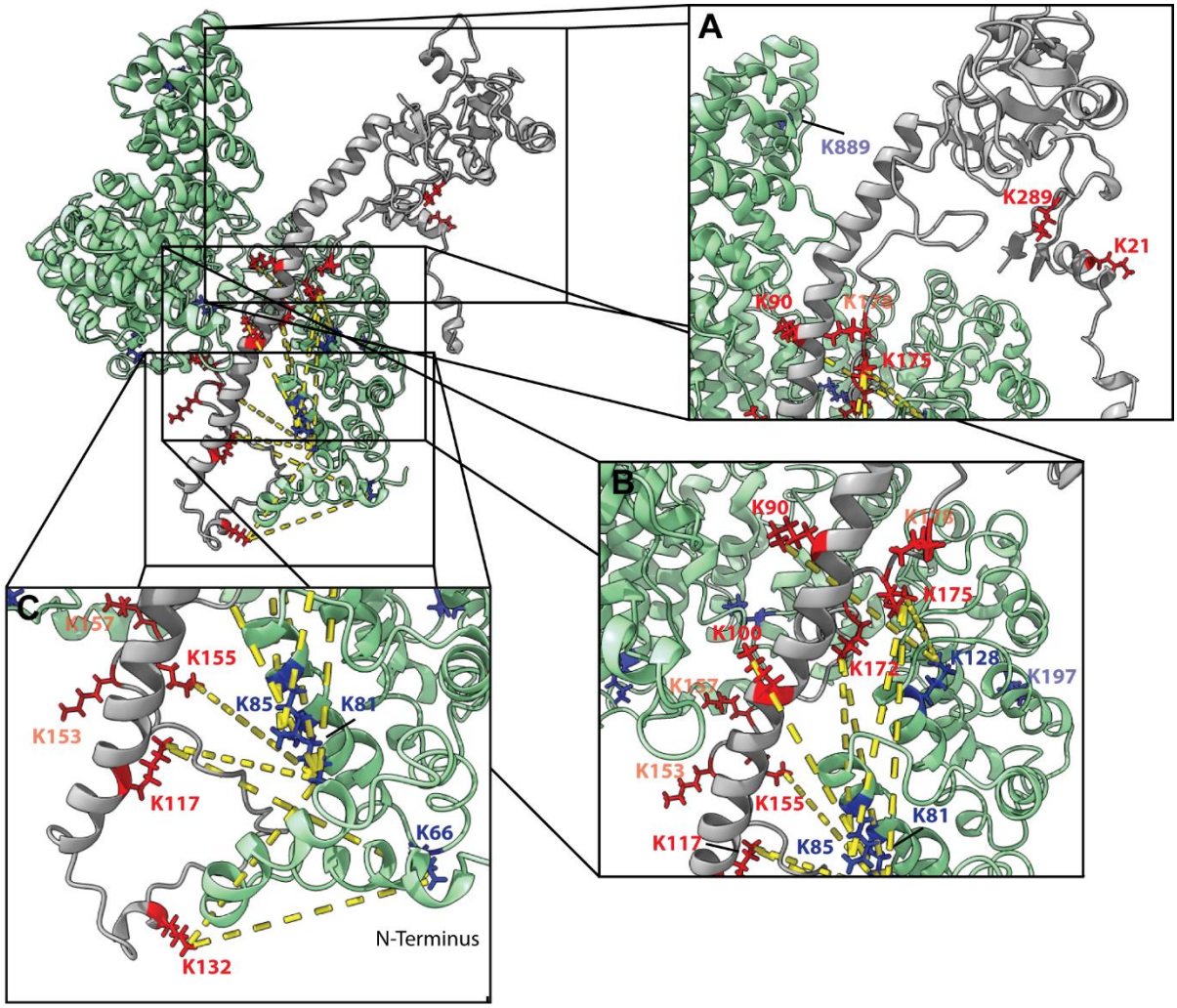

Figure 34: Docking of NOSIP to transportin 1 using ClusPro and Rosetta. (A-C) The AlphaFold model of NOSIP was docked to the crystal structure of transportin 1 (PDB: 1QBK) using the MS derived crosslinks. Only the transportin 1 structure of the PDB file was used for docking. NOSIP is depicted in gray, crosslinked lysins are shown as red sticks. Transportin 1 is colored in green and crosslinked lysins as blue sticks. Crosslinks in a distance of < 30 Å are depicted as yellow dashed lines. Images were generated using Chimera software.

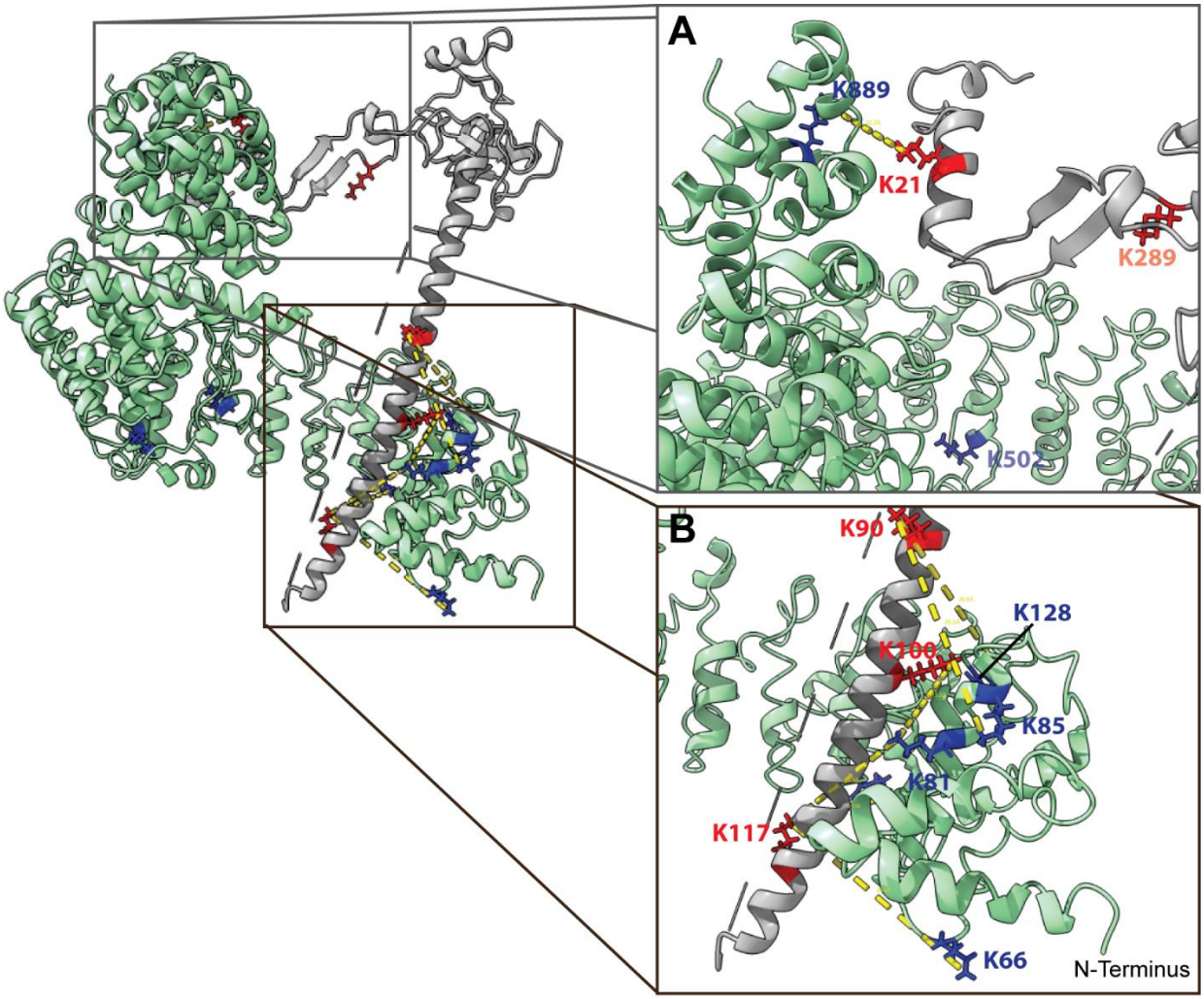

Figure 35: Docking of NOSIP without IDR to transportin 1 using ClusPro and Rosetta. (A-B) The IDR of NOSIP's AlphaFold model (126-188^{NOSIP}) was removed and the modified structure was then used for docking to the crystal structure of transportin 1 (PDB: 1QBK). Only the transportin 1 structure of the PDB file was used for docking. The MS derived crosslinks were used as restrains during the docking process. NOSIP is depicted in gray, with the removed IDR shown as dashed line and crosslinked lysins are shown as red sticks. Transportin 1 is colored in green and crosslinked lysins as blue sticks. Crosslinks in a distance of < 30 Å are depicted as yellow dashed line. Images were generated using Chimera software.

3.7 Cell-cycle regulated transport of NOSIP

NOSIP, with a size of 34 kDa, is small enough to shuttle between the nucleus and the cytoplasm, since it is below the threshold of the NPC. Nevertheless, NOSIP was shown to be mainly nuclear localized in HeLa or other cultured cells, as well as in some tissues (König *et al.* 2002; König *et al.* 2005; Schleicher *et al.* 2005). The prominent nuclear enrichment was shown to be based on active nuclear import, which outbalances passive nuclear export (Figure 11 - Figure 13). The best-known function of NOSIP takes place in the cytoplasm, where NOSIP regulates eNOS activity by translocating the enzyme from the plasma membrane to the cytoskeleton (Schleicher *et al.* 2005). This translocation occurs specifically in the G2-phase of the cell-cycle. In addition, NOSIP itself is enriched in the cytoplasm during this phase (Schleicher *et al.* 2005). This raises the question of how the cytoplasmic accumulation of NOSIP during the G2-phase of the cell-cycle is regulated. Active nuclear import is the driving force for the nuclear accumulation of NOSIP, but active nuclear export was not observed.

It is known that nuclear transport can be regulated through posttranslational modifications (PTM) like phosphorylation, ubiquitination, glycosylation or sumolyation (Nardozzi *et al.* 2010; Wang *et al.* 2012). The mechanism behind this regulation is either based on the modification of NPC components, and thus a more general effect, or on the modification of the cargo itself. An previous study showed, that NOSIP can be phosphorylated, when cells are treated with erythropoietin (Epo), IL 3 or G-CSF, even though this phosphorylation was transient for 5 to 15 min (Friedman *et al.* 2003). Additionally, NOSIP was shown to be an active E3-ubiquitin ligase, which can either ubiquitinate a target protein or itself (Friedman *et al.* 2003). Thus, it is possible that NOSIP is post-translationally modified in a cell-cycle dependent manner, which causes its accumulation in the cytoplasm.

3.7.1 Cell-cycle regulated localization of NOSIP in HeLa cells

First, the cell-cycle dependent re-localization of NOSIP in HeLa cells was analyzed, which was previously shown in another cell line (Schleicher *et al.* 2005). HeLa cells were synchronized in G1-phase or G2-phase of the cell-cycle using a double thymidine block, as depicted in (Figure 36 A). The cell-cycle stage was analyzed by flow cytometry using PI (propidium iodide) DNA staining. For comparison, unsynchronized

cells were analyzed, which showed 53.5% of cells in G1-phase, 19.4% in S-phase and 18.0% in G2-phase. In HeLa cells synchronized in G1-phase, 89.1% of the cells were in G1-phase, 7.51% in S-phase and 4.92% in G2-phase. In G2-phase synchronized cells, 73.5% were in G2-phase, 9.99% in G1-phase and 6.65% in S-phase, demonstrating that the synchronization was successful (Figure 36 B).

In addition to the flow cytometry analysis, cells were subjected to indirect immunofluorescence to visualize the localization of endogenous NOSIP. In unsynchronized HeLa cells, endogenous NOSIP localized to the nucleus, as shown before (Figure 36 C). Cells synchronized in G1-phase of the cell-cycle showed a similar distribution. A shift towards the cytoplasm was observed in cells synchronized in G2-phase of the cell-cycle, where NOSIP was almost equally distributed between cytoplasm and nucleus.

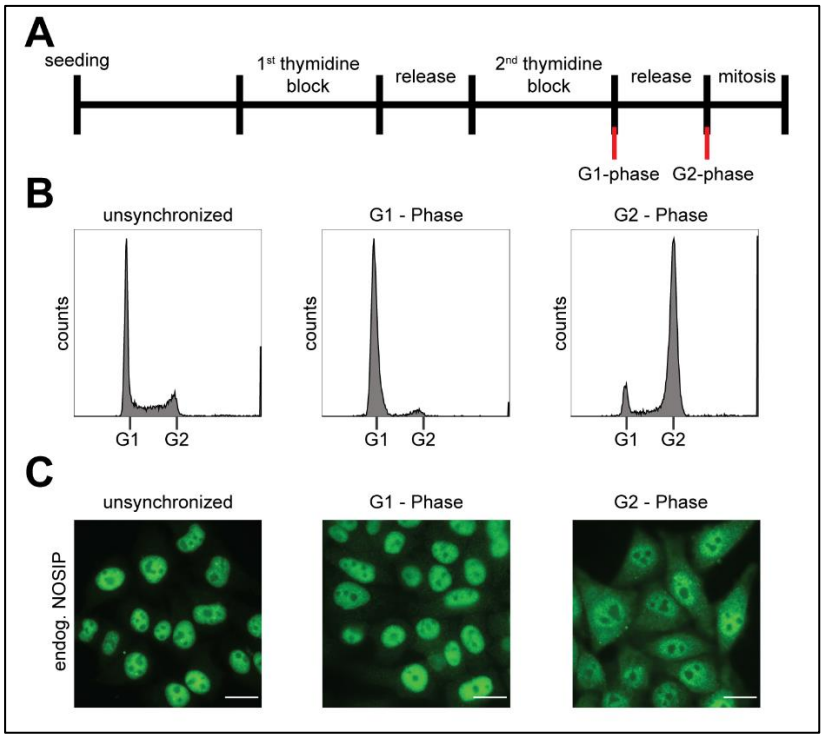

Figure 36: Localization of endogenous NOSIP during G1- and G2-phase of the cell-cycle. (A) HeLa cells were synchronized by a double thymidine block; a scheme of the procedure is depicted here. Cells were seeded and after 24 h, 2 mM thymidine were added for 18 h as a first blocking step. Afterwards, cells were released for 9 h, before another block with thymidine for 18 h was performed, followed by a release. At the beginning of the release, cells are synchronized in G1-phase of the cell-cycle, and after 8-9 h cells are in G2-Phase of the cell-cycle. After 9 h of release, the cells enter mitosis. (B) HeLa cells were synchronized as described in A and synchronization efficiency was analyzed by flow cytometry. Cell stages were analyzed by DNA staining with propidium iodide (PI), since cells in G2-phase have the double amount of DNA. The PI intensity is plotted against the cell-count. (C) Cells were synchronized and endogenous NOSIP was visualized by indirect immunofluorescence. Scale bar 20 µm.

3.7.2 Does phosphorylation affect the localization of NOSIP?

Many steps during mitosis are regulated through PTMs, like the activation of cyclin-dependent kinases (CDK), which are active upon autophosphorylation or due to phosphorylation by CDK activating kinases (Welburn and Jeyaprakash 2018). A proteomic screen analyzed the phosphorylation of the human proteome and showed that protein phosphorylation reaches the highest level during mitosis (Dephoure *et al.* 2008; Olsen *et al.* 2010). To examine whether phosphorylation of NOSIP plays a role for its localization, a broad-spectrum phosphatase inhibitor, okadaic acid, was used. This inhibitor increases the level of phosphorylation in HeLa cells through the inhibition of dephosphorylation. Further, a broad-spectrum kinase inhibitor, staurosporine, was used to prevent phosphorylation or to reverse the increased phosphorylation of proteins, as induced by okadaic acid (OA).

In this experiment, HeLa cells were treated with OA. The treatment with 0.5 µM OA for 1 h led to a shift of endogenous NOSIP towards the cytoplasm to an almost equal distribution of NOSIP compared to untreated cells (Figure 37). This effect was nearly completely reversed, when staurosporine (St) was used in a 2-fold molar excess (1 µM). The same was observed for transfected NOSIP-HA cells (Figure S 10). This indicated, that increased phosphorylation levels in HeLa cells led to a shift of NOSIP to the cytoplasm. To exclude that the protein level of NOSIP was altered upon treatments, it was analyzed overtime. It was observed that the protein level of NOSIP remained constant (Figure 37 B).

In order to analyze if the observed effect is specific for NOSIP, two reporter proteins, GFP_2-M9 and BFP-cNLS, for the transportin 1- and importin α/β- pathway were used. Cells transfected with GFP_2-M9 showed a mainly nuclear signal and treatment with OA or OA/St did not affect its localization (Figure 37 A). To examine the importin α/β pathway, BFP-cNLS reporter was treated with OA and St. As observed for GFP_2-M9, OA or OA/St treatment did not alter the localization of BFP-cNLS (Figure 37), showing that the observed effect of okadaic acid treatment on the localization of NOSIP was not based on a general alteration of nuclear import.

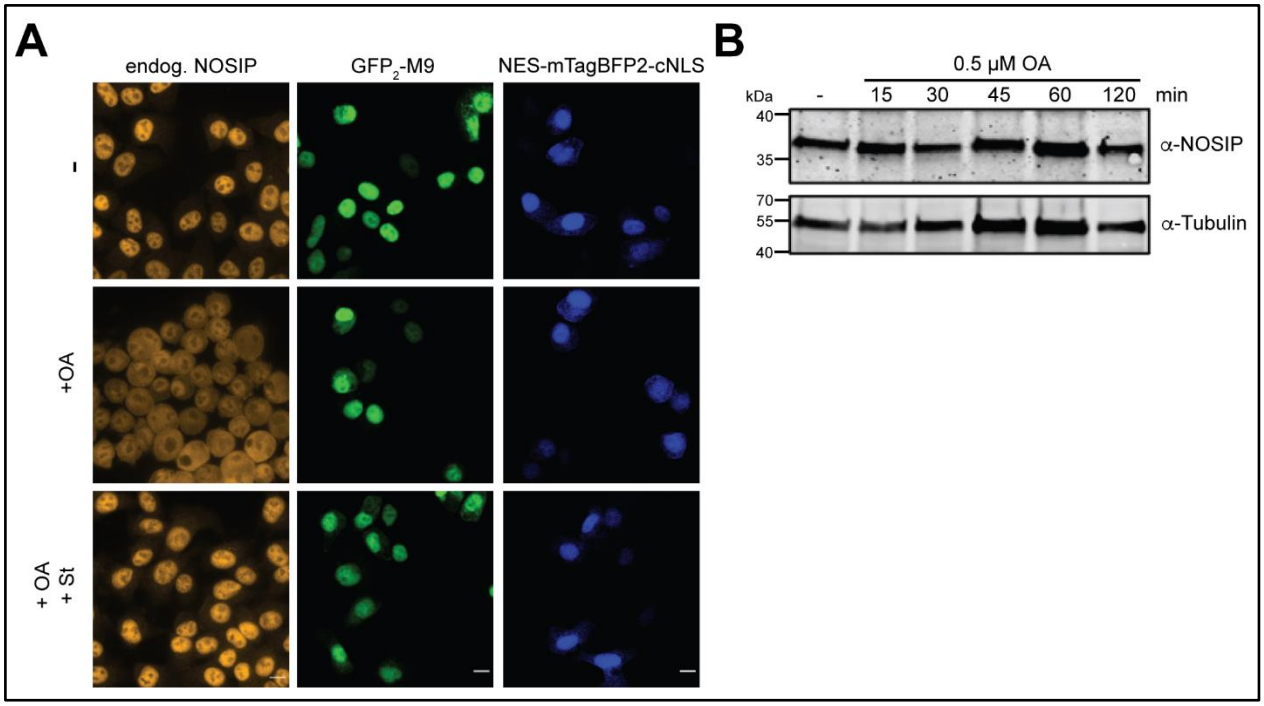

Figure 37: Okadaic acid treatment alters the localization of NOSIP in HeLa cells. (A) Cells were left untransfected or transfected with reporter proteins GFP_2-M9 and BFP-cNLS. To analyze the effect of phosphorylation on endogenous NOSIP or reporter proteins, cells were treated with the broad-spectrum phosphatase inhibitor, okadaic acid (OA), alone or in combination with the broad-spectrum kinase inhibitor staurosporine (St). Treatment was performed for 1 h at 37 °C with 0.5 µM OA or with 0.5 µM OA and 1 µM St. Reporter proteins were visualized through their fluorescence-tag and endogenous NOSIP was visualized by indirect immunofluorescence using a specific antibody. Scale bars 10 µm. (B) HeLa cells were treated over a period of 2 h with 0.5 µM OA and were harvested at indicated time-points. Lysates were analyzed by SDS-PAGE, followed by Western blotting using antibodies against NOSIP and Tubulin (loading control).

3.7.3 Mutation of potential phosphorylation sites of NOSIP

As seen above, phosphorylation possibly altered the nuclear shuttling of NOSIP. In order to analyze the effect of phosphorylation on the localization of NOSIP, potential phosphorylation sites of NOSIP were mutated to mimic the phosphate charge of a phosphorylation. Either serine (S), threonine (T) or tyrosine (Y) residues can be phosphorylated through specific kinases. In a proteomic screen analyzing the mitosis-dependent phospho-proteome, S36 of NOSIP was shown to be phosphorylated during mitosis. In addition, S107 was identified in the same screen, but not significantly enriched (Olsen *et al.* 2010). Another screen analyzing the cell-cycle dependent phosphorylation observed S138 of NOSIP to be phosphorylated (Dephoure *et al.* 2008). Moreover, Y14 of NOSIP was detected to be phosphorylated in various studies, for instance after ephrin-B1 treatment (Jørgensen *et al.* 2009). The study of Friedmann and co-workers, which showed that NOSIP ubiquitinates the Epo-receptor, also observed tyrosine phosphorylation of NOSIP (Friedman *et al.* 2003).

To analyze if phosphorylation of these sites affects the localization of NOSIP, initially S36 and S138 were mutated to aspartate (D) and Y14 to glutamate (E) to mimic the charge of a phosphorylation. Later, S107 was additionally mutated, albeit it was not a significant hit, but it is localized close to the bpNLS. Phosphorylation upstream or downstream of an NLSs can enhance or impair its recognition by NTRs (reviewed in (Nardozzi *et al.* 2010)). The mutations were introduced into NOSIP-HA and some of them also into GFP-GST-NOSIP. The mutations Y14E, S36D and S138D were all combined to double or triple mutations, the mutation S107D was only used as a single mutation.

HeLa cells were transfected with plasmids coding for wildtype (WT) or mutated NOSIP-HA (WT, Y14E, S36D, S138D, S36D/S138D, Y14E/S36D, Y14E/S138D, Y14E/S36D/S138D, S107D). As observed earlier (Figure 11), NOSIP-HA localized mainly to the nucleus and, in some cells, partially in the cytoplasm. Mutation of S36D or S138D did not alter the localization of NOSIP and showed the same distribution as the WT (Figure 38 A). The double mutation S36D/S138D did not have an effect, as the single mutations. Interestingly, the mutation Y14E resulted in a clear shift of NOSIP-HA towards the cytoplasm. Combining the mutation of Y14E with either S36D, S138D or both, resulted in an almost equal distribution between nucleus and cytoplasm, as the Y14E mutation alone (Figure 38 A). To clearly determine the effect of the mutants on the localization of NOSIP, the nucleocytoplasmic ratio (N/C ratio) of NOSIP was analyzed. In the quantification, the mutations S36D, S138D and S36D S138D showed a clear nuclear localization of NOSIP, similar to the WT (Figure 38 B). All mutants containing the mutation Y14E showed a shift of NOSIP to the cytoplasm, which was statistically significant (Figure 38 B).

The mutations Y14E and Y14E S36D S138D were introduced into the GFP-GST-NOSIP construct. Transfection of GFP-GST-NOSIP Y14E showed a pronounced enrichment in the cytoplasm, whereas GFP-GST-NOSIP WT localized mainly to the nucleus and only in single cells more to the cytoplasm (Figure S 11). The Y14E S36D S138D mutation introduced into GFP-GST-NOSIP, resulted in stronger cytoplasmic localization than Y14E alone (Figure S 11).

The mutation NOSIP-HA S107D led to an increased localization in the cytoplasm (Figure 38 A). This was confirmed by quantification, but the cytoplasmic enrichment

was lesser than for NOSIP-HA Y14E (Figure 38 B). This showed that both mutations, Y14E and S107D, altered the cellular localization of NOSIP, which was based on the introduced positive charge at these respective residues.

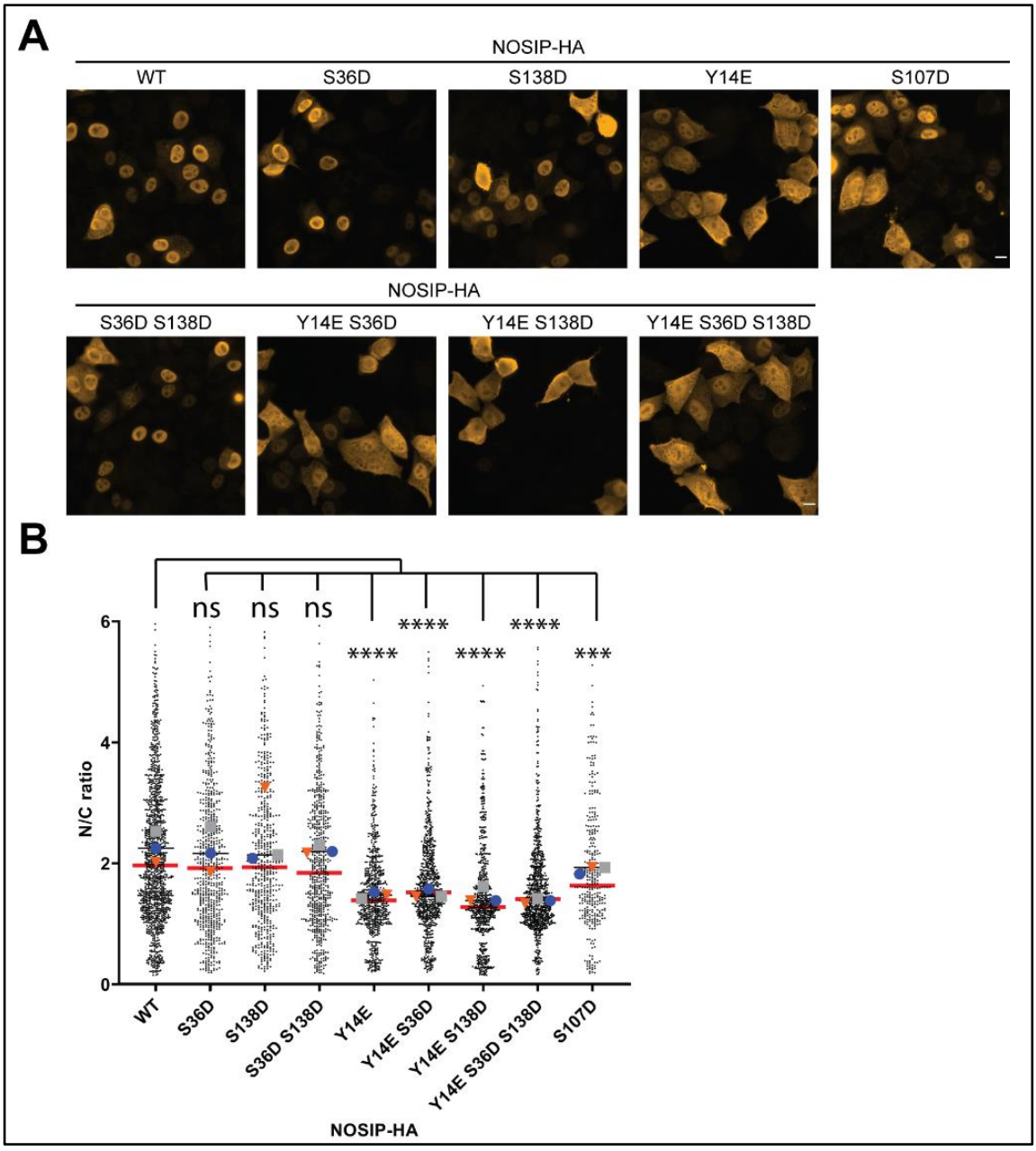

*Figure 38: Y14E mutation mimics phosphorylation and shifts NOSIP to the cytoplasm in HeLa P4 cells. (A) NOSIP S36, S107, S138 were mutated to asparagine (D) and Y14 was mutated to glutamate to mimic the charge of a phosphorylation. These mutations were introduced into NOSIP-HA either alone or in combinations with each other and transfected in HeLa cells using the calcium phosphate method. NOSIP-HA was visualized by indirect immunofluorescence using an HA antibody and analyzed by epifluorescence microscopy. Scale bar 10 µm. (B) Images, acquired in A, were used and the nuclear and cytoplasmic fluorescence were measured and divided to obtain the nucleocytoplasmic ratio (N/C ratio). Data was plotted in GraphPad prism 9. For each condition, 350-1000 cells were analyzed. All data points are plotted as small black symbols, the red line represents the mean of three independent experiments, bigger symbols (blue, orange, grey) represent the mean values of each experiment. Cells were analyzed using CellProfiler software. For statistical analysis a one-way ANOVA with Bonferroni post-test was done. P-values <0.05 were considered as significant (ns >0.05; *** = <0.001; **** = <0.0001)*

3.7.4 The Y14E mutation does not affect the interaction of NOSIP with NTRs

The mutation Y14E caused a shift of NOSIP to the cytoplasm. Y14E mimicked the negative charge of a phosphorylation at this residue. In the context of nuclear transport, it was observed that phosphorylation can enhance nuclear import of a cargo, as seen for SV40 T-antigen (Hübner *et al.* 1997), or to impair import activities, like in the case of PTHrP (Lam *et al.* 1999). Alternatively, it is possible that the phosphorylation does not impair the nuclear import of NOSIP, but instead promote interaction with a cytoplasmic binding partner, which in turn retains NOSIP in the cytoplasm. In order to analyze how the mutation Y14E caused the increased cytoplasmic localization, transport assays and binding assays were performed.

First, the binding of NOSIP to NTRs was analyzed by a pull-down and a binding assay, which were performed as described before. Immobilized mutant or WT His-NOSIP-MBP were incubated with HeLa lysate and an excess of RanQ69L$_{1-180}$-GTP was used as specificity control. When immobilizing His-NOSIP-MBP, all tested NTRs (importin -α, -β, -7, -13 and transportin 1) bound in the absence of Ran, but not in its presence as before (compare Figure 14 A). CRM1 bound in the presence of Ran, but not in its absence (Figure 39 A). The same was observed for His-NOSIP-MBP Y14E. In the binding assay, using purified NTRs, all tested His-tagged NTRs (importin -α/β, -β/7, -β, -7, -13, -5, transportin 1), except CRM1, bound to WT and mutant NOSIP. This indicates that the mutation Y14E did not affect the interaction with NTRs (Figure 39 B).

Since the binding of NTRs to His-NOSIP-MBP Y14E was not affected, it was tested if the mutant protein was able to form stable complexes with NTRs. As a representative NTR, transportin 1 was chosen and a complex was formed with His-NOSIP-MBP Y14E or the WT protein. Complex formation was analyzed by size exclusion chromatography. His-NOSIP-MBP has a molecular weight of ~78 kDa and His-transportin 1 of ~105 kDa. The similar size of both proteins led to partially over-lapping elution peaks of the proteins (Figure 40 A, C). A complex of His-NOSIP-MBP and His-transportin 1 would elute earlier from the column, based on the increased size of ~183 kDa.

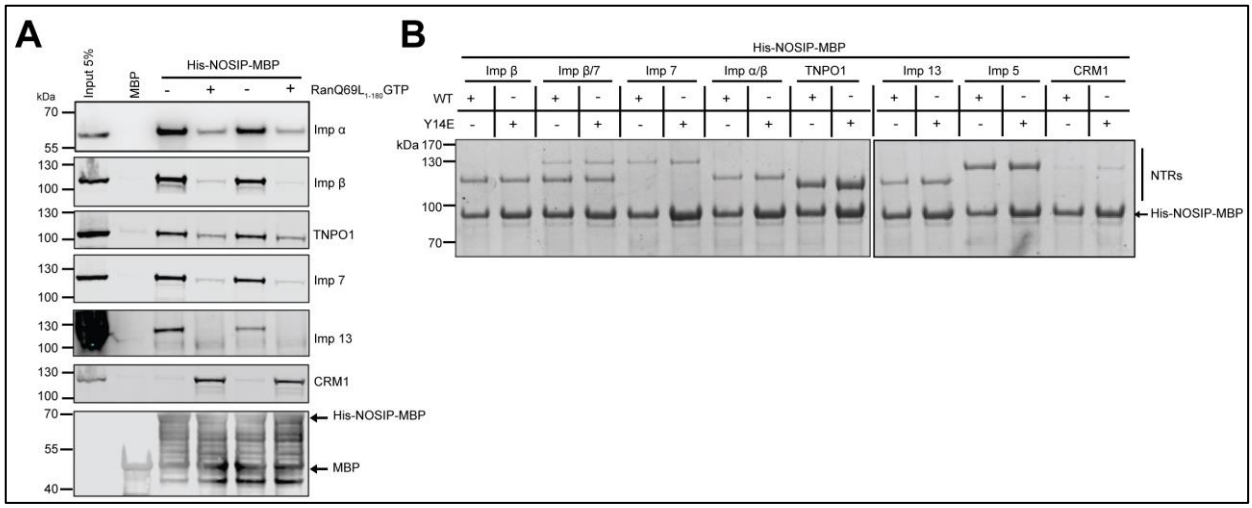

Figure 39: NOSIP Y14E is not impaired in its binding to NTRs. (A) Pulldown of NTRs out of HeLa cytosol using His-NOSIP-MBP WT (wildtype) compared to Y14E mutant. His-NOSIP-MBP WT or mutant or His-MBP protein (600 pmol) were immobilized on MBP-Trap and incubated with HeLa cytosol in the presence or absence of RanGTP$_{1-180}$ Q69L (2000 pmol). Unbound proteins were washed out and bound proteins were eluted using 4x SDS-sample buffer. Eluted proteins were separated by SDS-PAGE and analyzed by Western blotting approach with respective antibodies as indicated. For the bottom blot, anti-MBP antibody was used to control the immobilization of MBP or His-NOSIP-MBP. (B) The binding of purified NTRs to immobilized His-NOSIP-MBP (WT or Y14E) was analyzed using a binding assay. His-NOSIP-MBP (WT or MT) (100 pmol) was immobilized on amylose resin and incubated with 100 pmol of purified His-tagged NTR. Bound proteins were eluted using 4x SDS-sample buffer and analyzed by SDS-PAGE, followed by Coomassie staining.

His-NOSIP-MBP and His-transportin 1 were co-eluted from the SEC column, indicating that a complex was formed (Figure 40 A, B). However, His-NOSIP-MBP (WT and mutant) were used in a 2-fold molar excess, because His-NOSIP-MBP Y14E partially precipitated during the incubation time. Like His-NOSIP-MBP WT, the mutant formed a stable complex with His-transportin 1 (Figure 40 A black curve, B). As seen in the respective SDS-gels, (Figure 40 B) the total amount of His-NOSIP-MBP Y14E formed a complex with His-transportin 1, whereas in the complex His-NOSIP-MBP with His-transportin 1 free His-NOSIP-MBP was detectable. This was due to the precipitation of His-NOSIP-MBP Y14E. Nevertheless, this demonstrates that His-NOSIP-MBP Y14E was still able to form a complex with NTRs.

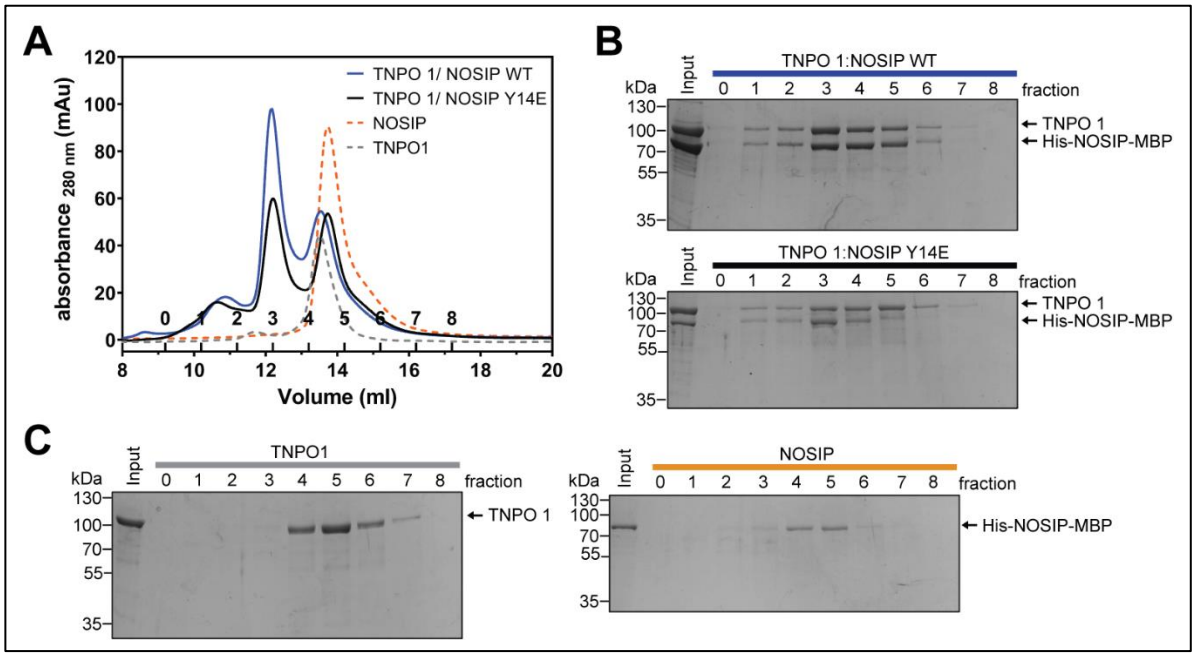

Figure 40: His-NOSIP-MBP Y14E formed a complex with His-transportin 1. (A) 20 µM His-transportin 1 were incubated with 40 µM His-NOSIP-MBP WT (wildtype) or Y14E for 1 h on ice in 1x TPB. Formed complexes and single proteins, as controls, were analyzed by gel filtration, while continously monitoring the absorbance at 280 nm. Note that His-NOSIP-MBP Y14E tended to precepitate during the incubation step on ice. Fractions were analyzed by SDS-PAGE, followed by Coomassie staining. (B) SDS-gels of His-transportin 1 and His-NOSIP-MBP (upper gel) or Y14E (lower gel) and of (C) His-transportin 1 (left gel) or His-NOSIP-MBP (right).

3.7.5 Characterization of the effect of NOSIP Y14E on nucleocytoplasmic transport

As shown before, NOSIP containing the mutation Y14E was not impaired in its interaction with NTRs (Figure 39) and formed a complex with His-transportin 1 (Figure 40). Hence, the increased cytoplasmic localization was not based on a reduced interaction with NTRs. To test if the efficiency of the nuclear import of NOSIP was altered, a heterokaryon assay and a GR-Assay were performed.

First, NOSIP-HA or GFP-GST-NOSIP containing the mutations Y14E and Y14E S36D S138D were used for a heterokaryon assay. NOSIP-HA Y14E and NOSIP-HA Y14E S36D S138D shuttled between NIH 3T3 and HeLa nuclei, similar to NOSIP-HA (Figure 41). Of note, the increased cytoplasmic localization of both mutants remained after fusion of cells and only the nuclear fraction of NOSIP-HA originating from HeLa nuclei was equally distributed between both nuclei. GFP-GST-NOSIP mutant proteins did not shuttle in this assay, indicating that the GFP-GST-NOSIP mutants were not actively exported, as the GFP-GST-NOSIP WT. Again, the cytoplasmic fraction of NOSIP before fusion of HeLa and NIH 3T3 cells remained after the fusion. Performing

the same assay in the presence of LMB did not alter the shuttling of NOSIP-HA or GFP-GST-NOSIP mutants (Figure S 12).

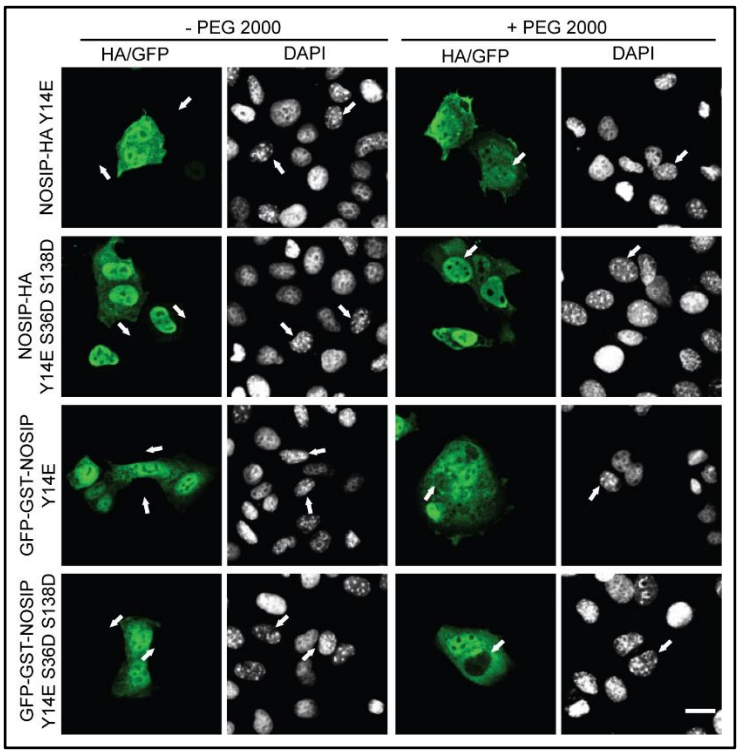

Figure 41: Y14E and Y14E S36D S138D mutations did not alter the nucleocytoplasmic shuttling of NOSIP. The heterokaryon assay was performed by fusing (+ PEG 2000 or as control – PEG 2000) HeLa P4 cells, transfected with NOSIP-HA or GFP-GST-NOSIP (Y14E or Y14E S36D S138D), and NIH 3T3 cells. Cell nuclei were distinguished by their DAPI staining, NIH 3T3 nuclei show several bright dots and are indicated by arrows. Proteins of interest were detected by their fluorescence tag or, in case of NOSIP-HA, by indirect immunofluorescence using an anti-HA antibody. Nuclear shuttling of fluorescently labeled proteins was analyzed by confocal microscopy. Scale bar 20 µm.

Second, the GR assay was used to analyze if the Y14E mutation led to increased nuclear export. In addition, the impact of the Y14E mutation on the transport efficiency could be analyzed, since the import and export could be controlled. Both, GR_2-GFP-NOSIP WT and Y14E, were retained in the cytoplasm through the fused GR fragment in the absence of dexamethasone. After 10 to 20 min of induced import, both proteins accumulated already partially in the nucleus. For GR_2-GFP-NOSIP WT Y14E, the import activity seemed to be reduced in some cells (Figure 42). After 40 to 60 min of nuclear import, GR_2-GFP-NOSIP WT accumulated exclusively in the nucleus, whereas GR_2-GFP-NOSIP WT Y14E showed a cytoplasmic retention in some cells (Figure 42). This indicates either slower import activity or an incomplete nuclear import in some cells. When nuclear export was induced, GR_2-GFP-NOSIP WT and Y14E were not exported, as observed before (compare Figure 13). Some cells, which were transfected with GR_2-GFP-NOSIP Y14E, showed a cytoplasmic signal after 120 min

of export. This was also seen for some cells after 60 min of import, suggesting that these cytoplasmic signals were based on an incomplete import reaction, instead of mediated active export. This is supported by the fact, that in the majority of cells GR_2-GFP-NOSIP Y14E was retained in the nucleus after 120 min of export.

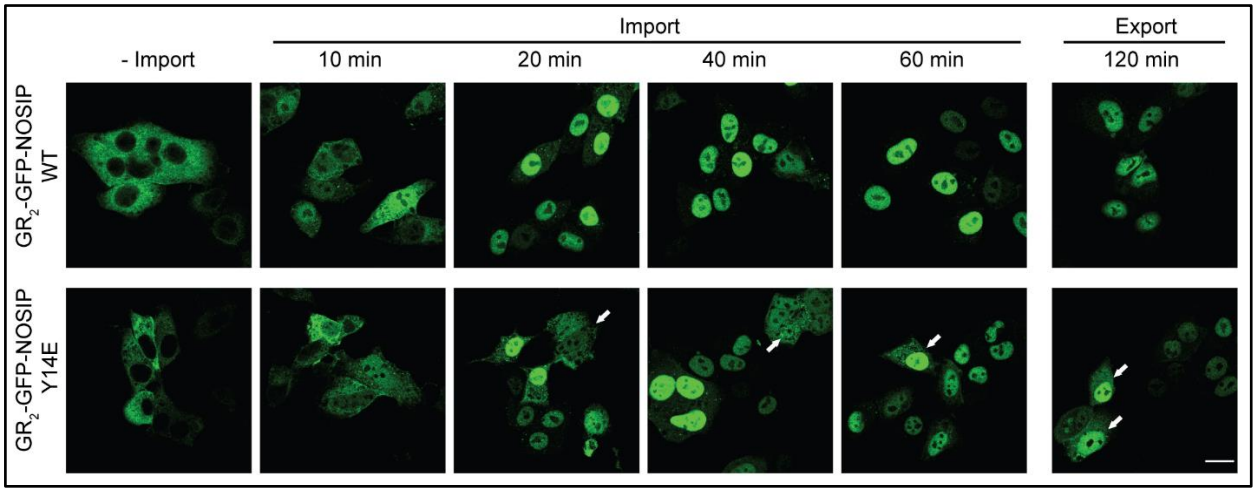

Figure 42: GR-assay using GR_2-GFP-NOSIP WT vs. Y14E mutant. Here, the import and export of NOSIP WT (wildtype) vs. Y14E was analyzed. In this in vivo transport assay, nuclear import and nuclear export can be controlled by treatment with steroid (dexamethasone) or removal of steroid, respectively. The GR fragment is bound to cytoplasmic structures in the absence of steroid and is imported upon steroid treatment. For import 5 µM dexamethasone were added and cells were fixed at indicated time-points to analyze import. After removal of steroid, proteins, if an NES is present, will be exported and retained in the cytoplasm again. Arrows indicate cells showing lower nuclear import of GR_2-GFP-NOSIP Y14E compared to the WT. Localization of proteins was analyzed by fluorescence microscopy. Scale bar 20 µM.

Third, nuclear import of His-NOSIP-MBP Y14E was analyzed in digitonin-permeabilized cells. The assay was performed as described before. As before (compare Figure 20), transportin 1 and importin 13 imported His-NOSIP-MBP most efficiently and importin β, importin 7 and importin β/7 also imported His-NOSIP-MBP, however, with a lower efficiency (Figure 43 A). When using His-NOSIP-MBP Y14E, the import efficiency was reduced and import was only observed in some cells (Figure 43). Again, controls using buffer only, cytosol or cytosol with WGA were performed to test the specificity of the assay (Figure 43 C). Of note, the positive control using cytosol showed a reduced nuclear import of His-NOSIP-MBP Y14E compared to His-NOSIP-MBP. Like His-NOSIP-MBP, His-NOSIP-MBP Y14E was imported most efficiently by transportin 1 and importin 13, but with a reduced efficiency compared to His-NOSIP-MBP (Figure 43 B). The import efficiency of importin β, -7 and -β/7 was already reduced for His-NOSIP-MBP and was further reduced for His-NOSIP-MBP Y14E. This pointed to a reduced nuclear import efficiency, but this result needs to be interpreted

with caution, since His-NOSIP-MBP Y14E was partially precipitating, as seen for the complex formation (Figure 43 B).

Taken together, mutant NOSIP proteins were observed to shuttle, as wildtype NOSIP, in a heterokaryon assay (Figure 41). Further, the GR-assay showed a slightly reduced nuclear import of the NOSIP Y14E mutant (Figure 42). In digitonin-permeabilized cells, performed with His-NOSIP-MBP WT and Y14E, the mutant was observed to enter the nucleus less efficiently (Figure 43). Taken together, NOSIP containing the mutation Y14E was still imported into the nucleus, but the experiments point to a reduced nuclear import.

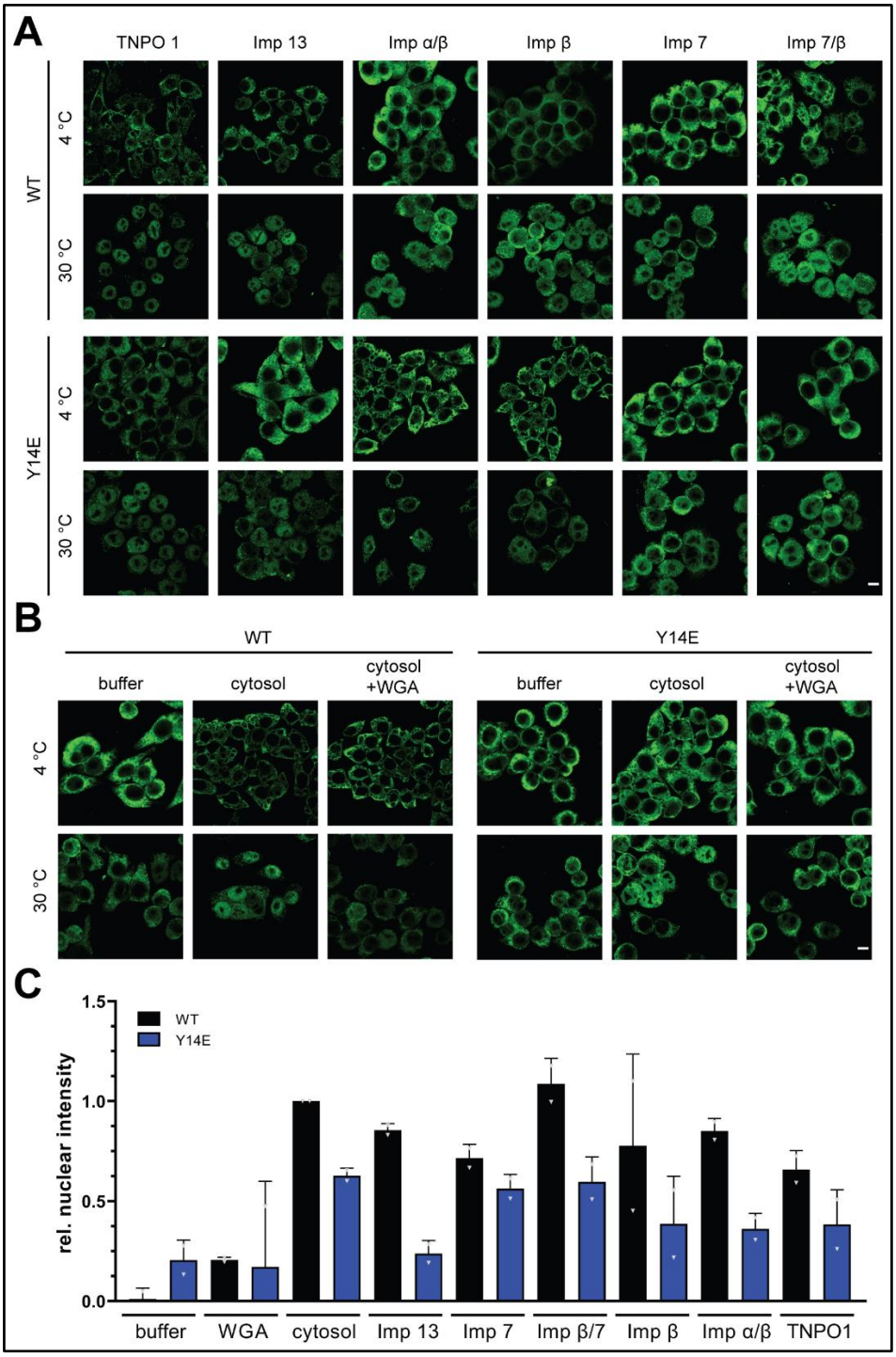

Figure 43: The import of His-NOSIP-MBP Y14E was lower compared to His-NOSIP-MBP WT in digitonin-permeabilized HeLa cells. (A) Nuclear import assay was performed using purified Imp 13, -7, -α, -β and TNPO 1. As cargo, either His-NOSIP-MBP WT (wildtype) or His-NOSIP^{Y14E}-MBP were used and visualized by indirect immunofluorescence using an MBP antibody. All reactions were carried out at 30 °C and at 4 °C, as control. Nuclear import was analyzed by confocal microscopy, scale bar 10 µM. (B) Quantification of the results are presented in A. The mean nuclear fluorescence intensities of 4 °C reactions were subtracted from the respective 30 °C values and normalized to the value obtained for the reaction containing cytosol of wildtype His-NOSIP-MBP, which was arbitrarily set to 1.

4 Discussion

4.1 Nuclear transport of Lipin 1

Lipin 1 functions as a transcriptional co-activator and in lipid metabolism and the subcellular localization is essential for both functions(Finck *et al.* 2006; Ren *et al.* 2010) The nuclear transport of Lipin 1 is very complex and regulated through multiple interactions or PTMs. In general, the nuclear localization of Lipin 1 is mediated by importin α/β through the interaction with an NLS (Ren *et al.* 2010). This could be confirmed in HeLa cells by knockdown experiments and the usage of inhibitors (Figure 6 and Figure 9). Interestingly, the interaction of Lipin 1 with importin 13 was also confirmed (Figure 7 and Figure 8). However, importin α/β was shown to be the preferred import pathway under physiological conditions. Nonetheless, importin 13 rescued the phenotype of an importin β knockdown, indicating a possible role of importin 13 in Lipin 1 nuclear import. The role of importin 13 could depend on specific cellular conditions. For instance, importin 13 is reported to play a key role in the transcriptional response of oxidative stress (Gajewska *et al.* 2021). Moreover, Lipin 1 expression is upregulated under oxidative stress conditions (Seo and Shin 2017). If importin 13 is involved in the oxidative stress-induced upregulation of Lipin 1 needs to be analyzed in the future.

Instead of regulating the nuclear import of Lipin 1 under specific cellular conditions, the preferred NTR can be tissue specific. In HeLa cells, importin 13 is only of low abundance, but in neuronal tissues importin 13 is expressed to higher levels. Lipin 1 nuclear localization in neuronal cells was shown to be regulated through sumoylation (Liu and Gerace 2009). A sumoylation depended nuclear import of Lipin 1 in HeLa cells was not observed, indicating that this regulation is tissue depended (data not shown). However, the specific NTR in neuronal tissue mediating the nuclear import of Lipin 1 was not analyzed. Lipin 1 can possibly be imported tissue specifically in neuronal cells by importin 13.

The nuclear export of Lipin 1 is CRM1 depended, since LMB treatment led to the accumulation of over-expressed Lipin 1 within the nuclei of HeLa cells (Figure 5 and (Ren *et al.* 2010). However, no functional NES is experimentally characterized. Predicting potential NESs using the LocNES prediction server

(http://prodata.swmed.edu/LocNES, (Xu *et al.* 2015)) resulted in two potential regions with a high-score, Lipin $1^{398-414}$ or Lipin $1^{624-640}$ (Table S 10). CRM1 bound to GST-Lipin 1 FL and GST-Lipin 1^{1-619}, which lacks the second potential NES, indicating that the first region Lipin $1^{398-414}$ may function as an NES for Lipin 1. To verify this region as true NES, mutational studies and export assays should be performed.

Taken together, the nuclear transport of Lipin 1 is mediated through importin α/β under physiological conditions. Importin 13 binds to Lipin 1 and can partially rescue an importin β knock down, indicating a role of importin 13 probably under certain conditions. Further, the observations indicate that the NES of Lipin 1 may be in region Lipin $1^{398-414}$ (^{398}Y**L**DD**L**TD**M**DPE**V**AA**L**^{414}).

4.2 Nucleocytoplasmic transport of NOSIP

4.2.1 Nuclear shuttling of NOSIP

NOSIP functions as an inhibitor of the eNOS enzyme (Dedio *et al.* 2001; König *et al.* 2002; König *et al.* 2005; Schleicher *et al.* 2005). eNOS is relocated from the plasma membrane to the cytoskeleton through the interaction with NOSIP (Schleicher *et al.* 2005). NOSIP, as a protein of 34 kDa, is small enough for passive diffusion through the NPC and should be present in the cytoplasm and nucleus. However, NOSIP shows a strong accumulation in the nucleus of cultured cells, which points to a higher active import rate compared to export (Dedio *et al.* 2001; König *et al.* 2002; Schleicher *et al.* 2005). For its function as an inhibitor of eNOS, NOSIP itself was shown to relocalize to the cytoplasm (Schleicher *et al.* 2005). This raised the question of how the subcellular localization of NOSIP is regulated.

Therefore, the nuclear transport of NOSIP was characterized in general and in a cell-cycle dependent manner, discussed in section 4.2.2. Various transport assays were used to examine the nuclear transport of NOSIP. In a HKA and GR assay, NOSIP was shown to accumulate in the nucleus. Further, the nuclear import of His-NOSIP-MBP can be reconstituted in digitonin permeabilized HeLa cells, indicating that NOSIP is actively imported into the nucleus by NTRs. This can explain the nuclear accumulation in the nucleus of cultured cells. However, several points exclude the possibility of active nuclear export in interphase HeLa cells. First, NOSIP with fused GFP-GST-tag,

to increase the size above the limit for passive diffusion, prevented any shuttling in HKA (Figure 12). Second, in the GR assay, GR-GFP-NOSIP was retained in the nucleus, whereas the control protein showed export activity, excluding active export of NOSIP (Figure 13). Third, NOSIP, neither HA-tagged, GFP-GST-tagged nor endogenous NOSIP, was affected by LMB treatment, ruling out CRM1 as an export receptor under these experimental conditions. However, in interphase HeLa cells, NOSIP was shuttling passively between nucleus and cytoplasm and was additionally imported actively into the nucleus. This showed that active and passive nuclear import outbalance passive nuclear export, leading to the strong nuclear accumulation of NOSIP.

4.2.2 Nuclear transport during G2-phase/mitosis

As mentioned above, NOSIP is enriched in the cytoplasm during G2-phase of the cell-cycle. Additionally, NOSIP was found to be phosphorylated during mitosis in proteomic screens (Dephoure *et al.* 2008; Olsen *et al.* 2010). This raised the possibility that phosphorylation regulates the cell-cycle dependent localization of NOSIP. These identified phosphorylation sites were mutated to mimic the charge of a phosphorylation to analyze the effect on NOSIPs localization. The phosphomimic mutants Y14E and to a lower extent S107D were enriched in the cytoplasm of HeLa cells. NOSIP-HA Y14E showed an equal distribution within cells and GFP-GST-NOSIP Y14E was partially excluded from the nucleus (Figure 38, Figure S 11). The cytoplasmic retention of NOSIP could be based on reduced or inhibited nuclear import within HeLa cells. For PTHrP it was shown that its nuclear import is reduced upon phosphorylation of its NLS (Lam *et al.* 1999). $Y14^{NOSIP}$ is not in the proximity of the bpNLS of NOSIP, but this can be a mechanism for residue $S107^{NOSIP}$, which is close to the bpNLS (see section 3.4). The Y14E mutant in HKA or GR assay did not change nuclear transport/shuttling of NOSIP (Figure 41 and Figure 42). The reduced import efficiency in the import assay using digitonin permeabilized HeLa cells needs to be interpreted with caution, since His-NOSIP-MBP Y14E was partially precipitating (Figure 43). Thus, Y14E did not affect the nuclear transport of NOSIP.

Cytoplasmic retention of NOSIP seems to be based on the interaction with a cytoplasmic binding partner and this binding is likely stimulated through phosphorylation. A similar scenario is known for Lipin 1, where insulin induced

phosphorylation of Lipin 1 promotes the interaction with the 14-3-3 protein and retains it in the cytoplasm (Péterfy *et al.* 2010). This interaction would sequester NOSIP away from the nuclear transport machinery. All NOSIP constructs, which contain the Y14E mutation, showed an equal distribution between nucleus and cytoplasm (see section 3.7). This equal distribution could be also observed in cells used for HKA or GR-assay. Surprisingly, the cytoplasmic fraction of NOSIP-HA Y14E remained in fused cells. This indicated that only the nuclear fraction of NOSIP, originating from HeLa nuclei, was distributed between both nuclei (Figure 41). In the GR-assay using GR-GFP-NOSIP Y14E some cells showed a cytoplasmic retention after induced nuclear import. This indicates that NOSIP is retained in the cytoplasm, when Y14 phosphorylation is mimicked.

Interestingly, eNOS enriched in a Triton X-100 insoluble fraction after stimulation with tyrosine phosphatase inhibitors (Fleming *et al.* 1998). The interaction of NOSIP and eNOS is based on the relocalization of eNOS to the cytoskeleton, which is known as the triton-insoluble fraction. The $Y14^{NOSIP}$ mutation to E, to mimic phosphorylation, lead to a localization of NOSIP to the cytoplasm, which could be explained through the interaction with eNOS. Phosphorylation of Y14 leads to the cytoplasmic retention of NOSIP, possibly through increased binding to eNOS. This binding leads to a shift of eNOS, which was bound to NOSIP, to the cytoskeleton and in turn prevented the nuclear import of NOSIP.

Another possibility is that the phosphorylation of NOSIP uncovered an NES, leading to active nuclear export or blocked the NLS, which leads to abolished import, increasing cytoplasmic NOSIP that interacts with eNOS. However, during G2-phase of the cell-cycle the balance between import and export seemed to be unchanged, pointing to the retention of NOSIP in the cytoplasm upon interaction with a binding partner, probably eNOS.

4.2.3 Interaction of NOSIP with CRM1

Surprisingly, NOSIP specifically interacted with CRM1 in a RanGTP-dependent manner. Despite this interaction, no active export was shown under our experimental conditions. It is likely that the export of NOSIP was based on passive diffusion in interphase cells (see section 4.2.1). The binding of NOSIP to importin β, transportin 1

and importin 13 was based on the interaction with the N-terminal arch, which is also the binding region of RanGTP (Chook and Blobel 1999; Vetter *et al.* 1999; Grünwald *et al.* 2013). The binding of CRM1 and NOSIP depended on the presence of RanGTP, indicating that the interaction of NOSIP and CRM1 is different. Using the NES prediction server LocNES (http://prodata.swmed.edu/LocNES), NOSIP$^{198-214}$ was only predicted as potential NES with a low score of 0.145 – 0.172 (Table S 9). Nonetheless, LMB did not affect NOSIPs localization (Figure 12) in HeLa cells. If NOSIP was exported by CRM1, the binding would be LMB independent. An LMB independent binding to CRM1 is reported for the CDK (cyclin dependent kinases) inhibitor p27. p27 binds to CRM1 through an unconventional NES to the classic NES cleft and an additional region, which is suggested to be responsible for the LMB insensitivity (Connor *et al.* 2003).

In the context of NOSIP's cellular function as a suppressor of eNOS activity, CRM1 could play a role in NOSIP's cytoplasmic accumulation during the G2-phase of the cell-cycle. During cell-cycle progression, NO levels need to be reduced, as elevated NO levels were shown to block the cell-cycle progression at G1/S or G2/M stage (Napoli *et al.* 2013). The progression of the cell-cycle is driven by phosphorylation through CDKs. Mimicking phosphorylation of some residues of NOSIP led to an accumulation of NOSIP in the cytoplasm (Figure 38). Cell-cycle dependent phosphorylation of NOSIP, as found in proteomic screens, could lead to active nuclear export of NOSIP. Phosphorylation of NOSIP can possibly induce a conformational change, which uncovers an NES like sequence, leading to the binding of an exportin and active export. A similar mechanism was observed to induce nuclear import. For instance, phosphorylation of the ERK5 NES prevents its export and lead to increased nuclear import (reviewed in (Nardozzi *et al.* 2010)). Alternatively, phosphorylation of NOSIP could lead to homodimerization, which could expose a dimer-specific NES. Likewise, STAT1 phosphorylation induces its homodimerization and exposes a dimer-specific NLS (reviewed in (Nardozzi *et al.* 2010)). To examine this, some functional assays are required or structural studies of a CRM1-NOSIP-RanGTP complex.

4.3 Interaction with NTRs

4.3.1 Interaction of NOSIP with multiple NTRs

NOSIP was reported to be imported into the nucleus by importin α/β (Schleicher *et al.* 2005). Here it was shown that NOSIP interacts with and is imported by multiple NTRs, but importin α did not seem to be involved. A previous study showed, that NOSIP from a cell lysate binds to immobilized GST-importin α (Schleicher *et al.* 2005). Such a binding was confirmed in a pulldown assay (Figure 14 A). *In vitro* no direct binding of importin α to NOSIP was observed (Figure 14 C). Instead, importin β bound independently of importin α to NOSIP and the binding of importin α and NOSIP to importin β was mutually exclusive (Figure 19) through distinct but maybe partially overlapping binding sites. Thus, the detection of importin α in the pulldown assay in both studies may be explained by the presence of additional factors in the cytosol. NOSIP as E3-ubiquitin ligase is probably interacting with several proteins, since E3 enzymes often function as scaffold proteins in the ubiquitination process. Binding of importin α was only observed in the presence of cytosol, but not *in vitro* using purified proteins, leading to the assumption that NOSIP interacts with importin α cargoes and is through this interaction detected in the pulldown assays. The indirect import of proteins, which bind through another cargo to importin α, is called piggybacking. This is known for cargoes like PP1 (protein phosphatase 1) (Lesage *et al.* 2004) and possibly plays a role in NOSIP nuclear import. This can explain the effect of the importin α/β inhibitor, Bimax2, which had an effect on over-expressed NOSIP only. In these experiments, NOSIP was highly expressed and the preferred NTR was the rate-limiting factor. The excess of NOSIP was then transported by other NTRs or piggybacked by importin α/β.

All other tested NTRs interacted specifically with NOSIP, since the binding was observed to be sensitive to RanGTP (Figure 14). Further, all NTRs *in vitro*, except importin 5, were able to specifically import NOSIP (Figure 20). The binding to multiple NTRs was already reported for other cargoes like c-Fos (Arnold *et al.* 2006b), HIV-1-Rev protein (Arnold *et al.* 2006a), FUS (Baade *et al.* 2021) and histones (Bernardes and Chook 2020). This redundancy of NTRs is also reflected in proteomic screens, where NTRs show over-lapping cargo-spectra (Kimura *et al.* 2017; Mackmull *et al.*

2017; Baade *et al.* 2018). Nevertheless, most cargoes show a preference for a specific NTR, e. g. HIV-1-Rev protein for importin β (Arnold *et al.* 2006a) and FUS for transportin 1 (Baade *et al.* 2021). NOSIP was shown to have a preference to transportin 1 (section 3.5). The interaction of several NTRs with NOSIP may result from its high conservation between species. It is well conserved between dinoflagellates, *X. laevis*, D. rerio and *H. sapiens* (Figure S 13). The high conservation of NOSIP is based on its involvement in the regulation of NOS, at least in mammals (Dedio *et al.* 2001). Like NOSIP, NTRs are well conserved in their structure, especially in the N-terminal part (Ran binding site) (Chook and Blobel 1999), where NOSIP binds. Since NOSIP binds to the well conserved N-terminal region of NTRs, it is possible that NOSIP bound to an ancestor of the NTRs. Cingolani and co-workers suggested, that the N-terminal arch, consisting of HEAT-repeat 1-11, is the ancestor of the NTRs, which retained during evolution to some degree (Cingolani *et al.* 2002). During time the NTR evolved to the NTRs known today, with specified cargo recognition sites at the C-terminal arch. NOSIP may represent and ancestral type of NLS, which binds the well-conserved N-terminal, this was also suggested for PTHrP (Cingolani *et al.* 2002).

Alternatively, NOSIP is transported in a tissue-specific manner by different import pathways. Here, nuclear transport of NOSIP was mainly analyzed in HeLa cells. It is known that the abundance of NTRs differs between tissues. Importin 13, for example, is of low abundance in most tissues, but higher expressed in the brain and testis. In line with this, NOSIP was shown to be important during brain development (Hoffmeister *et al.* 2014) and involved during the early development of the eye-anlagen (Flach *et al.* 2018). Importin 13 plays a role in developmental processes through the import of Arx (aristaless-related homeobox) (Lin *et al.* 2009), important during the development of the forebrain (Friocourt *et al.* 2006). Importin 13 itself is developmentally regulated in rat fetal lung (Tao *et al.* 2004). Perhaps, NOSIP is specifically transported by importin 13 in neuronal cells or during developmental processes. As transportin 1 is not tissue specifically expressed, it is probably the preferred pathway in most cells.

4.3.2 The bpNLS of NOSIP is not sufficient for the nuclear import of NOSIP

The bpNLS differs slightly from the consensus sequence of a bipartite NLS (Schleicher *et al.* 2005). Deletion or mutation of the bpNLS was shown to prevent the binding of NOSIP to importin α or the nuclear localization (Schleicher *et al.* 2005). This was confirmed by using the K78AK79A mutant of NOSIP (Figure 22). However, fusing the bpNLS to GFP-GST, only a weak nuclear accumulation was observed (Figure 21). A His-NOSIP-MBP construct comprising residues 1-110, including the bpNLS, bound only weakly to NTRs. Extending this fragment to residue 240, increased the binding of NTRs, indicating that some additional regions may promote its nuclear accumulation. In experiments using different fragments, the minimum residues for a clear nuclear accumulation were $NOSIP^{25\text{-}285}$ (Figure 25). This experiment showed that the residues $NOSIP^{26\text{-}55}$ promoted the nuclear accumulation, since the deletion led to a reduced nuclear accumulation. Additionally, $NOSIP^{111\text{-}240}$, which lacks the bpNLS, was required for the nuclear localization of NOSIP, because this construct localized like the bpNLS alone. Taken together, several regions are necessary for the strong nuclear accumulation of NOSIP. This points to a recognition of NOSIP through its folded structure, maybe through the exposure of an NLS-like domain. In the AlphaFold model, the bpNLS located in the beginning of the long α-helix. The lysins $K172^{NOSIP}$, $K175^{NOSIP}$ and $K178^{NOSIP}$ are located in the antiparallel IDR of NOSIP at the height of the bpNLS (Figure 44 A). This could increase the local concentration of positively charged residues, which are important for the interaction with NTRs (Figure 44 B). This hypothesis is supported by the fact that $NOSIP^{1\text{-}110}$ bound only weakly to NTRs, whereas the construct $NOSIP^{1\text{-}240}$, containing respective lysins, bound as strong as full-length NOSIP (Figure 24).

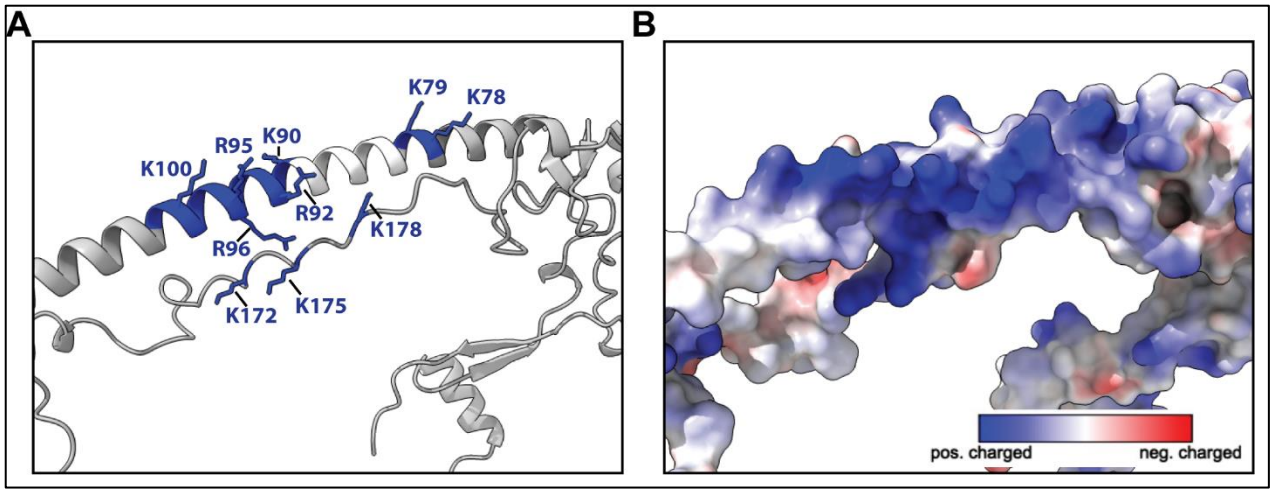

Figure 44: NOSIPs nuclear localization signal. (A) The AlphaFold model of NOSIP is depicted in grey. The two basic clusters of the bipartite NLS are marked in blue and the linker in white. Lysins and arginine are depicted as sticks, additionally the lysins K172, K175 and K178 are depicted as blue sticks. (B) The surface potential of the area from A is depicted. Positively charged regions are shown in blue and negatively charged regions in red. Images were generated using Chimera software.

4.3.3 Unusual binding-mode of NOSIP to NTRs

Interestingly, NOSIP bound mainly to the N-terminal arch of transportin 1, importin 13 and importin β, which is in contrast to the majority of cargoes (Figure 19, Figure 29, Figure 30, Figure 32). Most established cargoes bind to the C-terminal arch of the NTRs (Mboukou *et al.* 2021; Wing *et al.* 2022). The N-terminal arch, where RanGTP binds, is also referred as CRIME domain (CRM1, importin β etc.) (Monecke *et al.* 2014). RanGTP mainly binds to HEAT-repeats (H) 1-7 of the NTRs, one interface binds H 1-3 and the opposite site of Ran binds H 5-7, including the acidic H8-loop of NTRs (Chook and Blobel 1999; Vetter *et al.* 1999).

Only a few cargoes are known to bind to the N-terminal arch of importins. For instance, PTHrP to importin β, Ubc9 to importin 13 (Grünwald and Bono 2011) and the HIV-1-Rev protein and c-Fos to transportin 1 (Arnold *et al.* 2006a; Arnold *et al.* 2006b). PTHrP binds in an extended conformation to H2-11 of importin β and overlaps partially with the IBB binding site (H 7-19). Despite overlapping sites both were shown to bind simultaneously (Cingolani *et al.* 2002; Marfori *et al.* 2011). The importin β fragments used in this work comprise H 1-9 (importin β ΔC) and H 8-19 (importin β ΔN). Thus, the interaction of NOSIP with both fragments can be explained if NOSIP binds to H 2-11 of importin β, similar to PTHrP (Cingolani *et al.* 2002). The importin β ΔC fragment

contains H 2-8 of the PTHrP binding site and bound strongly to NOSIP, while binding of NOSIP to the importin β ΔN fragment, containing H 8-11, was weaker (Figure 19).

The HIV-1-Rev protein and c-Fos are reported to bind to an N-terminal fragment of transportin 1 (H 1-11) and, weaker, to the C-terminal fragment H 12-19 (Arnold *et al.* 2006a; Arnold *et al.* 2006b). For both proteins a similar binding to importin β fragments (N-terminal H 1-9 and C-terminal H8-19) was observed, but c-Fos bound exclusively N-terminal to importin β (Arnold *et al.* 2006b). Like c-Fos and HIV-1-Rev, NOSIP bound to both transportin 1 fragments, but stronger to the N-terminal fragment (Figure 32). Despite the interaction with transportin 1, none of the mentioned cargoes contain a PY-NLS nor an RG/RGG-rich motif. All proteins showed a strong binding to the N-terminal arch of transportin 1, which is clearly different from the typical cargo binding site on the C-terminal arch. However, a weak binding to the C-terminal arch, which contains the binding site for transportin 1 cargoes (for more information see introduction 1.1.5) (Cansizoglu *et al.* 2007), was observed, indicating that the N-terminal binding cargoes are bound to some extent to the C-terminal arch. When crosslinking the transportin 1-NOSIP complex, some crosslinks of the C-terminal arch of transportin 1 ($K502^{TNPO\ 1}$ and $K385^{TNPO\ 1}$) to $K178^{NOSIP}$ were identified (Figure 31). $K502^{TNPO1}$ and $K385^{TNPO\ 1}$ are located within binding site B of PY-NLS cargoes, near to epitope 2 and epitope 3, respectively (Soniat and Chook 2016). Epitope 2 and 3 are usually occupied by the R-X_{2-5}-PY part of the PY-NLS, where R binds to epitope 2 and the PY-motif to epitope 3 (Mboukou *et al.* 2021). Nevertheless, the binding to the C-terminal arch is not necessary for a strong interaction and has probably a stabilizing effect for the N-terminal bound cargo. To map the exact binding regions on transportin 1, further binding assays are needed as well as mutational studies.

However, NOSIP and HIV-1-Rev protein both bind importin β and transportin 1 fragments and both lack a typical PY-NLS sequence. This suggests a more common localization signal, which is rather based on a three-dimensional conformation than on a linear sequence. This point is further addressed in the next section.

4.3.4 Does NOSIP contain a three-dimensional NLS?

NOSIP, HIV-1-Rev, c-Fos and c-Jun bind to transportin 1 but lack a typical PY-NLS, as well as an RG/RGG-rich region (Arnold *et al.* 2006a; Arnold *et al.* 2006b; Waldmann

et al. 2007). This is not surprising, since these proteins, except c-Jun, were observed to bind to the N-terminal arch of transportin 1. Thus, the question arises of how these proteins interact with transportin 1. Comparing the amino acid sequences, no similarities were found. For HIV-1-Rev, c-Fos and c-Jun, basic regions, described as NLSs, are responsible for the interaction with various NTRs. The same was observed for NOSIP in this work. The need of a basic region for the interaction with all NTRs is expected, since the inner concave surface of NTRs is highly acidic. All mentioned proteins bind to NTRs at the N-terminal site. To examine if there was a common feature, the AlphaFold models of these proteins were compared. Only for HIV-1-Rev protein a partial experimental structure was available.

c-Jun and c-Fos, which can form the transcription factor AP-1 (Chiu *et al.* 1988), are structurally very similar. Both contain a long α-helix with a leucine-zipper domain through which they form a coiled-coil to bind DNA (Figure 45, A-B). The residual structure of the transcription factors is predicted to be unstructured. Like the transcription factors, NOSIP contains a long α-helix and an antiparallel oriented disordered region (Figure 45 C). For the HIV-1-Rev protein, no AlphaFold model was available, but a partial crystal structure including the NLS region (Daugherty 2010). The structure consists of two antiparallel oriented α-helices, which are connected by a short turn (Figure 45 D). Interestingly, c-Fos, c-Jun and NOSIP partially share a striking structural similarity. All proteins bind through a very basic region within the long α-helices (regions marked with a circle Figure 45) to NTRs. Further, closely located to this basic α-helical region, unstructured loops can be found, which have a basic character (as seen in the electrostatic depiction in Figure 45). c-Fos binds through this unstructured loop to transportin 1 and through the basic α-helical region to importin β (Arnold *et al.* 2006b). In general, all N-terminal binding cargoes interact with the NTRs via the very basic α-helix, whose positive charge is increased locally through surrounding loops.

Some NLSs are reported to be linear sequences and overall unstructured, but become partially ordered when bound to NTRs, like M9-sequences or classic and bipartite NLSs (Wing *et al.* 2022). The IBB-domain is a special kind of NLS, which is thought to be exclusive for adaptor proteins like importin α (Lott and Cingolani 2011). The IBB-domain consist of a short N-terminal α-helix, followed by a loop and a long α-helix.

The long α-helix has a very basic character with 40% basic residues (Lott and Cingolani 2011). The structure of the IBB domain is similar to the regions of c-Jun, c-Fos, NOSIP and HIV-1-Rev, which are reported to be important for the interaction with NTRs. But in contrast to the C-terminal binding IBB-domain, these proteins bind N-terminal to transportin 1 or importin β. These proteins may represent a class of proteins, containing a three-dimensional NLS, which is structurally similar to the well-defined IBB-domain. For further characterization of this NLS class, structural studies of these complexes are necessary to understand the interactions at an atomic level.

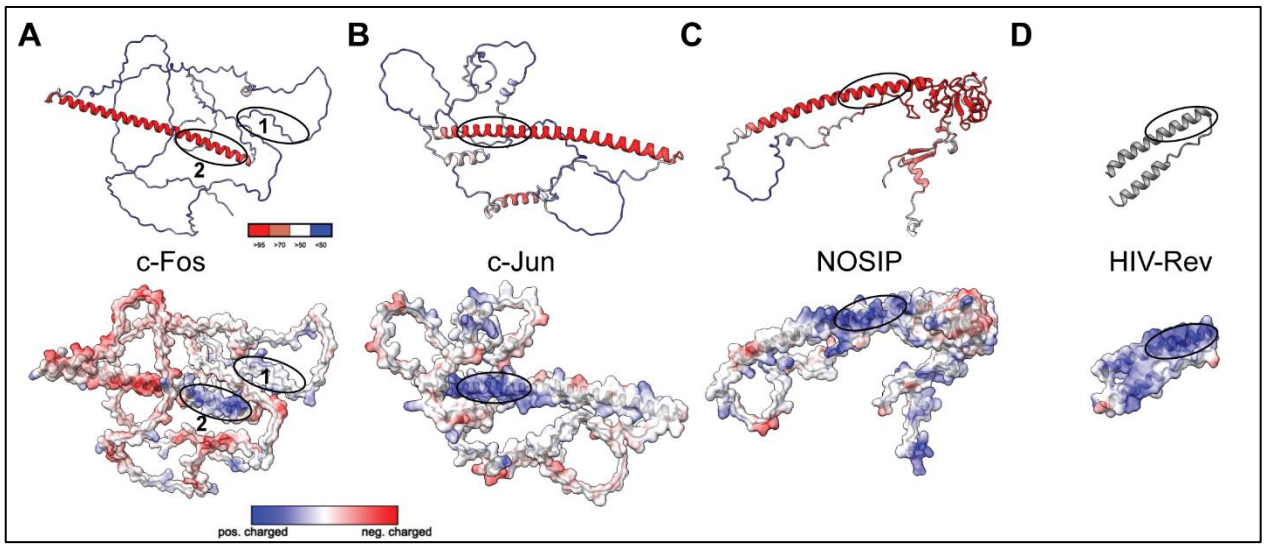

Figure 45: Structure comparison of N-terminal binding proteins. Predicted AlphaFold structures colored in per-residue confidence score (upper structure) and depicted electrostatic potential (lower structure) of c-Fos (A), c-Jun (B) and NOSIP (C). Per-residue confidence score, red residues have a confidence of >95, pale-red of <90 to >70, white <70 to >50 and blue <50. (D) Crystal-structure of the HIV-1-Rev protein (residues 1-70), PDB: 3LPH. Lower structure shows the electrostatic potential. (A-D) Regions identified as NLS binding to NTRs are marked with black circles. c-Fos aa138-160 (circle 2) binds to importin β and aa111-124 binds to transportin 1 (Arnold et al. 2006b); c-Jun aa273-276 binding to several NTRs (Waldmann et al. 2007); HIV-1-Rev aa34-50 binding to NTR (Arnold et al. 2006a); NOSIP aa78-101 binding to several NTRs.

4.3.5 Docking of NOSIP to transportin 1

The identified crosslinks allowed an unambiguous placement of NOSIP to the N-terminal arch of transportin 1 (Figure 31). However, the IDR of NOSIP, which is predicted with a low accuracy, could not be modeled sufficiently. The modelling algorithms of Rosetta and ClusPro dock proteins to each other with a rigid backbone. Some NLSs are known to be unstructured and to adopt a more ordered conformation, when binding to an NTR (Wing *et al.* 2022). It will need to be analyzed if the IDR of NOSIP adopts a different conformation upon binding to an NTR. Despite the clear positioning of NOSIP to the N-terminal Heat-repeats 1-4 of transportin 1, some

crosslinks cannot be explained. Either NOSIP can be bound in different orientations, with region-I facing up or down, close to the very N-terminal α-helices, or NOSIP can be bound as a dimer. Homodimerization of NOSIP would be likely through the long α-helices forming a coiled-coil. An orientation of region-I on opposite sides would correspond to the crosslinking of region-I to the very N- and C-terminal ends of transportin 1. Additionally, the crosslinks of both ends of the long α-helix to the cluster around $K81^{TNPO\ 1}$ and $K85^{TNPO\ 1}$ could be explained. A dimerization of purified His-NOSIP was only observed for a minor fraction (data not shown). Purified NOSIP-NTR complexes showed a retention time, corresponding to a bound monomer. *In vivo* additional factors or PTMs possibly can induce dimerization of NOSIP, which cannot be reconstituted *in vitro*.

However, this model needs to be interpreted carefully, since no experimental structure of NOSIP is available. Furthermore, the packing of NTRs can vary when bound to different cargoes and transportin 1 could adopt a more open conformation, allowing enough space for a homodimer, or in a more closed conformation. To test the model for its reliability, mutational studies need to be performed in the future.

5 Outlook

NOSIP was shown to bind to multiple NTRs, thus it should be analyzed, whether different NTRs transport NOSIP depending on the tissue. This could be tested by knocking-down different NTRs in various cell lines and analyzing the effect on endogenous NOSIP. Further, nuclear transport assays, in respective cell lines, should be performed to analyze the tissue dependency of NTRs by analyzing the transport efficiency.

An alternative hypothesis, stating that NOSIP is transported by different NTRs depending on the cellular conditions like oxidative stress, could be tested in a similar way. In a first step, it could be analyzed if different cellular stress conditions affected the binding of NOSIP to different NTRs. To determine the effect on NOSIPs cellular localization, cells should be exposed to such stress conditions and analyzed by indirect immunofluorescence.

Furthermore, it should be analyzed, if the phosphorylation at Y14 leads to a cytoplasmic retention of NOSIP through mediated binding to eNOS. This could be done by identifying the binding region of NOSIP on eNOS. This binding region should be mutated, the eNOS mutant and NOSIP Y14E mutant should be co-transfected and analyzed, if NOSIP still shows the cytoplasmic retention. Further, it could be interesting to test, if additional PTMs led to the cell-cycle dependent cytoplasmic retention of NOSIP. This could be determined by analyzing NOSIP out of cell lysates from G2-phase or G1-phase, for PTMs using mass spectrometry.

Structural studies, like crystallization, could be done to get more insight into the interaction of NOSIP with transportin 1 or other NTRs. Unfortunately, crystallizing His-tagged or untagged full-length NOSIP with importin 13 or transportin 1 failed. A deletion of the first 37 or the last 13 residues of NOSIP did not work either. In further trials, NOISP$^{75\text{-}180}$, containing the α-helix and the IDR, or NOSIP$^{25\text{-}285}$ could be used. It would be of great interest to identify the binding motif of NOSIP, which leads to the N-terminal NTR binding. Moreover, structural studies of c-Fos and HIV-1-Rev should be done to determine if there was a binding motif or three-dimensional NLS.

The role of importin 13-dependent nuclear import of Lipin 1 should be further analyzed. Lipin 1 is upregulated under oxidative stress conditions (Seo and Shin 2017) and importin 13 plays a key role in the transcriptional response to oxidative stress (Gajewska *et al.* 2021). It could be tested if different cellular conditions, especially oxidative stress, led to importin 13-dependent nuclear import.

References

Adam, E.J. and Adam, S.A. 1994 Identification of cytosolic factors required for nuclear location sequence-mediated binding to the nuclear envelope. *J Cell Biol* **125**, 547–555.

Adam, S.A. and Gerace, L. 1991 Cytosolic proteins that specifically bind nuclear location signals are receptors for nuclear import. *Cell* **66**, 837–847.

Adam, S.A., Marr, R.S. and Gerace, L. 1990 Nuclear protein import in permeabilized mammalian cells requires soluble cytoplasmic factors. *J Cell Biol* **111**, 807–816.

Agudo, D., Gómez-Esquer, F., Martínez-Arribas, F., Núñez-Villar, M.J., Pollán, M. and Schneider, J. 2004 Nup88 mRNA overexpression is associated with high aggressiveness of breast cancer. *Int J Cancer* **109**, 717–720.

Ahmadian, M., Duncan, R.E., Jaworski, K., Sarkadi-Nagy, E. and Sul, H.S. 2007 Triacylglycerol metabolism in adipose tissue. *Future Lipidol* **2**, 229–237.

Aksu, M., Pleiner, T., Karaca, S., Kappert, C., Dehne, H.-J., Seibel, K., Urlaub, H., Bohnsack, M.T. and Görlich, D. 2018 Xpo7 is a broad-spectrum exportin and a nuclear import receptor. *J Cell Biol* **217**, 2329–2340.

Allegretti, M., Zimmerli, C.E., Rantos, V., Wilfling, F., Ronchi, P., Fung, H.K.H., Lee, C.-W., Hagen, W., Turoňová, B., Karius, K., Börmel, M., Zhang, X., Müller, C.W., Schwab, Y., Mahamid, J., Pfander, B., Kosinski, J. and Beck, M. 2020 In-cell architecture of the nuclear pore and snapshots of its turnover. *Nature* **586**, 796–800.

Allen, N.P., Huang, L., Burlingame, A. and Rexach, M. 2001 Proteomic analysis of nucleoporin interacting proteins. *J Biol Chem* **276**, 29268–29274.

Amlacher, S., Sarges, P., Flemming, D., van Noort, V., Kunze, R., Devos, D.P., Arumugam, M., Bork, P. and Hurt, E. 2011 Insight into structure and assembly of the nuclear pore complex by utilizing the genome of a eukaryotic thermophile. *Cell* **146**, 277–289.

Andrade, M.A., Petosa, C., O'Donoghue, S.I., Müller, C.W. and Bork, P. 2001 Comparison of ARM and HEAT protein repeats. *J Mol Biol* **309**, 1–18.

Appen, A. von and Beck, M. 2016 Structure Determination of the Nuclear Pore Complex with Three-Dimensional Cryo electron Microscopy. *J Mol Biol* **428**, 2001–2010.

Aravind, L. and Koonin, E.V. 2000 The U box is a modified RING finger - a common domain in ubiquitination. *Curr Biol* **10**, R132-4.

Arnold, M., Nath, A., Hauber, J. and Kehlenbach, R.H. 2006a Multiple importins function as nuclear transport receptors for the Rev protein of human immunodeficiency virus type 1. *J Biol Chem* **281**, 20883–20890.

Arnold, M., Nath, A., Wohlwend, D. and Kehlenbach, R.H. 2006b Transportin is a major nuclear import receptor for c-Fos: a novel mode of cargo interaction. *J Biol Chem* **281**, 5492–5499.

Baade, I., Hutten, S., Sternburg, E.L., Pörschke, M., Hofweber, M., Dormann, D. and Kehlenbach, R.H. 2021 The RNA-binding protein FUS is chaperoned and imported into the nucleus by a network of import receptors. *J Biol Chem* **296**, 100659.

Baade, I., Spillner, C., Schmitt, K., Valerius, O. and Kehlenbach, R.H. 2018 Extensive Identification and In-depth Validation of Importin 13 Cargoes. *Mol Cell Proteomics* **17**, 1337–1353.

Bayliss, R., Littlewood, T. and Stewart, M. 2000 Structural basis for the interaction between FxFG nucleoporin repeats and importin-beta in nuclear trafficking. *Cell* **102**, 99–108.

Bayliss, R., Littlewood, T., Strawn, L.A., Wente, S.R. and Stewart, M. 2002 GLFG and FxFG nucleoporins bind to overlapping sites on importin-beta. *J Biol Chem* **277**, 50597–50606.

Bernardes, N.E. and Chook, Y.M. 2020 Nuclear import of histones. *Biochem Soc Trans* **48**, 2753–2767.

Bischoff, F.R. and Görlich, D. 1997 RanBP1 is crucial for the release of RanGTP from importin beta-related nuclear transport factors. *FEBS Lett* **419**, 249–254.

Bischoff, F.R., Klebe, C., Kretschmer, J., Wittinghofer, A. and Ponstingl, H. 1994 RanGAP1 induces GTPase activity of nuclear Ras-related Ran. *Proc Natl Acad Sci U S A* **91**, 2587–2591.

Bischoff, F.R., Krebber, H., Smirnova, E., Dong, W. and Ponstingl, H. 1995 Co-activation of RanGTPase and inhibition of GTP dissociation by Ran-GTP binding protein RanBP1. *EMBO J* **14**, 705–715.

Bischoff, F.R. and Ponstingl, H. 1991 Catalysis of guanine nucleotide exchange on Ran by the mitotic regulator RCC1. *Nature* **354**, 80–82.

Bitetto, G. and Di Fonzo, A. 2020 Nucleo-cytoplasmic transport defects and protein aggregates in neurodegeneration. *Transl Neurodegener* **9**, 25.

Bono, F., Cook, A.G., Grünwald, M., Ebert, J. and Conti, E. 2010 Nuclear import mechanism of the EJC component Mago-Y14 revealed by structural studies of importin 13. *Mol Cell* **37**, 211–222.

Bourgeois, B., Hutten, S., Gottschalk, B., Hofweber, M., Richter, G., Sternat, J., Abou-Ajram, C., Göbl, C., Leitinger, G., Graier, W.F., Dormann, D. and Madl, T. 2020 Nonclassical nuclear localization signals mediate nuclear import of CIRBP. *Proc Natl Acad Sci U S A* **117**, 8503–8514.

Brohée, L., Crémer, J., Colige, A. and Deroanne, C. 2021 Lipin-1, a Versatile Regulator of Lipid Homeostasis, Is a Potential Target for Fighting Cancer. *Int J Mol Sci* **22**.

Bui, K.H., Appen, A. von, DiGuilio, A.L., Ori, A., Sparks, L., Mackmull, M.-T., Bock, T., Hagen, W., Andrés-Pons, A., Glavy, J.S. and Beck, M. 2013 Integrated structural analysis of the human nuclear pore complex scaffold. *Cell* **155**, 1233–1243.

Bullock, T.L., Clarkson, W.D., Kent, H.M. and Stewart, M. 1996 The 1.6 angstroms resolution crystal structure of nuclear transport factor 2 (NTF2). *J Mol Biol* **260**, 422–431.

CALLAN, H.G. and TOMLIN, S.G. 1950 Experimental studies on amphibian oocyte nuclei. I. Investigation of the structure of the nuclear membrane by means of the electron microscope. *Proc R Soc Lond B Biol Sci* **137**, 367–378.

Cansizoglu, A.E., Lee, B.J., Zhang, Z.C., Fontoura, B.M.A. and Chook, Y.M. 2007 Structure-based design of a pathway-specific nuclear import inhibitor. *Nat Struct Mol Biol* **14**, 452–454.

Carpenter, A.E., Jones, T.R., Lamprecht, M.R., Clarke, C., Kang, I.H., Friman, O., Guertin, D.A., Chang, J.H., Lindquist, R.A., Moffat, J., Golland, P. and Sabatini, D.M. 2006 CellProfiler: image analysis software for identifying and quantifying cell phenotypes. *Genome Biol* **7**, R100.

Chen, B.B. and Mallampalli, R.K. 2009 Masking of a nuclear signal motif by monoubiquitination leads to mislocalization and degradation of the regulatory enzyme cytidylyltransferase. *Mol Cell Biol* **29**, 3062–3075.

Chen, Y., Rui, B.-B., Tang, L.-Y. and Hu, C.-M. 2015 Lipin family proteins--key regulators in lipid metabolism. *Ann Nutr Metab* **66**, 10–18.

Chiu, R., Boyle, W.J., Meek, J., Smeal, T., Hunter, T. and Karin, M. 1988 The c-fos protein interacts with c-JunAP-1 to stimulate transcription of AP-1 responsive genes. *Cell* **54**, 541–552.

Chook, Y.M. and Blobel, G. 1999 Structure of the nuclear transport complex karyopherin-beta2-Ran x GppNHp. *Nature* **399**, 230–237.

Chook, Y.M. and Süel, K.E. 2011 Nuclear import by karyopherin-βs: recognition and inhibition. *Biochim Biophys Acta* **1813**, 1593–1606.

Chou, C.-C., Zhang, Y., Umoh, M.E., Vaughan, S.W., Lorenzini, I., Liu, F., Sayegh, M., Donlin-Asp, P.G., Chen, Y.H., Duong, D.M., Seyfried, N.T., Powers, M.A., Kukar, T., Hales, C.M., Gearing, M., Cairns, N.J., Boylan, K.B., Dickson, D.W., Rademakers, R., Zhang, Y.-J., Petrucelli, L., Sattler, R., Zarnescu, D.C., Glass, J.D. and Rossoll, W. 2018 TDP-43 pathology disrupts nuclear pore complexes and nucleocytoplasmic transport in ALS/FTD. *Nat Neurosci* **21**, 228–239.

Chow, K.-H., Factor, R.E. and Ullman, K.S. 2012 The nuclear envelope environment and its cancer connections. *Nat Rev Cancer* **12**, 196–209.

Cingolani, G., Bednenko, J., Gillespie, M.T. and Gerace, L. 2002 Molecular Basis for the Recognition of a Nonclassical Nuclear Localization Signal by Importin β. *Mol Cell* **10**, 1345–1353.

Cingolani, G., Petosa, C., Weis, K. and Müller, C.W. 1999 Structure of importin-beta bound to the IBB domain of importin-alpha. *Nature* **399**, 221–229.

Connor, M.K., Kotchetkov, R., Cariou, S., Resch, A., Lupetti, R., Beniston, R.G., Melchior, F., Hengst, L. and Slingerland, J.M. 2003 CRM1/Ran-mediated nuclear export of p27(Kip1) involves a nuclear export signal and links p27 export and proteolysis. *Mol Biol Cell* **14**, 201–213.

Conti, E. and Kuriyan, J. 2000 Crystallographic analysis of the specific yet versatile recognition of distinct nuclear localization signals by karyopherin alpha. *Structure* **8**, 329–338.

Conti, E., Uy, M., Leighton, L., Blobel, G. and Kuriyan, J. 1998 Crystallographic Analysis of the Recognition of a Nuclear Localization Signal by the Nuclear Import Factor Karyopherin α. *Cell* **94**, 193–204.

Cook, A., Bono, F., Jinek, M. and Conti, E. 2007 Structural biology of nucleocytoplasmic transport. *Annu Rev Biochem* **76**, 647–671.

Cronshaw, J.M., Krutchinsky, A.N., Zhang, W., Chait, B.T. and Matunis, M.J. 2002 Proteomic analysis of the mammalian nuclear pore complex. *J Cell Biol* **158**, 915–927.

Csaki, L.S., Dwyer, J.R., Fong, L.G., Tontonoz, P., Young, S.G. and Reue, K. 2013 Lipins, lipinopathies, and the modulation of cellular lipid storage and signaling. *Prog Lipid Res* **52**, 305–316.

Daugherty, M.D. 2010 Crystal structure of the HIV-1 Rev dimer.

Dedio, J., König, P., Wohlfart, P., Schroeder, C., Kummer, W. and Müller-Esterl, W. 2001 NOSIP, a novel modulator of endothelial nitric oxide synthase activity. *FASEB J* **15**, 79–89.

DeJesus-Hernandez, M., Mackenzie, I.R., Boeve, B.F., Boxer, A.L., Baker, M., Rutherford, N.J., Nicholson, A.M., Finch, N.A., Flynn, H., Adamson, J., Kouri, N., Wojtas, A., Sengdy, P., Hsiung, G.-Y.R., Karydas, A., Seeley, W.W., Josephs, K.A., Coppola, G., Geschwind, D.H., Wszolek, Z.K., Feldman, H., Knopman, D.S., Petersen, R.C., Miller, B.L., Dickson, D.W., Boylan, K.B., Graff-Radford, N.R. and Rademakers, R. 2011 Expanded GGGGCC hexanucleotide repeat in noncoding region of C9ORF72 causes chromosome 9p-linked FTD and ALS. *Neuron* **72**, 245–256.

Dephoure, N., Zhou, C., Villén, J., Beausoleil, S.A., Bakalarski, C.E., Elledge, S.J. and Gygi, S.P. 2008 A quantitative atlas of mitotic phosphorylation. *Proc Natl Acad Sci U S A* **105**, 10762–10767.

Dickmanns, A., Kehlenbach, R.H. and Fahrenkrog, B. 2015 Nuclear Pore Complexes and Nucleocytoplasmic Transport: From Structure to Function to Disease. *Int Rev Cell Mol Biol* **320**, 171–233.

Ding, B. and Sepehrimanesh, M. 2021 Nucleocytoplasmic Transport: Regulatory Mechanisms and the Implications in Neurodegeneration. *Int J Mol Sci* **22**.

Donkor, J., Sariahmetoglu, M., Dewald, J., Brindley, D.N. and Reue, K. 2007 Three mammalian lipins act as phosphatidate phosphatases with distinct tissue expression patterns. *J Biol Chem* **282**, 3450–3457.

Donkor, J., Zhang, P., Wong, S., O'Loughlin, L., Dewald, J., Kok, B.P.C., Brindley, D.N. and Reue, K. 2009 A conserved serine residue is required for the phosphatidate phosphatase activity but not the transcriptional coactivator functions of lipin-1 and lipin-2. *J Biol Chem* **284**, 29968–29978.

Dreyer, J., Schleicher, M., Tappe, A., Schilling, K., Kuner, T., Kusumawidijaja, G., Müller-Esterl, W., Oess, S. and Kuner, R. 2004 Nitric oxide synthase (NOS)-interacting protein

interacts with neuronal NOS and regulates its distribution and activity. *J Neurosci* **24**, 10454–10465.

Eberhardt, R.Y., Chang, Y., Bateman, A., Murzin, A.G., Axelrod, H.L., Hwang, W.C. and Aravind, L. 2013 Filling out the structural map of the NTF2-like superfamily. *BMC Bioinformatics* **14**, 327.

Ederle, H., Funk, C., Abou-Ajram, C., Hutten, S., Funk, E.B.E., Kehlenbach, R.H., Bailer, S.M. and Dormann, D. 2018 Nuclear egress of TDP-43 and FUS occurs independently of Exportin-1/CRM1. *Sci Rep* **8**, 7084.

Eftekharzadeh, B., Daigle, J.G., Kapinos, L.E., Coyne, A., Schiantarelli, J., Carlomagno, Y., Cook, C., Miller, S.J., Dujardin, S., Amaral, A.S., Grima, J.C., Bennett, R.E., Tepper, K., DeTure, M., Vanderburg, C.R., Corjuc, B.T., DeVos, S.L., Gonzalez, J.A., Chew, J., Vidensky, S., Gage, F.H., Mertens, J., Troncoso, J., Mandelkow, E., Salvatella, X., Lim, R.Y.H., Petrucelli, L., Wegmann, S., Rothstein, J.D. and Hyman, B.T. 2019 Tau Protein Disrupts Nucleocytoplasmic Transport in Alzheimer's Disease. *Neuron* **101**, 349.

Fahrenkrog, B., Köser, J. and Aebi, U. 2004 The nuclear pore complex: a jack of all trades? *Trends Biochem Sci* **29**, 175–182.

Fan, X., Weng, Y., Bai, Y., Wang, Z., Wang, S., Zhu, J. and Zhang, F. 2018 Lipin-1 determines lung cancer cell survival and chemotherapy sensitivity by regulation of endoplasmic reticulum homeostasis and autophagy. *Cancer Med* **7**, 2541–2554.

Felix, R.S., Colleoni, G.W.B., Caballero, O.L., Yamamoto, M., Almeida, M.S.S., Andrade, V.C.C., Chauffaille, M.d.L.L.F., Da Silva, W.A., Begnami, M.D., Soares, F.A., Simpson, A.J., Zago, M.A. and Vettore, A.L. 2009 SAGE analysis highlights the importance of p53csv, ddx5, mapkapk2 and ranbp2 to multiple myeloma tumorigenesis. *Cancer Lett* **278**, 41–48.

Finck, B.N., Gropler, M.C., Chen, Z., Leone, T.C., Croce, M.A., Harris, T.E., Lawrence, J.C. and Kelly, D.P. 2006 Lipin 1 is an inducible amplifier of the hepatic PGC-1alpha/PPARalpha regulatory pathway. *Cell Metab* **4**, 199–210.

Finlay, D.R., Meier, E., Bradley, P., Horecka, J. and Forbes, D.J. 1991 A complex of nuclear pore proteins required for pore function. *J Cell Biol* **114**, 169–183.

Flach, H., Krieg, J., Hoffmeister, M., Dietmann, P., Reusch, A., Wischmann, L., Kernl, B., Riegger, R., Oess, S. and Kühl, S.J. 2018 Nosip functions during vertebrate eye and cranial cartilage development. *Dev Dyn* **247**, 1070–1082.

Fleming, I., Bauersachs, J., Fisslthaler, B. and Busse, R. 1998 Ca2+-independent activation of the endothelial nitric oxide synthase in response to tyrosine phosphatase inhibitors and fluid shear stress. *Circ Res* **82**, 686–695.

Fleming, I. and Busse, R. 2003 Molecular mechanisms involved in the regulation of the endothelial nitric oxide synthase. *Am J Physiol Regul Integr Comp Physiol* **284**, R1-12.

Fontana, P., Dong, Y., Pi, X., Tong, A.B., Hecksel, C.W., Wang, L., Fu, T.-M., Bustamante, C. and Wu, H. 2022 Structure of cytoplasmic ring of nuclear pore complex by integrative cryo-EM and AlphaFold. *Science* **376**, eabm9326.

Fontes, M.R.M., Teh, T., Jans, D., Brinkworth, R.I. and Kobe, B. 2003 Structural basis for the specificity of bipartite nuclear localization sequence binding by importin-alpha. *J Biol Chem* **278**, 27981–27987.

Förstermann, U. and Sessa, W.C. 2012 Nitric oxide synthases: regulation and function. *Eur Heart J* **33**, 829-37, 837a-837d.

Forwood, J.K., Lange, A., Zachariae, U., Marfori, M., Preast, C., Grubmüller, H., Stewart, M., Corbett, A.H. and Kobe, B. 2010 Quantitative structural analysis of importin-β flexibility: paradigm for solenoid protein structures. *Structure* **18**, 1171–1183.

Freibaum, B.D., Lu, Y., Lopez-Gonzalez, R., Kim, N.C., Almeida, S., Lee, K.-H., Badders, N., Valentine, M., Miller, B.L., Wong, P.C., Petrucelli, L., Kim, H.J., Gao, F.-B. and Taylor, J.P. 2015 GGGGCC repeat expansion in C9orf72 compromises nucleocytoplasmic transport. *Nature* **525**, 129–133.

Frey, S. and Görlich, D. 2007 A saturated FG-repeat hydrogel can reproduce the permeability properties of nuclear pore complexes. *Cell* **130**, 512–523.

Frey, S., Richter, R.P. and Görlich, D. 2006 FG-rich repeats of nuclear pore proteins form a three-dimensional meshwork with hydrogel-like properties. *Science* **314**, 815–817.

Fribourg, S., Braun, I.C., Izaurralde, E. and Conti, E. 2001 Structural basis for the recognition of a nucleoporin FG repeat by the NTF2-like domain of the TAP/p15 mRNA nuclear export factor. *Mol Cell* **8**, 645–656.

Fried, H. and Kutay, U. 2003 Nucleocytoplasmic transport: taking an inventory. *Cell Mol Life Sci* **60**, 1659–1688.

Friedman, A.D., Nimbalkar, D. and Quelle, F.W. 2003 Erythropoietin receptors associate with a ubiquitin ligase, p33RUL, and require its activity for erythropoietin-induced proliferation. *J Biol Chem* **278**, 26851–26861.

Friocourt, G., Poirier, K., Rakić, S., Parnavelas, J.G. and Chelly, J. 2006 The role of ARX in cortical development. *Eur J Neurosci* **23**, 869–876.

Fujiwara, A., Ozawa, M., Sumida, K., Hirawa, N., Yatsu, K., Ichihara, N., Haze, T., Komiya, S., Ohki, Y., Kobayashi, Y., Wakui, H. and Tamura, K. 2022 LPIN1 is a new target gene for essential hypertension. *J Hypertens* **40**, 536–543.

Fung, H.Y.J., Fu, S.-C. and Chook, Y.M. 2017 Nuclear export receptor CRM1 recognizes diverse conformations in nuclear export signals. *Elife* **6**.

Gajewska, K.A., Lescesen, H., Ramialison, M., Wagstaff, K.M. and Jans, D.A. 2021 Nuclear transporter Importin-13 plays a key role in the oxidative stress transcriptional response. *Nat Commun* **12**, 5904.

Gall, J.G. 1967 Octagonal nuclear pores. *J Cell Biol* **32**, 391–399.

García-García, M., Sánchez-Perales, S., Jarabo, P., Calvo, E., Huyton, T., Fu, L., Ng, S.C., Sotodosos-Alonso, L., Vázquez, J., Casas-Tintó, S., Görlich, D., Echarri, A. and Del Pozo, M.A. 2022 Mechanical control of nuclear import by Importin-7 is regulated by its dominant cargo YAP. *Nat Commun* **13**, 1174.

Gong, Z., Ye, S.-X., Nie, Z.-F. and Tang, C. 2020 The Conformational Preference of Chemical Cross-linkers Determines the Cross-linking Probability of Reactive Protein Residues. *J Phys Chem B* **124**, 4446–4453.

Gontan, C., Güttler, T., Engelen, E., Demmers, J., Fornerod, M., Grosveld, F.G., Tibboel, D., Görlich, D., Poot, R.A. and Rottier, R.J. 2009 Exportin 4 mediates a novel nuclear import pathway for Sox family transcription factors. *J Cell Biol* **185**, 27–34.

Gopal, P.P., Nirschl, J.J., Klinman, E. and Holzbaur, E.L.F. 2017 Amyotrophic lateral sclerosis-linked mutations increase the viscosity of liquid-like TDP-43 RNP granules in neurons. *Proc Natl Acad Sci U S A* **114**, E2466-E2475.

Gorello, P., La Starza, R., Di Giacomo, D., Messina, M., Puzzolo, M.C., Crescenzi, B., Santoro, A., Chiaretti, S. and Mecucci, C. 2010 SQSTM1-NUP214: a new gene fusion in adult T-cell acute lymphoblastic leukemia. *Haematologica* **95**, 2161–2163.

GORLICH, D. 1994 Isolation of a protein that is essential for the first step of nuclear protein import. *Cell* **79**, 767–778.

Görlich, D., Dabrowski, M., Bischoff, F.R., Kutay, U., Bork, P., Hartmann, E., Prehn, S. and Izaurralde, E. 1997 A novel class of RanGTP binding proteins. *J Cell Biol* **138**, 65–80.

Görlich, D. and Kutay, U. 1999 Transport between the cell nucleus and the cytoplasm. *Annu Rev Cell Dev Biol* **15**, 607–660.

Görlich, D., Panté, N., Kutay, U., Aebi, U. and Bischoff, F.R. 1996 Identification of different roles for RanGDP and RanGTP in nuclear protein import. *EMBO J* **15**, 5584–5594.

Gough, S.M., Slape, C.I. and Aplan, P.D. 2011 NUP98 gene fusions and hematopoietic malignancies: common themes and new biologic insights. *Blood* **118**, 6247–6257.

Gow, A.J. and Ischiropoulos, H. 2001 Nitric oxide chemistry and cellular signaling. *J Cell Physiol* **187**, 277–282.

Griffis, E.R., Xu, S. and Powers, M.A. 2003 Nup98 localizes to both nuclear and cytoplasmic sides of the nuclear pore and binds to two distinct nucleoporin subcomplexes. *Mol Biol Cell* **14**, 600–610.

Grimsey, N., Han, G.-S., O'Hara, L., Rochford, J.J., Carman, G.M. and Siniossoglou, S. 2008 Temporal and spatial regulation of the phosphatidate phosphatases lipin 1 and 2. *Journal of Biological Chemistry* **283**, 29166–29174.

Groves, M.R., Hanlon, N., Turowski, P., Hemmings, B.A. and Barford, D. 1999 The Structure of the Protein Phosphatase 2A PR65/A Subunit Reveals the Conformation of Its 15 Tandemly Repeated HEAT Motifs. *Cell* **96**, 99–110.

Grünwald, M. and Bono, F. 2011 Structure of Importin13-Ubc9 complex: nuclear import and release of a key regulator of sumoylation. *EMBO J* **30**, 427–438.

Grünwald, M., Lazzaretti, D. and Bono, F. 2013 Structural basis for the nuclear export activity of Importin13. *EMBO J* **32**, 899–913.

Hahn, S. and Schlenstedt, G. 2011 Importin β-type nuclear transport receptors have distinct binding affinities for Ran-GTP. *Biochem Biophys Res Commun* **406**, 383–388.

Han, G.-S. and Carman, G.M. 2010 Characterization of the human LPIN1-encoded phosphatidate phosphatase isoforms. *J Biol Chem* **285**, 14628–14638.

Han, G.-S., Wu, W.-I. and Carman, G.M. 2006 The Saccharomyces cerevisiae Lipin homolog is a Mg2+-dependent phosphatidate phosphatase enzyme. *J Biol Chem* **281**, 9210–9218.

Harreman, M.T., Hodel, M.R., Fanara, P., Hodel, A.E. and Corbett, A.H. 2003 The auto-inhibitory function of importin alpha is essential in vivo. *J Biol Chem* **278**, 5854–5863.

He, J., Zhang, F., Tay, L.W.R., Boroda, S., Nian, W., Levental, K.R., Levental, I., Harris, T.E., Chang, J.T. and Du, G. 2017 Lipin-1 regulation of phospholipid synthesis maintains endoplasmic reticulum homeostasis and is critical for triple-negative breast cancer cell survival. *FASEB J* **31**, 2893–2904.

Herold, A., Suyama, M., Rodrigues, J.P., Braun, I.C., Kutay, U., Carmo-Fonseca, M., Bork, P. and Izaurralde, E. 2000 TAP (NXF1) belongs to a multigene family of putative RNA export factors with a conserved modular architecture. *Mol Cell Biol* **20**, 8996–9008.

Hoelz, A., Debler, E.W. and Blobel, G. 2011 The structure of the nuclear pore complex. *Annu Rev Biochem* **80**, 613–643.

Hoffmeister, M., Krieg, J., Ehrke, A., Seigfried, F.A., Wischmann, L., Dietmann, P., Kühl, S.J. and Oess, S. 2017 Developmental neurogenesis in mouse and Xenopus is impaired in the absence of Nosip. *Dev Biol* **429**, 200–212.

Hoffmeister, M., Prelle, C., Küchler, P., Kovacevic, I., Moser, M., Müller-Esterl, W. and Oess, S. 2014 The ubiquitin E3 ligase NOSIP modulates protein phosphatase 2A activity in craniofacial development. *PLoS One* **9**, e116150.

Huang, G., Zhang, Y., Zhu, X., Zeng, C., Wang, Q., Zhou, Q., Tao, Q., Liu, M., Lei, J., Yan, C. and Shi, Y. 2020 Structure of the cytoplasmic ring of the Xenopus laevis nuclear pore complex by cryo-electron microscopy single particle analysis. *Cell Res* **30**, 520–531.

Huber, J., Cronshagen, U., Kadokura, M., Marshallsay, C., Wada, T., Sekine, M. and Lührmann, R. 1998 Snurportin1, an m3G-cap-specific nuclear import receptor with a novel domain structure. *EMBO J* **17**, 4114–4126.

Hübner, S., Xiao, C.Y. and Jans, D.A. 1997 The protein kinase CK2 site (Ser111/112) enhances recognition of the simian virus 40 large T-antigen nuclear localization sequence by importin. *J Biol Chem* **272**, 17191–17195.

Huebner, A., Kaindl, A.M., Knobeloch, K.P., Petzold, H., Mann, P. and Koehler, K. 2004 The triple A syndrome is due to mutations in ALADIN, a novel member of the nuclear pore complex. *Endocr Res* **30**, 891–899.

Hutten, S. and Dormann, D. 2020 Nucleocytoplasmic transport defects in neurodegeneration - Cause or consequence? *Semin Cell Dev Biol* **99**, 151–162.

Hutten, S., Flotho, A., Melchior, F. and Kehlenbach, R.H. 2008 The Nup358-RanGAP complex is required for efficient importin alpha/beta-dependent nuclear import. *Mol Biol Cell* **19**, 2300–2310.

Imasaki, T., Shimizu, T., Hashimoto, H., Hidaka, Y., Kose, S., Imamoto, N., Yamada, M. and Sato, M. 2007 Structural basis for substrate recognition and dissociation by human transportin 1. *Mol Cell* **28**, 57–67.

Isgro, T.A. and Schulten, K. 2005 Binding dynamics of isolated nucleoporin repeat regions to importin-beta. *Structure* **13**, 1869–1879.

Ivic, N., Potocnjak, M., Solis-Mezarino, V., Herzog, F., Bilokapic, S. and Halic, M. 2019 Fuzzy Interactions Form and Shape the Histone Transport Complex. *Mol Cell* **73**, 1191-1203.e6.

Izaurralde, E., Kutay, U., Kobbe, C. von, Mattaj, I.W. and Görlich, D. 1997 The asymmetric distribution of the constituents of the Ran system is essential for transport into and out of the nucleus. *EMBO J* **16**, 6535–6547.

Jainchill, J.L., Aaronson, S.A. and Todaro, G.J. 1969 Murine sarcoma and leukemia viruses: assay using clonal lines of contact-inhibited mouse cells. *J Virol* **4**, 549–553.

Jäkel, S., Albig, W., Kutay, U., Bischoff, F.R., Schwamborn, K., Doenecke, D. and Görlich, D. 1999 The importin beta/importin 7 heterodimer is a functional nuclear import receptor for histone H1. *EMBO J* **18**, 2411–2423.

Jäkel, S. and Görlich, D. 1998 Importin beta, transportin, RanBP5 and RanBP7 mediate nuclear import of ribosomal proteins in mammalian cells. *EMBO J* **17**, 4491–4502.

Jäkel, S., Mingot, J.-M., Schwarzmaier, P., Hartmann, E. and Görlich, D. 2002 Importins fulfil a dual function as nuclear import receptors and cytoplasmic chaperones for exposed basic domains. *EMBO J* **21**, 377–386.

Jang, S., Cook, N.J., Pye, V.E., Bedwell, G.J., Dudek, A.M., Singh, P.K., Cherepanov, P. and Engelman, A.N. 2019 Differential role for phosphorylation in alternative polyadenylation function versus nuclear import of SR-like protein CPSF6. *Nucleic Acids Res* **47**, 4663–4683.

Jarnik, M. and Aebi, U. 1991 Toward a more complete 3-D structure of the nuclear pore complex. *J Struct Biol* **107**, 291–308.

Jørgensen, C., Sherman, A., Chen, G.I., Pasculescu, A., Poliakov, A., Hsiung, M., Larsen, B., Wilkinson, D.G., Linding, R. and Pawson, T. 2009 Cell-specific information processing in segregating populations of Eph receptor ephrin-expressing cells. *Science* **326**, 1502–1509.

Jovičić, A., Mertens, J., Boeynaems, S., Bogaert, E., Chai, N., Yamada, S.B., Paul, J.W., Sun, S., Herdy, J.R., Bieri, G., Kramer, N.J., Gage, F.H., van den Bosch, L., Robberecht, W. and Gitler, A.D. 2015 Modifiers of C9orf72 dipeptide repeat toxicity connect nucleocytoplasmic transport defects to FTD/ALS. *Nat Neurosci* **18**, 1226–1229.

Jumper, J., Evans, R., Pritzel, A., Green, T., Figurnov, M., Ronneberger, O., Tunyasuvunakool, K., Bates, R., Žídek, A., Potapenko, A., Bridgland, A., Meyer, C., Kohl, S.A.A., Ballard, A.J., Cowie, A., Romera-Paredes, B., Nikolov, S., Jain, R., Adler, J., Back,

T., Petersen, S., Reiman, D., Clancy, E., Zielinski, M., Steinegger, M., Pacholska, M., Berghammer, T., Bodenstein, S., Silver, D., Vinyals, O., Senior, A.W., Kavukcuoglu, K., Kohli, P. and Hassabis, D. 2021 Highly accurate protein structure prediction with AlphaFold. *Nature* **596**, 583–589.

Kahraman, A., Malmström, L. and Aebersold, R. 2011 Xwalk: computing and visualizing distances in cross-linking experiments. *Bioinformatics* **27**, 2163–2164.

Kalab, P., Weis, K. and Heald, R. 2002 Visualization of a Ran-GTP gradient in interphase and mitotic Xenopus egg extracts. *Science* **295**, 2452–2456.

Kalderon, D., Richardson, W.D., Markham, A.F. and Smith, A.E. 1984 Sequence requirements for nuclear location of simian virus 40 large-T antigen. *Nature* **311**, 33–38.

Kalverda, B., Pickersgill, H., Shloma, V.V. and Fornerod, M. 2010 Nucleoporins directly stimulate expression of developmental and cell-cycle genes inside the nucleoplasm. *Cell* **140**, 360–371.

Katahira, J., Strässer, K., Podtelejnikov, A., Mann, M., Jung, J.U. and Hurt, E. 1999 The Mex67p-mediated nuclear mRNA export pathway is conserved from yeast to human. *EMBO J* **18**, 2593–2609.

Kau, T.R., Way, J.C. and Silver, P.A. 2004 Nuclear transport and cancer: from mechanism to intervention. *Nat Rev Cancer* **4**, 106–117.

Kehlenbach, R.H., Dickmanns, A., Kehlenbach, A., Guan, T. and Gerace, L. 1999 A role for RanBP1 in the release of CRM1 from the nuclear pore complex in a terminal step of nuclear export. *J Cell Biol* **145**, 645–657.

Kelley, J.B., Talley, A.M., Spencer, A., Gioeli, D. and Paschal, B.M. 2010 Karyopherin alpha7 (KPNA7), a divergent member of the importin alpha family of nuclear import receptors. *BMC Cell Biol* **11**, 63.

Kelley, K., Knockenhauer, K.E., Kabachinski, G. and Schwartz, T.U. 2015 Atomic structure of the Y complex of the nuclear pore. *Nat Struct Mol Biol* **22**, 425–431.

Kim, S.J., Fernandez-Martinez, J., Nudelman, I., Shi, Y., Zhang, W., Raveh, B., Herricks, T., Slaughter, B.D., Hogan, J.A., Upla, P., Chemmama, I.E., Pellarin, R., Echeverria, I., Shivaraju, M., Chaudhury, A.S., Wang, J., Williams, R., Unruh, J.R., Greenberg, C.H., Jacobs, E.Y., Yu, Z., La Cruz, M.J. de, Mironska, R., Stokes, D.L., Aitchison, J.D., Jarrold, M.F., Gerton, J.L., Ludtke, S.J., Akey, C.W., Chait, B.T., Sali, A. and Rout, M.P. 2018 Integrative structure and functional anatomy of a nuclear pore complex. *Nature* **555**, 475–482.

Kimura, M., Morinaka, Y., Imai, K., Kose, S., Horton, P. and Imamoto, N. 2017 Extensive cargo identification reveals distinct biological roles of the 12 importin pathways. *Elife* **6**.

Kita, K., Omata, S. and Horigome, T. 1993 Purification and characterization of a nuclear pore glycoprotein complex containing p62. *J Biochem* **113**, 377–382.

Kitamura, R., Sekimoto, T., Ito, S., Harada, S., Yamagata, H., Masai, H., Yoneda, Y. and Yanagi, K. 2006 Nuclear import of Epstein-Barr virus nuclear antigen 1 mediated by NPI-

1 (Importin alpha5) is up- and down-regulated by phosphorylation of the nuclear localization signal for which Lys379 and Arg380 are essential. *J Virol* **80**, 1979–1991.

Klebe, C., Bischoff, F.R., Ponstingl, H. and Wittinghofer, A. 1995 Interaction of the nuclear GTP-binding protein Ran with its regulatory proteins RCC1 and RanGAP1. *Biochemistry* **34**, 639–647.

Kobayashi, J. and Matsuura, Y. 2013 Structural basis for cell-cycle-dependent nuclear import mediated by the karyopherin Kap121p. *J Mol Biol* **425**, 1852–1868.

Kobe, B. 1999 Autoinhibition by an internal nuclear localization signal revealed by the crystal structure of mammalian importin alpha. *Nat Struct Biol* **6**, 388–397.

Koh, Y.-K., Lee, M.-Y., Kim, J.-W., Kim, M., Moon, J.-S., Lee, Y.-J., Ahn, Y.-H. and Kim, K.-S. 2008 Lipin1 is a key factor for the maturation and maintenance of adipocytes in the regulatory network with CCAAT/enhancer-binding protein alpha and peroxisome proliferator-activated receptor gamma 2. *J Biol Chem* **283**, 34896–34906.

König, P., Dedio, J., Müller-Esterl, W. and Kummer, W. 2002 Distribution of the novel eNOS-interacting protein NOSIP in the liver, pancreas, and gastrointestinal tract of the rat. *Gastroenterology* **123**, 314–324.

König, P., Dedio, J., Oess, S., Papadakis, T., Fischer, A., Müller-Esterl, W. and Kummer, W. 2005 NOSIP and its interacting protein, eNOS, in the rat trachea and lung. *J Histochem Cytochem* **53**, 155–164.

Kosinski, J., Mosalaganti, S., Appen, A. von, Teimer, R., DiGuilio, A.L., Wan, W., Bui, K.H., Hagen, W.J.H., Briggs, J.A.G., Glavy, J.S., Hurt, E. and Beck, M. 2016 Molecular architecture of the inner ring scaffold of the human nuclear pore complex. *Science* **352**, 363–365.

Kosugi, S., Hasebe, M., Entani, T., Takayama, S., Tomita, M. and Yanagawa, H. 2008 Design of peptide inhibitors for the importin alpha/beta nuclear import pathway by activity-based profiling. *Chem Biol* **15**, 940–949.

Kosugi, S., Hasebe, M., Tomita, M. and Yanagawa, H. 2009 Systematic identification of cell cycle-dependent yeast nucleocytoplasmic shuttling proteins by prediction of composite motifs. *Proc Natl Acad Sci U S A* **106**, 10171–10176.

Koyama, M. and Matsuura, Y. 2010 An allosteric mechanism to displace nuclear export cargo from CRM1 and RanGTP by RanBP1. *EMBO J* **29**, 2002–2013.

Kuhn, T.M. and Capelson, M. 2019 Nuclear Pore Proteins in Regulation of Chromatin State. *Cells* **8**.

Kumeta, M., Yamaguchi, H., Yoshimura, S.H. and Takeyasu, K. 2012 Karyopherin-independent spontaneous transport of amphiphilic proteins through the nuclear pore. *J Cell Sci* **125**, 4979–4984.

Kumeta, M., Yoshimura, S.H., Harata, M. and Takeyasu, K. 2010 Molecular mechanisms underlying nucleocytoplasmic shuttling of actinin-4. *J Cell Sci* **123**, 1020–1030.

Kutay, U., Bischoff, F.R., Kostka, S., Kraft, R. and Görlich, D. 1997 Export of importin alpha from the nucleus is mediated by a specific nuclear transport factor. *Cell* **90**, 1061–1071.

Lai, M.C., Lin, R.I., Huang, S.Y., Tsai, C.W. and Tarn, W.Y. 2000 A human importin-beta family protein, transportin-SR2, interacts with the phosphorylated RS domain of SR proteins. *J Biol Chem* **275**, 7950–7957.

Lam, M.H., House, C.M., Tiganis, T., Mitchelhill, K.I., Sarcevic, B., Cures, A., Ramsay, R., Kemp, B.E., Martin, T.J. and Gillespie, M.T. 1999 Phosphorylation at the cyclin-dependent kinases site (Thr85) of parathyroid hormone-related protein negatively regulates its nuclear localization. *J Biol Chem* **274**, 18559–18566.

Latta, E.J. and Golding, J.P. 2012 Regulation of PP2A activity by Mid1 controls cranial neural crest speed and gangliogenesis. *Mech Dev* **128**, 560–576.

Lee, B.J., Cansizoglu, A.E., Süel, K.E., Louis, T.H., Zhang, Z. and Chook, Y.M. 2006 Rules for nuclear localization sequence recognition by karyopherin beta 2. *Cell* **126**, 543–558.

Lee, S.J., Imamoto, N., Sakai, H., Nakagawa, A., Kose, S., Koike, M., Yamamoto, M., Kumasaka, T., Yoneda, Y. and Tsukihara, T. 2000 The adoption of a twisted structure of importin-beta is essential for the protein-protein interaction required for nuclear transport. *J Mol Biol* **302**, 251–264.

Lee, S.J., Matsuura, Y., Liu, S.M. and Stewart, M. 2005 Structural basis for nuclear import complex dissociation by RanGTP. *Nature* **435**, 693–696.

Lee, S.J., Sekimoto, T., Yamashita, E., Nagoshi, E., Nakagawa, A., Imamoto, N., Yoshimura, M., Sakai, H., Chong, K.T., Tsukihara, T. and Yoneda, Y. 2003 The structure of importin-beta bound to SREBP-2: nuclear import of a transcription factor. *Science* **302**, 1571–1575.

Lesage, B., Beullens, M., Nuytten, M., van Eynde, A., Keppens, S., Himpens, B. and Bollen, M. 2004 Interactor-mediated nuclear translocation and retention of protein phosphatase-1. *Journal of Biological Chemistry* **279**, 55978–55984.

Liker, E., Fernandez, E., Izaurralde, E. and Conti, E. 2000 The structure of the mRNA export factor TAP reveals a cis arrangement of a non-canonical RNP domain and an LRR domain. *EMBO J* **19**, 5587–5598.

Lin, D., Chen, J., Ehrlich, S., Bustillo, J.R., Perrone-Bizzozero, N., Walton, E., Clark, V.P., Wang, Y.-P., Sui, J., Du, Y., Ho, B.C., Schulz, C.S., Calhoun, V.D. and Liu, J. 2018 Cross-Tissue Exploration of Genetic and Epigenetic Effects on Brain Gray Matter in Schizophrenia. *Schizophr Bull* **44**, 443–452.

Lin, D.H. and Hoelz, A. 2019 The Structure of the Nuclear Pore Complex (An Update). *Annu Rev Biochem* **88**, 725–783.

Lin, D.H., Stuwe, T., Schilbach, S., Rundlet, E.J., Perriches, T., Mobbs, G., Fan, Y., Thierbach, K., Huber, F.M., Collins, L.N., Davenport, A.M., Jeon, Y.E. and Hoelz, A. 2016 Architecture of the symmetric core of the nuclear pore. *Science* **352**, aaf1015.

Lin, W., Ye, W., Cai, L., Meng, X., Ke, G., Huang, C., Peng, Z., Yu, Y., Golden, J.A., Tartakoff, A.M. and Tao, T. 2009 The roles of multiple importins for nuclear import of murine aristaless-related homeobox protein. *Journal of Biological Chemistry* **284**, 20428–20439.

Lin, Y.-C., Kumar, M.S., Ramesh, N., Anderson, E.N., Nguyen, A.T., Kim, B., Cheung, S., McDonough, J.A., Skarnes, W.C., Lopez-Gonzalez, R., Landers, J.E., Fawzi, N.L., Mackenzie, I.R.A., Lee, E.B., Nickerson, J.A., Grunwald, D., Pandey, U.B. and Bosco, D.A. 2021 Interactions between ALS-linked FUS and nucleoporins are associated with defects in the nucleocytoplasmic transport pathway. *Nat Neurosci* **24**, 1077–1088.

Lipowsky, G., Bischoff, F.R., Izaurralde, E., Kutay, U., Schäfer, S., Gross, H.J., Beier, H. and Görlich, D. 1999 Coordination of tRNA nuclear export with processing of tRNA. *RNA* **5**, 539–549.

Liu, G.-H. and Gerace, L. 2009 Sumoylation regulates nuclear localization of lipin-1alpha in neuronal cells. *PLoS One* **4**, e7031.

Liu, X., Lin, W., Shi, X., Davies, R.G., Wagstaff, K.M., Tao, T. and Jans, D.A. 2018 PKA-site phosphorylation of importin13 regulates its subcellular localization and nuclear transport function. *Biochem J* **475**, 2699–2712.

Loïodice, I., Alves, A., Rabut, G., van Overbeek, M., Ellenberg, J., Sibarita, J.-B. and Doye, V. 2004 The entire Nup107-160 complex, including three new members, is targeted as one entity to kinetochores in mitosis. *Mol Biol Cell* **15**, 3333–3344.

Lott, K. and Cingolani, G. 2011 The importin β binding domain as a master regulator of nucleocytoplasmic transport. *Biochim Biophys Acta* **1813**, 1578–1592.

Love, D.C., Sweitzer, T.D. and Hanover, J.A. 1998 Reconstitution of HIV-1 rev nuclear export: independent requirements for nuclear import and export. *Proc Natl Acad Sci U S A* **95**, 10608–10613.

Lu, J., Wu, T., Zhang, B., Liu, S., Song, W., Qiao, J. and Ruan, H. 2021 Types of nuclear localization signals and mechanisms of protein import into the nucleus. *Cell Commun Signal* **19**, 60.

Mackmull, M.-T., Klaus, B., Heinze, I., Chokkalingam, M., Beyer, A., Russell, R.B., Ori, A. and Beck, M. 2017 Landscape of nuclear transport receptor cargo specificity. *Mol Syst Biol* **13**, 962.

Marfori, M., Mynott, A., Ellis, J.J., Mehdi, A.M., Saunders, N.F.W., Curmi, P.M., Forwood, J.K., Bodén, M. and Kobe, B. 2011 Molecular basis for specificity of nuclear import and prediction of nuclear localization. *Biochim Biophys Acta* **1813**, 1562–1577.

Marrero, M.B., Venema, V.J., Ju, H., He, H., Liang, H., Caldwell, R.B. and Venema, R.C. 1999 Endothelial nitric oxide synthase interactions with G-protein-coupled receptors. *Biochem J* **343 Pt 2**, 335–340.

Maul, G.G. and Deaven, L. 1977 Quantitative determination of nuclear pore complexes in cycling cells with differing DNA content. *J Cell Biol* **73**, 748–760.

Mboukou, A., Rajendra, V., Kleinova, R., Tisné, C., Jantsch, M.F. and Barraud, P. 2021 Transportin-1: A Nuclear Import Receptor with Moonlighting Functions. *Front Mol Biosci* **8**, 638149.

Melchior, F., Sweet, D.J. and Gerace, L. 1995 [30] Analysis of Ran/TC4 function in nuclear protein import. In Small GTPases and their regulators. pp. 279–291. San Diego: Acad. Press.

Meyer, T., Begitt, A., Lödige, I., van Rossum, M. and Vinkemeier, U. 2002 Constitutive and IFN-gamma-induced nuclear import of STAT1 proceed through independent pathways. *EMBO J* **21**, 344–354.

Michel, J.B., Feron, O., Sacks, D. and Michel, T. 1997a Reciprocal regulation of endothelial nitric-oxide synthase by Ca2+-calmodulin and caveolin. *J Biol Chem* **272**, 15583–15586.

Michel, J.B., Feron, O., Sase, K., Prabhakar, P. and Michel, T. 1997b Caveolin versus calmodulin. Counterbalancing allosteric modulators of endothelial nitric oxide synthase. *J Biol Chem* **272**, 25907–25912.

Michel, T. and Vanhoutte, P.M. 2010 Cellular signaling and NO production. *Pflugers Arch* **459**, 807–816.

Michot, C., Hubert, L., Brivet, M., Meirleir, L. de, Valayannopoulos, V., Müller-Felber, W., Venkateswaran, R., Ogier, H., Desguerre, I., Altuzarra, C., Thompson, E., Smitka, M., Huebner, A., Husson, M., Horvath, R., Chinnery, P., Vaz, F.M., Munnich, A., Elpeleg, O., Delahodde, A., Keyzer, Y. de and Lonlay, P. de 2010 LPIN1 gene mutations: a major cause of severe rhabdomyolysis in early childhood. *Hum Mutat* **31**, E1564-73.

Mingot, J.M., Kostka, S., Kraft, R., Hartmann, E. and Görlich, D. 2001 Importin 13: a novel mediator of nuclear import and export. *EMBO J* **20**, 3685–3694.

Mishra, B.H., Mishra, P.P., Raitoharju, E., Marttila, S., Mononen, N., Sievänen, H., Viikari, J., Juonala, M., Laaksonen, M., Hutri-Kähönen, N., Kähönen, M., Raitakari, O.T. and Lehtimäki, T. 2021 Modular genome-wide gene expression architecture shared by early traits of osteoporosis and atherosclerosis in the Young Finns Study. *Sci Rep* **11**, 7111.

Mitchell, J.M., Mansfeld, J., Capitanio, J., Kutay, U. and Wozniak, R.W. 2010 Pom121 links two essential subcomplexes of the nuclear pore complex core to the membrane. *J Cell Biol* **191**, 505–521.

Miyamoto, Y., Yamada, K. and Yoneda, Y. 2016 Importin α: a key molecule in nuclear transport and non-transport functions. *J Biochem* **160**, 69–75.

Mohr, D., Frey, S., Fischer, T., Güttler, T. and Görlich, D. 2009 Characterisation of the passive permeability barrier of nuclear pore complexes. *EMBO J* **28**, 2541–2553.

Monecke, T., Dickmanns, A. and Ficner, R. 2014 Allosteric control of the exportin CRM1 unraveled by crystal structure analysis. *FEBS J* **281**, 4179–4194.

Monecke, T., Güttler, T., Neumann, P., Dickmanns, A., Görlich, D. and Ficner, R. 2009 Crystal structure of the nuclear export receptor CRM1 in complex with Snurportin1 and RanGTP. *Science* **324**, 1087–1091.

Monecke, T., Haselbach, D., Voß, B., Russek, A., Neumann, P., Thomson, E., Hurt, E., Zachariae, U., Stark, H., Grubmüller, H., Dickmanns, A. and Ficner, R. 2013 Structural basis for cooperativity of CRM1 export complex formation. *Proc Natl Acad Sci U S A* **110**, 960–965.

Moore, M.S. and Blobel, G. 1993 The GTP-binding protein Ran/TC4 is required for protein import into the nucleus. *Nature* **365**, 661–663.

Mosalaganti, S., Kosinski, J., Albert, S., Schaffer, M., Strenkert, D., Salomé, P.A., Merchant, S.S., Plitzko, J.M., Baumeister, W., Engel, B.D. and Beck, M. 2018 In situ architecture of the algal nuclear pore complex. *Nat Commun* **9**, 2361.

Mosalaganti, S., Obarska-Kosinska, A., Siggel, M., Taniguchi, R., Turoňová, B., Zimmerli, C.E., Buczak, K., Schmidt, F.H., Margiotta, E., Mackmull, M.-T., Hagen, W.J.H., Hummer, G., Kosinski, J. and Beck, M. 2022 AI-based structure prediction empowers integrative structural analysis of human nuclear pores. *Science* **376**, eabm9506.

Nadra, K., Preux Charles, A.-S. de, Médard, J.-J., Hendriks, W.T., Han, G.-S., Grès, S., Carman, G.M., Saulnier-Blache, J.-S., Verheijen, M.H.G. and Chrast, R. 2008 Phosphatidic acid mediates demyelination in Lpin1 mutant mice. *Genes Dev* **22**, 1647–1661.

Naim, B., Zbaida, D., Dagan, S., Kapon, R. and Reich, Z. 2009 Cargo surface hydrophobicity is sufficient to overcome the nuclear pore complex selectivity barrier. *EMBO J* **28**, 2697–2705.

Najbauer, E.E., Ng, S.C., Griesinger, C., Görlich, D. and Andreas, L.B. 2022 Atomic resolution dynamics of cohesive interactions in phase-separated Nup98 FG domains. *Nat Commun* **13**, 1494.

Napoli, C., Paolisso, G., Casamassimi, A., Al-Omran, M., Barbieri, M., Sommese, L., Infante, T. and Ignarro, L.J. 2013 Effects of nitric oxide on cell proliferation: novel insights. *J Am Coll Cardiol* **62**, 89–95.

Nardozzi, J.D., Lott, K. and Cingolani, G. 2010 Phosphorylation meets nuclear import: a review. *Cell Commun Signal* **8**, 32.

Neilson, D.E. 2010 The interplay of infection and genetics in acute necrotizing encephalopathy. *Curr Opin Pediatr* **22**, 751–757.

Nousiainen, H.O., Kestilä, M., Pakkasjärvi, N., Honkala, H., Kuure, S., Tallila, J., Vuopala, K., Ignatius, J., Herva, R. and Peltonen, L. 2008 Mutations in mRNA export mediator GLE1 result in a fetal motoneuron disease. *Nat Genet* **40**, 155–157.

Olsen, J.V., Vermeulen, M., Santamaria, A., Kumar, C., Miller, M.L., Jensen, L.J., Gnad, F., Cox, J., Jensen, T.S., Nigg, E.A., Brunak, S. and Mann, M. 2010 Quantitative phosphoproteomics reveals widespread full phosphorylation site occupancy during mitosis. *Sci Signal* **3**, ra3.

Onischenko, E., Stanton, L.H., Madrid, A.S., Kieselbach, T. and Weis, K. 2009 Role of the Ndc1 interaction network in yeast nuclear pore complex assembly and maintenance. *J Cell Biol* **185**, 475–491.

O'Reilly, A.J., Dacks, J.B. and Field, M.C. 2011 Evolution of the karyopherin-β family of nucleocytoplasmic transport factors; ancient origins and continued specialization. *PLoS One* **6**, e19308.

Ori, A., Banterle, N., Iskar, M., Andrés-Pons, A., Escher, C., Khanh Bui, H., Sparks, L., Solis-Mezarino, V., Rinner, O., Bork, P., Lemke, E.A. and Beck, M. 2013 Cell type-specific nuclear pores: a case in point for context-dependent stoichiometry of molecular machines. *Mol Syst Biol* **9**, 648.

Paciorkowski, A.R., Weisenberg, J., Kelley, J.B., Spencer, A., Tuttle, E., Ghoneim, D., Thio, L.L., Christian, S.L., Dobyns, W.B. and Paschal, B.M. 2014 Autosomal recessive mutations in nuclear transport factor KPNA7 are associated with infantile spasms and cerebellar malformation. *Eur J Hum Genet* **22**, 587–593.

Panté, N., Bastos, R., McMorrow, I., Burke, B. and Aebi, U. 1994 Interactions and three-dimensional localization of a group of nuclear pore complex proteins. *J Cell Biol* **126**, 603–617.

Paschal, B.M. and Gerace, L. 1995 Identification of NTF2, a cytosolic factor for nuclear import that interacts with nuclear pore complex protein p62. *J Cell Biol* **129**, 925–937.

Patel, S.S., Belmont, B.J., Sante, J.M. and Rexach, M.F. 2007 Natively unfolded nucleoporins gate protein diffusion across the nuclear pore complex. *Cell* **129**, 83–96.

Péterfy, M., Harris, T.E., Fujita, N. and Reue, K. 2010 Insulin-stimulated interaction with 14-3-3 promotes cytoplasmic localization of lipin-1 in adipocytes. *J Biol Chem* **285**, 3857–3864.

Péterfy, M., Phan, J. and Reue, K. 2005 Alternatively spliced lipin isoforms exhibit distinct expression pattern, subcellular localization, and role in adipogenesis. *J Biol Chem* **280**, 32883–32889.

Péterfy, M., Phan, J., Xu, P. and Reue, K. 2001 Lipodystrophy in the fld mouse results from mutation of a new gene encoding a nuclear protein, lipin. *Nat Genet* **27**, 121–124.

Pettersen, E.F., Goddard, T.D., Huang, C.C., Couch, G.S., Greenblatt, D.M., Meng, E.C. and Ferrin, T.E. 2004 UCSF Chimera--a visualization system for exploratory research and analysis. *J Comput Chem* **25**, 1605–1612.

Phan, J. and Reue, K. 2005 Lipin, a lipodystrophy and obesity gene. *Cell Metab* **1**, 73–83.

Picard, D. and Yamamoto, K.R. 1987 Two signals mediate hormone-dependent nuclear localization of the glucocorticoid receptor. *EMBO J* **6**, 3333–3340.

Port, S.A., Monecke, T., Dickmanns, A., Spillner, C., Hofele, R., Urlaub, H., Ficner, R. and Kehlenbach, R.H. 2015 Structural and Functional Characterization of CRM1-Nup214 Interactions Reveals Multiple FG-Binding Sites Involved in Nuclear Export. *Cell Rep* **13**, 690–702.

Radu, A., Moore, M.S. and Blobel, G. 1995 The peptide repeat domain of nucleoporin Nup98 functions as a docking site in transport across the nuclear pore complex. *Cell* **81**, 215–222.

Ren, H., Federico, L., Huang, H., Sunkara, M., Drennan, T., Frohman, M.A., Smyth, S.S. and Morris, A.J. 2010 A phosphatidic acid binding/nuclear localization motif determines lipin1 function in lipid metabolism and adipogenesis. *Mol Biol Cell* **21**, 3171–3181.

Renault, L., Kuhlmann, J., Henkel, A. and Wittinghofer, A. 2001 Structural Basis for Guanine Nucleotide Exchange on Ran by the Regulator of Chromosome Condensation (RCC1). *Cell* **105**, 245–255.

Ribbeck, K. and Görlich, D. 2001 Kinetic analysis of translocation through nuclear pore complexes. *EMBO J* **20**, 1320–1330.

Ribbeck, K., Lipowsky, G., Kent, H.M., Stewart, M. and Görlich, D. 1998 NTF2 mediates nuclear import of Ran. *EMBO J* **17**, 6587–6598.

Richards, S.A., Carey, K.L. and Macara, I.G. 1997 Requirement of guanosine triphosphate-bound ran for signal-mediated nuclear protein export. *Science* **276**, 1842–1844.

Robbins, J., Dilwortht, S.M., Laskey, R.A. and Dingwall, C. 1991 Two interdependent basic domains in nucleoplasmin nuclear targeting sequence: Identification of a class of bipartite nuclear targeting sequence. *Cell* **64**, 615–623.

Rout, M.P., Aitchison, J.D., Magnasco, M.O. and Chait, B.T. 2003 Virtual gating and nuclear transport: the hole picture. *Trends Cell Biol* **13**, 622–628.

Rout, M.P. and Wente, S.R. 1994 Pores for thought: nuclear pore complex proteins. *Trends Cell Biol* **4**, 357–365.

Sadaf, S., Nagarkoti, S., Awasthi, D., Singh, A.K., Srivastava, R.N., Kumar, S., Barthwal, M.K. and Dikshit, M. 2021 nNOS induction and NOSIP interaction impact granulopoiesis and neutrophil differentiation by modulating nitric oxide generation. *Biochim Biophys Acta Mol Cell Res* **1868**, 119018.

Sakuma, S. and D'Angelo, M.A. 2017 The roles of the nuclear pore complex in cellular dysfunction, aging and disease. *Semin Cell Dev Biol* **68**, 72–84.

Scheich, C., Kümmel, D., Soumailakakis, D., Heinemann, U. and Büssow, K. 2007 Vectors for co-expression of an unrestricted number of proteins. *Nucleic Acids Res* **35**, e43.

Schleicher, M., Brundin, F., Gross, S., Müller-Esterl, W. and Oess, S. 2005 Cell cycle-regulated inactivation of endothelial NO synthase through NOSIP-dependent targeting to the cytoskeleton. *Mol Cell Biol* **25**, 8251–8258.

Schneider, J., Martínez-Arribas, F. and Torrejón, R. 2010 Nup88 expression is associated with myometrial invasion in endometrial carcinoma. *Int J Gynecol Cancer* **20**, 804–808.

Seo, K. and Shin, S.M. 2017 Induction of Lipin1 by ROS-Dependent SREBP-2 Activation. *Toxicol Res* **33**, 219–224.

Shepard, P.J. and Hertel, K.J. 2009 The SR protein family. *Genome Biol* **10**, 242.

Snaebjornsson, M.T., Janaki-Raman, S. and Schulze, A. 2020 Greasing the Wheels of the Cancer Machine: The Role of Lipid Metabolism in Cancer. *Cell Metab* **31**, 62–76.

Soniat, M. and Chook, Y.M. 2016 Karyopherin-β2 Recognition of a PY-NLS Variant that Lacks the Proline-Tyrosine Motif. *Structure* **24**, 1802–1809.

Stade, K., Ford, C.S., Guthrie, C. and Weis, K. 1997 Exportin 1 (Crm1p) Is an Essential Nuclear Export Factor. *Cell* **90**, 1041–1050.

Starnawska, A., Hansen, C.S., Sparsø, T., Mazin, W., Olsen, L., Bertalan, M., Buil, A., Bybjerg-Grauholm, J., Bækvad-Hansen, M., Hougaard, D.M., Mortensen, P.B., Pedersen, C.B., Nyegaard, M., Werge, T. and Weinsheimer, S. 2017 Differential DNA methylation at birth associated with mental disorder in individuals with 22q11.2 deletion syndrome. *Transl Psychiatry* **7**, e1221.

Ström, A.C. and Weis, K. 2001 Importin-beta-like nuclear transport receptors. *Genome Biol* **2**, REVIEWS3008.

Stuwe, T., Correia, A.R., Lin, D.H., Paduch, M., Lu, V.T., Kossiakoff, A.A. and Hoelz, A. 2015 Nuclear pores. Architecture of the nuclear pore complex coat. *Science* **347**, 1148–1152.

Su, Y. 2014 Regulation of endothelial nitric oxide synthase activity by protein-protein interaction. *Curr Pharm Des* **20**, 3514–3520.

Süel, K.E., Gu, H. and Chook, Y.M. 2008 Modular organization and combinatorial energetics of proline-tyrosine nuclear localization signals. *PLoS Biol* **6**, e137.

Suntharalingam, M. and Wente, S.R. 2003 Peering through the Pore. *Developmental Cell* **4**, 775–789.

Takahashi, S. and Mendelsohn, M.E. 2003 Synergistic activation of endothelial nitric-oxide synthase (eNOS) by HSP90 and Akt: calcium-independent eNOS activation involves formation of an HSP90-Akt-CaM-bound eNOS complex. *J Biol Chem* **278**, 30821–30827.

Tao, T., Lan, J., Presley, J.F., Sweezey, N.B. and Kaplan, F. 2004 Nucleocytoplasmic shuttling of lgl2 is developmentally regulated in fetal lung. *Am J Respir Cell Mol Biol* **30**, 350–359.

Tayri-Wilk, T., Slavin, M., Zamel, J., Blass, A., Cohen, S., Motzik, A., Sun, X., Shalev, D.E., Ram, O. and Kalisman, N. 2020 Mass spectrometry reveals the chemistry of formaldehyde cross-linking in structured proteins. *Nat Commun* **11**, 3128.

Teng, S.-C., Wu, K.-J., Tseng, S.-F., Wong, C.-W. and Kao, L. 2006 Importin KPNA2, NBS1, DNA repair and tumorigenesis. *J Mol Histol* **37**, 293–299.

Thermo scientific - Double digest calculator *Double digest calculator*. https://www.thermofisher.com/de/de/home/brands/thermo-scientific/molecular-biology/thermo-scientific-restriction-modifying-enzymes/restriction-enzymes-thermo-scientific/double-digest-calculator-thermo-scientific.html.

Thermo scientific - Tm calculator *Tm calculator*. https://www.thermofisher.com/de/de/home/brands/thermo-scientific/molecular-biology/molecular-biology-learning-center/molecular-biology-resource-library/thermo-scientific-web-tools/tm-calculator.html.

Tomuschat, C., O'Donnell, A.-M., Coyle, D., Dreher, N., Kelly, D. and Puri, P. 2017 NOS-interacting protein (NOSIP) is increased in the colon of patients with Hirschsprungs's disease. *J Pediatr Surg* **52**, 772–777.

Trotman, L.C., Wang, X., Alimonti, A., Chen, Z., Teruya-Feldstein, J., Yang, H., Pavletich, N.P., Carver, B.S., Cordon-Cardo, C., Erdjument-Bromage, H., Tempst, P., Chi, S.-G., Kim, H.-J., Misteli, T., Jiang, X. and Pandolfi, P.P. 2007 Ubiquitination regulates PTEN nuclear import and tumor suppression. *Cell* **128**, 141–156.

Truant, R. and Cullen, B.R. 1999 The arginine-rich domains present in human immunodeficiency virus type 1 Tat and Rev function as direct importin beta-dependent nuclear localization signals. *Mol Cell Biol* **19**, 1210–1217.

Tsytlonok, M., Craig, P.O., Sivertsson, E., Serquera, D., Perrett, S., Best, R.B., Wolynes, P.G. and Itzhaki, L.S. 2013 Complex energy landscape of a giant repeat protein. *Structure* **21**, 1954–1965.

Tunyasuvunakool, K., Adler, J., Wu, Z., Green, T., Zielinski, M., Žídek, A., Bridgland, A., Cowie, A., Meyer, C., Laydon, A., Velankar, S., Kleywegt, G.J., Bateman, A., Evans, R., Pritzel, A., Figurnov, M., Ronneberger, O., Bates, R., Kohl, S.A.A., Potapenko, A., Ballard, A.J., Romera-Paredes, B., Nikolov, S., Jain, R., Clancy, E., Reiman, D., Petersen, S., Senior, A.W., Kavukcuoglu, K., Birney, E., Kohli, P., Jumper, J. and Hassabis, D. 2021 Highly accurate protein structure prediction for the human proteome. *Nature* **596**, 590–596.

Ullman, K.S., Shah, S., Powers, M.A. and Forbes, D.J. 1999 The nucleoporin nup153 plays a critical role in multiple types of nuclear export. *Mol Biol Cell* **10**, 649–664.

Upla, P., Kim, S.J., Sampathkumar, P., Dutta, K., Cahill, S.M., Chemmama, I.E., Williams, R., Bonanno, J.B., Rice, W.J., Stokes, D.L., Cowburn, D., Almo, S.C., Sali, A., Rout, M.P. and Fernandez-Martinez, J. 2017 Molecular Architecture of the Major Membrane Ring Component of the Nuclear Pore Complex. *Structure* **25**, 434–445.

van der Watt, P.J., Maske, C.P., Hendricks, D.T., Parker, M.I., Denny, L., Govender, D., Birrer, M.J. and Leaner, V.D. 2009 The Karyopherin proteins, Crm1 and Karyopherin beta1, are overexpressed in cervical cancer and are critical for cancer cell survival and proliferation. *Int J Cancer* **124**, 1829–1840.

van der Watt, P.J., Ngarande, E. and Leaner, V.D. 2011 Overexpression of Kpnβ1 and Kpnα2 importin proteins in cancer derives from deregulated E2F activity. *PLoS One* **6**, e27723.

Varadi, M., Anyango, S., Deshpande, M., Nair, S., Natassia, C., Yordanova, G., Yuan, D., Stroe, O., Wood, G., Laydon, A., Žídek, A., Green, T., Tunyasuvunakool, K., Petersen, S., Jumper, J., Clancy, E., Green, R., Vora, A., Lutfi, M., Figurnov, M., Cowie, A., Hobbs, N., Kohli, P., Kleywegt, G., Birney, E., Hassabis, D. and Velankar, S. 2022 AlphaFold Protein Structure Database: massively expanding the structural coverage of protein-sequence space with high-accuracy models. *Nucleic Acids Res* **50**, D439-D444.

Vetter, I.R., Arndt, A., Kutay, U., Görlich, D. and Wittinghofer, A. 1999 Structural View of the Ran–Importin β Interaction at 2.3 Å Resolution. *Cell* **97**, 635–646.

Villalobo, A. 2006 Nitric oxide and cell proliferation. *FEBS J* **273**, 2329–2344.

Waldmann, I., Wälde, S. and Kehlenbach, R.H. 2007 Nuclear import of c-Jun is mediated by multiple transport receptors. *J Biol Chem* **282**, 27685–27692.

Walther, T.C., Fornerod, M., Pickersgill, H., Goldberg, M., Allen, T.D. and Mattaj, I.W. 2001 The nucleoporin Nup153 is required for nuclear pore basket formation, nuclear pore complex anchoring and import of a subset of nuclear proteins. *EMBO J* **20**, 5703–5714.

Wang, H., Zhang, J., Qiu, W., Han, G.-S., Carman, G.M. and Adeli, K. 2011 Lipin-1γ isoform is a novel lipid droplet-associated protein highly expressed in the brain. *FEBS Lett* **585**, 1979–1984.

Wang, Y.E., Pernet, O. and Lee, B. 2012 Regulation of the nucleocytoplasmic trafficking of viral and cellular proteins by ubiquitin and small ubiquitin-related modifiers. *Biol Cell* **104**, 121–138.

Warda, A.S., Freytag, B., Haag, S., Sloan, K.E., Görlich, D. and Bohnsack, M.T. 2016 Effects of the Bowen-Conradi syndrome mutation in EMG1 on its nuclear import, stability and nucleolar recruitment. *Hum Mol Genet* **25**, 5353–5364.

WATSON, M.L. 1955 The nuclear envelope; its structure and relation to cytoplasmic membranes. *J Biophys Biochem Cytol* **1**, 257–270.

Weinberg, R.A. 2014 The biology of cancer. New York: Garland Science, Taylor & Francis Group.

Weis, K. 1998 Importins and exportins: how to get in and out of the nucleus. *Trends Biochem Sci* **23**, 185–189.

Weis, K., Mattaj, I.W. and Lamond, A.I. 1995 Identification of hSRP1 alpha as a functional receptor for nuclear localization sequences. *Science* **268**, 1049–1053.

Welburn, J.P.I. and Jeyaprakash, A.A. 2018 Mechanisms of Mitotic Kinase Regulation: A Structural Perspective. *Front Cell Dev Biol* **6**, 6.

Wing, C.E., Fung, H.Y.J. and Chook, Y.M. 2022 Karyopherin-mediated nucleocytoplasmic transport. *Nat Rev Mol Cell Biol* **23**, 307–328.

Wu, J., Matunis, M.J., Kraemer, D., Blobel, G. and Coutavas, E. 1995 Nup358, a cytoplasmically exposed nucleoporin with peptide repeats, Ran-GTP binding sites, zinc fingers, a cyclophilin A homologous domain, and a leucine-rich region. *J Biol Chem* **270**, 14209–14213.

Wu, K., He, J., Pu, W. and Peng, Y. 2018 The Role of Exportin-5 in MicroRNA Biogenesis and Cancer. *Genomics Proteomics Bioinformatics* **16**, 120–126.

Xu, D., Marquis, K., Pei, J., Fu, S.-C., Cağatay, T., Grishin, N.V. and Chook, Y.M. 2015 LocNES: a computational tool for locating classical NESs in CRM1 cargo proteins. *Bioinformatics* **31**, 1357–1365.

Yamada, J., Phillips, J.L., Patel, S., Goldfien, G., Calestagne-Morelli, A., Huang, H., Reza, R., Acheson, J., Krishnan, V.V., Newsam, S., Gopinathan, A., Lau, E.Y., Colvin, M.E., Uversky, V.N. and Rexach, M.F. 2010 A bimodal distribution of two distinct categories of intrinsically disordered structures with separate functions in FG nucleoporins. *Mol Cell Proteomics* **9**, 2205–2224.

Yashiroda, Y. and Yoshida, M. 2003 Nucleo-cytoplasmic transport of proteins as a target for therapeutic drugs. *Curr Med Chem* **10**, 741–748.

Yokoya, F., Imamoto, N., Tachibana, T. and Yoneda, Y. 1999 beta-catenin can be transported into the nucleus in a Ran-unassisted manner. *Mol Biol Cell* **10**, 1119–1131.

Yoshimura, S.H. and Hirano, T. 2016 HEAT repeats - versatile arrays of amphiphilic helices working in crowded environments? *J Cell Sci* **129**, 3963–3970.

Zhang, K., Donnelly, C.J., Haeusler, A.R., Grima, J.C., Machamer, J.B., Steinwald, P., Daley, E.L., Miller, S.J., Cunningham, K.M., Vidensky, S., Gupta, S., Thomas, M.A., Hong, I., Chiu, S.-L., Huganir, R.L., Ostrow, L.W., Matunis, M.J., Wang, J., Sattler, R., Lloyd, T.E. and Rothstein, J.D. 2015 The C9orf72 repeat expansion disrupts nucleocytoplasmic transport. *Nature* **525**, 56–61.

Zhang, K., Wang, M., Tamayo, A.T., Shacham, S., Kauffman, M., Lee, J., Zhang, L., Ou, Z., Li, C., Sun, L., Ford, R.J. and Pham, L.V. 2013 Novel selective inhibitors of nuclear export CRM1 antagonists for therapy in mantle cell lymphoma. *Exp Hematol* **41**, 67-78.e4.

Zhao, Z.-R., Zhang, Z.-Y., He, X.-Q., Hu, Y.-M., Tian, Y.-F., Zhang, L.-J. and Sun, X.-F. 2010 Nup88 mRNA overexpression in colorectal cancers and relationship with p53. *Cancer Biomark* **8**, 73–80.

Zheng, M., Tang, L., Huang, L., Ding, H., Liao, W.-T., Zeng, M.-S. and Wang, H.-Y. 2010 Overexpression of karyopherin-2 in epithelial ovarian cancer and correlation with poor prognosis. *Obstet Gynecol* **116**, 884–891.

Appendix

Synthesized gene fragments

In the following, ordered gene fragments from BioCat GmbH are listed. Mutated nucleotide, compared to the wildtype sequence, are marked in uppercase letters.

NOSIP fragment (aa 1-165)

>Y14E S36D S138D

atgacgcggcatggcaagaactgcaccgcaggggccgtcGAGacctaccacgagaagaagaaggacacagcggcctcg
ggctatgggacccagaacattcgactgGACcgggatgccgtgaaggacttcgactgctgttgtctctccctgcagccttgccac
gatcctgttgtcaccccagatggctacctgtatgagcgtgaggccatcctggagtacattctgcaccagaagaaggagattgccc
ggcagatgaaggcctacgagaagcagcggggcacccggcgcgaggagcagaaggagcttcagcgggcggcctcgcagg
accatgtgcggggcttcctggagaaggagtcggctatcgtgagccggcccctcaacccttcacagccaaggccctctcgggca
ccGACccagatgatgtccaacctgggcccagtgtgggtcctccaagtaaggacaaggacaaagtgctgcccagcttctggat
cccgt

>Y14E S138D

atgacgcggcatggcaagaactgcaccgcaggggccgtcGAGacctaccacgagaagaagaaggacacagcggcctcg
ggctatgggacccagaacattcgactgAGCcgggatgccgtgaaggacttcgactgctgttgtctctccctgcagccttgccac
gatcctgttgtcaccccagatggctacctgtatgagcgtgaggccatcctggagtacattctgcaccagaagaaggagattgccc
ggcagatgaaggcctacgagaagcagcggggcacccggcgcgaggagcagaaggagcttcagcgggcggcctcgcagg
accatgtgcggggcttcctggagaaggagtcggctatcgtgagccggcccctcaacccttcacagccaaggccctctcgggca
ccGACccagatgatgtccaacctgggcccagtgtgggtcctccaagtaaggacaaggacaaagtgctgcccagcttctggat
cccgt

>Y14E S36D

atgacgcggcatggcaagaactgcaccgcaggggccgtcGAGacctaccacgagaagaagaaggacacagcggcctcg
ggctatgggacccagaacattcgactgGACcgggatgccgtgaaggacttcgactgctgttgtctctccctgcagccttgccac
gatcctgttgtcaccccagatggctacctgtatgagcgtgaggccatcctggagtacattctgcaccagaagaaggagattgccc
ggcagatgaaggcctacgagaagcagcggggcacccggcgcgaggagcagaaggagcttcagcgggcggcctcgcagg
accatgtgcggggcttcctggagaaggagtcggctatcgtgagccggcccctcaacccttcacagccaaggccctctcgggca

ccAGCccagatgatgtccaacctgggcccagtgtgggtcctccaagtaaggacaaggacaaagtgctgcccagcttctggat
cccgt

>Y14E

atgacgcggcatggcaagaactgcaccgcaggggccgtcGAGacctaccacgagaagaagaaggacacagcggcctcg
ggctatgggacccagaacattcgactgAGCcgggatgccgtgaaggacttcgactgctgttgtctctccctgcagccttgccac
gatcctgttgtcaccccagatggctacctgtatgagcgtgaggccatcctggagtacattctgcaccagaagaaggagattgccc
ggcagatgaaggcctacgagaagcagcggggcacccggcgcgaggagcagaaggagcttcagcgggcggcctcgcagg
accatgtgcggggcttcctggagaaggagtcggctatcgtgagccggcccctcaacccctttcacagccaaggccctctcgggca
ccAGCccagatgatgtccaacctgggcccagtgtgggtcctccaagtaaggacaaggacaaagtgctgcccagcttctggat
cccgt

>S138D

atgacgcggcatggcaagaactgcaccgcaggggccgtcTACacctaccacgagaagaagaaggacacagcggcctcg
ggctatgggacccagaacattcgactgAGCcgggatgccgtgaaggacttcgactgctgttgtctctccctgcagccttgccac
gatcctgttgtcaccccagatggctacctgtatgagcgtgaggccatcctggagtacattctgcaccagaagaaggagattgccc
ggcagatgaaggcctacgagaagcagcggggcacccggcgcgaggagcagaaggagcttcagcgggcggcctcgcagg
accatgtgcggggcttcctggagaaggagtcggctatcgtgagccggcccctcaacccctttcacagccaaggccctctcgggca
ccGACccagatgatgtccaacctgggcccagtgtgggtcctccaagtaaggacaaggacaaagtgctgcccagcttctggat
cccgt

>S36D S138D

atgacgcggcatggcaagaactgcaccgcaggggccgtcTACacctaccacgagaagaagaaggacacagcggcctcg
ggctatgggacccagaacattcgactgGACcgggatgccgtgaaggacttcgactgctgttgtctctccctgcagccttgccac
gatcctgttgtcaccccagatggctacctgtatgagcgtgaggccatcctggagtacattctgcaccagaagaaggagattgccc
ggcagatgaaggcctacgagaagcagcggggcacccggcgcgaggagcagaaggagcttcagcgggcggcctcgcagg
accatgtgcggggcttcctggagaaggagtcggctatcgtgagccggcccctcaacccctttcacagccaaggccctctcgggca
ccGACccagatgatgtccaacctgggcccagtgtgggtcctccaagtaaggacaaggacaaagtgctgcccagcttctggat
cccgt

>S36D

atgacgcggcatggcaagaactgcaccgcaggggccgtcTACacctaccacgagaagaagaaggacacagcggcctcg
ggctatgggacccagaacattcgactgGACcgggatgccgtgaaggacttcgactgctgttgtctctccctgcagccttgccac
gatcctgttgtcaccccagatggctacctgtatgagcgtgaggccatcctggagtacattctgcaccagaagaaggagattgccc
ggcagatgaaggcctacgagaagcagcggggcacccggcgcgaggagcagaaggagcttcagcgggcggcctcgcagg

accatgtgcggggcttcctggagaaggagtcggctatcgtgagccggcccctcaacccttcacagccaaggccctctcgggca
ccAGCccagatgatgtccaacctgggcccagtgtgggtcctccaagtaaggacaaggacaaagtgctgcccagcttctggat
cccgt

Figures

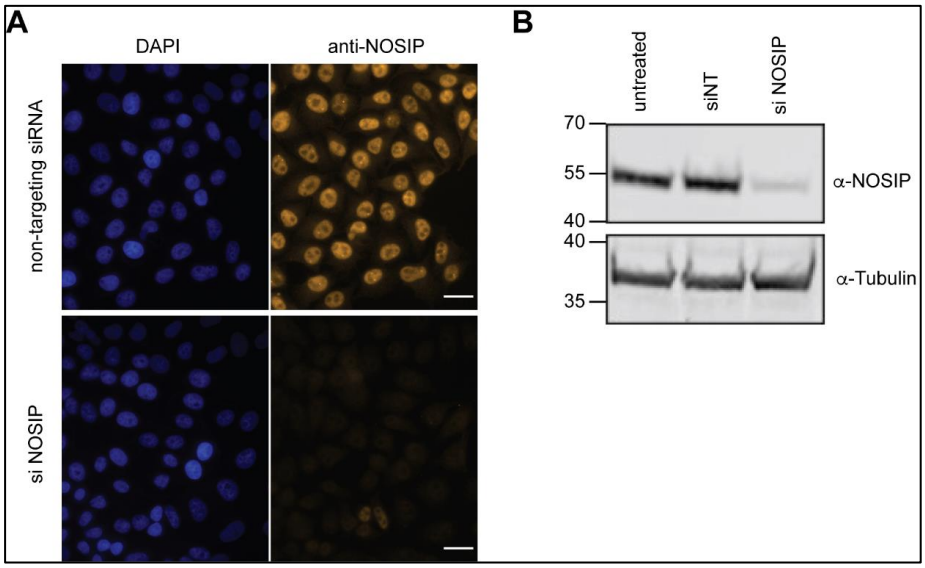

Figure S 1: Validation of anti-NOSIP antibody form Sigma (Ab411). (A) HeLa P4 cells were transfected with 50 nM siRNA against NOSIP or 50 nM nontargeting siRNA (siNT) using RNAiMax. NOSIP was visualized by indirect immunofluorescence using the NOSIP antibody (Ab411), cell nuclei were visualized using DAPI. Scale bar 20 µM. (B) Knockdown success was analyzed by Western blotting using antibodies against NOSIP and Tubulin (loading control)

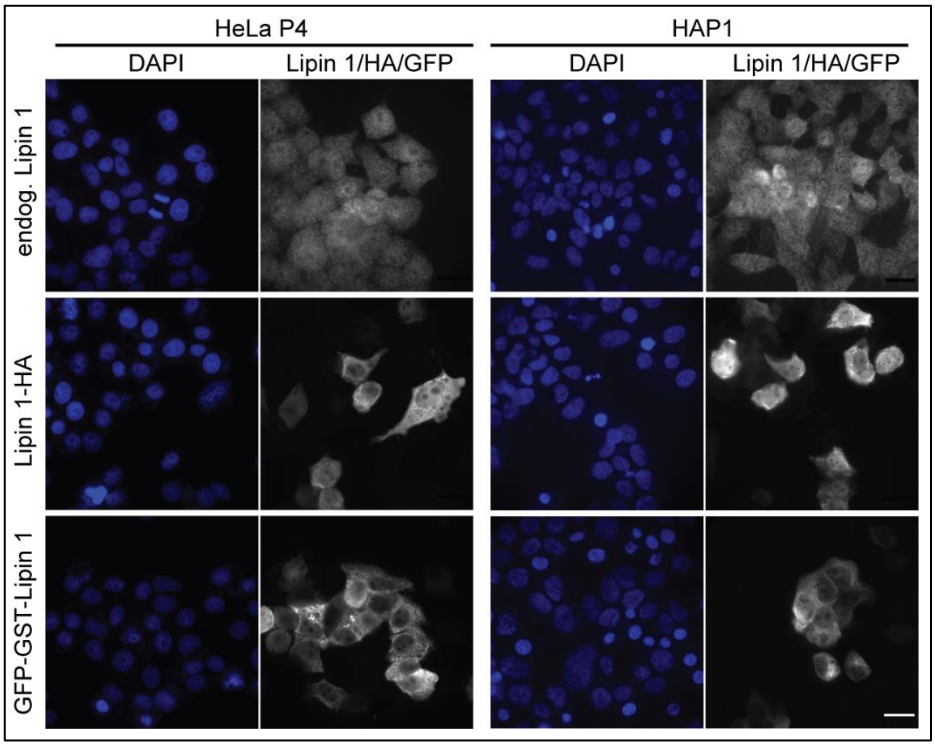

Figure S 2: Localization of Lipin 1 in HeLa cells and HAP1 cells. The localization of endogenous, HA-tagged and GFP-GST-tagged Lipin 1 was analyzed in HeLa cells and in HAP1 cells. Respective plasmids were transfected using the calcium phosphate method. Endogenous Lipin 1 and Lipin 1-HA were visualized by indirect immunofluorescence using antibodies against Lipin 1 or HA, respectively. GFP-GST-Lipin 1 was visualized by its fluorescence tag, images were acquired by epifluorescence microscopy. Scale bar 20 µm.

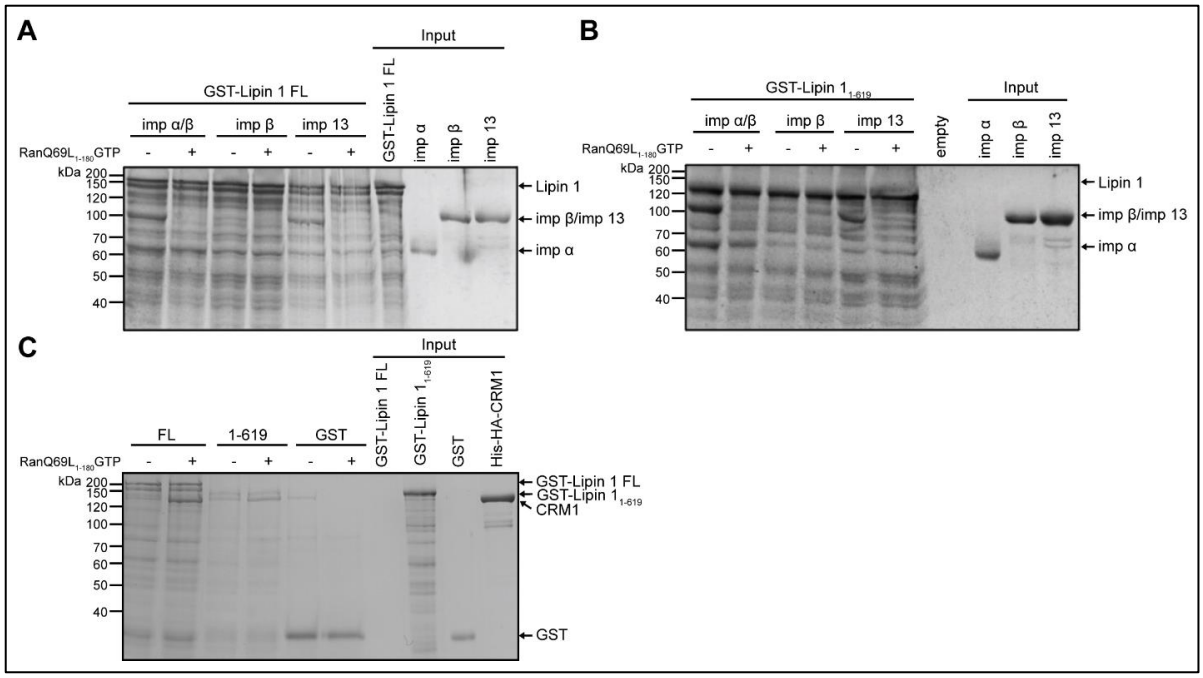

Figure S 3: Importin 13, CRM1 and importin α/β are binding to Lipin 1 in a binding assay. To analyze the binding of importin 13 and importin α/β to Lipin 1, either 100 pmol GST-Lipin 1 FL (full-length) (A) or GST-Lipin 1^{1-619} (B) were immobilized on glutathione sepharose beads. Immobilized Lipin 1 was incubated with 100 pmol His-importin 13, His-importin α/β or His- importin β in presence or absence of 300 pmol RanQ69L$_{1-180}$-GTP. Unbound proteins were washed out and bound proteins were eluted using 4xSDS sample buffer. Eluted proteins were analyzed by SDS-PAGE, followed by Coomassie staining. Protein purification and these binding assays were performed by Carmen Wassong. (C) GST-Lipin 1 FL or GST-Lipin 1^{1-619} were immobilized on glutathione sepharose beads and incubated with 100 pmol His-HA-CRM1 in presence or absence of 300 pmol RanQ69L$_{1-180}$-GTP. Bound proteins were eluted and analyzed as in A and B.

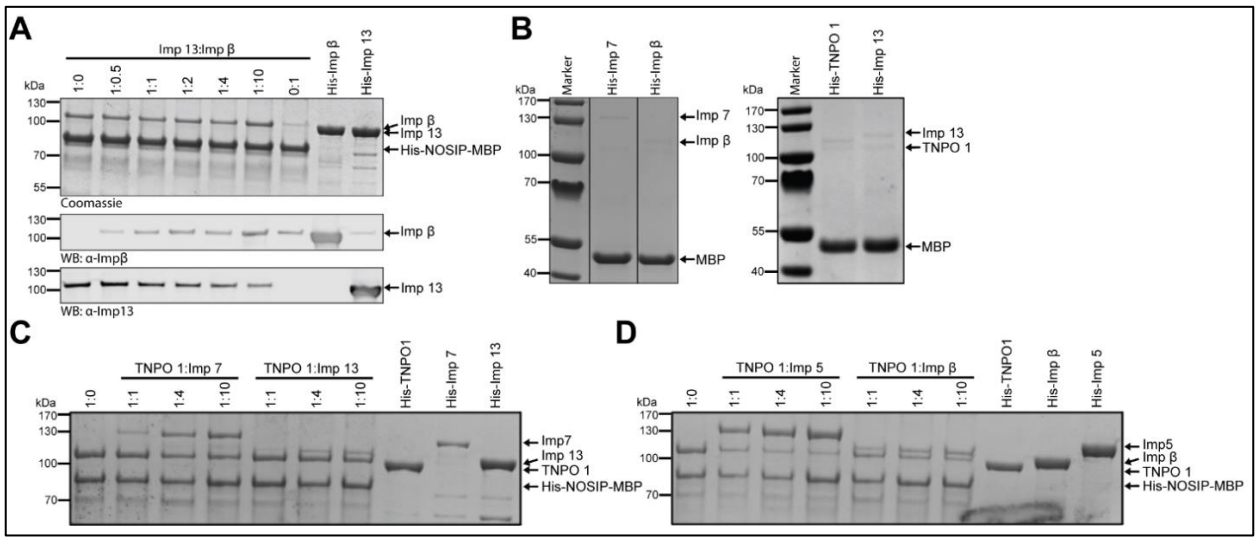

Figure S 4: Competition of NTRs for NOSIP. (A) His-NOSIP-MBP was immobilized to amylose resin and incubated with His-imp 13 or His-S-imp β or both at indicated molar ratios. Unbound proteins were washed out and bound proteins were eluted in 4xSDS-sample, analyzed by SDS-PAGE, followed by Coomassie staining. Since both NTRs have a similar size and running at a similar height in SDS-Gels, a Western blot using respective antibodies was performed to distinguish bound NTRs. (B) His-MBP was immobilized on amylose resin and incubated with His-tagged NTRs. Bound proteins were eluted and analyzed by SDS-PAGE, followed by Coomassie staining. (C-D) Competition binding assay of transportin 1 (TNPO 1) and other NTRs for NOSIP. His-NOSIP-MBP was immobilized as above and incubated with NTRs at indicated molar ratios. Bound proteins were eluted and analyzed by SDS-PAGE, followed by Coomassie staining.

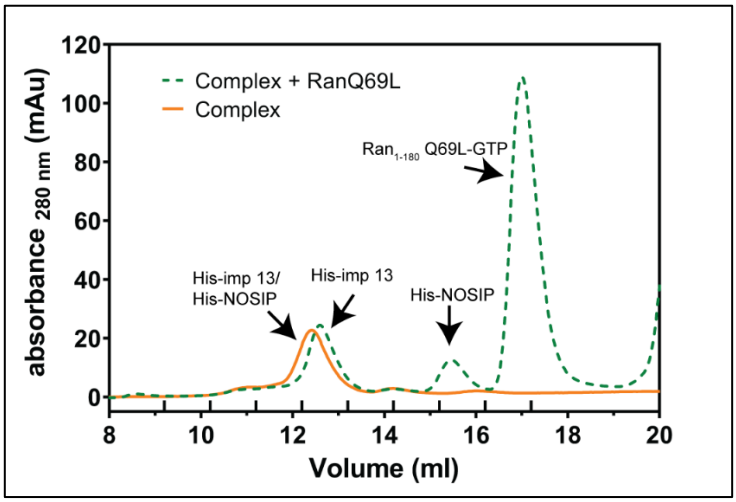

Figure S 5: The complex of importin 13-NOSIP is stable over-time. The complex of His-importin 13-His-NOSIP was formed by incubating 50 µM His-imp13 with 100 µM His-NOSIP in 1x TPB for 1 h on ice. The formed complex was centrifuged at 16100 x g prior to size exclusion chromatography using a Superdex 200 10/300 GL. Fractions containing His-imp13-His-NOSIP were pooled and concentrated using a Spin-X-UF concentrator (10K MWCO, 0.5 mL). The half of the concentrated complex was again subjected to SEC to validate the stability of the complex (orange curve). The other half was first incubated with 30 µM Ran_{1-180} Q69L-GTP for 1 h on ice, as specificity control, and then reapplied to SEC (green curve). Note, here another analytical SEC column (Superdex 200 10/300 GL vs. Superdex 200 10/300 GL increase) was used as in the experiments in Figure 17, curves are not directly comparable. Runs were performed using an Äkta purifier, data were plotted using GraphPad prism 9.

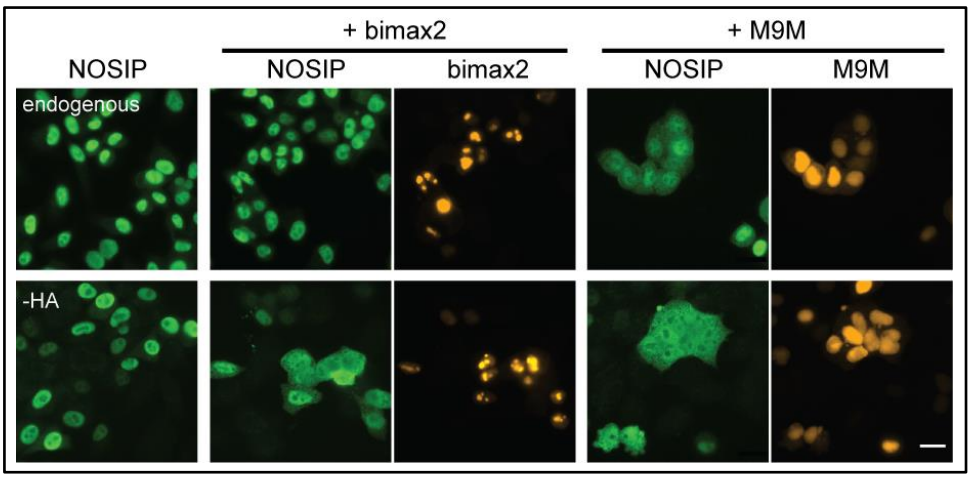

Figure S 6: Transfection of endogenous or HA-tagged NOSIP with RFP-tagged peptide inhibitors. HeLa P4 cells were transfected with RFP-tagged bimax2 or M9M which are peptide inhibitors of importin α/β or transportin 1, respectively. The effect of the inhibitors on endogenous NOSIP or co-transfected NOSIP was analyzed, therefore NOSIP was detected by indirect immunofluorescence using antibodies directed against NOSIP or the HA-tag. Cells were analyzed by epifluorescence microscopy, scale bar 20 µm.

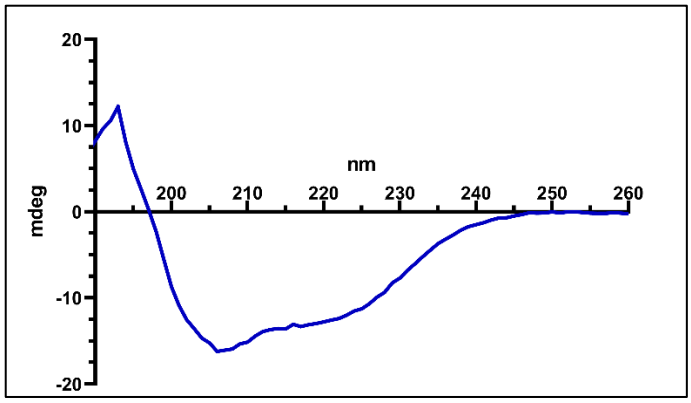

Figure S 7: CD-spectrum of untagged NOSIP. For analysis untagged NOSIP with a concentration of 0.1 mg/mL in 100 mM Na_2HPO_4/NaH_2PO_4 was measured at 20 °C using a Chirascan™ CD spectrometer. Depicted is the average of 20 spectra. Data was plotted in GraphPad prism 9. mdeg – millidegrees.

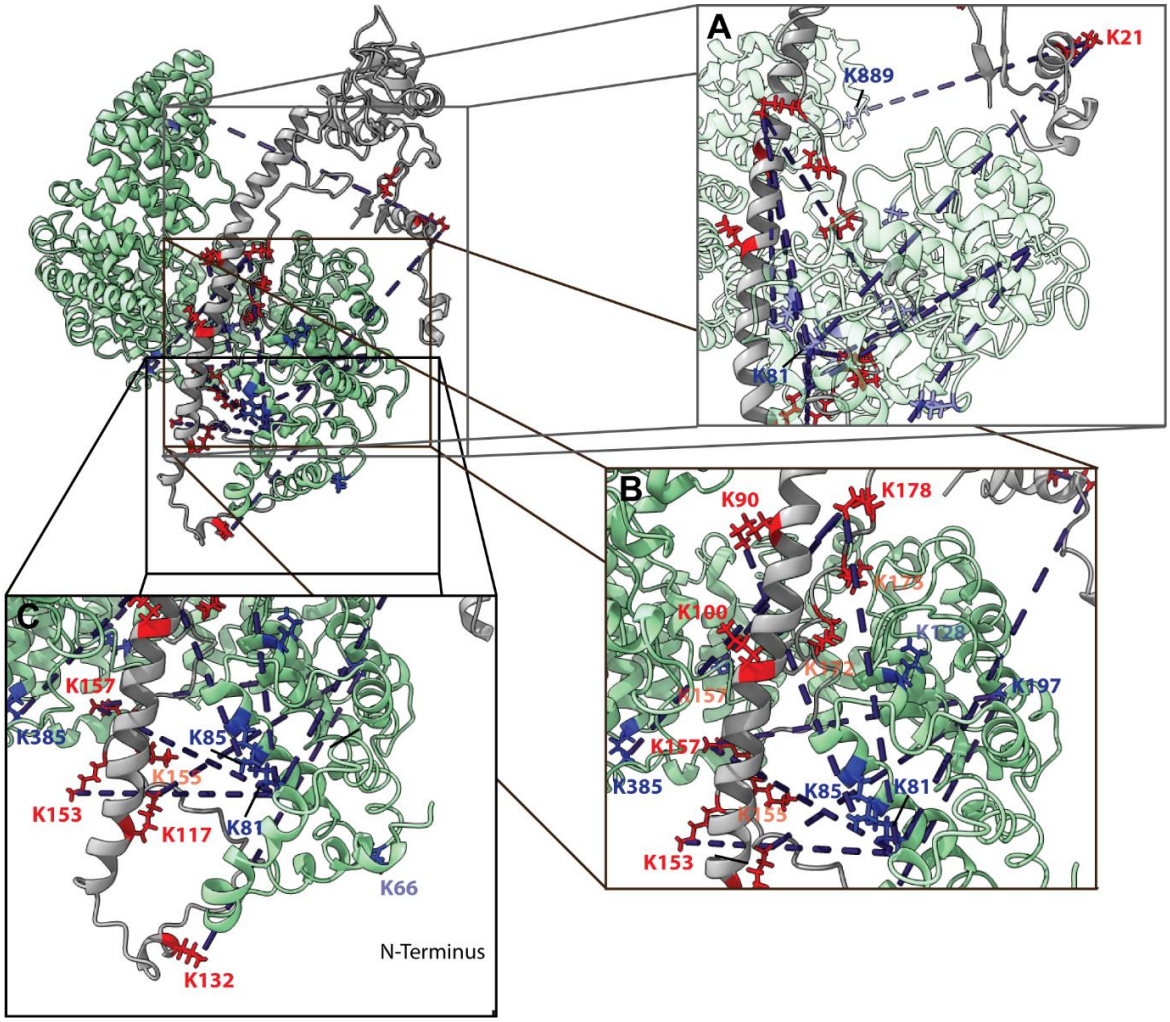

Figure S 8: Docking of NOSIP to transportin 1 using ClusPro and Rosetta. (A-C) The AlphaFold model of NOSIP was docked to the crystal structure of transportin 1 (PDB: 1QBK) using the MS derived crosslinks. Only the transportin 1 structure of the PDB file was used for docking, the structure of Ran was removed. NOSIP is depicted in gray, crosslinked lysins are shown as red sticks. Transportin 1 is colored in green and crosslinked lysins as blue sticks. Crosslinks in a distance of > 30 Å are depicted as dark blue dashed line. Images were generated using Chimera software

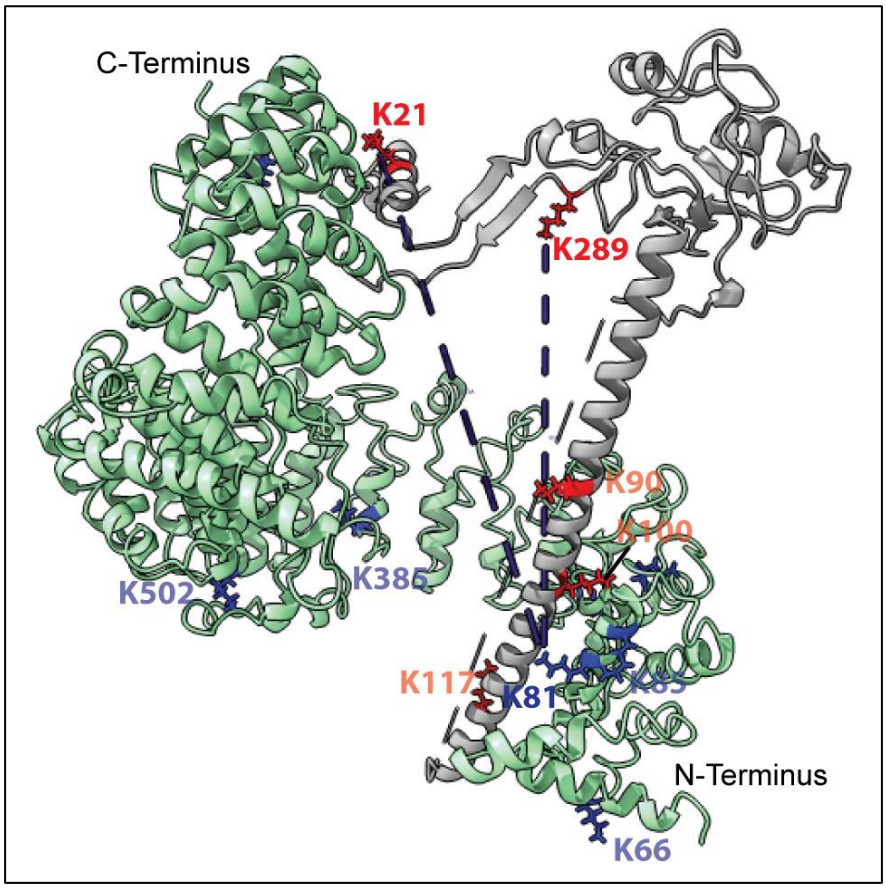

Figure S 9: Docking of NOSIP⊿IDR to transportin 1 using ClusPro and Rosetta. (A-B) The IDR of NOSIPs AlphaFold model (126-188^{NOSIP}) was removed and the modified structure was then used for docking to the crystal structure of transportin 1 (PDB: 1QBK). Only the transportin 1 structure of the PDB file was used for docking, the structure of Ran was removed. The MS derived crosslinks were used as restrains during the docking process. NOSIP is depicted in gray, with the removed IDR shown as dashed line and crosslinked lysins are shown as red sticks. Transportin 1 is colored in green and crosslinked lysins as blue sticks. Crosslinks in a distance of > 30 Å are depicted as dark blue dashed line. Images were generated using Chimera software

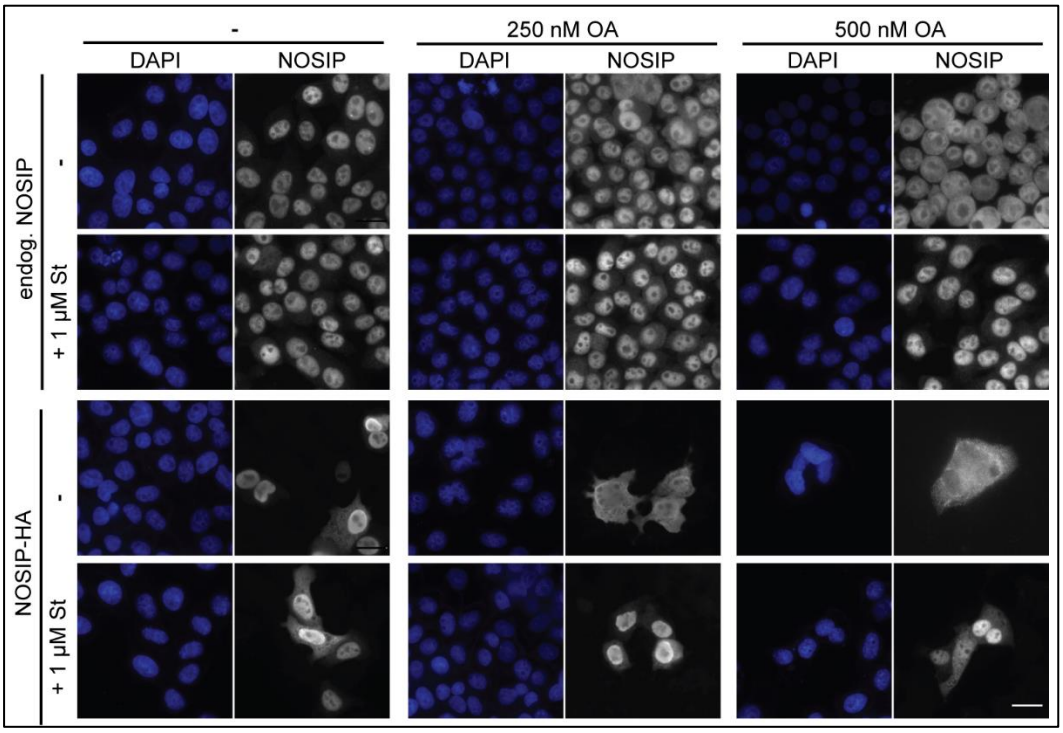

Figure S 10: Treatment of NOSIP with okadaic acid and staurosporine. HeLa cells were transfected with NOSIP-HA or untransfected cells were used. Cells were then treated with okadaicacid (OA) (250 or 500 nM) and with or without staurosporine (St) (1 µM) for 1 h. Afterwards cells were subjected to indirect imunofluorescence to detect endogenous NOSIP or NOSIP-HA using respective antibodies. Images were acquired by epifluoresence microscopy. Scale bar 20 µM.

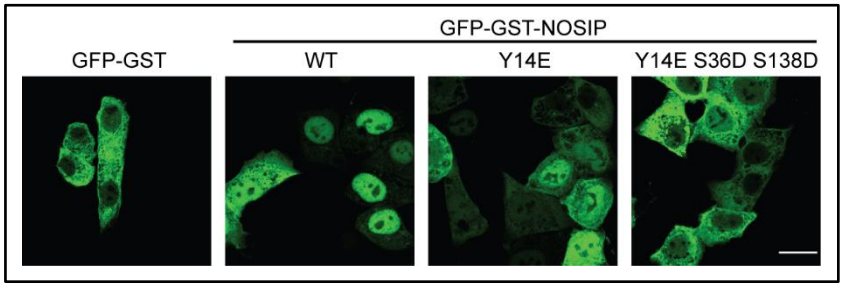

Figure S 11: Localization of GFP-GST-NOSIP phosphomimic mutants in HeLa P4 cells. HeLa P4 cells were transfected with plasmids coding for GFP-GST alone or GFP-GST-NOSIP WT (wildtype), Y14E and Y14E S36D S138D using calcium phosphate method. Localization of NOSIP was analyzed by confocal microscopy, Scale bar 20 µm.

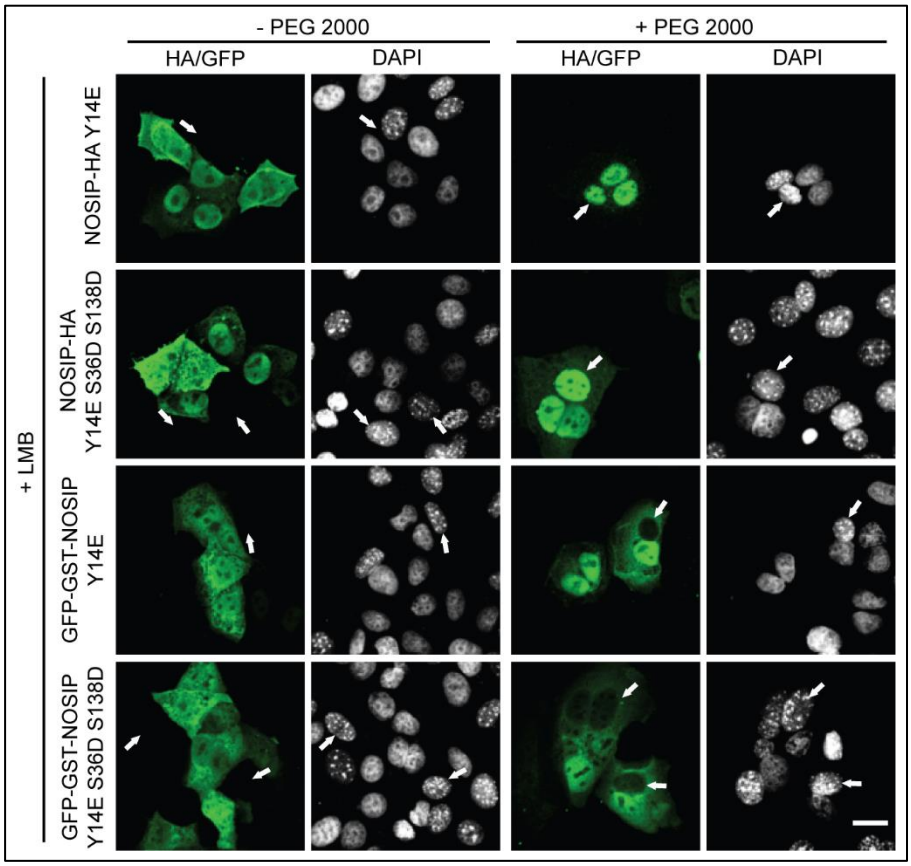

Figure S 12: NOSIP Y14E and Y14E S36D S138D showed still nucleocytoplasmic shuttling in presence of LMB. The heterokaryon assay was performed by fusing (+ PEG 2000 or as control – PEG 2000) HeLa P4 cells, transfected with NOSIP-HA or GFP-GST-NOSIP (Y14E or Y14E S36D S138D), and NIH 3T3 cells in the presence of 10 nM Leptomycin B (LMB). Cell nuclei were distinguished by their DAPI staining, NIH 3T3 nuclei show several bright dots and are indicated by arrows. Proteins of interest were detected by their fluorescence tag or in case of NOSIP-HA by indirect immunofluorescence using an anti-HA antibody. Nuclear shuttling of fluorescently labeled proteins was analyzed by confocal microscopy. Scale bar 20 µm

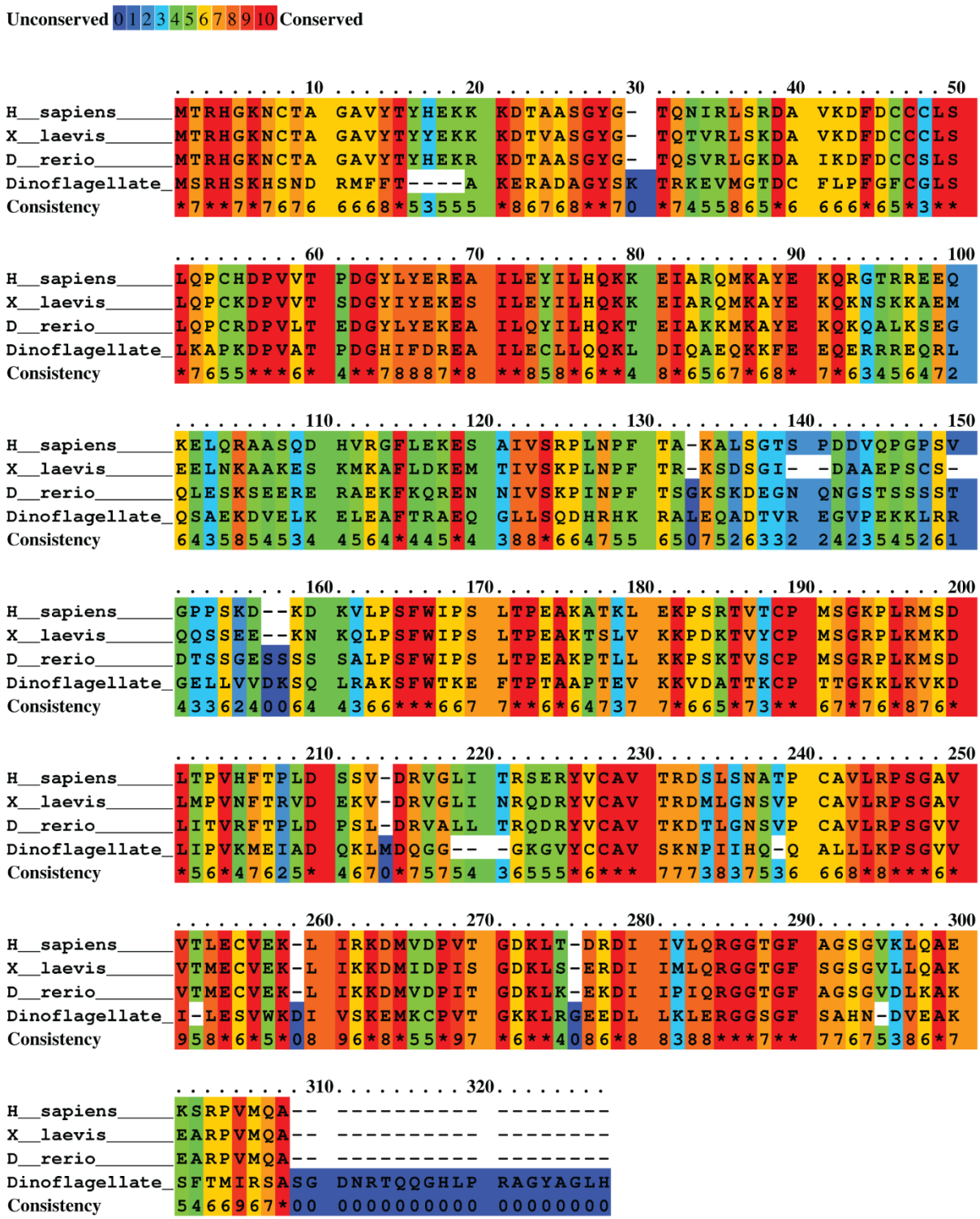

Figure S 13: Multiple sequence alignment of NOSIP from different species. The sequence of NOSIP from Homo sapiens (H. sapiens), Xenopus laevis (X. laevis), Danio rerio (D. rerio) and Symbiodinium pilosum (Dinoflagellate) were aligned using the PRALINE multiple sequence alignment webtool (https://www.ibi.vu.nl/programs/pralinewww/). Residues are depicted from red to blue, according to their conservation from high to low, respectively.

Tables

Table S 1: Table of constrains used for local docking of NOSIP and transportin 1 using Rosetta (see Figure 34)

Protein 1	Residue 1	Protein 2	Residue 2
transportin 1	K66	NOSIP	K117
transportin 1	K66	NOSIP	K132
transportin 1	K81	NOSIP	K21
transportin 1	K81	NOSIP	K100
transportin 1	K81	NOSIP	K117
transportin 1	K81	NOSIP	K132
transportin 1	K81	NOSIP	K153
transportin 1	K81	NOSIP	K155
transportin 1	K81	NOSIP	K157
transportin 1	K81	NOSIP	K172
transportin 1	K81	NOSIP	K175
transportin 1	K81	NOSIP	K178
transportin 1	K81	NOSIP	K289
transportin 1	K85	NOSIP	K90
transportin 1	K85	NOSIP	K172
transportin 1	K85	NOSIP	K175
transportin 1	K128	NOSIP	K90
transportin 1	K128	NOSIP	K175
transportin 1	K197	NOSIP	K117
transportin 1	K197	NOSIP	K132
transportin 1	K197	NOSIP	K157
transportin 1	K385	NOSIP	K178
transportin 1	K502	NOSIP	K178
transportin 1	K889	NOSIP	K21

Table S 2: Table of constrains used for local docking of NOSIP⊿IDR and transportin 1 using Rosetta (see Figure 35)

Protein 1	Residue 1	Protein 2	Residue 2
transportin 1	K66	NOSIP	K117
transportin 1	K81	NOSIP	K21
transportin 1	K81	NOSIP	K100
transportin 1	K81	NOSIP	K117
transportin 1	K81	NOSIP	K289
transportin 1	K85	NOSIP	K90
transportin 1	K128	NOSIP	K90
transportin 1	K197	NOSIP	K117
transportin 1	K889	NOSIP	K21

Table S 3: Filtered crosslinks of His-importin 13 His-NOSIP complex crosslinked by BS3 (lower band) (see Figure 29)

Protein 1	Residue 1	Protein 2	Residue 2	type	Spectral count
NOSIP	21	Importin 13	941	Inter-Protein	46
NOSIP	289	Importin 13	941	Inter-Protein	36
NOSIP	294	Importin 13	941	Inter-Protein	43
NOSIP	19	Importin 13	941	Inter-Protein	10
NOSIP	6	Importin 13	941	Inter-Protein	4
NOSIP	294	Importin 13	945	Inter-Protein	1
NOSIP	294	Importin 13	941	Inter-Protein	1
NOSIP	100	NOSIP	175	Intra-Protein	11
NOSIP	90	NOSIP	178	Intra-Protein	10
NOSIP	21	NOSIP	294	Intra-Protein	6
NOSIP	117	NOSIP	175	Intra-Protein	2
NOSIP	289	NOSIP	21	Intra-Protein	9
Importin 13	757	Importin 13	921	Intra-Protein	11
NOSIP	175	NOSIP	90	Intra-Protein	12
NOSIP	117	NOSIP	90	Intra-Protein	4
NOSIP	175	NOSIP	100	Intra-Protein	7
NOSIP	86	NOSIP	178	Intra-Protein	18
NOSIP	289	NOSIP	178	Intra-Protein	2
NOSIP	190	NOSIP	178	Intra-Protein	2
NOSIP	100	NOSIP	90	Intra-Protein	8
Importin 13	835	Importin 13	921	Intra-Protein	3
NOSIP	21	NOSIP	90	Intra-Protein	4
NOSIP	294	NOSIP	175	Intra-Protein	2
NOSIP	132	NOSIP	90	Intra-Protein	3
NOSIP	100	NOSIP	178	Intra-Protein	3
NOSIP	100	NOSIP	86	Intra-Protein	1

Table S 4: Filtered crosslinks of His-importin 13 His-NOSIP complex crosslinked by BS3 (upper band) (see Figure 29)

Protein 1	Residue 1	Protein 2	Residue 2	type	Spectral count
NOSIP	21	Importin 13	941	Inter-Protein	18
Importin 13	835	NOSIP	6	Inter-Protein	4
Importin 13	835	NOSIP	21	Inter-Protein	2
NOSIP	289	Importin 13	941	Inter-Protein	32
Importin 13	835	NOSIP	86	Inter-Protein	1
NOSIP	117	Importin 13	941	Inter-Protein	4
NOSIP	294	Importin 13	941	Inter-Protein	12
Importin 13	42	NOSIP	117	Inter-Protein	2
Importin 13	835	NOSIP	294	Inter-Protein	2
Importin 13	835	NOSIP	175	Inter-Protein	2
Importin 13	117	NOSIP	178	Inter-Protein	13
Importin 13	941	NOSIP	178	Inter-Protein	1
NOSIP	21	Importin 13	945	Inter-Protein	3
Importin 13	117	NOSIP	86	Inter-Protein	15
Importin 13	117	NOSIP	90	Inter-Protein	18
Importin 13	117	NOSIP	100	Inter-Protein	17
NOSIP	117	Importin 13	117	Inter-Protein	3
NOSIP	289	Importin 13	937	Inter-Protein	1
NOSIP	153	Importin 13	117	Inter-Protein	7
NOSIP	132	Importin 13	941	Inter-Protein	1
NOSIP	-20	NOSIP	21	Intra-Protein	10
NOSIP	289	NOSIP	21	Intra-Protein	27
Importin 13	835	Importin 13	941	Intra-Protein	55
NOSIP	21	NOSIP	117	Intra-Protein	4
NOSIP	175	NOSIP	90	Intra-Protein	21
NOSIP	6	NOSIP	21	Intra-Protein	19
NOSIP	21	NOSIP	294	Intra-Protein	14
NOSIP	19	NOSIP	21	Intra-Protein	11
NOSIP	132	NOSIP	117	Intra-Protein	10
NOSIP	90	NOSIP	178	Intra-Protein	14
NOSIP	100	NOSIP	175	Intra-Protein	12
NOSIP	172	NOSIP	90	Intra-Protein	11
NOSIP	117	NOSIP	175	Intra-Protein	12
NOSIP	172	NOSIP	178	Intra-Protein	9
NOSIP	117	NOSIP	100	Intra-Protein	12
NOSIP	21	NOSIP	175	Intra-Protein	9
NOSIP	117	NOSIP	86	Intra-Protein	3
NOSIP	175	NOSIP	100	Intra-Protein	19
NOSIP	157	NOSIP	175	Intra-Protein	3
NOSIP	6	NOSIP	178	Intra-Protein	2
NOSIP	78	NOSIP	178	Intra-Protein	20
NOSIP	132	NOSIP	175	Intra-Protein	5
Importin 13	937	Importin 13	941	Intra-Protein	13
NOSIP	253	NOSIP	257	Intra-Protein	2
NOSIP	117	NOSIP	178	Intra-Protein	24
NOSIP	6	NOSIP	20	Intra-Protein	1
NOSIP	117	NOSIP	90	Intra-Protein	17
NOSIP	78	NOSIP	86	Intra-Protein	22
NOSIP	21	NOSIP	90	Intra-Protein	13

Table S 4 continued

Protein 1	Residue 1	Protein 2	Residue 2	type	Spectral count
NOSIP	289	NOSIP	20	Intra-Protein	1
NOSIP	21	NOSIP	178	Intra-Protein	12
NOSIP	78	NOSIP	175	Intra-Protein	8
NOSIP	289	NOSIP	178	Intra-Protein	14
NOSIP	289	NOSIP	175	Intra-Protein	6
NOSIP	86	NOSIP	178	Intra-Protein	15
NOSIP	132	NOSIP	178	Intra-Protein	12
NOSIP	21	NOSIP	190	Intra-Protein	2
NOSIP	132	NOSIP	86	Intra-Protein	1
NOSIP	294	NOSIP	175	Intra-Protein	7
NOSIP	100	NOSIP	86	Intra-Protein	1
NOSIP	132	NOSIP	100	Intra-Protein	1
NOSIP	289	NOSIP	19	Intra-Protein	3
NOSIP	19	NOSIP	90	Intra-Protein	2
Importin 13	835	Importin 13	937	Intra-Protein	6
NOSIP	132	NOSIP	90	Intra-Protein	19
NOSIP	20	NOSIP	78	Intra-Protein	1

Table S 5: Filtered crosslinks of His-importin 13 His-NOSIP complex crosslinked by formaldehyde (see Figure 30)

Protein 1	Residue 1	Protein 2	Residue 2	type
importin 13	116	NOSIP	106	Inter-Protein
importin 13	924	NOSIP	110	Inter-Protein
importin 13	93	NOSIP	162	Inter-Protein
importin 13	924	NOSIP	106	Inter-Protein
importin 13	116	NOSIP	272	Inter-Protein
importin 13	37	NOSIP	205	Inter-Protein
importin 13	37	NOSIP	124	Inter-Protein
importin 13	37	NOSIP	106	Inter-Protein
importin 13	410	NOSIP	110	Inter-Protein
importin 13	924	NOSIP	272	Inter-Protein
importin 13	867	NOSIP	286	Inter-Protein
importin 13	93	NOSIP	118	Inter-Protein
importin 13	924	NOSIP	205	Inter-Protein
importin 13	109	NOSIP	118	Inter-Protein
importin 13	15	NOSIP	138	Inter-Protein
importin 13	924	NOSIP	200	Inter-Protein
importin 13	93	NOSIP	163	Inter-Protein
importin 13	15	NOSIP	144	Inter-Protein
importin 13	924	NOSIP	29	Inter-Protein
importin 13	93	NOSIP	261	Inter-Protein
importin 13	924	NOSIP	124	Inter-Protein
importin 13	37	NOSIP	110	Inter-Protein
importin 13	924	NOSIP	215	Inter-Protein
importin 13	793	NOSIP	106	Inter-Protein
importin 13	116	NOSIP	124	Inter-Protein
importin 13	650	NOSIP	27	Inter-Protein
importin 13	15	NOSIP	162	Inter-Protein
importin 13	116	NOSIP	82	Inter-Protein
importin 13	793	NOSIP	205	Inter-Protein
importin 13	924	NOSIP	82	Inter-Protein

Table S 5 continued

Protein 1	Residue 1	Protein 2	Residue 2	type
importin 13	914	NOSIP	27	Inter-Protein
importin 13	37	NOSIP	278	Inter-Protein
importin 13	37	NOSIP	28	Inter-Protein
importin 13	389	NOSIP	118	Inter-Protein
importin 13	410	NOSIP	106	Inter-Protein
importin 13	58	importin 13	79	Intra-Protein
importin 13	15	importin 13	37	Intra-Protein
importin 13	56	importin 13	79	Intra-Protein
importin 13	924	importin 13	928	Intra-Protein
importin 13	914	importin 13	924	Intra-Protein
importin 13	15	importin 13	924	Intra-Protein
importin 13	109	importin 13	924	Intra-Protein
importin 13	410	importin 13	650	Intra-Protein
importin 13	867	importin 13	924	Intra-Protein
importin 13	37	importin 13	109	Intra-Protein
importin 13	37	importin 13	93	Intra-Protein
importin 13	15	importin 13	284	Intra-Protein
importin 13	23	importin 13	389	Intra-Protein
importin 13	650	importin 13	924	Intra-Protein
importin 13	15	importin 13	410	Intra-Protein
importin 13	-7	importin 13	15	Intra-Protein
importin 13	93	importin 13	621	Intra-Protein
importin 13	37	importin 13	412	Intra-Protein
importin 13	393	importin 13	927	Intra-Protein
importin 13	15	importin 13	56	Intra-Protein
importin 13	37	importin 13	928	Intra-Protein
importin 13	-8	importin 13	16	Intra-Protein
importin 13	184	importin 13	924	Intra-Protein
importin 13	37	importin 13	867	Intra-Protein
importin 13	389	importin 13	924	Intra-Protein
importin 13	389	importin 13	410	Intra-Protein
importin 13	924	importin 13	935	Intra-Protein
importin 13	15	importin 13	63	Intra-Protein
importin 13	184	importin 13	284	Intra-Protein
importin 13	22	importin 13	93	Intra-Protein
importin 13	-7	importin 13	914	Intra-Protein
importin 13	79	importin 13	109	Intra-Protein
importin 13	410	importin 13	928	Intra-Protein
importin 13	14	importin 13	37	Intra-Protein
importin 13	15	importin 13	79	Intra-Protein
importin 13	37	importin 13	389	Intra-Protein
importin 13	855	importin 13	914	Intra-Protein
importin 13	389	importin 13	571	Intra-Protein
importin 13	15	importin 13	793	Intra-Protein
importin 13	410	importin 13	914	Intra-Protein
importin 13	116	importin 13	928	Intra-Protein
importin 13	116	importin 13	389	Intra-Protein
importin 13	99	importin 13	389	Intra-Protein
importin 13	23	importin 13	914	Intra-Protein
importin 13	621	importin 13	914	Intra-Protein
importin 13	412	importin 13	621	Intra-Protein
importin 13	855	importin 13	928	Intra-Protein

Table S 5 continued

Protein 1	Residue 1	Protein 2	Residue 2	type
importin 13	793	importin 13	914	Intra-Protein
importin 13	37	importin 13	914	Intra-Protein
importin 13	284	importin 13	914	Intra-Protein
importin 13	438	importin 13	474	Intra-Protein
importin 13	15	importin 13	621	Intra-Protein
importin 13	171	importin 13	186	Intra-Protein
importin 13	928	importin 13	942	Intra-Protein
importin 13	-8	importin 13	15	Intra-Protein
importin 13	-10	importin 13	22	Intra-Protein
importin 13	23	importin 13	109	Intra-Protein
importin 13	37	importin 13	184	Intra-Protein
importin 13	420	importin 13	571	Intra-Protein
importin 13	93	importin 13	924	Intra-Protein
NOSIP	26	NOSIP	124	Intra-Protein
NOSIP	106	NOSIP	118	Intra-Protein
NOSIP	27	NOSIP	106	Intra-Protein
NOSIP	27	NOSIP	110	Intra-Protein
NOSIP	261	NOSIP	280	Intra-Protein
NOSIP	124	NOSIP	163	Intra-Protein
NOSIP	124	NOSIP	166	Intra-Protein
NOSIP	82	NOSIP	118	Intra-Protein
NOSIP	261	NOSIP	272	Intra-Protein
NOSIP	118	NOSIP	272	Intra-Protein
NOSIP	27	NOSIP	280	Intra-Protein
NOSIP	272	NOSIP	286	Intra-Protein
NOSIP	110	NOSIP	264	Intra-Protein
NOSIP	103	NOSIP	118	Intra-Protein
NOSIP	124	NOSIP	261	Intra-Protein
NOSIP	100	NOSIP	124	Intra-Protein
NOSIP	110	NOSIP	118	Intra-Protein
NOSIP	118	NOSIP	215	Intra-Protein
NOSIP	215	NOSIP	261	Intra-Protein
NOSIP	110	NOSIP	286	Intra-Protein
NOSIP	106	NOSIP	187	Intra-Protein
NOSIP	27	NOSIP	200	Intra-Protein
NOSIP	118	NOSIP	182	Intra-Protein
NOSIP	26	NOSIP	110	Intra-Protein
NOSIP	163	NOSIP	272	Intra-Protein
NOSIP	73	NOSIP	106	Intra-Protein
NOSIP	110	NOSIP	261	Intra-Protein
NOSIP	106	NOSIP	162	Intra-Protein
NOSIP	27	NOSIP	215	Intra-Protein
NOSIP	27	NOSIP	82	Intra-Protein
NOSIP	124	NOSIP	144	Intra-Protein
NOSIP	99	NOSIP	106	Intra-Protein
NOSIP	222	NOSIP	261	Intra-Protein
NOSIP	261	NOSIP	278	Intra-Protein
NOSIP	86	NOSIP	124	Intra-Protein
NOSIP	106	NOSIP	295	Intra-Protein
NOSIP	187	NOSIP	215	Intra-Protein
NOSIP	73	NOSIP	110	Intra-Protein
NOSIP	106	NOSIP	261	Intra-Protein

Table S 5 continued

Protein 1	Residue 1	Protein 2	Residue 2	type
NOSIP	124	NOSIP	263	Intra-Protein
NOSIP	82	NOSIP	286	Intra-Protein
NOSIP	29	NOSIP	118	Intra-Protein
NOSIP	89	NOSIP	272	Intra-Protein
NOSIP	118	NOSIP	184	Intra-Protein
NOSIP	110	NOSIP	166	Intra-Protein
NOSIP	89	NOSIP	110	Intra-Protein
NOSIP	272	NOSIP	292	Intra-Protein
NOSIP	26	NOSIP	205	Intra-Protein
NOSIP	106	NOSIP	163	Intra-Protein
NOSIP	106	NOSIP	267	Intra-Protein
NOSIP	104	NOSIP	118	Intra-Protein
NOSIP	200	NOSIP	286	Intra-Protein
NOSIP	215	NOSIP	263	Intra-Protein
NOSIP	178	NOSIP	280	Intra-Protein
NOSIP	26	NOSIP	280	Intra-Protein
NOSIP	26	NOSIP	37	Intra-Protein
NOSIP	118	NOSIP	124	Intra-Protein
NOSIP	27	NOSIP	37	Intra-Protein
NOSIP	99	NOSIP	110	Intra-Protein
NOSIP	27	NOSIP	124	Intra-Protein
NOSIP	176	NOSIP	280	Intra-Protein
NOSIP	110	NOSIP	143	Intra-Protein
NOSIP	263	NOSIP	280	Intra-Protein
NOSIP	26	NOSIP	272	Intra-Protein
NOSIP	37	NOSIP	73	Intra-Protein
NOSIP	37	NOSIP	118	Intra-Protein
NOSIP	110	NOSIP	176	Intra-Protein
NOSIP	138	NOSIP	278	Intra-Protein
NOSIP	176	NOSIP	272	Intra-Protein
NOSIP	26	NOSIP	278	Intra-Protein
NOSIP	82	NOSIP	163	Intra-Protein
NOSIP	106	NOSIP	138	Intra-Protein
NOSIP	99	NOSIP	215	Intra-Protein
NOSIP	86	NOSIP	200	Intra-Protein
NOSIP	205	NOSIP	286	Intra-Protein
NOSIP	205	NOSIP	261	Intra-Protein
NOSIP	124	NOSIP	286	Intra-Protein
NOSIP	26	NOSIP	106	Intra-Protein
NOSIP	178	NOSIP	272	Intra-Protein
NOSIP	162	NOSIP	205	Intra-Protein
NOSIP	82	NOSIP	261	Intra-Protein
NOSIP	110	NOSIP	187	Intra-Protein
NOSIP	278	NOSIP	295	Intra-Protein
NOSIP	118	NOSIP	280	Intra-Protein
NOSIP	138	NOSIP	205	Intra-Protein
NOSIP	162	NOSIP	215	Intra-Protein
NOSIP	86	NOSIP	110	Intra-Protein
NOSIP	106	NOSIP	264	Intra-Protein
NOSIP	272	NOSIP	295	Intra-Protein
NOSIP	124	NOSIP	178	Intra-Protein
NOSIP	29	NOSIP	286	Intra-Protein

Table S 5 continued

Protein 1	Residue 1	Protein 2	Residue 2	type
NOSIP	118	NOSIP	200	Intra-Protein
NOSIP	100	NOSIP	110	Intra-Protein
NOSIP	187	NOSIP	272	Intra-Protein
NOSIP	110	NOSIP	178	Intra-Protein
NOSIP	124	NOSIP	143	Intra-Protein
NOSIP	110	NOSIP	267	Intra-Protein
NOSIP	163	NOSIP	205	Intra-Protein
NOSIP	110	NOSIP	292	Intra-Protein
NOSIP	163	NOSIP	200	Intra-Protein
NOSIP	124	NOSIP	295	Intra-Protein
NOSIP	106	NOSIP	286	Intra-Protein
NOSIP	280	NOSIP	292	Intra-Protein
NOSIP	264	NOSIP	280	Intra-Protein
NOSIP	118	NOSIP	267	Intra-Protein
NOSIP	100	NOSIP	278	Intra-Protein
NOSIP	118	NOSIP	278	Intra-Protein
NOSIP	29	NOSIP	264	Intra-Protein
NOSIP	110	NOSIP	138	Intra-Protein
NOSIP	176	NOSIP	215	Intra-Protein
NOSIP	166	NOSIP	182	Intra-Protein
NOSIP	73	NOSIP	82	Intra-Protein
NOSIP	163	NOSIP	278	Intra-Protein
NOSIP	178	NOSIP	278	Intra-Protein
NOSIP	99	NOSIP	272	Intra-Protein
NOSIP	178	NOSIP	200	Intra-Protein
NOSIP	163	NOSIP	280	Intra-Protein
NOSIP	176	NOSIP	278	Intra-Protein
NOSIP	73	NOSIP	200	Intra-Protein
NOSIP	73	NOSIP	272	Intra-Protein
NOSIP	37	NOSIP	162	Intra-Protein
NOSIP	29	NOSIP	187	Intra-Protein
NOSIP	200	NOSIP	261	Intra-Protein
NOSIP	26	NOSIP	82	Intra-Protein
NOSIP	162	NOSIP	278	Intra-Protein
NOSIP	267	NOSIP	278	Intra-Protein
NOSIP	124	NOSIP	187	Intra-Protein
NOSIP	26	NOSIP	182	Intra-Protein
NOSIP	27	NOSIP	205	Intra-Protein
NOSIP	280	NOSIP	295	Intra-Protein
NOSIP	82	NOSIP	166	Intra-Protein
NOSIP	215	NOSIP	267	Intra-Protein
NOSIP	143	NOSIP	215	Intra-Protein
NOSIP	267	NOSIP	286	Intra-Protein
NOSIP	200	NOSIP	267	Intra-Protein
NOSIP	82	NOSIP	100	Intra-Protein
NOSIP	26	NOSIP	215	Intra-Protein
NOSIP	27	NOSIP	278	Intra-Protein
NOSIP	82	NOSIP	176	Intra-Protein
NOSIP	86	NOSIP	278	Intra-Protein
NOSIP	73	NOSIP	124	Intra-Protein
NOSIP	124	NOSIP	176	Intra-Protein
NOSIP	205	NOSIP	267	Intra-Protein

Table S 5 continued

Protein 1	Residue 1	Protein 2	Residue 2	type
NOSIP	106	NOSIP	166	Intra-Protein
NOSIP	37	NOSIP	267	Intra-Protein
NOSIP	28	NOSIP	138	Intra-Protein
NOSIP	182	NOSIP	286	Intra-Protein
NOSIP	162	NOSIP	272	Intra-Protein
NOSIP	200	NOSIP	292	Intra-Protein
NOSIP	37	NOSIP	261	Intra-Protein
NOSIP	26	NOSIP	200	Intra-Protein
NOSIP	118	NOSIP	222	Intra-Protein
NOSIP	124	NOSIP	138	Intra-Protein
NOSIP	13	NOSIP	28	Intra-Protein
NOSIP	124	NOSIP	162	Intra-Protein
NOSIP	263	NOSIP	297	Intra-Protein
NOSIP	215	NOSIP	286	Intra-Protein
NOSIP	73	NOSIP	215	Intra-Protein
NOSIP	103	NOSIP	138	Intra-Protein
NOSIP	162	NOSIP	200	Intra-Protein
NOSIP	82	NOSIP	295	Intra-Protein
NOSIP	110	NOSIP	263	Intra-Protein
NOSIP	108	NOSIP	118	Intra-Protein
NOSIP	138	NOSIP	184	Intra-Protein
NOSIP	82	NOSIP	143	Intra-Protein
NOSIP	118	NOSIP	205	Intra-Protein
NOSIP	267	NOSIP	295	Intra-Protein
NOSIP	29	NOSIP	100	Intra-Protein
NOSIP	26	NOSIP	267	Intra-Protein
NOSIP	178	NOSIP	267	Intra-Protein
NOSIP	187	NOSIP	205	Intra-Protein
NOSIP	29	NOSIP	263	Intra-Protein
NOSIP	29	NOSIP	261	Intra-Protein
NOSIP	138	NOSIP	200	Intra-Protein
NOSIP	29	NOSIP	138	Intra-Protein
NOSIP	99	NOSIP	124	Intra-Protein
NOSIP	27	NOSIP	272	Intra-Protein
NOSIP	267	NOSIP	272	Intra-Protein
NOSIP	215	NOSIP	292	Intra-Protein
NOSIP	106	NOSIP	144	Intra-Protein
NOSIP	176	NOSIP	200	Intra-Protein
NOSIP	110	NOSIP	163	Intra-Protein
NOSIP	200	NOSIP	263	Intra-Protein
NOSIP	89	NOSIP	104	Intra-Protein
NOSIP	26	NOSIP	29	Intra-Protein
NOSIP	82	NOSIP	144	Intra-Protein
NOSIP	118	NOSIP	295	Intra-Protein
NOSIP	37	NOSIP	286	Intra-Protein
NOSIP	26	NOSIP	104	Intra-Protein
NOSIP	162	NOSIP	280	Intra-Protein
NOSIP	82	NOSIP	187	Intra-Protein
NOSIP	215	NOSIP	295	Intra-Protein
NOSIP	37	NOSIP	163	Intra-Protein
NOSIP	82	NOSIP	162	Intra-Protein
NOSIP	166	NOSIP	205	Intra-Protein

Table S 5 continued

Protein 1	Residue 1	Protein 2	Residue 2	type
NOSIP	29	NOSIP	295	Intra-Protein
NOSIP	99	NOSIP	278	Intra-Protein
NOSIP	100	NOSIP	205	Intra-Protein
NOSIP	11	NOSIP	29	Intra-Protein
NOSIP	82	NOSIP	138	Intra-Protein
NOSIP	166	NOSIP	215	Intra-Protein
NOSIP	29	NOSIP	267	Intra-Protein
NOSIP	82	NOSIP	267	Intra-Protein
NOSIP	162	NOSIP	267	Intra-Protein
NOSIP	175	NOSIP	278	Intra-Protein
NOSIP	110	NOSIP	144	Intra-Protein
NOSIP	29	NOSIP	162	Intra-Protein
NOSIP	143	NOSIP	200	Intra-Protein
NOSIP	163	NOSIP	267	Intra-Protein
NOSIP	100	NOSIP	280	Intra-Protein
NOSIP	86	NOSIP	267	Intra-Protein
NOSIP	89	NOSIP	124	Intra-Protein
NOSIP	29	NOSIP	143	Intra-Protein
NOSIP	264	NOSIP	278	Intra-Protein
NOSIP	166	NOSIP	200	Intra-Protein
NOSIP	205	NOSIP	264	Intra-Protein
NOSIP	106	NOSIP	176	Intra-Protein
NOSIP	215	NOSIP	264	Intra-Protein
NOSIP	124	NOSIP	292	Intra-Protein
NOSIP	82	NOSIP	178	Intra-Protein
NOSIP	29	NOSIP	176	Intra-Protein
NOSIP	99	NOSIP	114	Intra-Protein
NOSIP	27	NOSIP	267	Intra-Protein
NOSIP	28	NOSIP	118	Intra-Protein
NOSIP	124	NOSIP	267	Intra-Protein
NOSIP	267	NOSIP	292	Intra-Protein
NOSIP	99	NOSIP	200	Intra-Protein
NOSIP	86	NOSIP	205	Intra-Protein
NOSIP	37	NOSIP	263	Intra-Protein
NOSIP	143	NOSIP	278	Intra-Protein
NOSIP	29	NOSIP	73	Intra-Protein
NOSIP	267	NOSIP	283	Intra-Protein
NOSIP	73	NOSIP	205	Intra-Protein
NOSIP	106	NOSIP	263	Intra-Protein
NOSIP	176	NOSIP	267	Intra-Protein
NOSIP	144	NOSIP	278	Intra-Protein
NOSIP	29	NOSIP	163	Intra-Protein
NOSIP	166	NOSIP	278	Intra-Protein
NOSIP	37	NOSIP	86	Intra-Protein
NOSIP	175	NOSIP	185	Intra-Protein
NOSIP	182	NOSIP	267	Intra-Protein
NOSIP	144	NOSIP	205	Intra-Protein
NOSIP	82	NOSIP	89	Intra-Protein
NOSIP	138	NOSIP	182	Intra-Protein
NOSIP	264	NOSIP	272	Intra-Protein
NOSIP	138	NOSIP	272	Intra-Protein
NOSIP	176	NOSIP	187	Intra-Protein

Table S 5 continued

Protein 1	Residue 1	Protein 2	Residue 2	type
NOSIP	166	NOSIP	280	Intra-Protein
NOSIP	89	NOSIP	200	Intra-Protein
NOSIP	106	NOSIP	122	Intra-Protein
NOSIP	163	NOSIP	182	Intra-Protein
NOSIP	118	NOSIP	297	Intra-Protein
NOSIP	106	NOSIP	143	Intra-Protein
NOSIP	205	NOSIP	263	Intra-Protein
NOSIP	144	NOSIP	272	Intra-Protein
NOSIP	143	NOSIP	205	Intra-Protein
NOSIP	98	NOSIP	118	Intra-Protein
NOSIP	26	NOSIP	99	Intra-Protein
NOSIP	143	NOSIP	272	Intra-Protein
NOSIP	110	NOSIP	295	Intra-Protein
NOSIP	163	NOSIP	215	Intra-Protein
NOSIP	99	NOSIP	118	Intra-Protein
NOSIP	86	NOSIP	106	Intra-Protein
NOSIP	29	NOSIP	86	Intra-Protein
NOSIP	98	NOSIP	138	Intra-Protein
NOSIP	37	NOSIP	187	Intra-Protein
NOSIP	138	NOSIP	280	Intra-Protein
NOSIP	110	NOSIP	162	Intra-Protein
NOSIP	28	NOSIP	267	Intra-Protein
importin 13	116	NOSIP	106	Inter-Protein
importin 13	924	NOSIP	110	Inter-Protein
importin 13	93	NOSIP	162	Inter-Protein
importin 13	924	NOSIP	106	Inter-Protein
importin 13	116	NOSIP	272	Inter-Protein

Table S 6: Filtered crosslinks of His-transportin 1 His-NOSIP complex crosslinked by BS3 (see Figure 31)

Protein 1	Residue 1	Protein 2	Residue 2	type	Spectral count
NOSIP	117	transportin 1	81	Inter-Protein	67
transportin 1	85	NOSIP	175	Inter-Protein	42
NOSIP	172	transportin 1	81	Inter-Protein	28
NOSIP	21	transportin 1	81	Inter-Protein	31
transportin 1	128	NOSIP	175	Inter-Protein	12
NOSIP	157	transportin 1	81	Inter-Protein	50
NOSIP	132	transportin 1	66	Inter-Protein	6
transportin 1	85	NOSIP	90	Inter-Protein	20
NOSIP	117	transportin 1	66	Inter-Protein	20
transportin 1	85	NOSIP	172	Inter-Protein	17
NOSIP	21	transportin 1	889	Inter-Protein	8
transportin 1	385	NOSIP	178	Inter-Protein	70
NOSIP	155	transportin 1	81	Inter-Protein	24
NOSIP	289	transportin 1	81	Inter-Protein	5
NOSIP	132	transportin 1	81	Inter-Protein	33
transportin 1	81	NOSIP	175	Inter-Protein	116
transportin 1	502	NOSIP	178	Inter-Protein	9
transportin 1	128	NOSIP	90	Inter-Protein	8
transportin 1	81	NOSIP	100	Inter-Protein	157
NOSIP	153	transportin 1	81	Inter-Protein	23
NOSIP	117	transportin 1	197	Inter-Protein	26
NOSIP	132	transportin 1	197	Inter-Protein	9
transportin 1	81	NOSIP	178	Inter-Protein	10
NOSIP	157	transportin 1	197	Inter-Protein	4
NOSIP	78	NOSIP	175	Intra-Protein	4
NOSIP	6	NOSIP	21	Intra-Protein	34
NOSIP	78	NOSIP	178	Intra-Protein	27
transportin 1	128	transportin 1	85	Intra-Protein	14
NOSIP	100	NOSIP	90	Intra-Protein	10
NOSIP	100	NOSIP	175	Intra-Protein	12
NOSIP	289	NOSIP	21	Intra-Protein	41
NOSIP	117	NOSIP	100	Intra-Protein	66
NOSIP	253	NOSIP	257	Intra-Protein	31
NOSIP	100	NOSIP	178	Intra-Protein	57
NOSIP	90	NOSIP	178	Intra-Protein	15
NOSIP	41	NOSIP	289	Intra-Protein	5
NOSIP	175	NOSIP	100	Intra-Protein	11
NOSIP	132	NOSIP	100	Intra-Protein	26
NOSIP	132	NOSIP	157	Intra-Protein	6
transportin 1	42	transportin 1	66	Intra-Protein	13
NOSIP	78	NOSIP	117	Intra-Protein	3
NOSIP	21	NOSIP	175	Intra-Protein	6
NOSIP	172	NOSIP	90	Intra-Protein	9
NOSIP	132	NOSIP	117	Intra-Protein	29
NOSIP	6	NOSIP	289	Intra-Protein	14
NOSIP	21	NOSIP	294	Intra-Protein	30
NOSIP	21	NOSIP	178	Intra-Protein	18
NOSIP	289	NOSIP	175	Intra-Protein	9
NOSIP	172	NOSIP	178	Intra-Protein	2
NOSIP	132	NOSIP	155	Intra-Protein	4
NOSIP	157	NOSIP	100	Intra-Protein	10

Table S 6 continued

Protein 1	Residue 1	Protein 2	Residue 2	type	Spectral count
NOSIP	78	NOSIP	86	Intra-Protein	19
NOSIP	289	NOSIP	178	Intra-Protein	11
transportin 1	327	transportin 1	502	Intra-Protein	16
NOSIP	117	NOSIP	178	Intra-Protein	19
NOSIP	19	NOSIP	21	Intra-Protein	12
NOSIP	132	NOSIP	175	Intra-Protein	3
NOSIP	117	NOSIP	157	Intra-Protein	4
NOSIP	132	NOSIP	90	Intra-Protein	4
NOSIP	132	NOSIP	178	Intra-Protein	9
NOSIP	157	NOSIP	117	Intra-Protein	5
NOSIP	6	NOSIP	20	Intra-Protein	2
NOSIP	117	NOSIP	90	Intra-Protein	8
NOSIP	155	NOSIP	100	Intra-Protein	19
NOSIP	153	NOSIP	178	Intra-Protein	3
NOSIP	117	NOSIP	139	Intra-Protein	7
transportin 1	128	transportin 1	81	Intra-Protein	9
transportin 1	5	transportin 1	42	Intra-Protein	2
NOSIP	21	NOSIP	117	Intra-Protein	2
NOSIP	175	NOSIP	90	Intra-Protein	10
NOSIP	21	NOSIP	90	Intra-Protein	5
NOSIP	172	NOSIP	100	Intra-Protein	3
NOSIP	153	NOSIP	100	Intra-Protein	18

Table S 7: Xwalk measured distances of NOSIP intra-protein crosslinks from transportin 1/NOSIP crosslinking (see Figure 33)

Residue 1	Residue 2	Dist. in sequence	Euclidean distance (Å)	SAS distance (Å)
LYS-19	LYS-21	2	7,3	8,4
LYS-253	LYS-257	4	7,8	11,4
LYS-41	LYS-289	248	12,9	13,3
LYS-78	LYS-86	8	12,7	17,2
LYS-172	LYS-90	82	15,6	17,6
LYS-175	LYS-90	85	13	18,6
LYS-78	LYS-178	100	16,4	20,1
LYS-172	LYS-178	6	18,1	21
LYS-21	LYS-294	273	16,4	21,2
LYS-100	LYS-90	10	16,1	21,3
LYS-100	LYS-175	75	17,7	21,5
LYS-90	LYS-178	88	12,9	22,5
LYS-100	LYS-178	78	20,6	23,5
LYS-172	LYS-100	72	17,8	25,2
LYS-6	LYS-20	14	23,7	28
LYS-132	LYS-117	15	25,8	28,7
LYS-117	LYS-100	17	26,1	31,4
LYS-78	LYS-175	97	23,9	31,6
LYS-289	LYS-21	268	25,2	31,9
LYS-6	LYS-21	15	25,7	32,3
LYS-117	LYS-157	40	26,6	33,4

Table S 7 continued

Residue 1	Residue 2	Dist. in sequence	Euclidean distance (Å)	SAS distance (Å)
LYS-289	LYS-175	114	34,9	-3
LYS-132	LYS-157	25	37,7	-3
LYS-117	LYS-90	27	40,9	-3
LYS-117	LYS-178	61	43,2	-3
LYS-21	LYS-175	154	45,9	-3
LYS-153	LYS-178	25	46	-3
LYS-21	LYS-178	157	48,7	-3
LYS-132	LYS-100	32	51	-3
LYS-21	LYS-90	69	52,5	-3
LYS-132	LYS-175	43	57,7	-3
LYS-78	LYS-117	39	58	-3
LYS-132	LYS-90	42	64,1	-3
LYS-132	LYS-178	46	65,7	-3
LYS-21	LYS-117	96	76,7	-3
LYS-155	LYS-100	55	26,8	-1
LYS-157	LYS-100	57	30,1	-1
LYS-289	LYS-178	111	32,6	-1
LYS-78	LYS-100	22	32,9	-1
LYS-132	LYS-155	23	33,1	-1
LYS-6	LYS-289	283	37,9	-1

Table S 8: Predicted bipartite NLSs for NOSIP using cNLS Mapper

Amino acid position	Sequence of NOSIP	Score
18-45	EKKKDTAASGYGTQNIRLSRDAVKDFDC	2,1
77-105	QKKEIARQMKAYEKQRGTRREEQKELQRA	2,1
124-158	RPLNPFTAKALSGTSPDDVQPGPSVGPPSKDKDKV	3
150-177	PPSKDKDKVLPSFWIPSLTPEAKATKLE	2,9
150-180	PPSKDKDKVLPSFWIPSLTPEAKATKLEKPS	6,7
154-180	DKDKVLPSFWIPSLTPEAKATKLEKPS	3
249-279	ECVEKLIRKDMVDPVTGDKLTDRDIIVLQRG	2,1
264-294	TGDKLTDRDIIVLQRGGTGFAGSGVKLQAEK	2,8

Table S 9: Predicted NESs for NOSIP using LocNES

Amino acid position	Sequence of NOSIP	Score
188-202	SGKPLRMSDLTPVHF	0.005
198-212	TPVHFTPLDSSVDRV	0.145
200-214	VHFTPLDSSVDRVGL	0.172

Table S 10: Predicted NESs for Lipin 1 using LocNES

Amino acid position	Sequence of Lipin 1	Score
1-13	MNYVGQLAGQVFV	0.018
14-18	VGQLAGQVFVTVKEL	0.020
22-36	LNPATLSGCIDIIVI	0.007
43-57	LQCSPFHVRFGKMGV	0.009
346-360	EDLETLGAAAPLLPM	0.195
347-361	DLETLGAAAPLLPMI	0.209
350-364	TLGAAAPLLPMIEEL	0.105
385-399	RDKRSRHLGADGVYL	0.036
398-412	YLDDLTDMDPEVAAL	0.768
400-414	DDLTDMDPEVAALYF	0.719
447-461	VDSGVESTSDGLRDL	0.139
452-466	ESTSDGLRDLPSIAI	0.196
515-529	NWTTAAPLLLAMQAF	0.207
624-638	YKKTLRLTSEQLKSL	0.212
626-640	KTLRLTSEQLKSLKL	0.437
715-729	NGYKFLYCSARAIGM	0.021
774-788	KFKVQCLTDIKNLFF	0.015
807-821	SYKQVGVSLNRIFTV	0.009
828-842	VQEHAKTNISSYVRL	0.026
838-852	SYVRLCEVVDHVFPL	0.009

List of Figures

List of Tables

Abbreviations

aa	amino acid
AP	aprotinin
ATP	adenosine-5'-triphosphate
BSA	bovine-serum albumin
C-terminus	carboxy terminus
CRIME	CRM1, importin β etc.
CRM1	chromosome maintenance region 1
D	asparagine
D. rerio	*Danio rerio*
DAPI	4',6-diamidino-2-phenylindole
DMEM	Dulbecco's modified eagles' medium
DMSO	dimethyl sulfoxide
dNTPs	2'-desoxynucleoside-5'-triphosphate
DTT	dithiothreitol
E	glutamine
E. coli	*Escherichia coli*
FG	phenylalanine glycine
g	units of gravity
GFP	green fluorescence protein
GR	glucocorticoid-receptor
GST	glutathione-S-transferase
GTP	guanosine-5'-triphosphate
HA	hemagglutinin
HEAT	huntingtin, elongation factor 3, protein phosphatase 2A and TOR1
His	histidine tag
HIV-1	human-immunodeficiency virus 1
HKA	heterokaryon assay
IDR	intrinsically disordered region
IDR	intrinsically disordered region
Imp	importin
IPTG	Isopropyl b-D-1-thiogalactopyranoside
K	lysine
Kap	karyopherin
kDa	kilo dalton
LMB	leptomycin B
LP	leupeptin
M9	PY-NLS described for hnRNP A1
MBP	maltose-binding protein
MWCO	molecular weight cut-off
N-terminus	amino terminus
NES	nuclear export signal
NLS	nuclear localization signal
NPC	nuclear pore complex
NT	non-targeting
NTF2	nuclear transport factor 2
NTR	Nuclear transport receptor
Nup	nucleoporin
OA	okadaic acid
OD	optical density
PAGE	polyacrylamide gel electrophoresis
PBS	phosphate-buffered saline
PCR	polymerase-chain reaction
PDB	protein data bank
PEG	polyethylenglycol
PMSF	phenylmethylsulphonyl fluoride
PTHrP	parathyroid hormone-related protein
Ran	Ras-related nuclear protein
RanGAP	RanGTPase activating protein
RanGEF	Ran guanine exchange factor
RCC1	regulator of chromatin condensation 1
RNA	ribonucleic acid
rpm	rounds per minute
S	serine
S. cerevisiae	*Saccharomyces cerevisiae*
SDS	sodiumdodecylsulfate

siRNA	small interfering RNA
St	staurosporine
SV40	simian virus large T-antigen
TAE	Tris/Acetate/EDTA
TAP	tip-associated protein
TNPO 1	transportin 1
w/v	weight/volume
WGA	wheat-germ-agglutinin
WT	wildtype
X. laevis	*Xenopus laevis*
Y	tyrosine

Acknowledgements

First of all, I want to thank my supervisor Prof. Ralph Kehlenbach for giving me the opportunity to work on this project and for the scientific freedom and the support during this time.

I would like to thank my thesis committee Prof. Michael Meinecke and Dr. Achim Dickmanns for very helpful discussion and input to my project. A big thank you to Prof. Hauke Hillen who kindly accepted to evaluate my work as a reviewer.

Thank you, Dr. Imke Baade, for teaching me most of the techniques and the project and also for your support during the beginning of my thesis. I would also like to thank all the members of the Kehlenbach lab. Thanks to David Kohlhause, Inés Rodríguez González, Dr. Floriane Lagadec and Dr. Mohamed Hamed for the nice coffee breaks, scientific and non-scientific discussions, I enjoyed it a lot. Dr. Christina James for your support and proof-reading of my thesis. Dr. Marina Blenski, Christiane Spillner, Ulrike Möller and all the others for the great working atmosphere.

I also thank all members of the Department of Molecular Biology for the support and help during my PhD. Special thanks to Rebecca Rossen Falk, Nicolas Lemus, Nidhi Kanwal and Nicole Kleiber for so nice lunch times and coffee breaks!

I would like to thank Mike Blüggel, for your scientific input during our hour lasting calls aka Mario Kart races.

A very special thank you goes to the love of my life, Johanna Pörschke! Thank you for supporting me all the time, for helping me up when I got stocked, for forcing me to keep my work life balance, for your scientific input, your ideas and the willing to listen to all my complains and problems during the journey of this project. I love you!

Publications

Baade I, Hutten S, Sternburg EL, **Pörschke M**, Hofweber M, Dormann D, Kehlenbach RH. The RNA-binding protein FUS is chaperoned and imported into the nucleus by a network of import receptors. J Biol Chem. 2021

Meiners A, Bäcker S, Hadrović I, Heid C, Beuck C, Ruiz-Blanco YB, Mieres-Perez J, **Pörschke M**, Grad JN, Vallet C, Hoffmann D, Bayer P, Sánchez-García E, Schrader T, Knauer SK. Specific inhibition of the Survivin-CRM1 interaction by peptide-modified molecular tweezers. Nat Commun. 2021

Parts of this work are currently under revision:

Pörschke M, Rodríguez-González I, Parfentev I, Urlaub H, Kehlenbach RH. Transportin 1 is the major nuclear transport receptor for the nitric oxide synthase interacting protein (NOSIP).